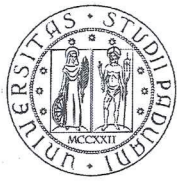

UNIVERSITÀ
DEGLI STUDI
DI PADOVA

Sede Amministrativa: Università degli Studi di Padova

Dipartimento di Ingegneria Civile, Edile e Ambientale

SCUOLA DI DOTTORATO DI RICERCA IN: Scienze dell'Ingegneria Civile e Ambientale
INDIRIZZO: Meccanica computazionale ed Ingegneria strutturale
CICLO: XXVI

THREE-DIMENSIONAL COUPLED FEM MODELLING AND PROGRAMMING OF PARTIALLY SATURATED POROUS MEDIA

Direttore della Scuola : Ch.mo Prof. Stefano Lanzoni

Supervisori : Ch. mo Prof. Carmelo Majorana
Dott. Ing. Valentina Salomoni

Dottorando: Daniele Muraro

Index

Acknowledgements

This work as well my doctorate studies wouldn't have been possible without the efforts of so many people that during these years encouraged me to fight and carry on my research activities, helped me on keeping high my self-esteem when things went wrong and that participated to the small successes of every day. I would to thank all of you, from the deep of my heart you have helped to my happiness and to the success of my work.

My special thanks goes to my family that supported me during these years as well as in each instant of my life, my mother that takes care of me with her infinite love and my father that lights me with his wisdom and courage, my sister Angela that is by my side every day and Daniele that is like a brother for me.

Particularly I want to thanks Prof. Carmelo Majorana and Prof. Valentina Salomoni, my supervisors that believed in me, taught me with great patience and gave me the possibility to increase my capabilities in this wonderful adventure.

Huge thanks goes to my friends and colleagues Gianluca, Riccardo, Giovanna, Nicolò and Beatrice for having contributed actively to my work, helping me with problems and sustaining me with a lot of advises, and with which I have shared unforgettable moments. Neverthless, I have to express my gratitude to all the friends I've met during these years here at the Padua University, in particular the guys of my office Marco, Teo, Giuseppe and Mattia, for the beautiful friendship that we have built all together and which I want to carry with me for all my life.

I would like to thank also all my closest friends that I have out of the academic environment and with which I share my free time, because they have cancelled every preoccupation I have had, giving me a lot of happy moments.

My prayers of thanksgiving go to you God, because you give me life, you put on me a strange mixture of gifts that I have yet to understand and you give me the health and the empathy to stay among people in happiness. You give me a good brain, a good family, invaluable friends and you put Elena by my side.

I want to dedicate all my work to you, Elena. Because you have taken my hand every time I was fallen, you helped me to stand up and you brought us, hand in hands, outside the wall.

Abstract

The purpose of the work presented in this thesis is to investigate the fully and partially saturated behaviour of soils, behaviour that can be extended also to geomaterials like concrete.

The physical - mathematical approach proposed within this manuscript is a coupled thermo-hydro-mechanical model, suitable for consolidation / subsidence analyses of unsaturated soils. This coupled formulation, can therefore be qualified as $\boldsymbol{u - p_w - p_g - (T)}$, by the introduction of basic state variables involved in the processes, that here are: the displacements field $\boldsymbol{u}$, the liquid (water) pressure field $\boldsymbol{p_w}$, the gas (dry air and water vapour) pressure field $\boldsymbol{p_g}$, and eventually the temperature $\boldsymbol{T}$ that is involved on the modelling of non – isothermal process. Due to the coexistence of two different fluid phases, liquid and gaseous one, this model can be regarded as a multiphase approach to a deforming porous medium as proposed by Lewis and Schrefler [1] in the framework of the hybrid mixture theory for porous media firstly presented by Hassanizadeh and Gray [2, 3] and Zienkiewicz *et al.* [4, 5].

The evolution at macroscopic scale of the state variables above mentioned, in particular of pressures of both liquid and gas, is basically influenced by the microstructure of the material that characterizes the behaviour of a soil with relation on capillary effects and deformability. The physical approach proposed here is based on averaging techniques applied to the physical quantities that can be estimated in a representative elementary volume (REV) [6, 7]. With the addition of water retention functions that provide a description of the relation that exists among capillary pressure and the degree of water saturation [8-10], a complete set of fluid balance equations and mechanical and thermodynamic equilibrium equations can be obtained for the medium in a macroscopic scale.

A coupled (thermo)-hydro-mechanical formulation $\boldsymbol{u - p - (T)}$ that deals with a fully saturated porous medium has been implemented with success in the past in the F.E. two-dimensional program PLASCON [11] and its further extensions to three-dimensionality with PLASCON3D [12-14].

The present work focused on the extension and upgrading of the relative simple single phase theory along with its numerical implementations, towards a more realistic multiphase description of the porous material, where voids may be filled up with both liquid and gas that interacts each other by mean of the concept of capillary pressure. An improved code PLASCON3D_PS based on the fully coupled $\boldsymbol{u - p_w - p_g - (T)}$ formulation and developed from previous versions has been realized. Due to the lack in literature of three-dimensional coupled numerical and

experimental tests, some numerical results of benchmark tests and real case problems, that derive from two-dimensional domains [15, 16], will be presented.

Abstract (Italian)

Lo scopo del lavoro presentato con questa tesi è di studiare il comportamento dei terreni in stato di totale e parziale saturazione, comportamento che può essere anche esteso ad altri geomateriali come il calcestruzzo.

Il modello fisico - matematico proposto in questo lavoro è denominato termo- idro-meccanico in formulazione accoppiata, adatto ad analisi di consolidazione / subsidenza per suoli non saturi. La formulazione accoppiata può essere quindi qualificata come $\boldsymbol{u - p_w - p_g - (T)}$, attraverso l'introduzione delle variabili di stato, che qui sono: il campo degli spostamenti $\boldsymbol{u}$, il campo di pressione liquida (acqua) $\boldsymbol{p_w}$ e quello di pressione del gas (aria secca e vapore acqueo) $\boldsymbol{p_g}$ ed eventualmente la temperatura $\boldsymbol{T}$ coinvolta nella modellazione di processi non isotermi. Data la coesistenza di due differenti fasi fluide, liquida e gassosa, il modello può essere visto come un approccio multifase al mezzo poroso deformabile, come già proposto da Lewis and Schrefler [1] nel contesto della teoria delle miscele ibride per mezzo poroso, inizialmente presentata da Hassanizadeh and Gray [2, 3] e Zienkiewicz *et al.* [4, 5].

L'evoluzione a scala macroscopica delle variabili di stato menzionate sopra, in particolare delle pressioni del liquido e del gas, sono fondamentalmente influenzate dalla microstruttura del materiale che caratterizza il comportamento del suolo in relazione agli effetti capillari e alla deformabilità. L'approccio fisico proposto qui è basato sull'uso di tecniche di media applicate alle grandezze fisiche stimate su un volume rappresentativo elementare (REV) [6, 7]. Con l'aggiunta di funzioni di ritenzione dell'acqua che forniscono una descrizione della relazione che esiste tra pressione capillare e grado di saturazione dell'acqua [8-10], si può ottenere un set completo di equazioni di bilancio di massa per i fluidi e di equilibrio meccanico e termodinamico per il mezzo a scala macroscopica.

Una formulazione accoppiata termo-idro-meccanica $\boldsymbol{u - p - (T)}$ che tratta mezzi porosi completamente saturi è stata implementata con successo in passato nel codice bidimensionale a elementi finiti PLASCON [11] e le successive estensioni alla tridimensionalità con PLASCON3D [12-14].

Il presente lavoro si focalizza sull'estensione e aggiornamento della relativamente semplice teoria a singola fase, con relative implementazioni numeriche, verso una più realistica descrizione multifase del materiale poroso, dove i vuoti possono essere riempiti da liquido e gas che interagiscono tra loro attraverso il concetto di pressione capillare. Sulla base delle versioni precedenti è stato realizzato un codice chiamato PLASCON3D_PS che implementa la formulazione accoppiata $\boldsymbol{u - p_w - p_g}$

– *(T)*. Data la mancanza in letteratura di test sperimentali e numerici su domini tridimensionali, verranno presentati alcuni risultati numerici di benchmark test e casi reali derivanti da domini bidimensionali [15, 16].

Bibliography

1. Lewis, R.W. and B.A. Schrefler, *The finite element method in the deformation and consolidation of porous media.* 1987.

2. Hassanizadeh, M. and W.G. Gray, *General conservation equations for multi-phase systems: 1. Averaging procedure.* Advances in Water Resources, 1979. **2**: p. 131-144.

3. Hassanizadeh, M. and W.G. Gray, *General conservation equations for multi-phase systems: 2. Mass, momenta, energy, and entropy equations.* Advances in Water Resources, 1979. **2**: p. 191-203.

4. Zienkiewicz, O.C., et al., *Static and dynamic behaviour of soils: a rational approach to quantitative solutions. I. Fully saturated problems.* Proceedings of the Royal Society of London. A. Mathematical and Physical Sciences, 1990. **429**(1877): p. 285-309.

5. Zienkiewicz, O.C., et al., *Static and dynamic behaviour of soils: a rational approach to quantitative solutions. II. Semi-saturated problems.* Proceedings of the Royal Society of London. A. Mathematical and Physical Sciences, 1990. **429**(1877): p. 311-321.

6. Lewis, R.W. and B.A. Schrefler, *The finite element method in the deformation and consolidation of porous media.* 1998.

7. Bachmat, Y. and J. Bear, *On the concept and size of a representative elementary volume (REV)*, in *Advances in transport phenomena in porous media*. 1987, Springer. p. 3-20.

8. Brooks, R.H. and A.T. Corey. *Properties of porous media affecting fluid flow*. in *Journal of the Irrigation and Drainage Division, Proceedings of the American Society of Civil Engineers*. 1966.

9. Lloret, A. and E.E. Alonso, *State surfaces for partially saturated soils.* Proceedings of the 11th International Conference on Soil Mechanics and Foundation Engineering, San Francisco, 12-16 august 1985. Publication of Balkema, 1985.

10. van Genuchten, M.T., *A closed-form equation for predicting the hydraulic conductivity of unsaturated soils.* Soil Science Society of America Journal, 1980. **44**(5): p. 892-898.

11. Majorana, C., R. Lewis, and B. Schrefler, *Two-dimensional non-linear thermo-elastoplastic consolidation program Plascon.* The Finite Element Method in the Deformation and Consolidation of Porous Media, Lewis RW, Schrefler BA (eds), 1987.

12. Salomoni, V.A. and R. Fincato. *3D modelling of geomaterials accounting for an unconventional plasticity approach*. 2011.

13. Befi, M., *Modelli tridimensionali per l'analisi termomeccanica di geomateriali* Department of Civil, Environmental and Architectural Engineering, 1993: p. 271.

14. Majorana, C., *Modelli tridimensionali per l'analisi termomeccanica di geomateriali.* Tecnica Italiana, 1994. **59**(4): p. 265-290.

15. Meiri, D., *Two-phase flow simulation of air storage in an aquifer.* Water Resources Research, 1981. **17**(5): p. 1360-1366.

16. Schrefler, B. and Z. Xiaoyong, *A fully coupled model for water flow and airflow in deformable porous media.* Water Resources Research, 1993. **29**(1): p. 155-167.

Introduction

The study of the soils as well as a wide range of porous media, is a very challenging topic by way of the diversity that characterizes each geomaterial that we can encounter every day and the variety in terms of physical and chemical behaviour that can be observed in nature and in the engineering practice.

In the past, like today, the Science tried to give a mathematical description to the various phenomena that occurs when these material are subjected to general load processes (e.g. mechanical, thermal or hydraulic loads conditions), that can be caused by natural events or man activities. Often simply theories, (such the one proposed by Terzaghi [1] for soils) and related formulae, were the most robust, cheapest and affordable solutions to get rid of the problems in the most of cases.

However, these approaches that have great validity in practice, are not suitable to predict the complexity of each porous medium, the response in terms of mechanics and hydraulic quantities, that each sample that have an unique genesis, can give when analysed or reworked. Biot M.A. [2-8] understood this fact and followed and extended the work of Terzaghi trying to find the effects of the fluid phase on the solid one and to describe the three-dimensional effects that arise during consolidation processes in soils. Later, Ghaboussi and Wilson [9] introduced the concept of fluid compressibility and the change in volume for the solid phase, usually constituted by grains, was presented by Zienkiewicz [10].

From this point of view, it's clear that the interaction between solid and fluid phases is a key concept of paramount importance to understand and model as best as possible the real nature of each porous medium. Most of engineering applications deal with a fully saturated material approach and neglect in part or totally of the capillarity effects that arise from the coexistence among grains of a gas phase. To understand the effects of capillarity phenomena on the behaviour of the material at a macroscopic scale, a multiphase framework is necessary, and the multiphase approach to a deforming porous medium as proposed by Lewis and Schrefler [11] in the context of the hybrid mixture theory by Hassanizadeh and Gray [12, 13] and Zienkiewicz *et al.* [14, 15], represents the ideal mathematical theory to model the saturated – unsaturated material.

The physical - mathematical model proposed within this work, and based on the above mentioned approach considers the effects of each phase coupled with others, trying to catch the thermo-hydro-mechanical response of the medium at a macroscopic scale as close as possible to the reality.

This coupled formulation, that suits well for consolidation / subsidence analyses of unsaturated soils, can therefore be qualified as $\boldsymbol{u - p_w - p_g - (T)}$, and represents an extension of the classical fully saturated formulation $\boldsymbol{u - p - (T)}$ [11].

The present work focused on the extension and upgrading of the relative simple single phase theory, already implemented in a research numerical code towards the above mentioned fully coupled multiphase formulation, implemented concretely on an improved code, named PLASCON3D_PS.

Chapter 1 introduces the physical model approach and gives the theoretical framework with the necessary equilibrium, balance and constitutive equations that govern the hydro-, thermo-, mechanical behaviour of a porous medium with respect to partial saturated states. Water retention characteristics of soil are also widely explained.

Chapter 2 recalls the final equations obtained from mechanical and thermodynamic equilibrium and from the mass balances introducing the boundary value problem and the necessary initial and boundary conditions. The F.E. formulation is then presented applied to the set of equations for the solid, liquid and gas phases both for isothermal and non-isothermal problem. Spatial and time discretizations as well as the monolithic solving procedure are also presented.

In *Chapter 3*, the upgraded numerical code PLASCON3D_PS is explained and a comparison with the previous versions is also carried out. The main modifications and upgrades are pointed out giving an idea of the new contributes added to the original form.

Chapter 5 reports the numerical analyses starting from the validation of the code with a benchmark test and the approach and solution of two other different problems.

In the *Appendix* is reported my contribution to the structural analyses performed on a nuclear beam test facility that is actually in construction. The design of the MITICA Injector device integrated with the surrounding building is presented [16].

Bibliography

1. Terzaghi, K., *Die Berechnung der Durchlässigkeitsziffer des Tones aus dem Verlauf der hydrodynamischen Spannungserscheinungen.* Ak. der Wissenschaften in Wien, Sitzungsberichte mathematisch-naturwissenschaftliche Klasse, part IIa, 1923. **132 (3/4)**: p. 125 - 138.

2. Biot, M.A., *General theory of three-dimensional consolidation.* Journal of applied physics, 1941. **12**(2): p. 155-164.

3. Biot, M.A., *Consolidation settlement under a rectangular load distribution.* Journal of Applied Physics, 1941. **12**(5): p. 426-430.

4. Biot, M.A., *Theory of elasticity and consolidation for a porous anisotropic solid.* Journal of Applied Physics, 1955. **26**(2): p. 182-185.

5. Biot, M., *General solutions of the equations of elasticity and consolidation for a porous material.* J. appl. Mech, 1956. **23**(1): p. 91-96.

6. Biot, M.A., *Thermoelasticity and irreversible thermodynamics.* Journal of Applied Physics, 1956. **27**(3): p. 240-253.

7. Biot, M.A. and P.G. Willis, *The elastic coefficients of the theory of consolidation.* J. Appl. Mech., 1957. **24**: p. 594 - 601.

8. Biot, M., *Theory of stability and consolidation of a porous medium under initial stress.* 1963.

9. Ghaboussi, J., E.L. Wilson, and J. Isenberg, *Finite element for rock joints and interfaces.* Journal of the soil mechanics and foundations division, 1973. **99**(10): p. 849-862.

10. Zienkiewicz, O.C., C. Humpheson, and R.W. Lewis, *A unified approach to soil mechanics problems (including plasticity and viscoplasticity)*, 1977, Wiley: New York. p. 151-179

11. Lewis, R.W. and B.A. Schrefler, *The finite element method in the deformation and consolidation of porous media.* 1987.

12. Hassanizadeh, M. and W.G. Gray, *General conservation equations for multi-phase systems: 1. Averaging procedure.* Advances in Water Resources, 1979. **2**: p. 131-144.

13. Hassanizadeh, M. and W.G. Gray, *General conservation equations for multi-phase systems: 2. Mass, momenta, energy, and entropy equations.* Advances in Water Resources, 1979. **2**: p. 191-203.

14. Zienkiewicz, O.C., et al., *Static and dynamic behaviour of soils: a rational approach to quantitative solutions. I. Fully saturated problems.* Proceedings of the Royal Society of London. A. Mathematical and Physical Sciences, 1990. **429**(1877): p. 285-309.

15. Zienkiewicz, O.C., et al., *Static and dynamic behaviour of soils: a rational approach to quantitative solutions. II. Semi-saturated problems.* Proceedings of the Royal Society of London. A. Mathematical and Physical Sciences, 1990. **429**(1877): p. 311-321.

16. Mazzucco, G., et al., *Structural analyses and integrated design of the MITICA Injector assembly.* Fusion Engineering and Design, 2013.

1 A physical model for a partial saturated porous medium

1.1. Introduction

In order to give and affordable theoretical treatment of equations involved on the macroscopic description of the behaviour of a partial saturated geomaterial, a physical approach has been chosen, as presented in literature at [1, 2]. This approach is an alternative point of view, rather than a necessary part, of the more formal and basic principle at the base of the hybrid mixture theory.

The hybrid mixture theory, first observes the porous medium at microscopic scale with clear distinction of phases among the skeleton structure, and then defines on each phase, not only fluid ones, the physical quantities (such temperature, pressure etc.) that will be then averaged by the introduction averaging principles on a representative elementary volume (REV). This theoretical procedure makes available these physical quantities at macroscopic scale over a porous medium that can be considered as homogeneous.

Here the equilibrium equations and the mass balance equations are derived in a more direct way, along with constitutive relations, in order to provide a complete set of governing equations able to describe states of partial saturation in a deforming material. For a complete framework on hybrid mixture theory and to better contextualize this approach along with this theory, the reader can refer to [1, 2].

1.2. The physical model

The porous medium can be represented with a solid skeleton or matrix that is constituted by the solid grains and eventually petals of cohesive material like clay. The voids between the grains are filled by the fluid phases that in general, are liquid (water, oil) or gaseous (air, water vapour or other gas like hydrocarbons). In the following, for sake of simplicity, three fluid phases will be considered: the liquid phase constituted by water, and the gas phase constituted by dry air and water

vapour. Figure 1.2.1a gives an example of the three coexisting phases on a soil matrix that is the porous medium par excellence.

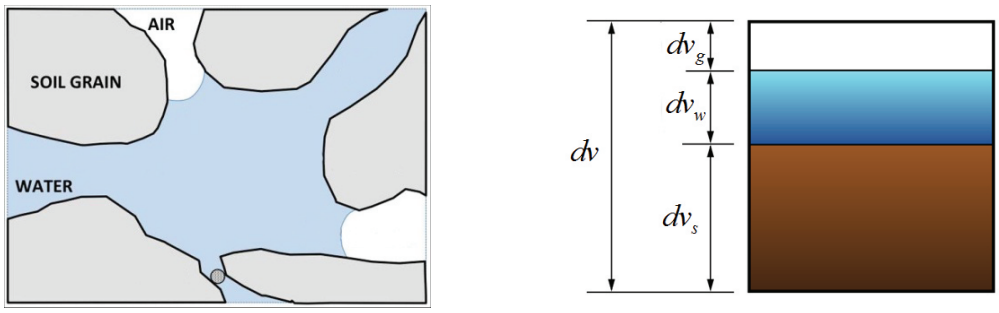

(a) (b)

Figure 1.2.1: Unsaturated voids between grains (a); Phases volume with respect to total volume (b).

In order to treat a partial saturated porous medium is mandatory to define the main parameters that qualify the soak process of voids.

The volumetric water content, θ, is defined mathematically as the ratio between the volume occupied by the liquid (water) phase and the total volume of the specimen considered

$$\theta = \frac{dv_w}{dv} \tag{1.2.1}$$

where dv is the total volume of REV and is the sum of the infinitesimal volume of solid skeleton dv_s and the infinitesimal volume occupied by voids dv_v (air or gas dv_g and water dv_w)

$$dv = dv_s + dv_g + dv_w \tag{1.2.2}$$

as showed by Figure 1.2.1b. The water content concept is widely used in Hydrogeology, but in Soil Mechanics and Petroleum Engineering, the term water saturation or degree of water saturation, S_w is preferred. It can be defined it as:

$$S_w = \frac{dv_w}{dv_v} = \frac{dv_w}{dv_w + dv_g} = \frac{dv_w}{n\,dv} = \frac{\theta}{n} \tag{1.2.3}$$

where the porosity n relative to a REV is defined as following:

$$n = \frac{dv_w + dv_g}{dv} = \frac{dv_v}{dv} \tag{1.2.4}$$

The degree of water saturation S_w , hence, is the ratio between the volume occupied by the water and the total pore volume in the representative elementary volume (REV). Values of S_w can range from 0 (dry) to 1 (complete saturation of voids with water). In reality, S_w never reaches 0 or 1, due to the irregular nature of the soil matrix. These limits are idealizations for engineering use and will be further explained when the retention curves will be described on section 1.5. The definition of degree of gas saturation S_g is immediate:

$$S_g = \frac{dv_g}{dv_f} = \frac{dv_g}{dv_w + dv_g} \tag{1.2.5}$$

The void volume occupied by the gas is referred to both dry air and water vapour. It is clear that both the degrees of saturations sum to one, i.e. $S_w + S_g = 1$.

The degree of water saturation (and so on the degree of gas saturation) can be expressed as function of the temperature T and of the capillary pressure p_c as:

$$S_w = S_w\left(p_c, T\right) \tag{1.2.6}$$

and the capillary pressure can be defined as:

$$p_c = p_g - p_w \tag{1.2.7}$$

where p_w and p_g are the water and gas pressure. Usually, the inverse relation of $S_w = S_w\left(p_c, T\right)$ is more used. In fact $p_c = p_c\left(S_w, T\right)$ is determined experimentally and usually shows hysteresis characteristic, that have to take into account in the case of cyclic processes of saturation – desaturation, as wetting by rain and drying processes. In fact, the retention curves of saturation and desaturation depend

mainly by the matrix texture of the porous medium. The relations between capillary pressure and saturation will be widely discussed on section 1.5.

The effective stress principle can express the solid-phase relation:

$$\boldsymbol{\sigma}' = \boldsymbol{\sigma} - \mathbf{I}\,\mathbf{p}^{s} \tag{1.2.8}$$

Here $\boldsymbol{\sigma}'$ is the effective stress tensor and $\boldsymbol{\sigma}$ the total stress tensor. The second-order unit tensor is expressed by $\mathbf{I}$ and the average pressure of both the water and air surrounding the grains is expressed by $\mathbf{p}^{s}$.

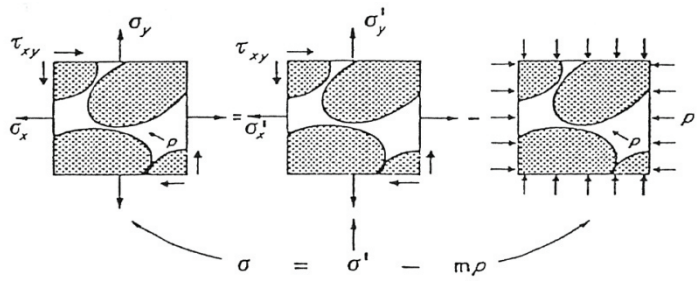

Figure 1.2.2 – Total and effective stresses in the porous media.

The stress tensor for the fluid phases (here the π phase is general) is given by

$$\boldsymbol{\sigma}^{\pi} = \tau^{\pi} - \mathbf{I}\,\mathbf{p}^{\pi} \tag{1.2.9}$$

where τ is the shear stress. For the fluids, it can be assumed that shear stress is negligible and so the following expression can be obtained:

$$\boldsymbol{\sigma} = (1-n)\boldsymbol{\sigma}^{s} - n\mathbf{I}\left[S_{w}\,p^{w} + S_{g}\,p^{g}\right] \tag{1.2.10}$$

where

$$p_{s} = \left(S_{w}\,p_{w} + S_{g}\,p_{g}\right) \tag{1.2.11}$$

represents the intrinsically averaged (or mean) pressure of the fluid phases.

Grains are usually assumed incompressible and in this case no stress state in the grains is produced by the effects of this weighted pore pressure. Due to this fact, here, the deformation of the solid skeleton, which depends on the effective stress, is due only to the skeleton matrix.

Equation (1.2.10) can be updated to

$$\begin{aligned}\boldsymbol{\sigma} &= (1-n)\boldsymbol{\sigma}^s - n\mathbf{I}\,p^s \\ &= (1-n)\left(\boldsymbol{\sigma}^s + \mathbf{I}\,p^s\right) - (1-n)\mathbf{I}\,p^s - n\mathbf{I}\,p^s \\ &= \boldsymbol{\sigma}' - \mathbf{I}\,p^s\end{aligned} \tag{1.2.12}$$

The presence of several fluid phases, allows the splitting of the effective stress tensor similarly to the Terzaghi's principle. It becomes:

$$\boldsymbol{\sigma}' = \boldsymbol{\sigma} + \mathbf{I}\left(S_w\,p^w + S_g\,p^g\right) \tag{1.2.13}$$

The α Biot's constant can be assumed here as a corrective coefficient that takes into account of the deformability of the solid grains and in such way, the previous equation becomes:

$$\boldsymbol{\sigma} = \boldsymbol{\sigma}'' - \alpha\,\mathbf{m}^T\left(S_w\,p^w + S_g\,p^g\right) \tag{1.2.14}$$

where $\mathbf{m}$ is the vector $\mathbf{m}^T = [1,1,1,0,0,0]^T$. The value of the corrective term α will be discussed further.

1.3. Constitutive equations

The Constitutive equations are now introduced in order to give a complete description of the mechanical behaviour of the medium.

Under small displacements hypothesis with the addition of linear elastic and isotropic material, it can be assumed that strain as well displacements remain small and limited during the deformation process due to external load conditions or environmental conditions variation. Due to this fact, in the following the constitutive equations are principally expressed with infinitesimal terms.

The effective stress is responsible for all major deformations in the skeleton and the constitutive equations, which relate this effective stress, with the infinitesimal deformations of the solid skeleton, are independent from the pore pressure. In general, in the case of linear elastic isotropic and homogeneous material the following relation holds:

$$d\boldsymbol{\sigma}' = \mathbf{D}_e\left(d\boldsymbol{\varepsilon} - d\boldsymbol{\varepsilon}_0 - d\boldsymbol{\varepsilon}_T\right) \tag{1.3.1}$$

And in the case of a non - linear material, remaining in the small strain field, the (1.3.1) becomes

$$d\boldsymbol{\sigma}' = \mathbf{D}_T \left(d\boldsymbol{\varepsilon} - d\boldsymbol{\varepsilon}_0 - d\boldsymbol{\varepsilon}_v^s - d\boldsymbol{\varepsilon}_T \right) \tag{1.3.2}$$

Where $\mathbf{D}_T$ is the tangent constitutive tensor that substitutes the elastic constitutive tensor $\mathbf{D}_e$ when material non-linearity occurs. Creep effects are neglected for the moment.

The term

$$d\boldsymbol{\varepsilon} = \left\{ \varepsilon_x, \varepsilon_y, \varepsilon_z, \gamma_{xy}, \gamma_{yz}, \gamma_{zx} \right\} \tag{1.3.3}$$

is the vector form for the total deformation tensor of the skeleton, and can be considered as:

$$d\boldsymbol{\varepsilon} = \boldsymbol{L}\, d\mathbf{u} \tag{1.3.4}$$

Where $d\mathbf{u} = \left\{ du_x, du_y, du_z \right\}$ is the displacements field and $\boldsymbol{L}$ is the differential operator defined as

$$\boldsymbol{L} = \begin{Bmatrix} \frac{\partial}{\partial x} & 0 & 0 \\ 0 & \frac{\partial}{\partial y} & 0 \\ 0 & 0 & \frac{\partial}{\partial z} \\ \frac{\partial}{\partial y} & \frac{\partial}{\partial x} & 0 \\ 0 & \frac{\partial}{\partial z} & \frac{\partial}{\partial y} \\ \frac{\partial}{\partial z} & 0 & \frac{\partial}{\partial x} \end{Bmatrix} \tag{1.3.5}$$

The deformation caused by the uniform compression of the particles by means of the pore fluid pressure, named $d\boldsymbol{\varepsilon}_v^s$ can be expressed as:

$$d\boldsymbol{\varepsilon}_v^s = -\mathbf{I} \left(\frac{dp^s}{3K_S} \right) \tag{1.3.6}$$

where K_S is the compressibility bulk modulus for the solid phase. In soils this last term is generally not relevant compared to the others due that the solid grains have the bulk modulus much greater than the skeleton one. This is why it has been omitted in (1.3.1). However in rocks mechanics, where the compressibility of the solid grains is comparable to the skeleton one this term cannot be neglected.

The deformation due to thermal effects is given by the following relation:

$$d\boldsymbol{\varepsilon}_T = \mathbf{m}\left(\frac{\beta_s}{3}\right)T \tag{1.3.7}$$

Where T is the temperature β_s is the thermal expansion coefficient. At least, $d\boldsymbol{\varepsilon}_0$ represent all the other deformations which cannot be directly associated to a stress variation (i.e. swelling, thermal, chemical, etc.) and named “autogeneous deformations”.

The effective stress relation rewritten for the non-linear case and taking into account of grain compression using the Biot’s constant α is:

$$d\boldsymbol{\sigma}' = \mathbf{D}_T\left[\left(\, d\boldsymbol{\varepsilon} - d\boldsymbol{\varepsilon}_v^s\right)\right] = \mathbf{D}_T\left[d\boldsymbol{\varepsilon}\right] + \mathbf{D}_T\left[I\right]\frac{dp^s}{3K_S} \tag{1.3.8}$$

The equations (1.2.11) and (1.2.13) become:

$$d\boldsymbol{\sigma} = d\boldsymbol{\sigma}' - \mathbf{I}\,dp^s = d\boldsymbol{\sigma}'' + D_T\left[\mathbf{I}\right]\frac{dp^s}{3K_s} - \mathbf{I}\,dp^s \tag{1.3.9}$$

where $d\boldsymbol{\sigma}''$ represents the stress responsible for all the deformation of the solid. Replacing the unity tensor $\mathbf{I}$ with the Kronecker symbol the (1.3.9) can be rewritten as given by Zinkiewicz and Shiomi [3]:

$$d\sigma_{ij} = d\sigma_{ij}'' - \frac{1}{3}\left(\delta_{\mathrm{mn}}\,\delta_{\mathrm{nm}} - \delta_{\mathrm{mn}}\,D_{\mathrm{mnkl}}\,\delta_{\mathrm{kl}}\,\frac{1}{3K_s}\right)\delta_{ij}\,dp^s \tag{1.3.10}$$

Introducing the isotropic elastic material characterised by the Young’s elastic modulus E and the Poisson’s coefficient ν holds

$$\delta_{\mathrm{mn}}\,D_{\mathrm{mnkl}}\,\delta_{\mathrm{kl}} = \frac{3E}{1-2\nu} = 9K_T \tag{1.3.11}$$

The bulk modulus of the overall skeleton is given by K_T. The (1.3.10) can be written as

$$d\sigma_{ij} = d\sigma_{ij}'' - \left(1 - \frac{K_T}{K_s}\right)\delta_{ij}\, dp^s = d\sigma_{ij}'' - \alpha\,\delta_{ij}\, dp^s \tag{1.3.12}$$

where α is Biot's constant. Therefore, the resultant expression of the constitutive relationship can be written with this compact form

$$d\boldsymbol{\sigma}'' = \boldsymbol{D}_T\left[d\boldsymbol{\varepsilon}\right] \tag{1.3.13}$$

Each fluid phase π is characterized by its intrinsic pore pressure p^π that causes a purely volumetric strain for the considered phase, again represented by

$$\boldsymbol{\varepsilon}_v^\pi = -\frac{p_\pi}{K_\pi} \tag{1.3.14}$$

K_π is the bulk modulus of the considered fluid phase.

In the section 1.4 will be presented the balance equations for the phases that constitute the porous medium. In order to understand them some useful relations will be now introduced.

Density of the solid phase

To deal with the density of the solid phase, a material time derivative relationship will be now introduced for a compressible solid phase. From the mass conservation equation in differential form, with total material time derivatives can be obtained:

$$\frac{D^s\left(\rho_s V_s\right)}{Dt} = 0 \tag{1.3.15}$$

Further, the use of partial derivative instead of material time one will be adopted. In the case of small displacements the two derivatives coincide. For a shake of generality here and in the following relations the time derivative will be maintained.

The solid density ρ_s is assumed to be a function of (1.2.11), a function of the temperature and of the first invariant of the effective stress. The (1.3.15) becomes

$$\frac{1}{\rho_s}\frac{D^s\rho_s}{Dt} = -\frac{1}{V_s}\frac{D^s V_s}{Dt} = \frac{1}{K_S}\frac{D^s p_s}{Dt} - \beta_s\frac{D^s T}{Dt} - \frac{1}{3\left(n-1\right)K_S}\frac{D^s\left(\operatorname{tr}\boldsymbol{\sigma}'\right)}{Dt} \tag{1.3.16}$$

where it must be kept in mind that

$$\frac{1}{\rho_s}\frac{\partial \rho_s}{\partial p_s}=\frac{1}{K_S},\quad \frac{1}{\rho_s}\frac{\partial \rho_s}{\partial T}=-\beta_s,\quad \frac{1}{\rho_s}\frac{\partial \rho_s}{\partial \mathbf{I}_{I\sigma'}}=-\frac{1}{3(n-1)K_S} \tag{1.3.17}$$

where K_S, is the bulk modulus of the grain material, β_s, is the thermal expansion coefficient for the solid and $\operatorname{tr}\boldsymbol{\sigma}'=\mathbf{I}_{I\sigma'}$, is the first stress invariant.

The constitutive relationship for the first stress invariant can be now introduced

$$\frac{D^s\left(\mathbf{I}_{I\sigma'}\right)}{Dt}=3K_T\left(\operatorname{div}\mathbf{v}^s+\frac{1}{K_S}\frac{D^s\rho_s}{Dt}-\beta_s\frac{D^sT}{Dt}\right) \tag{1.3.18}$$

and the term

$$-\frac{1}{K_S}\frac{D^s\rho_s}{Dt} \tag{1.3.19}$$

represents an overall volumetric strain rate caused by uniform compression of particles (as opposed to the skeleton) by the average pressure p_s.

Soils present a compressibility of the solid phase that is significantly higher than the compressibility of the medium. Due to this fact this volumetric strain is relatively insignificant and can be ignored, but it is important in rock mechanics and in concrete, where the compressibility of the solid phase is comparable to that of the skeleton.

Hence, the α Biot's constant [4] can be defined as

$$1-\alpha=\frac{K_T}{K_S} \tag{1.3.20}$$

Reworking the (1.3.16) the following result can be obtained

$$\frac{1}{\rho_s}\frac{D^s\rho_s}{Dt}=\frac{1}{1-n}\left[(\alpha-n)\frac{1}{K_S}\frac{D^s\rho_s}{Dt}-\beta_s(\alpha-n)\frac{D^sT}{Dt}\ -(1-\alpha)\operatorname{div}\mathbf{v}^s\right] \tag{1.3.21}$$

For incompressible grain material $1/K_S=0,\ \alpha=1$ .This does not imply that the solid skeleton is rigid, because of rearrangements of the voids. The necessary evolution

equation is the mass balance equation for the solid phase that expressed with total derivatives is

$$\frac{D^s\left(1-n\right)\rho_s}{Dt}+\rho_s\left(1-n\right)\operatorname{div}\mathbf{v}^s=0 \tag{1.3.22}$$

Permeability effects. The Darcy's law

Due to the impossibility to describe analytically and univocally the texture of the porous medium matrix, to describe the filtration process of both phases among the porous matrix, averaged variables must be considered in order to simplify and generalize the approach.

The averaged filtration velocity vector $\mathbf{v}_w$, also known as *Darcy's velocity* or *volume velocity*, for a fully water saturated medium can be written as

$$\mathbf{v}_w=-\frac{1}{\mu_w}\mathbf{k}_w(-\operatorname{grad}p_w+\rho_w\mathbf{g}) \tag{1.3.23}$$

Where $\mathbf{k}_w$ is the absolute water permeability tensor of the medium, which is different for every material (usually soil) considered, μ_w is the dynamic viscosity of the water, $\mathbf{g}$ is the gravity vector.

When dealing with a multiphase fluid flowing in a porous matrix (e.g. water and air), some dissipative terms arise at fluid - solid and fluid - fluid interfaces. Due to this fact, the (1.3.23) has to be modified to take into account of the presence of the other fluids.

Starting from the (1.3.23) the water permeability tensor of the fully saturated case $\mathbf{k}_w$, can be rewritten as

$$\mathbf{k_w}=\mathbf{k}\,k_{rw} \tag{1.3.24}$$

The term $\mathbf{k}$ that is called intrinsic permeability of the medium, has the dimension of [L²], and depends only on the internal geometry and structure of voids among the solid skeleton, is multiplied by a relative permeability k_{rw}, a dimensionless parameter that can take values from 0 to 1. k_{rw} quantify the reduction, or better, the magnitude with respect to the intrinsic permeability, that has to be adopted in the case of multiphase flow, in order to express an equivalent absolute permeability

$\mathbf{k}_w$ for the water phase. Like the (1.3.24) the absolute gas permeability tensor can be rewritten as

$$\mathbf{k}_g = \mathbf{k}\, k_{rg} \tag{1.3.25}$$

A more general expression for the π - phase Darcy's velocity can be rewritten as

$$\mathbf{v}_\pi = -\frac{\mathbf{k} k_{r\pi}}{\mu_\pi}(-\text{grad}\, p_\pi + \rho_\pi \mathbf{g}) \tag{1.3.26}$$

Where all the constants and variable have the same mean of the previous ones but referred to the generic phase π.

The Darcy's velocity formulation here presented doesn't take into account of temperature gradients, that have a significant effect only in heat conduction (by fluid) phenomena and that inertial and macroscopic viscous effects are neglected [5].

The relative permeability varies with the void ratio

$$e = \frac{dv_w + dv_g}{dv_s} \tag{1.3.27}$$

and degree of saturation. For many situations the change of void ratio may be of secondary importance and $k_{r\pi}$ may be defined mainly as a function of the degree of saturation.

For each particular porous medium, the relations $k_{r\pi}(S_w)$ are either predicted by models based on some more or less realistic capillary assumption, or experimentally determined under laboratory and field conditions. The relation that exist between relative permeability coefficients will be widely explained in section 1.5

Gaseous mixture of dry air and water vapour

Gas phase that fill totally the voids partially or in some cases totally can be regarded usually as a perfect mixture of dry air and water vapour, which behaviour is assumed to be ideal. With this assumption, the ideal gas law can be used and the partial pressure $p_{g\pi}$ of the gas phase π, can be related to the mass concentration (density) $\rho_{g\pi}$ of species π in the gas phase and the absolute temperature ϑ using the molar mass M_π of constituent π and R that is universal gas constant.

The state equations of a perfect gas applied to dry air (ga), vapour (gw) and moist air (g) are

$$\begin{aligned} p_{ga} &= \rho_{ga}\, \vartheta R / M_a \\ p_{gw} &= \rho_{gw}\, \vartheta R / M_w \end{aligned} \tag{1.3.28}$$

$$\begin{aligned} \rho_g &= \rho_{ga} + \rho_{gw} \\ p_g &= p_{ga} + p_{gw} \end{aligned} \tag{1.3.29}$$

$$M_g = \left(\frac{\rho_{gw}}{\rho_g} \frac{1}{M_w} + \frac{\rho_{ga}}{\rho_g} \frac{1}{M_a} \right)^{-1} \tag{1.3.30}$$

The Dalton's law [6] is the second equation in (1.3.29). The volume fraction occupied by dry air, vapour and moist air is expressed by $n S_g$. This is useful when dealing with averaged quantities such the relative volume velocities as reported in (1.3.26).

Relative Humidity and capillary effects

When exposing to a wet environment, a dehydrated sample of the medium (after drying it on oven), the water present in the moist air is absorbed resulting in an increasing of the sample weight. The sorption process starts filling by water the finest pores and continuing with the ones of bigger size. The condensed water in pores is separated from its vapour by a concave meniscus, because of the surface tension. Recalling the definition of capillary pressure already defined in the (1.2.7), i.e. the pressure difference between the gas phase and the liquid one, the relationship between the relative humidity (RH) and the capillary pressure in the pores, the Kelvin - Laplace law is assumed to be valid:

$$\ln RH = \ln \frac{p_{gw}}{p_{gws}} = \frac{p_c\, M_w}{\rho_w\, \vartheta R} \tag{1.3.31}$$

The water vapour saturation pressure p_{gws}, which is a function of the temperature only, can be obtained from the Clausius - Clapeyron equation indicated below at number (1.3.33). Empirical formulas have been also used in literature to predict this parameter, such as the one proposed by Hyland and Wexler [24].

The contact angle between the liquid phase and the solid phase, as is usually accepted for pore water, is assumed to be zero.

The capillary pressure can be obtained through the Young – Laplace equation:

$$p_c = \frac{2\sigma_{st}}{r} \tag{1.3.32}$$

where r is the pore radius and σ_{st} is the surface tension. Water present in molecular layers adsorbed on the surface of a solid because of the van der Waals and/or other interactions are here neglected. These considerations apply if the water is present in the pores as a condensed liquid (capillary region).

Water vapour saturation pressure as function of temperature

To link the water vapour saturation pressure with temperature, the Clausius - Clapeyron equation must be used:

$$p_{gws}(\vartheta) = p_{gws}^0 \exp\left[-\frac{M_w \Delta H_{gw}}{R}\left(\frac{1}{\vartheta} - \frac{1}{\vartheta_0}\right)\right] \tag{1.3.33}$$

Where p_{gws} is the water vapour saturation pressure at the reference temperature ϑ, p_{gws}^0 is the water vapour saturation pressure at the temperature ϑ_0 and ΔH_{gw} is the specific enthalpy of evaporation. This equation derived from the laws of the thermodynamics and holds for temperatures next to ϑ_0.

State Equation for water

To express the changes in terms of water density by effects of temperature and pressure (environmental conditions), an equation, named equation of state for water, must be given. The relationship presented here was obtained by Fernandez [7, 8], and states

$$\rho_w = \rho_w^0 \exp\left[-\beta_w(\vartheta - \vartheta_0) + C_w\left(p_w - p_w^0\right)\right] \tag{1.3.34}$$

ρ_w^0 and p_w^0 refer respectively to the density and pressure of water at the initial steady state with all the phases at the standard conditions. The thermal expansion coefficient β_w quantifies the effects of relative temperature variations and the compressibility coefficient C_w denotes the effects caused by confinement pressure.

A series expansion of the (1.3.34) can be done and, once maintained only the first order terms, what it can be obtained is:

$$\rho_w = \rho_{w0}\left[1 - \beta_w(\vartheta - \vartheta_0) + C_w\left(p_w - p_{w0}\right)\right] \tag{1.3.35}$$

Following, the mass conservation equation for water, written in in material time derivatives reads

$$\frac{D^w\left(\rho_w V_w\right)}{Dt}=0 \tag{1.3.36}$$

Carrying out the differentiation of the product $\rho_w V_w$ and considering as before the density as function of states variables, i.e. $\rho_w=\rho_w\left(p_w,T\right)$, it results in

$$\frac{1}{\rho_w}\frac{D^w\rho_w}{Dt}=-\frac{1}{V_w}\frac{D^w V_w}{Dt}=\frac{1}{\rho_w}\left(\frac{\partial\rho_w}{\partial p_w}\frac{D^w p_w}{Dt}+\frac{\partial\rho_w}{\partial T}\frac{D^w T}{Dt}\right) \tag{1.3.37}$$

The following relations also hold

$$\frac{1}{\rho_{w0}}\frac{\partial\rho_w}{\partial p_w}=\frac{1}{K_W},\quad \frac{1}{\rho_{w0}}\frac{\partial\rho_w}{\partial T}=-\beta_w \tag{1.3.38}$$

and so, it follows

$$\frac{1}{\rho_{w0}}\frac{D^w\rho_w}{Dt}=\frac{1}{K_W}\frac{D^w p_w}{Dt}-\beta_w\frac{D^w T}{Dt} \tag{1.3.39}$$

In the (1.3.39) the term $1/K_W$ corresponds to the water compressibility C_w. This result obtained here by derivation of the mass balance equation of water, can be obtained with the (1.3.35) from the series expansion of (1.3.34).

Diffusive – dispersive mass flux. The Fick's law

To consider the diffusive-dispersive mass flux that occurs in the medium the Fick's law is now introduced

$$\mathbf{J}_\alpha^\pi=-\rho_\alpha\,\mathbf{D}_\varpi^\pi\,\mathrm{grad}\left(\frac{\rho_\pi}{\rho_\varpi}\right) \tag{1.3.40}$$

To quantify these fluxes, an effective dispersion tensor $\mathbf{D}_\alpha^\pi$ must be taken into account. The dispersion tensor depends strictly on which phase diffuses (π) and on the phase in which diffusion takes place (ϖ, where $\varpi=w,g$). $\mathbf{D}_\varpi^\pi$ is a function of the tortuosity that the diffusing phase encounters in the diffusion process in the medium. $\mathbf{D}_\varpi^\pi$ is also correlated with seepage velocity, when a diffusion caused by mechanical deformation contribute is considered.

For a binary system of dry air and water vapour the following set can be written

$$\mathbf{J}_g^{ga} = -\rho_g \mathbf{D}_g^{ga} \operatorname{grad}\left(\frac{\rho_{ga}}{\rho_g}\right) \quad \text{and} \quad \mathbf{J}_g^{gw} = -\rho_g \mathbf{D}_g^{gw} \operatorname{grad}\left(\frac{\rho_{gw}}{\rho_g}\right) \tag{1.3.41}$$

The first equation of (1.3.29) leads to

$$\operatorname{grad}\left(\frac{\rho_{ga}}{\rho_g}\right) = \operatorname{grad}\left(\frac{\rho_g - \rho_{gw}}{\rho_g}\right) = -\operatorname{grad}\left(\frac{\rho_{gw}}{\rho_g}\right) \tag{1.3.42}$$

A diffusive – dispersive velocity $\mathbf{u}^{\pi}$ with π = *ga*, *gw* can be now defined as reported by [7, 8]:

$$\mathbf{u}^{\pi} = \overline{\mathbf{v}}^{\pi g} = \overline{\mathbf{v}}^{\pi} - \overline{\mathbf{v}}^{g} \tag{1.3.43}$$

The over-bar sign in (1.3.43) denotes averaged quantities. It holds

$$\rho^{ga}\mathbf{u}^{ga} + \rho^{gw}\mathbf{u}^{gw} = \rho^{g} \sum_{\pi} c^{\pi}\mathbf{u}^{\pi} = 0 \tag{1.3.44}$$

Each component π can be related to its mass fraction by the expression

$$c^{\pi} = \rho^{\pi} / \rho^{g} \tag{1.3.45}$$

and

$$\sum_{\pi} c^{\pi} = 1 \qquad \pi = gw,\ ga \tag{1.3.46}$$

From (1.3.44) and (1.3.42) it follows, that

$$\mathbf{D}_g^{ga} = \mathbf{D}_g^{gw} = \mathbf{D}_g \tag{1.3.47}$$

Using (1.3.47) in the case of binary gas it results

$$\mathbf{J}_g^{ga} = -\rho_g \frac{M_w M_g}{M_g^2} \mathbf{D}_g \operatorname{grad}\left(\frac{\rho_{ga}}{\rho_g}\right) = \rho_g \frac{M_w M_g}{M_g^2} \mathbf{D}_g \operatorname{grad}\left(\frac{\rho_{gw}}{\rho_g}\right) = -\mathbf{J}_g^{gw} \tag{1.3.48}$$

The gas diffusion phenomena take place even in the absence of a gas pressure gradient. The mass-weighted velocity of the gas phase in this case is

$$\overline{\mathbf{v}}^{g} = \frac{1}{\rho_g}\left(\rho_{ga}\overline{\mathbf{v}}^{ga} + \rho_{gw}\overline{\mathbf{v}}^{gw}\right) = 0 \tag{1.3.49}$$

Temperature induced transport expressions for the diffusive - dispersive flux can be derived from the entropy inequality [9] and [8].

Heat flux in the porous medium. The Fourier's law

A constitutive expression for the heat flux is given by the generalized version of Fourier's law, written as follow

$$\overline{\mathbf{q}} = -\chi_{\text{eff}} \operatorname{grad} T \tag{1.3.50}$$

The effective thermal conductivity tensor is reported as χ_{eff} and $\overline{\mathbf{q}}$ is the heat flux of the multiphase medium and $\overline{\mathbf{q}}$ is the sum of the partial heat fluxes $\overline{\mathbf{q}}_{\pi}$.

The empirical version of Fourier's law is

$$\mathbf{q} = -\chi_{\text{eff}} \operatorname{grad} T \tag{1.3.51}$$

The effective thermal conductivity can be predicted theoretically as well as determined experimentally. A wider description of methods to determine the parameter χ_{eff} is given by Whitaker [10] and Nozad *et al.* [11].

Bomberg and Shirtlitfe [12] gave a linear relationship for porous building material:

$$\chi_{\text{eff}} = \chi_{\text{dry}} \left(1 + 4 \frac{n S_w \rho_w}{(1-n)\rho_s} \right) \tag{1.3.52}$$

1.4. Governing equations

The following section has the role to present the governing equations used for the model. In following equations the convective terms are neglected. For convenience the fluid velocities are conveniently referred to the velocity of the solid phase. Expression for the relative velocities for water and gas can be obtained:

$$\mathbf{v}^{ws} = \mathbf{v}^{w} - \mathbf{v}^{s} \tag{1.4.1}$$

and

$$\mathbf{v}^{gs} = \mathbf{v}^{g} - \mathbf{v}^{s} \tag{1.4.2}$$

As well for the velocities, also for the accelerations, the relative expressions can be obtained, without convective terms:

$$\mathbf{a}^{ws} = \mathbf{a}^{w} - \mathbf{a}^{s} \tag{1.4.3}$$

$$\mathbf{a}^{gs} = \mathbf{a}^{g} - \mathbf{a}^{s} \tag{1.4.4}$$

where $\mathbf{a}^{ws}$ is the acceleration of water relative to the solid phase and $\mathbf{a}^{gs}$ is the relative acceleration of gas. Full expressions are reported on [13].

Linear momentum balance equation: multiphase medium

Writing the dynamics equations for the individual phases, relative to the solid phase via (1.4.3) and (1.4.4), a first expression for the linear momentum balance equation for the multiphase system can be obtained:

$$-\rho\mathbf{a}^{s} - nS_{w}\rho_{w}\mathbf{a}^{ws} - nS_{g}\rho_{g}\mathbf{a}^{gs} + \operatorname{div}\boldsymbol{\sigma} + \rho\mathbf{g} = 0 \tag{1.4.5}$$

The acceleration of the solid phase is multiplied by the averaged density of the multiphase system

$$\rho = \left(1-n\right)\rho_{s} + nS_{w}\rho_{w} + nS_{g}\rho_{g} \tag{1.4.6}$$

The densities ρ_{π} are to be considered as intrinsic densities, i.e. referred to the volume of each phase as discussed in the section 1.2. The acceleration $\mathbf{g}$ is usually related to gravitational effects.

As well as the intrinsic densities in the (1.4.6) are multiplied by the volume fraction of the respective fluid phase (nS_{w} and nS_{g}), also the expression of the phases velocities, as given by Darcy's law have to be referred to the phase volume fraction, due to the fact that Darcy's law is expressed in terms of volume-averaged relative velocities. The generalised form of Darcy's laws takes the following form:

$$nS_{w}\mathbf{v}^{ws} = \rho_{w}\frac{\mathbf{k}\,k_{rw}}{\mu_{w}}\left[-\operatorname{grad}p_{w} + \rho_{w}\left(\mathbf{g} - \mathbf{a}^{s} - \mathbf{a}^{ws}\right)\right] \tag{1.4.7}$$

$$nS_{g}\mathbf{v}^{gs} = \rho_{g}\frac{\mathbf{k}\,k_{rg}}{\mu_{g}}\left[-\operatorname{grad}p_{g} + \rho_{g}\left(\mathbf{g} - \mathbf{a}^{s} - \mathbf{a}^{gs}\right)\right] \tag{1.4.8}$$

Again, as in the previous section, $\mathbf{k}$ is the intrinsic permeability tensor, k_{rw} and k_{rg} are the relative permeabilities of water and gas. The relative permeabilities vary between 0 and 1 and they are a function of the degree of saturation (Section 1.5). μ_w and μ_g are the dynamic viscosities, which are temperature dependent, i.e. $\mu_\pi = \mu_\pi(T), \pi = w, g$. In the generalised form of Darcy's law for the gas phase, the body forces are usually neglected. These are the velocities measured from experimental works like the ones presented in [14].

Mass balance equations

The mass balance equation for the solid takes the following form

$$\frac{\partial(1-n)\rho_s}{\partial t} + \operatorname{div}\left[(1-n)\rho_s \mathbf{v}^s\right] = 0 \tag{1.4.9}$$

whereas the equation of balance for the generic π- fluid phase holds

$$\frac{\partial(n S_\pi \rho_\pi)}{\partial t} + \operatorname{div}\left(n S_\pi \rho_\pi \mathbf{v}^\pi\right) = \pm \dot{m} \tag{1.4.10}$$

again $\dot{m}$ is the mass exchange term between the two phases, principally given by evaporation processes and this term takes negative values for water and positive values for the gas.

After and after the gradient of $(1-n)\rho^s$ has been neglected, the (1.4.9) can be divided by ρ_s, and becomes

$$\frac{(1-n)}{\rho^s}\frac{\partial \rho^s}{\partial t} - \frac{\partial n}{\partial t} + (1-n)\operatorname{div}\mathbf{v}^s = 0 \tag{1.4.11}$$

The relative velocities (1.4.1) and (1.4.2) are now introduced into the (1.4.10). After the time derivative have been carried out and every term has been divided by $S_\pi \rho_\pi$ the following vector identity can be applied

$$\operatorname{div}(\rho_s \overline{\mathbf{v}}^s) = \rho_s \operatorname{div}\overline{\mathbf{v}}^s + \operatorname{grad}\rho_s \cdot \overline{\mathbf{v}}^s \tag{1.4.12}$$

and the (1.4.10) can be written as:

$$\frac{\partial n}{\partial t}+\frac{n}{\rho_\pi}\frac{\partial \rho_\pi}{\partial t}+\frac{n}{S_\pi}\frac{\partial S_\pi}{\partial t}+\frac{1}{S_\pi \rho_\pi}\operatorname{div}\left(n S_\pi \rho_\pi \mathbf{v}^{\pi s}\right)+n\operatorname{div}\mathbf{v}^s=\pm\frac{\dot{m}}{S_\pi \rho_\pi} \tag{1.4.13}$$

Summing the (1.4.11) and the (1.4.13) the time derivative of the porosity can be eliminated and the continuity equation of the fluid phases can be finally obtained

$$\frac{1-n}{\rho_s}\frac{\partial \rho_s}{\partial t}+\operatorname{div}\mathbf{v}^s+\frac{n}{\rho_\pi}\frac{\partial \rho_\pi}{\partial t}+\frac{n}{S_\pi}\frac{\partial S_\pi}{\partial t}+\frac{1}{S_\pi \rho_\pi}\operatorname{div}\left(n S_\pi \rho_\pi \mathbf{v}^{\pi s}\right)=\pm\frac{\dot{m}}{S_\pi \rho_\pi} \tag{1.4.14}$$

Using partial derivatives instead of material time derivatives is possible due to the fact that, considering small displacements, the two derivatives coincide.

The introduction of the constitutive relationships for the time derivatives of water density (1.3.39) and solid density (1.3.21) along with the pressure in the solid phase (1.2.11), and the multiplication by S_w to the water continuity equation reads

$$\begin{aligned}&\left(\frac{\alpha-n}{K_S}S_w^2+\frac{n S_w}{K_W}\right)\frac{\partial p_w}{\partial t}+\frac{\alpha-n}{K_S}S_w S_g\frac{\partial p_g}{\partial t}+\alpha S_w\operatorname{div}\mathbf{v}^s-\beta_{sw}\frac{\partial T}{\partial t}\\&+\left(\frac{\alpha-n}{K_S}p_w S_w-\frac{\alpha-n}{K_S}p_g S_w+n\right)\frac{\partial S_w}{\partial t}+\frac{1}{\rho_w}\operatorname{div}\left(nS_w\rho_w\mathbf{v}^{ws}\right)=-\frac{\dot{m}}{\rho_w}\end{aligned} \tag{1.4.15}$$

where T is the temperature above a reference value and β_π is the thermal expansion coefficient that has to be introduced into

$$\beta_{sw}=S_w\left[\left(\alpha-n\right)\beta_{sw}+n\beta_w\right] \tag{1.4.16}$$

The following relationship has also to be taken into account

$$\frac{\partial S_g}{\partial t}=-\frac{\partial S_w}{\partial t} \tag{1.4.17}$$

The Darcy's law (1.4.7) can be now introduced as well as the capillary pressure definition (1.2.7). What it can be obtained is

$$\begin{aligned}&\left(\frac{\alpha-n}{K_S}S_w^2+\frac{n S_w}{K_W}\right)\frac{\partial p_w}{\partial t}+\frac{\alpha-n}{K_S}S_w S_g\frac{\partial p_g}{\partial t}+\alpha S_w\operatorname{div}\mathbf{v}^s+\frac{\alpha-n}{K_S}p_c S_w\frac{\partial S_w}{\partial t}\\&+n\frac{\partial S_w}{\partial t}-\beta_{sw}\frac{\partial T}{\partial t}+\frac{1}{\rho_w}\operatorname{div}\left\{\rho_w\frac{\mathbf{k}\,k_{rw}}{\mu_w}\left[-\operatorname{grad}p_w+\rho_w\left(\mathbf{g}-\mathbf{a}^s-\mathbf{a}^{ws}\right)\right]\right\}=-\frac{\dot{m}}{\rho_w}\end{aligned} \tag{1.4.18}$$

where

$$\beta_{sw} = \rho_w S_w \left[\beta_s \left(\alpha - n \right) + n \beta_w \right] \tag{1.4.19}$$

Recalling that the (1.2.6) implies

$$\frac{\partial S_w}{\partial t} = \frac{\partial S_w}{\partial p_c} \frac{\partial p_c}{\partial t} + \frac{\partial S_w}{\partial T} \frac{\partial T}{\partial t} \tag{1.4.20}$$

The continuity equation for gas can be obtained in a very similar way to that used for water. Thus, the time derivative of the gas density has to be considered along with the use of the (1.3.28) , of the (1.3.30) and of time derivative of solid density. The (1.4.14) has to be multiplied by S_g and again with the definition of capillary pressure, it yields:

$$\begin{aligned} &\frac{\alpha - n}{K_S} S_w S_g \frac{\partial p_w}{\partial t} + \frac{\alpha - n}{K_S} S_g^2 \frac{\partial p_g}{\partial t} - \left(\frac{\alpha - n}{K_S} p_c S_g + n \right) \frac{\partial S_w}{\partial t} + \alpha S_g \operatorname{div} \mathbf{v}^s \\ &- \beta_s \left(\alpha - n \right) S_g \frac{\partial T}{\partial t} + \frac{n S_g}{\rho_g} \frac{\partial}{\partial t} \left(\frac{p_g M_g}{\vartheta R} \right) + \frac{1}{\rho_g} \operatorname{div} \left(n S_g \rho_g \mathbf{v}^{gs} \right) = + \frac{\dot{m}}{\rho_g} \end{aligned} \tag{1.4.21}$$

with M_g as molar mass of gas, obtained with the (1.3.30). The term ϑ is the absolute temperature. Now, Darcy's law for gas (1.4.8) can be introduced and the final expression for the gas mass balance equation can be obtained

$$\begin{aligned} &\frac{\alpha - n}{K_S} S_w S_g \frac{\partial p_w}{\partial t} + \frac{\alpha - n}{K_S} S_g^2 \frac{\partial p_g}{\partial t} - \left(\frac{\alpha - n}{K_S} p_c S_g + n \right) \frac{\partial S_w}{\partial t} + \\ &- \beta_s \left(\alpha - n \right) S_g \frac{\partial T}{\partial t} + \alpha S_g \operatorname{div} \mathbf{v}^s + \frac{n S_g}{\rho_g} \frac{\partial}{\partial t} \left(\frac{p_g M_g}{\vartheta R} \right) + \\ &+ \frac{1}{\rho_g} \operatorname{div} \left\{ \rho_g \frac{\mathbf{k} k_{rg}}{\mu_g} \left[- \operatorname{grad} p_g + \rho_g \left(\mathbf{g} - \mathbf{a}^s - \mathbf{a}^{gs} \right) \right] \right\} = + \frac{\dot{m}}{\rho_g} \end{aligned} \tag{1.4.22}$$

The use of equations (1.4.18) and (1.4.22), both with $\dot{m} = 0$, can be found in a model of heat and mass transfer in deforming porous media with low or absent temperature gradients, where phase change phenomena are negligible [15]. This assumption can be done also in the case of pollutant transport analysis [16].

Analyses that involve heat transfer processes, it is more convenient to consider the mass balance equation for dry air separated from the water vapour one. As

consequence a mass balance equations for both water species, liquid water and water vapour must be written [17, 18].

Thus, the term relative to the mass rate of water evaporation $\dot{m}$ can be cancelled from both mass balance equations. Furthermore, an expression for $\dot{m}$ must be specified from the energy balance equation. In this way, the mass rate of water evaporation doesn't need of a constitutive model.

Detailed derivation of the expressions to obtain the vapour phase mass balance equation is reported in [2]. The vapour phase mass balance equation gives $\dot{m}$ as:

$$\begin{aligned}\dot{m} = &\frac{\alpha - n}{K_s} S_w S_g \rho_{gw} \frac{\partial p_w}{\partial t} + \frac{\alpha - n}{K_s} S_g^2 \rho_{gw} \frac{\partial p_g}{\partial t} - \left(\frac{\alpha - n}{K_s} S_g p_c + n \right) \rho_{gw} \frac{\partial S_w}{\partial t} \\ &- \rho_{gw} \beta_{sg} \frac{\partial T}{\partial t} + \alpha S_g \rho_{gw} \mathbf{m}^T \boldsymbol{L} \frac{\partial \mathbf{u}}{\partial t} + S_g \, n \frac{\partial}{\partial t} \left(\frac{1}{\vartheta R} p_{gw} M_w \right) \\ &+ \nabla^T \left[\rho_{gw} \frac{\mathbf{k} \, k^{rg}}{\mu^g} \left(-\nabla p_g + \rho_g \mathbf{g} \right) \right] - \nabla^T \left[\rho_g \frac{M_a M_w}{M_g^2} \mathbf{D}_g \nabla \left(\frac{p_{gw}}{p_w} \right) \right]\end{aligned} \tag{1.4.23}$$

The mass source term is now eliminated by substituting the (1.4.23) into the (1.4.18), obtaining the so called water species mass balance equation:

$$\begin{aligned}&\left(\frac{\alpha - n}{K_s} S_w \left(\rho_{gw} S_g + \rho_w S_w \right) + \rho_w S_w \frac{n}{K_w} \right) \frac{\partial p_w}{\partial t} \\ &+ \frac{\alpha - n}{K_s} S_g \left(\rho_{gw} S_g + \rho_w S_w \right) \frac{\partial p_g}{\partial t} + \alpha \left(\rho_{gw} S_g + \rho_w S_w \right) \mathbf{m}^T \boldsymbol{L} \frac{\partial \mathbf{u}}{\partial t} \\ &+ \left[\frac{\alpha - n}{K_s} \left(\rho_{gw} S_g p_c + \rho_w S_w p_w - \rho_w S_w p_c \right) + n \left(\rho_w - \rho_{gw} \right) \right] \frac{\partial S_w}{\partial t} \\ &- S_w \beta_{swg} \frac{\partial T}{\partial t} + n S_g \frac{\partial}{\partial t} \left(\frac{M_w}{\vartheta R} p_{gw} \right) - \nabla^T \left[\rho_g \frac{M_a M_w}{M_g^2} \mathbf{D}_g \nabla \left(\frac{p_{gw}}{p_w} \right) \right] \\ &+ \nabla^T \left[\rho_{gw} \frac{\mathbf{k} \, k^{rg}}{\mu^g} \left(-\nabla p_g + \rho_g \mathbf{g} \right) \right] + \nabla^T \left[\rho_w \frac{\mathbf{k} \, k^{rw}}{\mu^r} \left(-\nabla p_w + \rho_w \mathbf{g} \right) \right] = 0\end{aligned} \tag{1.4.24}$$

where

$$\beta_{swg} = \beta_s \left(\alpha - n \right) \left(\rho_{gw} S_g + \rho_w S_w \right) + n \beta_w \rho_w S_w \tag{1.4.25}$$

Taking into account that $\rho_{ga} = \rho_g - \rho_{gw}$ and substituting the (1.4.23) into the (1.4.22), the mass balance equation for dry air phase results:

$$\begin{aligned}
&\frac{\alpha - n}{K_s} S_w S_g \rho_{ga} \frac{\partial p_w}{\partial t} + \frac{\alpha - n}{K_s} S_g^2 \rho_{ga} \frac{\partial p_g}{\partial t} - \left(\frac{\alpha - n}{K_s} S_g p_c + n \right) \rho_{ga} \frac{\partial S_w}{\partial t} \\
&- \rho_{ga} \beta_{sg} \frac{\partial T}{\partial t} + \alpha S_g \rho_{ga} \mathbf{m}^T \boldsymbol{L} \frac{\partial \mathbf{u}}{\partial t} + S_g \, n \frac{\partial}{\partial t} \left(\frac{p_{ga} M_a}{\vartheta R} \right) \\
&+ \nabla^T \left[\rho_{ga} \frac{\mathbf{k} \, k^{rg}}{\mu^g} \left(-\nabla p_g + \rho_g \mathbf{g} \right) \right] + \nabla^T \left[\rho_g \frac{M_a M_w}{M_g^2} \mathbf{D}_g \nabla \left(\frac{p_{gw}}{p_g} \right) \right] = 0
\end{aligned} \tag{1.4.26}$$

Where

$$\beta_{sg} = \beta_s \left(\alpha - n \right) S_g \tag{1.4.27}$$

With the assumption of small displacements and quasi static loads (i.e. neglecting dynamic loads and assuming that relative accelerations (1.4.3) and (1.4.4) are negligible) only the gravity acceleration $\mathbf{g}$ is relevant, and so it is the only acceleration term that can be taken into account from the (1.4.23) to the (1.4.26).

Energy balance equations

The following equations represents the balance equation of thermal energy written for constituent π [19] and can be obtained after a subtraction of the kinetic energy term from a global energy balance:

$$\frac{\partial}{\partial t} \left(\rho_\pi E_\pi \right) = -\operatorname{div} \left(\rho_\pi E_\pi \mathbf{v}^\pi \right) - \operatorname{div} \overline{\mathbf{q}}_\pi - \overline{p}^\pi \operatorname{div} \mathbf{v}^\pi + \boldsymbol{\tau}^\pi : \operatorname{grad} \mathbf{v}^\pi + \rho_\pi R_\pi \tag{1.4.28}$$

here E_π is the specific internal energy, $\boldsymbol{\tau}^\pi$ is the deviatoric part of the stress tensor and $\overline{p}^\pi$ the hydrostatic part (or mean stress). The rate of accumulation of internal energy in a control volume is given by left-hand side terms. The rate of internal energy changed due to convection, the rate of internal energy changed due to conduction, the reversible rate of internal energy increased due to pressure, the irreversible rate of internal energy increased by viscous dissipation, and the contribution of heat sources are given, respectively, by the right-hand side terms.

Using the following vector identity:

$$\operatorname{div} \left(\rho_\pi E_\pi \mathbf{v}^\pi \right) = \rho_\pi E_\pi \operatorname{div} \mathbf{v}^\pi + \operatorname{grad} \left(\rho_\pi E_\pi \right) \cdot \mathbf{v}^\pi \tag{1.4.29}$$

and writing the (1.4.28) as

$$\frac{\partial}{\partial t}\left(\rho_\pi E_\pi\right)+\mathbf{v}^\pi\cdot\ \operatorname{grad}\left(\rho_\pi E_\pi\right)+\rho_\pi E_\pi \operatorname{div}\mathbf{v}^\pi=-\operatorname{div}\overline{\mathbf{q}}_\pi+ \\ -\overline{p}^\pi\operatorname{div}\mathbf{v}^\pi+\tau^\pi:\operatorname{grad}\mathbf{v}^\pi\ +\rho_\pi R_\pi \tag{1.4.30}$$

The following form for the continuity equation can be taken into account when (1.4.29) is considered along with the equation (1.4.9) with $n=0$:

$$\frac{\partial}{\partial t}\rho_\pi+\mathbf{v}^\pi\cdot\ \operatorname{grad}\rho_\pi+\rho_\pi\operatorname{div}\mathbf{v}^\pi=\frac{\partial}{\partial t}\rho_\pi+\operatorname{div}\left(\rho_\pi\mathbf{v}^\pi\right)=0 \tag{1.4.31}$$

At the end the energy balance equation becomes

$$\rho_\pi\frac{\partial E_\pi}{\partial t}+\rho_\pi\mathbf{v}^\pi\cdot\ \operatorname{grad}E_\pi=-\operatorname{div}\overline{\mathbf{q}}_\pi-\overline{p}^\pi\operatorname{div}\mathbf{v}^\pi+\boldsymbol{\tau}^\pi:\operatorname{grad}\mathbf{v}^\pi+\rho_\pi R_\pi \tag{1.4.32}$$

Viscous dissipation effects are neglected in the following. Through the concept of enthalpy, the (1.4.30) can be expressed in a more conveniently way, i.e. in terms of temperature and heat capacity instead of internal energy [19]. Hence, the energy balance equation can be rewritten as

$$\rho_\pi C_p^\pi\left(\frac{\partial T_\pi}{\partial t}+\mathbf{v}^\pi\cdot\ \operatorname{grad}T_\pi\right)=-\operatorname{div}\overline{\mathbf{q}}_\pi\ +\rho_\pi R_\pi \tag{1.4.33}$$

For π = s, w. These two phases can be considered incompressible regarding their use in the energy balance.

$$\rho_g C_p^g\left(\frac{\partial T_g}{\partial t}+\mathbf{v}^g\cdot\ \operatorname{grad}T_g\right)=-\operatorname{div}\overline{\mathbf{q}}_g\ +\frac{\partial p_g}{\partial t}+\ \mathbf{v}^g\cdot\ \operatorname{grad}p_g+\rho_g R_g \tag{1.4.34}$$

where C_p^g is the specific heat at constant pressure. The time derivatives of gas pressure, as well as the convective terms, are negligible with respect to the other terms in (1.4.34). A local equilibrium state is assumed to hold, i.e.

$$T_g=T_w=T_s=\vartheta \tag{1.4.35}$$

Introducing the constitutive equation far heat fluxes (1.3.50) and adding together the (1.4.33) and the (1.4.34), then is possible to introduce the appropriate heat sources to obtain the following form of the energy balance equation:

$$\left(\rho_\pi C_p\right)_{\text{eff}}\frac{\partial T}{\partial t}+\left(\rho_w C_p^w\mathbf{v}^w+\rho_g C_p^g\mathbf{v}^g\ \right)\cdot\operatorname{grad}T-\operatorname{div}\left(\chi_{\text{eff}}\operatorname{grad}T\right)=-\dot{m}\Delta H_{vap} \tag{1.4.36}$$

where the effective thermal capacity $\left(\rho_\pi C_p\right)_{\text{eff}}$ and the effective thermal conductivity χ_{eff} are defined by

$$\left(\rho_\pi C_p\right)_{\text{eff}} = \rho_s C_p^s + \rho_w C_p^w + \rho_g C_p^g \tag{1.4.37}$$

$$\chi_{\text{eff}} = \chi_s + \chi_w + \chi_g \tag{1.4.38}$$

$$\Delta H_{vap} = H_{gw} - H_w \tag{1.4.39}$$

The convective heat flux in the solid phase has been neglected. ΔH_{vap} is the latent heat of evaporation. The mass rate of water evaporation is eliminated from the (1.4.35) by means of the mass balance equation for water (1.4.14).

1.5. Water retention characteristics of soil

Describing the heterogeneity and the variety of all the soil compositions and structures in nature is quite impossible with the use of few parameters and the same is for the hydraulic features of a soil, in terms of the capacity to absorb, retain and release water and fluids. However, starting from empirical observations, some simplified relations were created in the past, with the aim to easy describe the retention behaviour of the most commons soils, achieving a good agreement with most of the experimental results.

Here, in a concise but exhaustive way, some retention models are now presented, with particular attention to the mathematical forms that are suitable for the numerical implementations. Part of the theory presented here as well as further insights can be found in literature at [20] and [21].

Assuming that water and air are the only wetting and non-wetting fluid, respectively, present in the soil. Hence, the notation will pertain to air - water systems only, and might be different for other multi-fluid soil systems. As further assumed, here the soil is considered homogeneous.

A schematic representation from of a typical soil water retention curve is presented in Figure 1.5.1 [20].

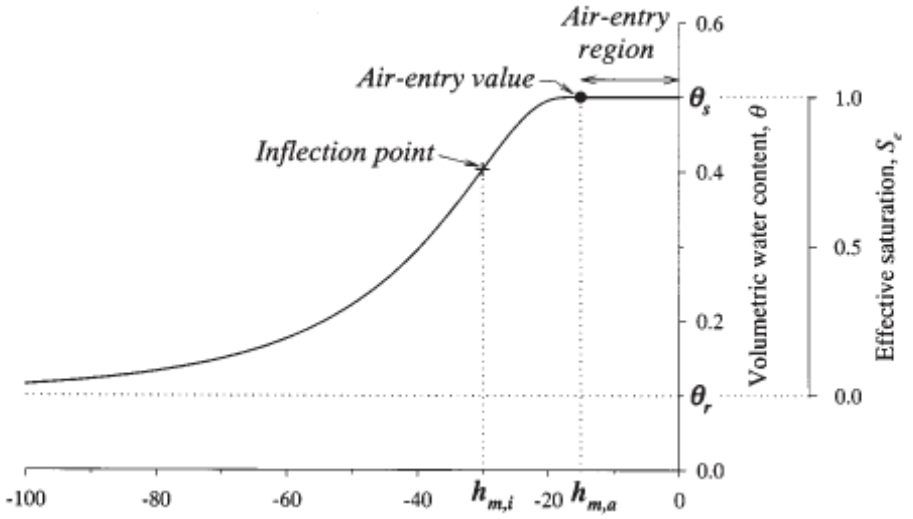

Figure 1.5.1: Water retention curve in plotted in terms of volumetric water content vs. matrix suction.

By definition, the volumetric water content θ, is equal to the saturated water content, θ_s, when the soil matrix head h_m, defined as

$$h_m = -\frac{p_c}{\gamma_w} \tag{1.5.1}$$

is equal to zero. h_m denotes a suction effect on matrix, i.e. a negative head. However, only under specific circumstances the water content is equal to the porosity *n*. Due to entrapped air, it generally can be determined that θ_s ≤ 0.85 - 0.9*n*.

For many soils, the value of θ will remain at θ_s for values of h_m slightly less than zero. The value of h_m at which the soil starts to desaturate is defined as air entry value $h_{m,a}$. The air entry value is related to the air pressure required to force air through a porous medium, which has been thoroughly wetted with water. The relation of the pore size to the air entry value is often defined by the equation [22]:

$$D = 30Y / P \tag{1.5.2}$$

where D is the pore diameter measured in microns; P is the air entry value or air entry value measured in [mmHg]; and Y is the surface tension of water measured in [dynes/cm].

It is assumed to be inversely proportional to the maximum pore size forming a continuous network of flow paths within the soil. As h_m decreases below $h_{m,a}$, θ usually decreases according to a S-shaped curve with an inflection point. In Figure 1.5.1 [20], the matrix head at the inflection point is denoted by $h_{m,i}$. As h_m decreases further, θ decreases seemingly asymptotically towards a soil-specific minimum water content known as the residual water content θ_r. More in detail, θ_r, is the water content value for which the gradient $\partial\theta/\partial h$ becomes 0.

The reason for the finite value of θ_r is that the preponderance of historical water content measurements were in the wet range and the typical soil water retention models assumed asymptotic behaviour at low water content values. As a result, most retention models describe retention curves in the range of $\theta_r \le \theta \le \theta_s$. It is convenient to define an effective saturation as define by van Genuchten [23] :

$$S_e = \frac{\theta - \theta_r}{\theta_s - \theta_r} = \frac{S_w - S_{w,irr}}{1 - S_{w,irr}} \qquad (1.5.3)$$

which varies between zero and one.

Due to the relation between water content θ and water saturation S_w, related by the porosity *n*, also an expression in terms of degree of saturation has been given in the previous equation.

It should be noted that the nature of θ_r is still controversial since the water content theoretically goes to zero as h_m becomes infinitely negative. In practice, θ_r is treated as a fitting parameter.

In addition to the four parameters $h_{m,a}$, $h_{m,i}$, θ_s, and θ_r, most retention models include a dimensionless parameter, which characterizes the width of the soil pore size distribution, the so called pore size distribution index λ (Brooks and Corey [24]).

The parameter λ depends on the range of pore sizes that can be observed in the porous medium. The more the porous medium presents regular sized pores, the more λ is higher.

Many functions have been proposed to relate the matrix head to volumetric water content. Most of these functional relationships are empirical in nature, but might

include parameters that have a physical basis. The following sections include the most widely used expressions.

Brooks and Corey Type Power Function

Among the earlier models proposed is the Brooks and Corey [24, 25] water retention model, which expresses the effective saturation S_e , as a power function of h_m :

$$S_e = \left(\frac{h_{m,a}}{h_m} \right)^{\lambda} \quad for\ h_m < h_{m,a}$$
$$S_e = 1 \qquad for\ h_m \geq h_{m,a} \tag{1.5.4}$$

The dimensionless parameter λ characterizes the pore-size distribution, as above explained. Theoretically, its value approaches to infinity for a medium with a uniform pore-size distribution, whereas it approaches to zero for soils with a wide range of pore sizes. Usually, λ values are in the range between 0.3 and 10.0. Assuming that soil pore structure satisfies the general fractal geometry conditions, Tyler and Wheatcraft [26, 27] showed that λ can be determined from the fractal dimension of soil texture. Approximate values of both $h_{m,a}$ and λ can be obtained by plotting log(S_e) vs. log(- h_m).

The absolute value of the slope of the resulting straight lines is equal to the value of λ and the $h_{m,a}$ is determined from the intercept.

However, a more straightforward estimation of the parameters can be achieved by model fitting by means of nonlinear least squares optimization procedures. Parameters are optimized to minimize an objective function $\phi(\mathbf{p})$, which contains the residual sum of squares of observed and fitted water content and/or hydraulic conductivity values:

$$\phi(\mathbf{p}) = \sum_{i=1}^{I_\theta} \left(\theta_i - \hat{\theta}_i \right)^2 + w \sum_{i=1}^{I_K} \left(\log K_i - \log \hat{K}_i \right)^2 \tag{1.5.5}$$

where $\mathbf{p}$ is the vector containing the fitted parameters, θ_i and $\hat{\theta}_i$ are the observed and fitted water content data, respectively, K_i and $\hat{K}_i$ are the observed and fitted unsaturated hydraulic conductivity values, respectively, l_θ and l_K are the number of measured retention and hydraulic conductivity data points, respectively, and *w* is

a weighting factor to correct for differences in the number of data points and units between θ and K data.

Since the (1.5.4) does not include an inflection point, but instead identifies a distinct air-entry value, the Brooks and Corey expression usually shows excellent agreement with experimental data for soils with well-defined air-entry values and J-shaped retention curves Figure 1.5.2.

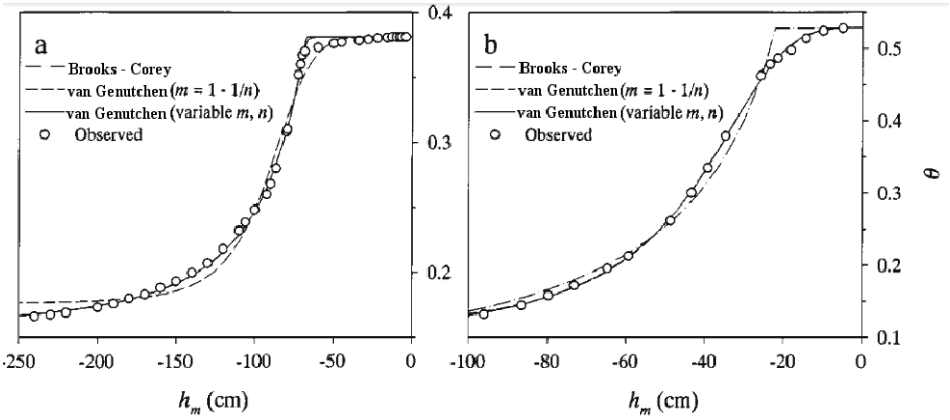

Figure 1.5.2: (a) Observed and fitted retention curves for a Rubicon sandy loam, and (b) a Touchet silt loam. The observed data were taken from the soil catalog of Mualem [28]. The saturated water content values, θ_s , were fixed as listed in the Mualem catalog.

However, as van Genuchten and Nielsen [29] and Milly [30] pointed out, the model may give relatively poor fits for soils with S-shaped retention data Figure 1.5.2 [20], such as finer-textured soils and undisturbed field soils.

The retention model used by Campbell [31] is identical to the power function of Brooks and Corey (1.5.4). However, the dependent variable is defined as the degree of saturation, that is θ / θ_s, instead of effective saturation

$$\begin{aligned} \frac{\theta}{\theta_S} &= \left(\frac{h_{m,a}}{h_m} \right)^{\lambda} \qquad for\, h_m < h_{m,a} \\ \frac{\theta}{\theta_S} &= 1 \qquad\qquad for\, h_m \geq h_{m,a} \end{aligned} \tag{1.5.6}$$

In order to provide a more affordable relation in order to be numerically implemented along with the formulation presented in this work a slightly different Brooks and Corey equation will be now provided.

Due to the relation between water content and water saturation, mentioned above, the (1.5.6) can be rewritten as:

$$\begin{aligned} S_w &= S_{w,irr} + \left(1 - S_{w,irr}\right)\left[\frac{p_b}{s}\right]^{\lambda} \quad for\ s > p^b \\ S_w &= 1 \qquad\qquad for\ s < p_b \end{aligned} \tag{1.5.7}$$

where S_w is the degree of saturation, $S_{w,irr}$ the irreducible degree of saturation, i.e. the residual saturation due to adhesive water that remains attached to the grains of the porous matrix and that can be eliminated only via thermal treatments, s is the so called suction that here coincide with the capillary pressure $s = p_c = p_g - p_w$, λ is again the pore size distribution index and p_b is the bubbling pressure. A plot of the Brooks & Corey relationship between capillary pressure and the degree of water saturation is given in Figure 1.5.3a [21]. The bubbling pressure is the equivalent value of the capillary pressure to $h_{m,a}$. It denotes the value at which the air starts to naturally enter in the porous medium.

As the capillary pressure approaches to the p_b value, the degree of water saturation S_w increases rapidly. Otherwise, for high values of capillary pressure the saturation reaches asymptotically the irreducible value of saturation.

To improve the numerical behaviour of the above mentioned equation, the $S_{g,irr}$ term has been introduced:

$$\begin{aligned} S_w &= S_{w,irr} + \left(1 - S_{w,irr} - S_{g,irr}\right)\left[\frac{p_b}{s}\right]^{\lambda} \quad for\ s > p_b \\ S_w &= 1 - S_{g,irr} \qquad\qquad for\ s < p_b \end{aligned} \tag{1.5.8}$$

This term physically can be identified as a small percentage of air trapped between the grains and the liquid phase. Numerically, it prevents (in the same way of $S_{w,irr}$) that when the bubbling pressure value is reached the degree of gas saturation S_g, involved as S_w in the equations of the model, doesn't assume a null value, as stated by the relation $S_w + S_g = 1$. A null value for S_g can lead in some cases to a numerical labilities of the system matrix, i.e. the determinant $\det\left[\boldsymbol{B} + \theta \Delta t\, \boldsymbol{C}\right] = 0$. However the $S_{g,irr}$ value must assume small values, such 0.01 – 0.05 or less.

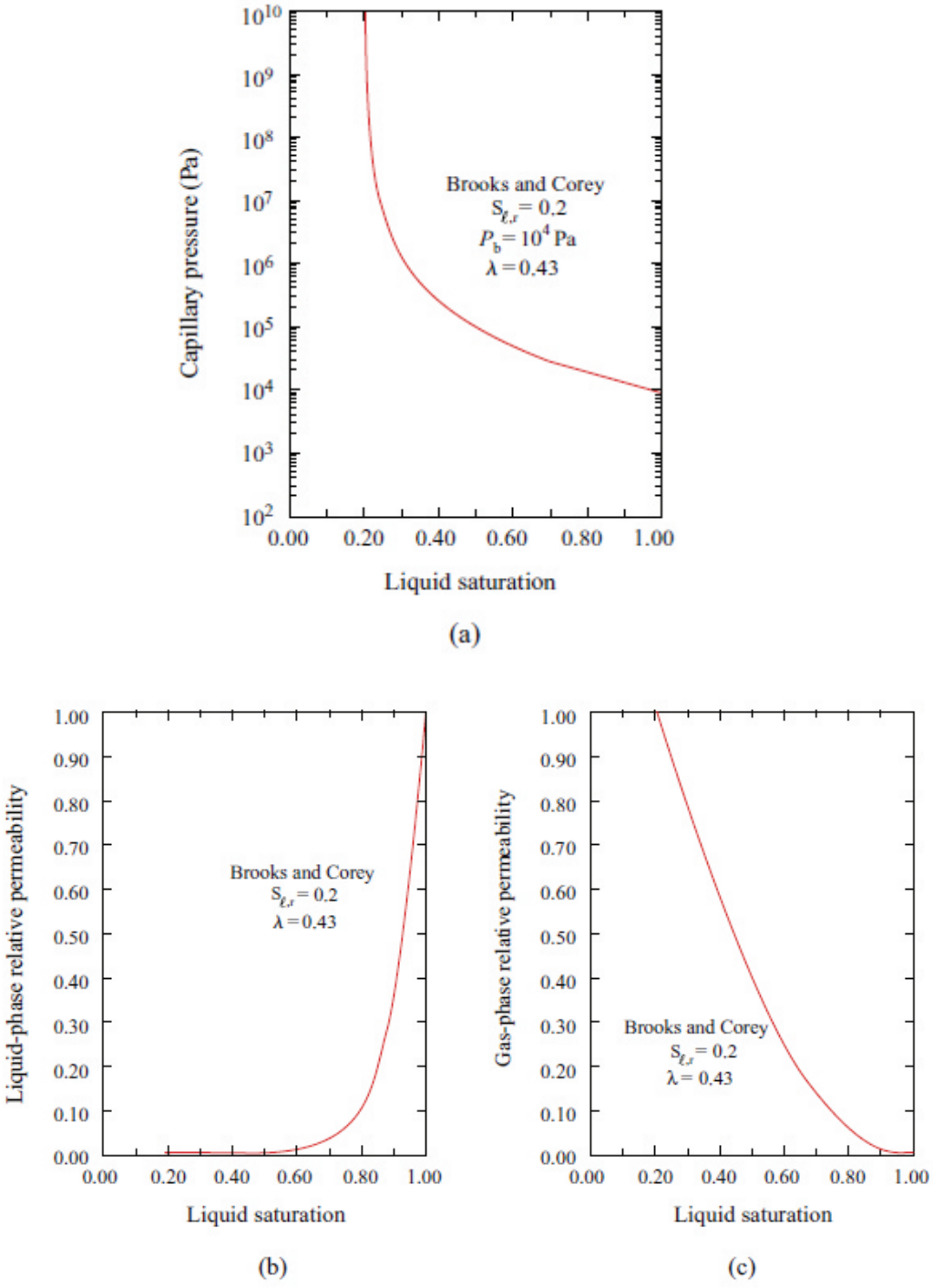

Figure 1.5.3: Representative Brooks and Corey two-phase characteristic curves (a) Capillary pressure, (b) Liquid relative permeability, (c) Gas relative permeability.

Brooks and Corey used the Burdine [32] theory to derive expressions for the wetting (liquid) and non-wetting (gas) phases relative permeabilities. Expressions for the relative permeabilities are the followings:

$$k_{rw} = S_e^{(2+3\lambda)/\lambda}$$
$$k_{rg} = (1 - S_e)^2 \left(1 - S_e^{(2+\lambda)/\lambda}\right) \tag{1.5.9}$$

Plots of relative permeabilities functions are given in Figure 1.5.3b-c [21].

Lloret and Alonso Function

Lloret and Alonso starting from experimental tests [33], tried to provide a number of analytical simple models, in order to describe the state surfaces for volume (in terms of void ratio *e*) and the degree of saturation change of partially saturated soils subjected to confined or isotropic compression.

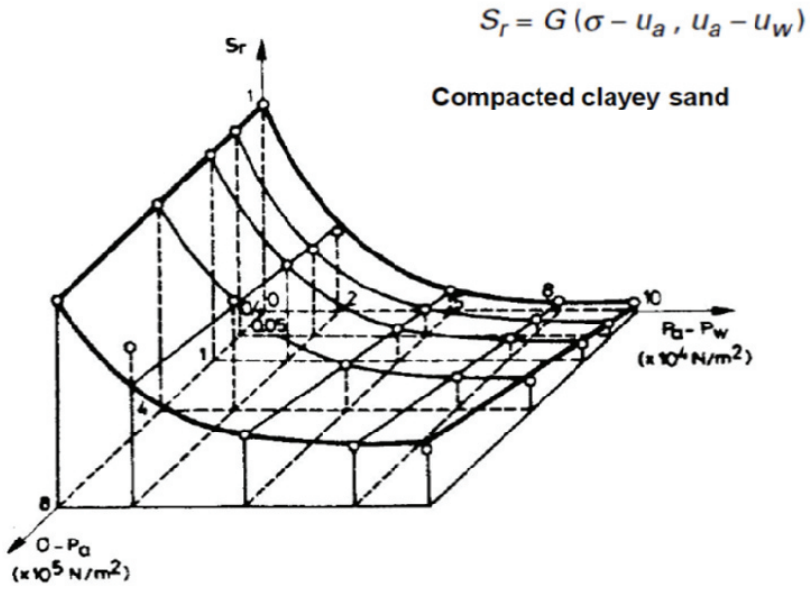

Figure 1.5.4: State surface for clayey sand.

Lloret and Alonso observed [33] that the same soil subjected to increasing effective stress loads presents a progressive evolution of the $S_w - p_c$ curve. The curve plotted versus the effective stress describes the above mentioned "state surface" for the water saturation in this case. Figure 1.5.4 shows a state surface for clayey sand. Is immediate to see that the state surface shows that the same soil, at higher effective stress loads, presents at the same value of capillary pressure a higher degree of saturation, i.e. is more difficult to desaturate a loaded soil than a unloaded one.

This effect can be easily taken into account once found the proper $S_w - p^c$ law that describes in the best way the retention behaviour of the analysed soil.

Excellent results in terms of experimental data agreement have been obtained with the following two expressions:

$$\begin{aligned} S_w &= a - \tanh\left[bp^c\right]\cdot\left[c + d\left(\sigma - p^g\right)\right] \\ S_w &= a - \left\{1 - \exp\left[-b\,p^c\right]\right\}\cdot\left[c + d\left(\sigma - p^g\right)\right] \end{aligned} \tag{1.5.10}$$

where *a, b, c, d* are material parameter deriving from the data fitting and optimization techniques based on data collect from experimental tests. Providing an effective stress evolution of these parameters, is possible to obtain the best description of the $S_w - p_c$ for each load state. However, for sake of simplicity, this feature hasn't been taken into account in the present work, opting for a fixed parameter law, leaving the stress state evolution for further development.

In order to implement this law accordingly with the theory presented in this work, the first of (1.5.10) can be rewritten as:

$$S_w = 1 - m\tanh\left(l\cdot s\right) \quad s > 0 \tag{1.5.11}$$

Where m and l again are material constants (in particular m is equivalent to $1 - S_{w,irr}$) and s is the suction, again equivalent to a positive value of the capillary pressure. Figure 1.5.5 [2] shows a comparison between Brooks and Corey power law and Lloret and Alonso law. As the same as the (1.5.8) to improve the numerical behaviour of the previous equation the term $S_{g,irr}$ has been introduced such that:

$$\begin{aligned} S_w &= 1 - S_{g,irr} - m\tanh\left(l\cdot s\right) \quad s > 0 \\ S_w &= 1 - S_{g,irr} \qquad\qquad\qquad\qquad\quad s = 0 \end{aligned} \tag{1.5.12}$$

van Genuchten law

Brutsaert [34] proposed the following power function model, which describes an *S-shaped* retention curve

$$S_e = a \Big/ \left[a + \left(-h_m\right)\right]^b \tag{1.5.13}$$

where a and b are fitting parameters, which can either be determined from moment analysis (Brutsaert, [34]) or by model fitting with similar procedure described with

the (1.5.5). The retention model suggested by Ahuja and Swartzendruber [35] has the same functional form as (1.5.13), whereas Haverkamp *et al.* [36] used (1.5.13) to test various numerical algorithms for the solution of one-dimensional infiltration.

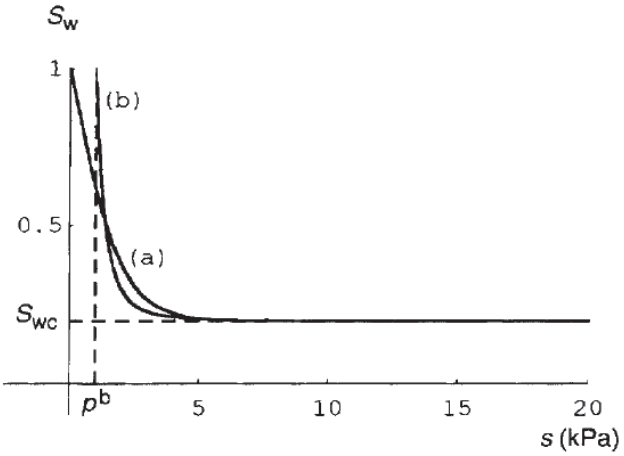

Figure 1.5.5:Comparison between Lloret and Alonso (a) relationship and Brooks and Corey relationship (b).

A more general version of (1.5.13) was suggested by van Genuchten [23, 37] and is currently one of the most commonly used soil water retention models.

$$S_e = \left[1 + \left(-\alpha h_m\right)^n\right]^{-m} \tag{1.5.14}$$

where $\alpha\left[L^{-1}\right]$ is a parameter (α > 0) to scale the matrix head, and both n and m are dimensionless parameters. The n value is generally restricted to values larger than one, so that the slope of the soil water retention curve, $\partial\theta/\partial h_m$, is zero as the water content approaches the saturated water content (van Genuchten & Nielsen, [29]). If m is fixed at a value 1, the model reduces to (1.5.13).

Instead of using a constant m value, van Genuchten (1980) proposed the relationship of $m = 1 - 1/n$ $(n > 1, 0 < m < 1)$. Using this relationship (1.5.14) does not account for an air-entry value, but does include an inflection point, allowing this model to perform better than the Brooks and Corey type model for soils with S-shaped retention curves as is shown in Figure 1.5.2b [20]. However, the model cannot accurately describe retention characteristics for soils with distinct air-entry regions Figure 1.5.2a [20]. Table 1.5.1 summarizes approximate parameter values for typical soil textural groups as estimated by Carsel and Parrish [38].

Table 1.5.1: Average values of the parameters in the van Genuchten retention model (1.5.14).

Texture	θ_s	θ_r	α	n	K_s
			cm^{-1}		cm d^{-1}
Sand	0.43	0.045	0.145	2.68	712.8
Loamy sand	0.41	0.057	0.124	2.28	350.2
Sandy loam	0.41	0.065	0.075	1.89	106.1
Loam	0.43	0.078	0.036	1.56	24.96
Silt	0.46	0.034	0.016	1.37	6.00
Silt loam	0.45	0.067	0.020	1.41	10.80
Sandy clay loam	0.39	0.100	0.059	1.48	31.44
Clay loam	0.41	0.095	0.019	1.31	6.24
Silty clay loam	0.43	0.089	0.010	1.23	1.68
Sandy clay	0.38	0.100	0.027	1.23	2.88
Silty clay	0.36	0.070	0.005	1.09	0.48
Clay	0.38	0.068	0.008	1.09	4.80

Although van Genuchten [37] provides various graphical and analytical procedures to estimate α and m, routinely parameters are obtained using fitting algorithms such as RETC software (van Genuchten *et al.* [39]) and UNSODA (Leij *et al.*, [40]).

Whereas the parameter α is related to the inverse of the air-entry value (van Genuchten [23]), the strict definition of this parameter is unclear.

Assuming $m = 1 - 1/n$, van Genuchten [37] differentiated (1.5.14) twice with respect to h_m to obtain the matrix head at the inflection point ($h_{m,i}$):

$$h_{m,i} = \frac{m^{1-m}}{\alpha} \tag{1.5.15}$$

Inverting this equation with respect to α and substituting the result into (1.5.14), yields an alternative equivalent expression for the soil water retention curve Kosugi, [41]):

$$S_e = \left[1 + m \left(\frac{h_m}{h_{m,i}} \right)^n \right]^{-m} \tag{1.5.16}$$

where $m = 1 - 1/n$.

Although van Genuchten includes special cases for $m = 1 - 1/n$ $(n > 1,\ 0 < m < 1)$ and $m = 1 - 2/n$ $(n > 2,\ 0 < m < 1)$, to derive hydraulic conductivity relations, the most general form of (1.5.14) includes the case for which m $(m > 0)$ is independent of n. Increasing the number of parameters from two to three (excluding θ_s and θ_r), allows more flexibility in the fitting of soil water retention data. Van Genuchten and

Nielsen demonstrated that (1.5.14) is almost equivalent to the Brooks and Corey model if n is increased and m is simultaneously decreased so that the product mn remains constant. Under this condition, the values of mn and $(-\alpha^{-1})$ of the (1.5.14) correspond to λ and $h_{m,a}$ of (1.5.4), respectively. Therefore, the case with m independent of n provides acceptable fits for soils with distinct air-entry values (Figure 1.5.2a), whereas the model simultaneously retains its capability to fit sigmoidal-shaped retention curves as shown in Figure 1.5.2b.

Two other three-parameter related models have been presented that allow the inclusion of an air-entry value, while maintaining the general form of (1.5.14). First, Vogel and Císlerová [42] modified the (1.5.14) to allow for a non-zero $h_{m,a}$ value:

$$\begin{aligned} \theta &= \theta_r + \left(\theta_s' + \theta_r\right)\left[1+\left(-\alpha\, h_m\right)^n\right]^{-m} && \text{for } h_m < h_{m,a} \\ \theta &= \theta_s && \text{for } h_m \geq h_{m,a} \end{aligned} \qquad (1.5.17)$$

where $m = 1 - 1/n\,(n>1)$ and $\theta_s'\,(\theta_s' \geq \theta_s)$ is a fitting parameter. The selected value of $h_{m,a}$ will depend on values of the other parameters to ensure the continuity of the θ value at $h_m = h_{m,a}$. The case of $\theta_s' \geq \theta_s$ leads to $h_{m,a} = 0$, so that (1.5.17) is identical to (1.5.14). The added flexibility of (1.5.17) is included in Simnek *et al.* [43] for the simulation of variably saturated water flow. Second, Kosugi [41] modified (1.5.16) to include an air-entry head value as well, while maintaining the physical meaning of $h_{m,i}$ as the matrix head at the inflection point:

$$\begin{aligned} S_e &= \left\{1 + m\left[\left(h_{m,a} - h_m\right)/\left(h_{m,a} - h_{m,i}\right)\right]^n\right\}^{-m} && \text{for } h_m < h_{m,a} \\ S_e &= 1 && \text{for } h_m \geq h_{m,a} \end{aligned} \qquad (1.5.18)$$

where $m = 1 - 1/n\,(n>1)$. Again, if $h_{m,a} = 0$, (1.5.18) reduces to (1.5.16), which is equivalent to (1.5.14).

In order to give a more practical relation to implement in the code the following capillary pressure relationship has been chosen:

$$S_e = \left[\frac{1}{1+\left(\bar{\alpha}\, p_c\right)^n}\right]^m \qquad (1.5.19)$$

This can be rearranged as

$$p_c = \frac{1}{\bar{\alpha}}\left[S_e^{-1/m} - 1\right]^{1/n} \tag{1.5.20}$$

where now $\bar{\alpha} = \alpha/\gamma_w$, and has the dimension of [Pa^{-1}], in order to maintain S_e dimensionless. The coefficients m and n are the same used in the previous relations written in terms of water content and matrix head. A plot of the van Genuchten relationship between capillary pressure and the degree of water saturation is given in Figure 1.5.6a [21].

The relative permeability of the liquid phase can be predicted from the capillary pressure curve expression using the integral expressions of Mualem [44] or Burdine [32]. The resulting liquid phase relative permeability integral can be expressed as a closed form expression for certain relationships between the m and n fitting parameters as detailed by van Genuchten [23, 37]. For Mualem [44], the relationship $m = 1 - 1/n$ leads to a closed form solution for the liquid-phase relative permeability, which is given by

$$k_{rw} = S_e^{1/2}\left(1-\left(1-S_e^{1/m}\right)^m\right)^2 \quad \left(m=1-1/n\right) \tag{1.5.21}$$

For Burdine [32], the relationship $m = 1-2/n$ leads to a closed form expression, or

$$k_{rw} = S_e^2\left(1-\left(1-S_e^{1/m}\right)^m\right) \quad \left(m=1-2/n\right) \tag{1.5.22}$$

In both cases, m must be between 0 and 1. With these restricted forms, the limits on the parameter n are $n \geq 1$ for Mualem and $n \geq 2$ for Burdine. As discussed by van Genuchten [23, 37] and van Genuchten and Nielsen [29], both forms give similar results, but the Mualem form is preferred because of it has more general applicability due to the larger range for n, and the Mualem restricted form with $m = 1 - 1/n$ is generally recommended.

An important point for the present discussion is that van Genuchten [23, 37] did not address gas-phase relative permeability. Parker *et al.* [45, 46] extended the van Genuchten–Mualem characteristic curves to include the gas-phase relative permeability, or

$$k_{rg} = \left(1-S_e\right)^{1/2}\left(1-S_e^{1/m}\right)^{2m} \tag{1.5.23}$$

Similarly, Luckner *et al.* [47] present a gas-phase relative permeability expression for the van Genuchten–Mualem characteristic curves.

$$k_{rg} = \left(1 - S_e\right)^{1/3} \left(1 - S_e^{1/m}\right)^{2m} \tag{1.5.24}$$

Figure 1.5.6 shows some generic van Genuchten–Mualem two-phase characteristic curves for some typical parameters as noted on the figures. The van Genuchten capillary pressure curve exhibits unphysical behavior as the liquid saturation is reduced (gas saturation is increased). As the liquid residual value (0.2 in this case) is approached, the value of capillary pressure goes to infinity. The liquid relative permeability starts out low and increases dramatically with increasing liquid saturation. The gas-phase relative permeability decreases with increasing liquid saturation and is concave down. The difference between the Parker *et al.* [45, 46] and Luckner *et al.* [47] expressions is small for these parameter values. Plots of relative permeability functions are given in Figure 1.5.6b-c [21].

Typical values of the van Genuchten – Mualem parameters for 34 soils are tabulated by Stephens [48] , and the original tabulations in Stephens *et al.* [49] and van Genuchten [23, 37]. The parameter ranges are *α* from 0.004 to 0.12 cm^{-1} ($1/\alpha$ from 817 to 24500 Pa), n from 1.17 to 7.62 (m from 0.15 to 0.87), and S_r from 0 to $0.4/n$ (Stephens *et al.* [49], used a water content form of the effective saturation equation).

While the van Genuchten and Brooks and Corey two-phase characteristic curves may look similar, there are important differences when they are used in flow situations. McWhorter and Sunada [50] and Webb [51] evaluated the differences between the two sets of characteristic curves for analytical two-phase flow situations. The differences in the saturation profiles are significant, probably due to the different shape of the gas-phase relative permeability expressions. In general, the van Genuchten (and Parker) set of curves lead to a much sharper interface, while the Brooks and Corey predictions are much blunter.

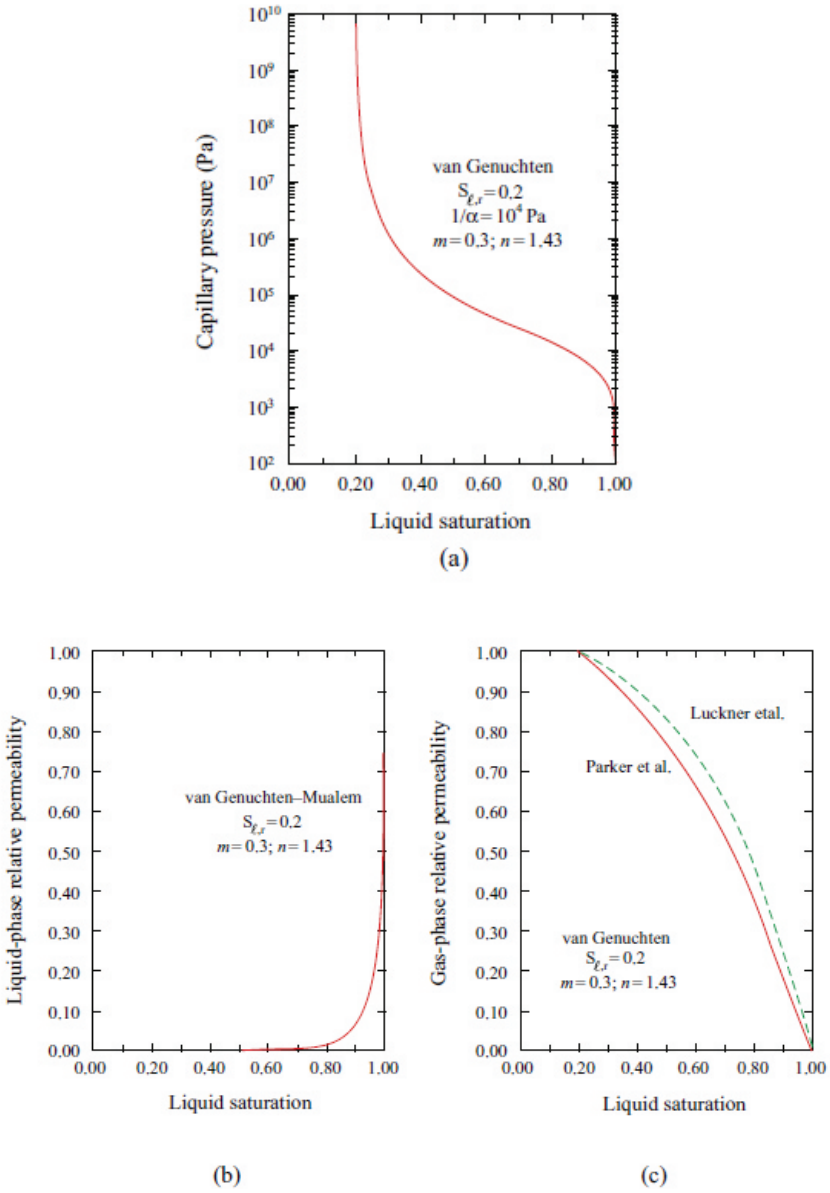

Figure 1.5.6: Representative van Genuchten–Mualem two-phase characteristic curves (a) Capillary pressure, (b) Liquid relative permeability, (c) Gas relative permeability.

Bibliography

1. Lewis, R.W. and B.A. Schrefler, *The finite element method in the deformation and consolidation of porous media.* 1987.

2. Lewis, R.W. and B.A. Schrefler, *The finite element method in the deformation and consolidation of porous media.* 1998.

3. Zienkiewicz, O.C. and T. Shiomi, *Dynamic behaviour of saturated porous media; the generalized Biot formulation and its numerical solution.* International journal for numerical and analytical methods in geomechanics, 1984. **8**(1): p. 71-96.

4. Biot, M.A. and P.G. Willis, *The elastic coefficients of the theory of consolidation.* J. Appl. Mech., 1957. **24**: p. 594 - 601.

5. Hassanizadeh, M. and W.G. Gray, *General conservation equations for multi-phase systems: 3. Constitutive theory for porous media flow.* Advances in Water Resources, 1980. **3**(1): p. 25-40.

6. Moran, M.J., et al., *Fundamentals of engineering thermodynamics*. 2010: Wiley. com.

7. Hassanizadeh, S.M., *Derivation of basic equations of mass transport in porous media, Part 1. Macroscopic balance laws.* Adv. Water Resour, 1986. **9**: p. 196-206.

8. Hassanizadeh, S.M., *Derivation of basic equations of mass transport in porous media, Part 2. Generalized Darcy's law and Fick's law.* Adv. Water Resources, 1986. **9**: p. 207-222.

9. de Boer, R., *Porous Media: A Survey of Differential Approaches*. 1991: Universität-Gesamthochschule-Essen, Fachbereich Bauwesen.

10. Withaker, S., *Simultaneous heat, mass and momentum transfer in porous media. A theory of drying porous media.* Adv. Heat Transfer, 1977. **13**: p. 119-200.

11. Nozad, I., R. Carbonell, and S. Whitaker, *Heat conduction in multiphase systems—I: theory and experiment for two-phase systems.* Chemical Engineering Science, 1985. **40**(5): p. 843-855.

12. Bomberg, M. and C. Shirtliffe, *Influence of moisture and moisture gradients on heat transfer through porous building materials.* ASTM STP, 1978. **660**: p. 211-233.

13. Lewis, R.W., B.A. Schrefler, and N.A. Rahman, *A finite element analysis of multiphase immiscible flow in deforming porous media for subsurface systems.* Communications in numerical methods in engineering, 1998. **14**(2): p. 135-149.

14. Fleureau, J. and S. Taibi. *Water-air permeabilities of unsaturated soils*. in *Proceedings of the first international conference on unsaturated soils (UNSAT'95) Paris (France), 6-8 september 1995. Volume 2*. 1995.

15. Schrefler, B.A., X. Zhan, and L. Simoni, *A coupled model for water flow, airflow and heat flow in deformable porous media.* International Journal of Numerical Methods for Heat & Fluid Flow, 1995. **5**(6): p. 531-547.

16. Schrefler, B., et al., *Pollutant transport in deforming porous media.* European journal of mechanics. A. Solids, 1994. **13**: p. 175-194.

17. Baggio, P., C. Bonacina, and M. Strada, *Trasporto di calore e massa nel calcestruzzo cellulare.* Termotecnica, 1993. **47**(12): p. 53-59.

18. Gawin, D., P. Baggio, and B.A. Schrefler, *Coupled heat, water and gas flow in deformable porous media.* International Journal for numerical methods in fluids, 1995. **20**(8-9): p. 969-987.

19. Bird, R.B., W.E. Stewart, and E.N. Lightfoot, *Transport phenomena*. 2007: Wiley. com.

20. *Soil Science Sociery of America - Methods of Soil Analysis. Part 4. Physical Methods.* SSSA Book Series, no. 5, 2002.

21. Ho, C.K. and S.W. Webb, *Gas transport in porous media*. Vol. 20. 2006: Springer.

22. *Soilmoisture equipment Corp. - The Use of Porous Materials in Devices for Sampling Moisture in the Vadose Zone.* Engineering details, 2001. **05/2001**.

23. van Genuchten, M.T., *A closed-form equation for predicting the hydraulic conductivity of unsaturated soils.* Soil Science Society of America Journal, 1980. **44**(5): p. 892-898.

24. Brooks, R. and A. Corey, *Hydraulic properties of porous media.* Hydrology Papers, Colorado State University, Fort Collins, 1964. **3**.

25. Brooks, R.H. and A.T. Corey. *Properties of porous media affecting fluid flow*. in *Journal of the Irrigation and Drainage Division, Proceedings of the American Society of Civil Engineers*. 1966.

26. Tyler, S.W. and S.W. Wheatcraft, *Application of fractal mathematics to soil water retention estimation.* Soil Science Society of America Journal, 1989. **53**(4): p. 987-996.

27. Tyler, S.W. and S.W. Wheatcraft, *Fractal processes in soil water retention.* Water Resources Research, 1990. **26**(5): p. 1047-1054.

28. Mualem, Y., *catalogue of the hydraulic properties of unsaturated soils.* 1976.

29. van Genuchten, M.T. and D. Nielsen, *On describing and predicting the hydraulic properties of unsaturated soils.* Ann. Geophys, 1985. **3**(5): p. 615-628.

30. Milly, P., *Estimation of Brooks-Corey parameters from water retention data.* Water Resources Research, 1987. **23**(6): p. 1085-1089.

31. Campbell, G.S., *A simple method for determining unsaturated conductivity from moisture retention data.* Soil Science, 1974. **117**(6): p. 311-314.

32. Burdine, N., *Relative permeability calculations from pore size distribution data.* Journal of Petroleum Technology, 1953. **5**(3): p. 71-78.

33. Lloret, A. and E.E. Alonso, *State surfaces for partially saturated soils.* Proceedings of the 11th International Conference on Soil Mechanics and Foundation Engineering, San Francisco, 12-16 august 1985. Publication of Balkema, 1985.

34. Brutsaert, W., *Probability laws for pore-size distributions.* Soil Science, 1966. **101**(2): p. 85-92.

35. Ahuja, L. and D. Swartzendruber, *An improved form of soil-water diffusivity function.* Soil Science Society of America Journal, 1972. **36**(1): p. 9-14.

36. Haverkamp, R., et al., *A comparison of numerical simulation models for one-dimensional infiltration.* Soil Science Society of America Journal, 1977. **41**(2): p. 285-294.

37. van Genuchten, R., *Calculating the unsaturated hydraulic conductivity with a new closed-form analytical model*. 1978: International Ground Water Modeling Center.

38. Carsel, R.F. and R.S. Parrish, *Developing joint probability distributions of soil water retention characteristics.* Water Resources Research, 1988. **24**(5): p. 755-769.

39. van Genuchten, M.T., F. Leij, and S. Yates, *The RETC code for quantifying the hydraulic functions of unsaturated soils.* 1991.

40. Leij, F.J., *UNSODA unsaturated soil hydraulic database.* 1996.

41. Kosugi, K.i., *Three-parameter lognormal distribution model for soil water retention.* Water Resources Research, 1994. **30**(4): p. 891-901.

42. Císlerová, M., J. Šimůnek, and T. Vogel, *Changes of steady-state infiltration rates in recurrent ponding infiltration experiments.* Journal of Hydrology, 1988. **104**(1): p. 1-16.

43. Šimůnek, J., et al., *Parameter estimation of unsaturated soil hydraulic properties from transient flow processes.* Soil and Tillage Research, 1998. **47**(1): p. 27-36.

44. Mualem, Y., *A new model for predicting the hydraulic conductivity of unsaturated porous media.* Water resources research, 1976. **12**(3): p. 513-522.

45. Parker, J. and R. Lenhard, *A model for hysteretic constitutive relations governing multiphase flow: 1. Saturation-pressure relations.* Water Resources Research, 1987. **23**(12): p. 2187-2196.

46. Parker, J., R. Lenhard, and T. Kuppusamy, *A parametric model for constitutive properties governing multiphase flow in porous media.* Water Resources Research, 1987. **23**(4): p. 618-624.

47. Luckner, L., M.T. Van Genuchten, and D. Nielsen, *A consistent set of parametric models for the two-phase flow of immiscible fluids in the subsurface.* Water Resources Research, 1989. **25**(10): p. 2187-2193.

48. Stephens, D.B., *Vadose zone hydrology*. 1996: CRC press.

49. Stephens, D.B., K. Lambert, and D. Watson, *Regression models for hydraulic conductivity and field test of the borehole permeameter.* Water Resources Research, 1987. **23**(12): p. 2207-2214.

50. McWhorter, D.B. and D.K. Sunada, *Exact integral solutions for two-phase flow.* Water Resources Research, 1990. **26**(3): p. 399-413.

51. Webb, S.W., *Steady-state saturation profiles for linear immiscible fluid displacement in porous media*, 1991, Sandia National Labs., Albuquerque, NM (United States)

2 Discretized equations for the deforming porous medium

2.1. Introduction

In this chapter some shorts recalls of basic equilibrium and mass balances equations for water species and dry air are given, in order to introduce properly the boundary value problem and boundary conditions. The Finite Element Method is then shortly presented, applied to the boundary value problem presented before. Discretized equations for the solid phase, water species, dry air and thermal coupling are therefore presented for the non-isothermal problem. The isothermal case of air flow and water flow in a deforming porous medium is then discussed and the relative simplifications to the general problem introduced. An ideal finite element that can be used in the spatial discretization of three-dimensional domains is presented.

Solving techniques and time discretization are finally discussed. Further insights can be found on literature on [1].

2.2. Governing equations: recall

The linear momentum balance equation (1.4.5) in terms of total stress can be expressed as

$$L^T \boldsymbol{\sigma} + \rho \mathbf{g} = 0 \tag{2.2.1}$$

with effective stress principle that is given by (1.2.14):

$$\boldsymbol{\sigma} = \boldsymbol{\sigma}'' - \alpha \, \mathbf{m}^T \left(S_w \, p^w + S_g \, p^g \right) \tag{2.2.2}$$

For the multiphase medium the density is given from the (1.4.6):

$$\rho = \left(1 - n\right) \rho_s + n S_w \rho_w + n S_g \rho_g \tag{2.2.3}$$

The water and gas mass balance equations are given by the (1.4.18) and the (1.4.22). An expression of the mass balance equation for the water species (vapour and liquid water) can be given by the (1.4.23). i.e.

$$\begin{aligned}
&\left(\frac{\alpha-n}{K_s}S_w\left(\rho_{gw}S_g+\rho_w S_w\right)+\rho_w S_w\frac{n}{K_w}\right)\frac{\partial p_w}{\partial t}\\
&+\frac{\alpha-n}{K_s}S_g\left(\rho_{gw}S_g+\rho_w S_w\right)\frac{\partial p_g}{\partial t}+\alpha\left(\rho_{gw}S_g+\rho_w S_w\right)\mathbf{m}^T\boldsymbol{L}\frac{\partial \mathbf{u}}{\partial t}\\
&+\left[\frac{\alpha-n}{K_s}\left(\rho_{gw}S_g p_c+\rho_w S_w p_w-\rho_w S_w p_c\right)+n\left(\rho_w-\rho_{gw}\right)\right]\frac{\partial S_w}{\partial t}\\
&-S_w\beta_{swg}\frac{\partial T}{\partial t}+nS_g\frac{\partial}{\partial t}\left(\frac{M_w}{\vartheta R}p_{gw}\right)-\nabla^T\left[\rho_g\frac{M_a M_w}{M_g^2}\mathbf{D}_g\nabla\left(\frac{p_{gw}}{p_w}\right)\right]\\
&+\nabla^T\left[\rho_{gw}\frac{\mathbf{k}\,k^{rg}}{\mu^g}\left(-\nabla p_g+\rho_g\mathbf{g}\right)\right]+\nabla^T\left[\rho_w\frac{\mathbf{k}\,k^{rw}}{\mu^r}\left(-\nabla p_w+\rho_w\mathbf{g}\right)\right]=0
\end{aligned}\tag{2.2.4}$$

Summing both the mass conservation equations for the liquid water equation (1.4.18) and for the vapour equation (1.4.22), it results a null right hand side term in the previous equation. Even if the mass source term is not explicitly present, this equation takes into account any phase change, i.e. evaporation condensation phenomena.

Along with the (2.2.4) a mass balance equation for dry air must be expressed:

$$\begin{aligned}
&\frac{\alpha-n}{K_s}S_w S_g\rho_{ga}\frac{\partial p_w}{\partial t}+\frac{\alpha-n}{K_s}S_g^2\rho_{ga}\frac{\partial p_g}{\partial t}-\left(\frac{\alpha-n}{K_s}S_g p_c+n\right)\rho_{ga}\frac{\partial}{\partial}\\
&-\rho_{ga}\beta_{sg}\frac{\partial T}{\partial t}+\alpha S_g\rho_{ga}\mathbf{m}^T\boldsymbol{L}\frac{\partial \mathbf{u}}{\partial t}+S_g\,n\frac{\partial}{\partial t}\left(\frac{p_{ga}M_a}{\vartheta R}\right)\\
&+\nabla^T\left[\rho_{ga}\frac{\mathbf{k}\,k^{rg}}{\mu^g}\left(-\nabla p_g+\rho_g\mathbf{g}\right)\right]+\nabla^T\left[\rho_g\frac{M_a M_w}{M_g^2}\mathbf{D}_g\nabla\left(\frac{p_{gw}}{p_g}\right)\right]=
\end{aligned}\tag{2.2.5}$$

Last balance equation recalled regards the enthalpy as given in the (1.4.33):

$$\begin{aligned}
&\left(\rho_\pi C_p\right)_{\text{eff}}\frac{\partial T}{\partial t}+\left(nS_w\rho_w C_p^w\mathbf{v}^w+nS_g\rho_g C_p^g\mathbf{v}^g\right)\cdot\nabla T\\
&-\nabla^T\left(\chi_{\text{eff}}\nabla T\right)=-\dot{m}\,\Delta H_{vap}
\end{aligned}\tag{2.2.6}$$

With the effective heat capacity that in this case is:

$$\left(\rho_\pi C_p\right)_{\text{eff}} = \left(1-n\right)\rho_s C_p^s + nS_w\rho_w C_p^w + nS_g\rho_g C_p^g \tag{2.2.7}$$

For completeness, also the mass source term that comes from the water mass conservation equation is reported here:

$$\begin{aligned}\dot{m} = &-\rho_w\left(\frac{\alpha-n}{K_s}S_w^2 + S_w\frac{n}{K_W}\right)\frac{\partial p_w}{\partial t} - \rho_w\frac{\alpha-n}{K_s}S_wS_g\frac{\partial p_g}{\partial t}\\ &-\alpha\rho_w S_w\mathbf{m}^T\boldsymbol{L}\frac{\partial\mathbf{u}}{\partial t} + \beta_{sw}\frac{\partial T}{\partial t}\\ &-\rho_w\left[\frac{\alpha-n}{K_s}S_wp_w - \frac{\alpha-n}{K_s}S_wp_g + n\right]\frac{\partial S_w}{\partial t}\\ &-\nabla^T\left[\rho_w\frac{\mathbf{k}\,k^{rw}}{\mu^w}\left(-\nabla p_w + \rho_w\mathbf{g}\right)\right]\end{aligned} \tag{2.2.8}$$

The constitutive relationship for a linear isotropic material, in infinitesimal form, is given with the (1.3.1) and now can be rewritten in total form

$$\boldsymbol{\sigma}' = \mathbf{D}_e\left(\boldsymbol{\varepsilon} - \boldsymbol{\varepsilon}_0 - \boldsymbol{\varepsilon}_T\right) \tag{2.2.9}$$

As widely discussed on section 1.5, where the degree of water saturation has been related to the capillary pressure, the equation (1.2.6) express briefly the relation

$$S_w = S_w\left(p_c, T\right) \tag{2.2.10}$$

or its inverse

$$p_c = p_c\left(S_w, T\right) \tag{2.2.11}$$

with the condition that

$$S_w + S_g = 1 \tag{2.2.12}$$

The relationships between relative permeabilities and degrees of saturation, pressures and temperature are briefly expressed as

$$k_{rw} = k_{rw}\left(S_w, T\right) \;or\; k_{rw} = k_{rw}\left(p_w, T\right) \tag{2.2.13}$$

$$k_{rg} = k_{rg}\left(S_g, T\right) \;or\; k_{rg} = k_{rg}\left(p_g, T\right) \tag{2.2.14}$$

as dealt in section 1.5.

2.3. The boundary value problem

The following problem

$$\mathbf{A(u)} = \mathbf{C(u)} + \mathbf{p} = \mathbf{0} \qquad \text{in } \Omega \tag{2.3.1}$$

with

$$\mathbf{B(u)} = \mathbf{M(u)} + \mathbf{q} = \mathbf{0} \qquad \text{in } \Gamma \tag{2.3.2}$$

represents a boundary value problem, where $\mathbf{C}$ is differential operator, $\mathbf{u}$ a generic field variable and $\mathbf{p}$ is a known function, that is independent of $\mathbf{u}$. $\mathbf{M}$ is again an appropriate operator and $\mathbf{q}$ a known function independent of $\mathbf{u}$ which is the exact solution of the boundary value problem.

The following integral form:

$$\int_{\Omega} \mathbf{v}^T \mathbf{A(u)}\, d\Omega + \int_{\Gamma} \overline{\mathbf{v}}^T \mathbf{B(u)}\, d\Gamma = 0 \tag{2.3.3}$$

is satisfied for a proper choice of the set of functions, i.e. the differential equation (2.3.1) and the boundary condition (2.3.2) are satisfied. If an arbitrary choice of $\mathbf{v}$ and $\overline{\mathbf{v}}$ satisfy the (2.3.3), (2.3.1) and (2.3.2) has to be satisfied in each point within the domain Ω and on the boundary Γ.

Functions for which any term in the integrals (2.3.3) becomes infinite, have to be avoided as proper choice for the functions $\mathbf{v}$ and $\overline{\mathbf{v}}$. In the literature at [2] can be found details on the restrictions to be applied on the choice of $\mathbf{v}$ and $\overline{\mathbf{v}}$ in order to maintain the validity of the integral statement

When solving the boundary value problem with the finite element method, an approximation of the solution, as most of practical problems require, is sought in the class of functions

$$\mathbf{u} \approx \hat{\mathbf{u}} = \sum_{i}^{r} \mathbf{N}_i \boldsymbol{a}_i = \mathbf{N}\mathbf{a} \tag{2.3.4}$$

In (2.3.4) a set of so called shape function $\mathbf{N}$ has been introduced. These functions depend from independent variables as the coordinates. $\boldsymbol{a}_i$ is a vector that represents the values of the unknowns at the i-th points or nodes defined in the domain Ω. Further insights on shape functions can be found on standard finite

element textbooks as [2] and the section 2.5. Substituting $\hat{\mathbf{u}}$ into the (2.3.1) and the (2.3.2) an error occurs and so a residual can be found as

$$\mathbf{R} = \mathbf{R}_{\Omega} + \mathbf{R}_{\Gamma} = \mathbf{A}(\hat{\mathbf{u}}) + \mathbf{B}(\hat{\mathbf{u}}) \tag{2.3.5}$$

The goal would be to minimize the residual for each node on the domain Ω and the boundary Γ and this can done, for example, with the weighted residual method, briefly applied to the (2.3.3)

$$\int_{\Omega} \mathbf{w}^T \mathbf{A}(\hat{\mathbf{u}})\, d\Omega + \int_{\Gamma} \bar{\mathbf{w}}^T \mathbf{B}(\hat{\mathbf{u}})\, d\Gamma = 0 \tag{2.3.6}$$

where in general, the functions $\mathbf{w}$ and $\bar{\mathbf{w}}$ can be independently chosen.

The system that results approximating the (2.3.3) with the (2.3.6) can be written as

$$\mathbf{K}\mathbf{a} = \mathbf{f} \tag{2.3.7}$$

With

$$\mathbf{K}_{ij} = \sum_{e=1}^{m} \mathbf{K}_{ij}^{e} \quad \mathbf{f}_i = \sum_{e=1}^{m} \mathbf{f}_i^{e} \tag{2.3.8}$$

Weighting functions $\mathbf{w}$ and $\bar{\mathbf{w}}$ have to be chosen carefully in order to preserve possible symmetries of the system (2.3.7). Shape functions have to possess at least the same order of derivative of the differential operators $\mathbf{A}$ and $\mathbf{B}$ and these derivatives must be continuous.

2.4. Initial and boundary conditions

In order to solve the equations recalled in the previous section, the displacements in the three Cartesian directions u_x, u_y, u_z, the water pressure p_w, the gas pressure p_g, and the temperature T have been chosen as basic variables of the previous equations.

In order to solve the boundary value problem (2.3.1) a set of conditions that represent the initial state of the system, in terms of basic variables and the value that these variables assume at the boundary of the domain, has to be stated. At time t = 0 the full field of displacements water and gas pressures and temperature is:

$$\mathbf{u} = \mathbf{u}^0 \quad p_w = p_w^0 \quad p_g = p_g^0 \quad T = T^0 \ \text{ in } \Omega \text{ and } \Gamma \tag{2.4.1}$$

where Ω is the domain of interest and Γ its boundary. The boundary conditions can be either fixed values on Γ_π or fluxes on Γ_π^q, where the boundary $\Gamma = \Gamma_\pi \cup \Gamma_\pi^q$.

The imposed boundary values for the six variables can be of the Dirichlet type as follows:

$$\begin{aligned} &\mathbf{u} = \hat{\mathbf{u}} \quad \text{in } \Gamma_u, \quad p_w = \hat{p}_w \text{ in } \Gamma_w \\ &p_g = \hat{p}_g \text{ in } \Gamma_g, \quad T = \hat{T} \quad \text{in } \Gamma_T \end{aligned} \tag{2.4.2}$$

Or of the Neumann type i.e.

$$\mathbf{I}^T \boldsymbol{\sigma} = \bar{\mathbf{t}} \quad \text{on } \Gamma_u^q \tag{2.4.3}$$

That represent the boundary traction for stress on the boundary Γ_u^q and for the water and gas phase the relative Neumann condition is represented by the fluxes, i.e.

$$\begin{aligned} &\left[\rho_w \frac{\mathbf{k}\, k_{rw}}{\mu_w} \left(-\nabla p_w + \rho_w \mathbf{g} \right)^T + \rho_{gw} \frac{\mathbf{k}\, k_g}{\mu_g} \left(-\nabla p_g + \rho_g \mathbf{g} \right)^T \right. \\ &\left. + \rho_g \frac{M_a M_w}{M_g^2} \mathbf{D}_g \nabla \left(\frac{p_{gw}}{p_w} \right) \right] \cdot \mathbf{n} = q_w + q_{gw} + \beta_c \left(\rho_{gw} - \rho_{gw}^\infty \right) \text{ on } \Gamma_w^q \end{aligned} \tag{2.4.4}$$

and

$$\left[\rho_{ga} \frac{\mathbf{k}\, k_{rg}}{\mu_g} \left(-\nabla p_g + \rho_g \mathbf{g} \right)^T - \rho_g \frac{M_a M_w}{M_g^2} \mathbf{D}_g \nabla \left(\frac{p_{gw}}{p_g} \right) \right] \cdot \mathbf{n} = q_{ga} \text{ on } \Gamma_g^q \tag{2.4.5}$$

The heat flux has the form

$$\left(\rho_w \mathbf{v}^w \Delta H_{vap} - \chi_{eff} \nabla T \right) \cdot \mathbf{n} = q_T + \alpha_C \left(T - T^\infty \right) \text{ on } \Gamma_T^q \tag{2.4.6}$$

where q_{ga} is the imposed mass flux of dry air. β_c is the convective mass transfer coefficient and ρ_{gw}^∞ is the partial density of vapour in the surrounding air at a great distance from the interface, q_T is the imposed heat flux, α_C the convective heat transfer coefficient and finally the T^∞ is the temperature for the gas phase that can be observed at a not disturbed point of the domain. The term at right hand side of the (2.4.4) is analogous to the last term in the (2.4.6). They are representative of the cooling process as the porous bodies dry.

2.5. Discretized equations for the non-isothermal airflow and water flow in a deforming porous medium with the Finite Element Method. Boundary problem solution

By applying the weighted residual method to the linear momentum balance equation (2.2.1), i.e. the integral equation (2.3.6) with the boundary condition (2.4.3) results

$$\int_{\Omega} \mathbf{w}^T \left(L^T \boldsymbol{\sigma} + \rho \mathbf{g} \right) d\Omega + \int_{\Gamma} \overline{\mathbf{w}}^T \left(\mathbf{I}^T \boldsymbol{\sigma} - \overline{\mathbf{t}} \right) d\Gamma = 0 \tag{2.5.1}$$

The choice of the weighting functions is limited in such a way that

$$\mathbf{w} = 0 \qquad \text{on} \, \Gamma_u \tag{2.5.2}$$

and

$$\overline{\mathbf{w}} = -\mathbf{w} \quad \text{on} \, \Gamma_u^q \tag{2.5.3}$$

The Green 's theorem can be applied to the left hand side of (2.5.1) and it can be proved that [2]:

$$\int_{\Omega} \phi \frac{\partial \Psi}{\partial x} d\Omega = -\int_{\Omega} \frac{\partial \phi}{\partial x} \psi \, d\Omega + \int_{\Gamma} \phi \psi \, n_x \, d\Gamma \tag{2.5.4}$$

Hence the (2.5.1) becomes

$$-\int_{\Omega} \left(\boldsymbol{L} \mathbf{w} \right)^T \boldsymbol{\sigma} \, d\Omega + \int_{\Gamma} \mathbf{w}^T \mathbf{I}^T \, \boldsymbol{\sigma} \, d\Gamma + \int_{\Omega} \mathbf{w}^T \, \rho \mathbf{g} \, d\Omega + \int_{\Gamma} \overline{\mathbf{w}}^T \left(\mathbf{I}^T \boldsymbol{\sigma} - \overline{\mathbf{t}} \right) d\Gamma \tag{2.5.5}$$

If weighting functions are chosen in order to satisfy the (2.5.2) and the (2.5.3). The previous equation can be rewritten as:

$$\int_{\Omega} \left(L \mathbf{w} \right)^T \boldsymbol{\sigma} \, d\Omega = \int_{\Omega} \mathbf{w}^T \rho \mathbf{g} \, d\Omega + \int_{\Gamma} \mathbf{w}^T \overline{\mathbf{t}} \, d\Gamma \tag{2.5.6}$$

After a proper expressions for the weighting functions has been taken (here w^* stands for water species and $w^\bullet$ for dry air), the Green's theorem can be applied to the water mass conservation equation and the corresponding boundary equation.

It yields

$$
\begin{aligned}
&\int_{\Omega} \mathbf{w}^{*T} \left[\left(\frac{\alpha - n}{K_S} S_w \left(\rho_{gw} S_g + \rho_w S_w \right) + \rho_w S_w \frac{n}{K_W} \right) \frac{\partial p_w}{\partial t} + \right. \\
&\left. + \frac{\alpha - n}{K_S} S_g \left(\rho_{gw} S_g + \rho_w S_w \right) \frac{\partial p_g}{\partial t} \right] d\Omega + \\
&+ \int_{\Omega} \mathbf{w}^{*T} \left[+ \alpha \left(\rho_{gw} S_g + \rho_w S_w \right) \mathbf{m}^T \boldsymbol{L} \frac{\partial \mathbf{u}}{\partial t} + \right. \\
&\left. - S_w \beta_{swg} \frac{\partial T}{\partial t} + n S_g \frac{\partial}{\partial t} \left(\frac{M_w}{\vartheta R} p_{gw} \right) \right] d\Omega + \\
&+ \int_{\Omega} \mathbf{w}^{*T} \left\{ \left[\frac{\alpha - n}{K_S} \left(\rho_{gw} S_g p_c + \rho_w S_w p_w - \rho_w S_w p_c \right) + n \left(\rho_w - \rho_{gw} \right) \right] \frac{\partial S_w}{\partial t} \right\} d\Omega + \\
&- \int_{\Omega} \left(\nabla \mathbf{w}^{*T} \right) \left[- \rho_g \frac{M_a M_w}{M_g^2} \mathbf{D}_g \nabla \left(\frac{p_{gw}}{p_w} \right) + \rho_{gw} \frac{\mathbf{k} k_{rg}}{\mu_g} \left(- \nabla p_g + \rho_g \mathbf{g} \right) \right] d\Omega + \\
&- \int_{\Omega} \left(\nabla \mathbf{w}^{*T} \right) \left[\rho_w \frac{\mathbf{k} k_{rw}}{\mu_w} \left(- \nabla p_w + \rho_w \mathbf{g} \right) \right] d\Omega + \\
&+ \int_{\Gamma_w^q} \mathbf{w}^{*T} \left[q_w + q_{gw} + \beta_c \left(\rho_{gw} - \rho_{gw}^{\infty} \right) \right] d\Gamma = 0
\end{aligned}
\tag{2.5.7}
$$

Applying the Green's theorem to the gas mass conservation equation, taking into account that $\rho_{ga} = \rho_g - \rho_{gw}$ gives

$$
\begin{aligned}
&\int_{\Omega} \mathbf{w}^{\bullet T} \left[\frac{\alpha - n}{K_S} S_w S_g \rho_{ga} \frac{\partial p_w}{\partial t} + \frac{\alpha - n}{K_S} S_g^2 \rho_{ga} \frac{\partial p_g}{\partial t} + \right. \\
&\left. - \left(\frac{\alpha - n}{K_S} S_g p_c + n \right) \rho_{ga} \frac{\partial S_w}{\partial t} - \rho_{ga} \beta_{sg} \frac{\partial T}{\partial t} \right] d\Omega + \\
&+ \int_{\Omega} \mathbf{w}^{\bullet T} \left[+ \alpha S_g \rho_{ga} \mathbf{m}^T \boldsymbol{L} \frac{\partial \mathbf{u}}{\partial t} + S_g \, n \frac{\partial}{\partial t} \left(\frac{p_{ga} M_a}{\vartheta R} \right) \right] d\Omega + \\
&- \int_{\Omega} \left(\nabla \mathbf{w}^{\bullet T} \right) \left\{ \left[\rho_{ga} \frac{\mathbf{k} k_{rg}}{\mu_g} \left(- \nabla p_g + \rho_g \mathbf{g} \right) \right] + \nabla^T \left[\rho_g \frac{M_a M_w}{M_g^2} \mathbf{D}_g \nabla \left(\frac{p_{gw}}{p_g} \right) \right] \right\} d\Omega + \\
&- \int_{\Omega} \left(\nabla \mathbf{w}^{\bullet T} \right) \left[\rho_w \frac{\mathbf{k} k_{rw}}{\mu_w} \left(- \nabla p_w + \rho_w \mathbf{g} \right) \right] d\Omega + \int_{\Gamma_g^q} \mathbf{w}^{\bullet T} q_{ga} \, d\Gamma = 0
\end{aligned}
\tag{2.5.8}
$$

Applying the weighted residual method to the energy conservation equation it yields

$$
\begin{aligned}
&\int_{\Omega} \mathbf{w}^{\circ T} \left(\rho_{\pi} C_{p}\right)_{\text{eff}} \frac{\partial T}{\partial t} d\Omega + \int_{\Omega} \left(\nabla \mathbf{w}^{\circ}\right)^{T} \chi_{\text{eff}} \nabla T \, d\Omega \\
&+ \int_{\Omega} \mathbf{w}^{\circ T} \left\{ \begin{bmatrix} nS_w \rho_w C_p^w \dfrac{\mathbf{k}\, k_{rw}}{\mu_w} \left(-\nabla p_w + \rho_w \mathbf{g}\right)^T \\ + nS_g \rho_g C_p^g \dfrac{\mathbf{k}\, k_{rg}}{\mu_g} \left(-\nabla p_g + \rho_g \mathbf{g}\right)^T \end{bmatrix} \cdot \nabla T \right\} d\Omega \\
&+ \int_{\Omega} \mathbf{w}^{\circ T} \Delta H_{vap} \left\{ \begin{matrix} -\rho_w \left(\dfrac{\alpha - n}{K_S} S_w^2 + S_w \dfrac{n}{K_W} \right) \dfrac{\partial p_w}{\partial t} \\ -\rho_w \dfrac{\alpha - n}{K_S} S_w S_g \dfrac{\partial p_g}{\partial t} - \alpha \rho_w S_w \mathbf{m}^T \boldsymbol{L} \dfrac{\partial \mathbf{u}}{\partial t} \end{matrix} \right\} d\Omega \\
&+ \int_{\Omega} \mathbf{w}^{\circ T} \Delta H_{vap} \left\{ \beta_{sw} \frac{\partial T}{\partial t} - \rho_w \left[\frac{\alpha - n}{K_S} S_w p_w - \frac{\alpha - n}{K_S} S_w p_g + n \right] \frac{\partial S_w}{\partial t} \right\} d\Omega \\
&+ \int_{\Omega} \left(\nabla \mathbf{w}^{\circ}\right)^{T} \Delta H_{vap} \left[\rho_w \frac{\mathbf{k}\, k_{rw}}{\mu_w} \left(-\nabla p_w + \rho_w \mathbf{g}\right) \right] d\Omega \\
&+ \int_{\Gamma_T^q} \mathbf{w}^{\circ T} \left[q_T + \alpha_c \left(T - T^{\infty}\right) \right] d\Gamma = 0
\end{aligned}
\tag{2.5.9}
$$

Where the weighting functions for the boundary are

$$0 \qquad \text{on } \Gamma_u \tag{2.5.10}$$

and

$$\mathbf{w}^{\circ T} \quad \text{on } \Gamma_u^q \tag{2.5.11}$$

The finite element method can be applied now to (2.5.6), (2.5.7), (2.5.8) and (2.5.9). This consists on considering the basic variables $\mathbf{u}$, p_w, p_g and T expressed in the form of (2.3.4):

$$\mathbf{u} = \mathbf{N}_u \overline{\mathbf{u}}, \quad p_w = \mathbf{N}_p \overline{\mathbf{p}}_w, \quad p_g = \mathbf{N}_p \overline{\mathbf{p}}_g, \quad T = \mathbf{N}_t \overline{\mathbf{T}} \tag{2.5.12}$$

where $\overline{\mathbf{u}}$, $\overline{\mathbf{p}}_w$, $\overline{\mathbf{p}}_g$ and $\overline{\mathbf{T}}$ are the vectors of the nodal values of the unknowns.

Taking into account of (2.2.1), (2.2.2) and (2.2.3), is possible to use the (2.5.12) and further the Galerkin method [3] can be applied, to the equations (2.5.6) to (2.5.9).

Thus, the weighting functions are replaced by the shape functions, yielding to

$$\int_{\Omega} \mathbf{B}^T \boldsymbol{\sigma}'' \, d\Omega - \int_{\Omega} \alpha \, \mathbf{m}^T \left(S_w \mathbf{N}_p \overline{\mathbf{p}}_w + S_g \mathbf{N}_p \overline{\mathbf{p}}_g \right) d\Omega = \int_{\Omega} \mathbf{N}_u^T \rho \, \mathbf{g} \, d\Omega + \int_{\Gamma_u^q} \mathbf{N}_u^T \overline{\mathbf{t}} \, d\Gamma \tag{2.5.13}$$

The following relationships hold:

$$\frac{\partial S_w}{\partial t}=\frac{\partial S_w}{\partial p_c}\frac{\partial p_c}{\partial t}+\frac{\partial S_w}{\partial T}\frac{\partial T}{\partial t}=\frac{\partial S_w}{\partial p_c}\frac{\partial p_g}{\partial t}-\frac{\partial S_w}{\partial p_c}\frac{\partial p_w}{\partial t}+\frac{\partial S_w}{\partial T}\frac{\partial T}{\partial t} \tag{2.5.14}$$

$$\frac{\partial}{\partial t}\left(\frac{M_w}{\vartheta R}p_{gw}\right)=\frac{M_w}{\vartheta R}\frac{\partial p_{gw}}{\partial p_c}\left(\frac{\partial p_g}{\partial p_c}-\frac{\partial p_w}{\partial p_c}\right)+\frac{M_w}{\vartheta R}\left(\frac{\partial p_{gw}}{\partial T}-\frac{p_{gw}}{\vartheta}\right)\frac{\partial T}{\partial t} \tag{2.5.15}$$

$$\nabla\left(\frac{p_{gw}}{p_g}\right)=\frac{\nabla p_{gw}}{p_g}-\frac{p_{gw}}{\left(p_g\right)^2}\nabla p_g=\frac{1}{p_g}\frac{\partial p_{gw}}{\partial p_c}\left(\nabla p_g-\nabla p_w\right)-\frac{p_{gw}}{\left(p_g\right)^2}\nabla p_g \tag{2.5.16}$$

$$\begin{aligned}\frac{\partial}{\partial t}\left(\frac{p_{ga}M_a}{\vartheta R}\right)&=\frac{\partial}{\partial t}\left[\frac{\left(p_g-p_{gw}\right)M_a}{\vartheta R}\right]=\frac{M_a}{\vartheta R}\frac{\partial p_g}{\partial t}-\frac{M_a}{\vartheta^2 R}\frac{\partial T}{\partial t}+\\&-\frac{M_w}{\vartheta R}\frac{\partial p_{gw}}{\partial p_c}\left(\frac{\partial p_g}{\partial t}-\frac{\partial p_w}{\partial t}\right)-\frac{M_w}{\vartheta R}\left(\frac{\partial p_{gw}}{\partial T}-\frac{p_{gw}}{\vartheta}\right)\frac{\partial T}{\partial t}\end{aligned} \tag{2.5.17}$$

The final set of discretized equations started with the (2.5.13), has to be completed with the discretized equation for water phase (water species):

$$\begin{aligned}&\int_\Omega \mathbf{N}_p^T\left[\left(\frac{\alpha-n}{K_S}S_w\left(\rho_{gw}S_g+\rho_w S_w\right)+\rho_w S_w\frac{n}{K_W}\right)\mathbf{N}_p\frac{\partial\overline{\mathbf{p}}_w}{\partial t}+\right.\\&\left.+\frac{\alpha-n}{K_S}S_g\left(\rho_{gw}S_g+\rho_w S_w\right)\mathbf{N}_p\frac{\partial\overline{\mathbf{p}}_g}{\partial t}\right]d\Omega+\\&+\int_\Omega \mathbf{N}_p^T\left[\begin{array}{l}+\alpha\left(\rho_{gw}S_g+\rho_w S_w\right)\mathbf{m}^T\boldsymbol{L}\mathbf{N}_u\frac{\partial\overline{\mathbf{u}}}{\partial t}-S_w\beta_{swg}\mathbf{N}_T\frac{\partial\overline{\mathbf{T}}}{\partial t}+\\+nS_g\frac{M_w}{\vartheta R}\frac{\partial p_{gw}}{\partial p_c}\mathbf{N}_p\left(\frac{\partial\overline{\mathbf{p}}_g}{\partial t}-\frac{\partial\overline{\mathbf{p}}_w}{\partial t}\right)\end{array}\right]d\Omega+\\&+\int_\Omega \mathbf{N}_p^T\left[nS_g\frac{M_w}{\vartheta R}\left(\frac{\partial p_{gw}}{\partial T}-\frac{p_{gw}}{\vartheta}\right)\mathbf{N}_T\frac{\partial\overline{\mathbf{T}}}{\partial t}\right]d\Omega+\\&+\int_\Omega \mathbf{N}_p^T\left\{\begin{array}{l}\left[\frac{\alpha-n}{K_S}\left(\rho_{gw}S_g p_c+\rho_w S_w p_w-\rho_w S_w p_c\right)+n\left(\rho_w-\rho_{gw}\right)+\right]\\\left(\frac{\partial S_w}{\partial p_c}\mathbf{N}_p\frac{\partial\overline{\mathbf{p}}_g}{\partial t}-\frac{\partial S_w}{\partial p_c}\mathbf{N}_p\frac{\partial\overline{\mathbf{p}}_w}{\partial t}+\frac{\partial S_w}{\partial T}\mathbf{N}_T\frac{\partial\overline{\mathbf{T}}}{\partial t}\right)\end{array}\right\}d\Omega+\\&-\int_\Omega\left(\nabla\mathbf{N}_p\right)^T\left\{-\rho_g\frac{M_a M_w}{M_g^2}\mathbf{D}_g\left[\begin{array}{l}\frac{1}{p_g}\frac{\partial p_{gw}}{\partial p_c}\left(\nabla\mathbf{N}_p\overline{\mathbf{p}}_g-\nabla\mathbf{N}_p\overline{\mathbf{p}}_w\right)+\\-\frac{p_{gw}}{\left(p_g\right)^2}\nabla\mathbf{N}_p\overline{\mathbf{p}}_g\end{array}\right]\right\}d\Omega+\end{aligned} \tag{2.5.18}$$

continued

from previous page

$$-\int_{\Omega}\left(\nabla\mathbf{N}_p\right)^T\left[\rho_{gw}\frac{\mathbf{k}\,k_{rg}}{\mu_g}\left(-\nabla\mathbf{N}_p\bar{\mathbf{p}}_g+\rho_g\mathbf{g}\right)\right]d\Omega+$$

$$-\int_{\Omega}\left(\nabla\mathbf{N}_p\right)^T\left[\rho_w\frac{\mathbf{k}\,k_w}{\mu_w}\left(-\nabla\mathbf{N}_p\bar{\mathbf{p}}_w+\rho_w\mathbf{g}\right)\right]d\Omega+$$

$$+\int_{\Gamma_w^q}\mathbf{N}_p^T\left[q_w+q_{gw}+\beta_c\left(\rho_{gw}-\rho_{gw}^{\infty}\right)\right]d\Gamma=0$$

along with the equation for the gas phase (dry air):

$$\begin{aligned}
&\int_{\Omega}\mathbf{N}_p^T\begin{bmatrix}\dfrac{\alpha-n}{K_S}S_wS_g\rho_{ga}\mathbf{N}_p\dfrac{\partial\bar{\mathbf{p}}_w}{\partial t}+\dfrac{\alpha-n}{K_S}S_g^2\rho_{ga}\mathbf{N}_p\dfrac{\partial\bar{\mathbf{p}}_g}{\partial t}\\ -\rho_{ga}\beta_{sg}\mathbf{N}_T\dfrac{\partial\bar{\mathbf{T}}}{\partial t}\end{bmatrix}d\Omega\\
&-\int_{\Omega}\mathbf{N}_p^T\begin{bmatrix}\left(\dfrac{\alpha-n}{K_S}S_gp_c+n\right)\rho_{ga}\\ \left(\dfrac{\partial S_w}{\partial p_c}\mathbf{N}_p\dfrac{\partial\bar{\mathbf{p}}_g}{\partial t}-\dfrac{\partial S_w}{\partial p_c}\mathbf{N}_p\dfrac{\partial\bar{\mathbf{p}}_w}{\partial t}+\dfrac{\partial S_w}{\partial T}\mathbf{N}_T\dfrac{\partial\bar{\mathbf{T}}}{\partial t}\right)\end{bmatrix}d\Omega\\
&+\int_{\Omega}\mathbf{N}_p^T\begin{bmatrix}+\alpha S_g\rho_{ga}\mathbf{m}^T\boldsymbol{L}\mathbf{N}_u\dfrac{\partial\bar{\mathbf{u}}}{\partial t}+S_g\,n\dfrac{M_a}{\vartheta R}\mathbf{N}_p\dfrac{\partial\bar{\mathbf{p}}_g}{\partial t}\\ -S_g\,n\dfrac{M_a}{\vartheta^2R}\mathbf{N}_T\dfrac{\partial\bar{\mathbf{T}}}{\partial t}\end{bmatrix}d\Omega\\
&-\int_{\Omega}\mathbf{N}_p^T\left[S_gn\frac{M_w}{\vartheta R}\left(\frac{\partial p_{gw}}{\partial T}-\frac{p_{gw}}{\vartheta}\right)\mathbf{N}_T\frac{\partial\bar{\mathbf{T}}}{\partial t}\right]d\Omega\\
&+\int_{\Omega}\mathbf{N}_p^T\left[-S_gn\frac{M_w}{\vartheta R}\frac{\partial p_{gw}}{\partial p_c}\mathbf{N}_p\left(\frac{\partial\bar{\mathbf{p}}_g}{\partial t}-\frac{\partial\bar{\mathbf{p}}_w}{\partial t}\right)\right]d\Omega\\
&-\int_{\Omega}\left(\nabla\mathbf{N}_p\right)^T\left[\rho_{ga}\frac{\mathbf{k}\,k_{rg}}{\mu_g}\left(-\nabla\mathbf{N}_p\bar{\mathbf{p}}_g+\rho_g\mathbf{g}\right)\right]d\Omega+\int_{\Gamma_g^q}\mathbf{N}_p^Tq_{ga}\,d\Gamma\\
&-\int_{\Omega}\left(\nabla\mathbf{N}_p\right)^T\left\{\rho_g\frac{M_aM_w}{M_g^2}\mathbf{D}_g\begin{bmatrix}\dfrac{1}{p_g}\dfrac{\partial p_{gw}}{\partial p_c}\left(\nabla\mathbf{N}_p\bar{\mathbf{p}}_g-\nabla\mathbf{N}_p\bar{\mathbf{p}}_w\right)\\ -\dfrac{p_{gw}}{\left(p_g\right)^2}\nabla\mathbf{N}_p\bar{\mathbf{p}}_g\end{bmatrix}\right\}d\Omega=0
\end{aligned}\tag{2.5.19}$$

and the last for the energy conservation (in terms of temperature)

$$
\begin{aligned}
&\int_{\Omega} \mathbf{N}_T^T \left(\rho_\pi C_p\right)_{\text{eff}} \mathbf{N}_T \frac{\partial \overline{\mathbf{T}}}{\partial t} d\Omega + \int_{\Omega} \left(\nabla \mathbf{N}_T\right)^T \chi_{\text{eff}} \nabla \mathbf{N}_T \overline{\mathbf{T}}\, d\Omega \\
&+ \int_{\Omega} \mathbf{N}_T^T \left\{ \begin{bmatrix} nS_w \rho_w C_p^w \dfrac{\mathbf{k}\, k_{rw}}{\mu_w} \left(-\nabla p_w + \rho_w \mathbf{g}\right)^T \\ + nS_g \rho_g C_p^g \dfrac{\mathbf{k}\, k_{rg}}{\mu_g} \left(-\nabla p_g + \rho_g \mathbf{g}\right)^T \end{bmatrix} \cdot \nabla \mathbf{N}_T \overline{\mathbf{T}} \right\} d\Omega \\
&+ \int_{\Omega} \mathbf{N}_T^T \Delta H_{vap} \begin{Bmatrix} -\rho_w \left(\dfrac{\alpha - n}{K_S} S_w^2 + S_w \dfrac{n}{K_W} \right) \mathbf{N}_p \dfrac{\partial \overline{\mathbf{p}}_w}{\partial t} \\ -\rho_w \dfrac{\alpha - n}{K_S} S_w S_g \mathbf{N}_p \dfrac{\partial \overline{\mathbf{p}}_g}{\partial t} - \alpha \rho_w S_w \mathbf{m}^T \boldsymbol{L} \mathbf{N}_u \dfrac{\partial \overline{\mathbf{u}}}{\partial t} \end{Bmatrix} d\Omega \\
&+ \int_{\Omega} \mathbf{N}_T^T \Delta H_{vap} \begin{Bmatrix} \beta_{sw} \mathbf{N}_T \dfrac{\partial \overline{\mathbf{T}}}{\partial t} - \rho_w \left[\dfrac{\alpha - n}{K_S} S_w p_w - \dfrac{\alpha - n}{K_S} S_w p_g + n \right] \\ \left(\dfrac{\partial S_w}{\partial p_c} \mathbf{N}_p \dfrac{\partial \overline{\mathbf{p}}_g}{\partial t} - \dfrac{\partial S_w}{\partial p_c} \mathbf{N}_p \dfrac{\partial \overline{\mathbf{p}}_w}{\partial t} + \dfrac{\partial S_w}{\partial T} \mathbf{N}_T \dfrac{\partial \overline{\mathbf{T}}}{\partial t} \right) \end{Bmatrix} d\Omega \\
&+ \int_{\Omega} \left(\nabla \mathbf{N}_T\right)^T \Delta H_{vap} \left[\rho_w \frac{\mathbf{k}\, k_{rw}}{\mu_w} \left(-\nabla \mathbf{N}_p \overline{\mathbf{p}}_w + \rho_w \mathbf{g}\right) \right] d\Omega \\
&+ \int_{\Gamma_T^q} \mathbf{N}_T^T \left[q_T + \alpha_c \left(T - T^\infty\right) \right] d\Gamma = 0
\end{aligned}
\tag{2.5.20}
$$

Remembering that derivatives of shape functions are

$$
\mathbf{B} = L\mathbf{N}_u, \quad \mathbf{B}^T = \left(L\mathbf{N}_u\right)^T \tag{2.5.21}
$$

And considering the (2.5.13) for a linear elastic solid medium, it results

$$
\mathbf{P}(\overline{\mathbf{u}}) = \int_{\Omega} \mathbf{B}^T \sigma''\, d\Omega = \mathbf{K}_E \overline{\mathbf{u}} + \mathbf{K}_{TE} \overline{\mathbf{T}} \tag{2.5.22}
$$

A time differentiation can be performed and the discretised mechanical equilibrium equation can be obtained in the following form:

$$
\mathrm{K_E} \frac{\partial \overline{\mathbf{u}}}{\partial t} + \mathrm{K_{TE}} \frac{\partial \overline{\mathbf{T}}}{\partial t} - C_{\mathrm{sw}} \frac{\partial \overline{\mathbf{p}}^w}{\partial t} - C_{\mathrm{sg}} \frac{\partial \overline{\mathbf{p}}^g}{\partial t} = \frac{\partial \mathbf{f}^u}{\partial t} \tag{2.5.23}
$$

where the matrices $\mathrm{K_E}$, $\mathrm{K_{TE}}$, C_{sw} and C_{sg} are defined as:

$$\mathrm{K_E} = \int_{\Omega} \mathbf{B}^{\mathrm{T}} \mathbf{D}_{\mathrm{E}} \mathbf{B} \mathrm{d}\Omega \tag{2.5.24}$$

$$\mathrm{K_{TE}} = \int_{\Omega} \mathbf{B}^{\mathrm{T}} \mathbf{D}_{\mathrm{E}}\, \mathbf{m} \frac{\beta_s}{3} \mathbf{N}_{\mathbf{t}} \mathrm{d}\Omega \tag{2.5.25}$$

$$C_{\mathrm{sw}} = \int_{\Omega} \mathbf{B}^{\mathrm{T}} \mathrm{S}_{\mathrm{w}} \alpha\, \mathbf{m}\, \mathbf{N}_{\mathbf{p}}\, \mathrm{d}\Omega \tag{2.5.26}$$

$$C_{\mathrm{sg}} = \int_{\Omega} \mathbf{B}^{\mathrm{T}} \mathrm{S}_{\mathrm{g}} \alpha\, \mathbf{m}\, \mathbf{N}_{\mathbf{p}} \mathrm{d}\Omega \tag{2.5.27}$$

For the non-linear solid-phase behaviour, the elastic matrices have to be substituted by the proper tangent matrices

$$\frac{\partial \mathbf{P}(\bar{\mathbf{u}})}{\partial \bar{\mathbf{u}}} = \mathbf{K}_{\mathrm{T}} = \int_{\Omega} \mathbf{B}^{\mathrm{T}} \mathbf{D}_{\mathrm{T}} \mathbf{B}\, \mathrm{d}\Omega \tag{2.5.28}$$

$$\frac{\partial \mathbf{P}(\bar{\mathbf{u}})}{\partial \bar{\mathbf{T}}} = \mathbf{K}_{\mathrm{TT}} = \int_{\Omega} \mathbf{B}^{\mathrm{T}} \mathbf{D}_{\mathrm{T}}\, \mathbf{m} \frac{\beta_s}{3} \mathbf{N}_{\mathbf{t}} \mathrm{d}\Omega \tag{2.5.29}$$

where $\mathrm{K_E}$ and $\mathrm{K_{TE}}$ may be replaced by $\mathrm{K_T}$ and $\mathrm{K_{TT}}$ respectively. The discretised mass and energy conservation equations can be written as:

$$C_{ws} \frac{\partial \bar{\mathbf{u}}}{\partial t} + P_{\mathrm{ww}} \frac{\partial \bar{\mathbf{p}}^{w}}{\partial t} + C_{\mathrm{wg}} \frac{\partial \bar{\mathbf{p}}^{g}}{\partial t} + C_{\mathrm{wt}} \frac{\partial \bar{\mathbf{T}}}{\partial t} + H_{\mathrm{ww}}\, \bar{\mathbf{p}}^{w} + K_{\mathrm{wg}}\, \bar{\mathbf{p}}^{g} = \mathbf{f}^{w} \tag{2.5.30}$$

$$C_{gs} \frac{\partial \bar{\mathbf{u}}}{\partial t} + C_{\mathrm{gw}} \frac{\partial \bar{\mathbf{p}}^{w}}{\partial t} + P_{\mathrm{gg}} \frac{\partial \bar{\mathbf{p}}^{g}}{\partial t} + C_{\mathrm{gt}} \frac{\partial \bar{\mathbf{T}}}{\partial t} + K_{gw}\, \bar{\mathbf{p}}^{w} + H_{\mathrm{gg}}\, \bar{\mathbf{p}}^{g} = \mathbf{f}^{g} \tag{2.5.31}$$

$$C_{ts} \frac{\partial \bar{\mathbf{u}}}{\partial t} + C_{\mathrm{tw}} \frac{\partial \bar{\mathbf{p}}^{w}}{\partial t} + C_{\mathrm{gt}} \frac{\partial \bar{\mathbf{p}}^{g}}{\partial t} + P_{\mathrm{tt}} \frac{\partial \bar{\mathbf{T}}}{\partial t} + K_{tw}\, \bar{\mathbf{p}}^{w} + H_{tt}\, \bar{\mathbf{p}}^{g} = \mathbf{f}^{t} \tag{2.5.32}$$

The equations (2.5.23) to (2.5.32) can finally be written in the following matrix from:

$$\boldsymbol{H}\boldsymbol{X} + \boldsymbol{S} \frac{\partial \boldsymbol{X}}{\partial t} = \boldsymbol{F} \tag{2.5.33}$$

Where hyper - matrices are:

$$\boldsymbol{S}=\begin{bmatrix} \mathrm{K}_{\mathrm{T}} & -C_{\mathrm{sw}} & -C_{\mathrm{sg}} & \mathrm{K}_{\mathrm{tT}} \\ C_{\mathrm{ws}} & P_{\mathrm{ww}} & C_{\mathrm{wg}} & C_{\mathrm{wt}} \\ C_{\mathrm{gs}} & C_{\mathrm{gw}} & P_{\mathrm{gg}} & C_{\mathrm{gt}} \\ C_{\mathrm{ts}} & C_{\mathrm{tw}} & C_{\mathrm{tg}} & P_{\mathrm{tt}} \end{bmatrix} \tag{2.5.34}$$

$$\boldsymbol{H}=\begin{bmatrix} 0 & 0 & 0 & 0 \\ 0 & H_{\mathrm{ww}} & K_{\mathrm{wg}} & 0 \\ 0 & K_{\mathrm{gw}} & H_{\mathrm{gg}} & 0 \\ 0 & K_{\mathrm{tw}} & 0 & H_{\mathrm{tt}} \end{bmatrix} \tag{2.5.35}$$

$$\boldsymbol{X}=\begin{Bmatrix} \overline{\mathbf{u}} \\ \overline{\mathbf{p}}^{\mathrm{w}} \\ \overline{\mathbf{p}}^{\mathrm{g}} \\ \overline{\mathbf{T}} \end{Bmatrix} \tag{2.5.36}$$

$$\boldsymbol{F}=\begin{Bmatrix} \dfrac{\partial \mathbf{f}^{\mathrm{u}}}{\partial t} \\ \mathbf{f}^{\mathrm{w}} \\ \mathbf{f}^{\mathrm{g}} \\ \mathbf{f}^{\mathrm{t}} \end{Bmatrix} \tag{2.5.37}$$

The matrices are defined as following:

$$C_{\mathrm{ws}}=\int_{\Omega}\mathbf{N}_{\mathbf{p}}^{\mathbf{T}}\left[\alpha\left(\rho_{gw}\mathrm{S}_{\mathrm{g}}+\rho_{w}\mathrm{S}_{\mathrm{w}}\right)\right]\mathbf{m}^{T}\,\mathbf{L}\,\mathbf{N}_{\mathbf{u}}\mathrm{d}\Omega \tag{2.5.38}$$

$$\begin{aligned} P_{\mathrm{ww}}=&\int_{\Omega}\mathbf{N}_{\mathbf{p}}^{\mathbf{T}}\left[\left(\frac{\alpha-n}{K_{s}}\mathrm{S}_{\mathrm{w}}\left(\rho_{gw}\mathrm{S}_{\mathrm{g}}+\rho_{w}\mathrm{S}_{\mathrm{w}}\right)+\rho_{w}\mathrm{S}_{\mathrm{w}}\frac{n}{K_{w}}\right)\mathbf{N}_{\mathbf{p}}\right]\mathrm{d}\Omega \\ &-\int_{\Omega}\mathbf{N}_{\mathbf{p}}^{\mathbf{T}}\left(\mathrm{S}_{\mathrm{g}}\,n\frac{M_{w}}{\vartheta R}\frac{\partial p_{gw}}{\partial p_{c}}\mathbf{N}_{\mathbf{p}}\right)\mathrm{d}\Omega \\ &-\int_{\Omega}\mathbf{N}_{\mathbf{p}}^{\mathbf{T}}\left\{\left[\frac{\alpha-n}{K_{s}}\left(\rho_{gw}\mathrm{S}_{\mathrm{g}}p_{c}+\rho_{w}\mathrm{S}_{\mathrm{w}}p_{w}-\rho_{w}\mathrm{S}_{\mathrm{w}}p_{c}\right)\right.\right. \\ &\left.\left.+n\left(\rho_{w}-p_{gw}\right)\frac{\partial S_{\mathrm{w}}}{\partial p_{c}}\mathbf{N}_{\mathbf{p}}\right]\right\}\mathrm{d}\Omega \end{aligned} \tag{2.5.39}$$

$$C_{\mathrm{wg}}=\int_{\Omega}\mathbf{N}_{\mathbf{p}}^{\mathbf{T}}\left[\frac{\alpha-n}{K_s}\mathrm{S_g}\left(\rho_{gw}\mathrm{S_g}+\rho_w\mathrm{S_w}\right)\mathbf{N}_{\mathbf{p}}\right]\mathrm{d}\Omega$$
$$+\int_{\Omega}\mathbf{N}_{\mathbf{p}}^{\mathbf{T}}\left(\mathrm{S_g}\,n\frac{M_w}{\vartheta R}\frac{\partial p_{gw}}{\partial p_c}\mathbf{N}_{\mathbf{p}}\right)\mathrm{d}\Omega \qquad (2.5.40)$$
$$\int_{\Omega}\mathbf{N}_{\mathbf{p}}^{\mathbf{T}}\left\{\left[\frac{\alpha-n}{K_s}\left(\rho_{gw}\mathrm{S_g}p_c+\rho_w\mathrm{S_w}p_w-\rho_w\mathrm{S_w}p_w\right)+n\left(\rho_w-\rho_{gw}\right)\frac{\partial S_{\mathrm{w}}}{\partial p_c}\mathbf{N}_{\mathbf{p}}\right]\right\}\mathrm{d}\Omega$$

$$C_{\mathrm{wt}}=-\int_{\Omega}\mathbf{N}_{\mathbf{p}}^{\mathbf{T}}\left(S_{\mathrm{w}}\beta_{sgw}\right)\mathbf{N}_{\mathbf{t}}\mathrm{d}\Omega+\int_{\Omega}\mathbf{N}_{\mathbf{p}}^{\mathbf{T}}\left[\mathrm{S_g}\,n\frac{M_w}{\vartheta R}\left(\frac{\partial p_{gw}}{\partial T}-\frac{p_{gw}}{\vartheta}\right)\mathbf{N}_{\mathbf{t}}\right]\mathrm{d}\Omega$$
$$+\int_{\Omega}\mathbf{N}_{\mathbf{p}}^{\mathbf{T}}\left\{\left[\frac{\alpha-n}{K_s}\left(\rho_{gw}\mathrm{S_g}p_c+\rho_w\mathrm{S_w}p_w-\rho_w\mathrm{S_w}p_c\right)\right.\right. \qquad (2.5.41)$$
$$\left.\left.+n\left(\rho_w-\rho_{gw}\right)\right]\frac{\partial S_{\mathrm{w}}}{\partial T}\mathbf{N}_{\mathbf{t}}\right\}\mathrm{d}\Omega$$

$$H_{\mathrm{ww}}=\int_{\Omega}\left(\nabla\mathbf{N}_{\mathbf{p}}\right)^{T}\rho_w\frac{\mathbf{k}k_{rw}}{\mu_w}\nabla\mathbf{N}_{\mathbf{p}}\,\mathrm{d}\Omega$$
$$+\int_{\Omega}\left(\nabla\mathbf{N}_{\mathbf{p}}\right)^{T}\rho_g\frac{M_aM_w}{M_{\mathrm{g}}^2}\mathbf{D}_{\mathbf{g}}\frac{1}{p_g}\frac{\partial p_{gw}}{\partial p_c}\nabla\mathbf{N}_{\mathbf{p}}\,\mathrm{d}\Omega \qquad (2.5.42)$$

$$K_{\mathrm{wg}}=-\int_{\Omega}\left(\nabla\mathbf{N}_{\mathbf{p}}\right)^{T}\left[-\rho_g\frac{M_aM_w}{M_{\mathrm{g}}^2}\mathbf{D}_{\mathbf{g}}\right.$$
$$\left.\cdot\left(\frac{1}{p_g}\frac{\partial p_{gw}}{\partial p_c}\nabla\mathbf{N}_{\mathbf{p}}-\frac{p_{gw}}{\left(\rho_g\right)^2}\nabla\mathbf{N}_{\mathbf{p}}\right)-\rho_{gw}\frac{\mathbf{k}k_{rg}}{\mu_g}\nabla\mathbf{N}_{\mathbf{p}}\right]\mathrm{d}\Omega \qquad (2.5.43)$$

$$C_{\mathrm{gs}}=\int_{\Omega}\mathbf{N}_{\mathbf{p}}^{\mathbf{T}}\,\alpha\,\rho_{ga}\mathrm{S_g}\mathbf{m}^{T}\,\mathbf{L}\,\mathbf{N}_{\mathbf{u}}\mathrm{d}\Omega \qquad (2.5.44)$$

$$C_{\mathrm{gw}}=\int_{\Omega}\mathbf{N}_{\mathbf{p}}^{\mathbf{T}}\frac{\alpha-n}{K_s}\mathrm{S_w}\mathrm{S}_g\rho_{ga}\mathbf{N}_{\mathbf{p}}\mathrm{d}\Omega+\int_{\Omega}\mathbf{N}_{\mathbf{p}}^{\mathbf{T}}\left[\left(\frac{\alpha-n}{K_s}\mathrm{S_g}p_c+n\right)\rho_{ga}\frac{\partial S_{\mathrm{w}}}{\partial p_c}\mathbf{N}_{\mathbf{p}}\right]\mathrm{d}\Omega$$
$$+\int_{\Omega}\mathbf{N}_{\mathbf{p}}^{\mathbf{T}}\,\mathrm{S_g}\,n\frac{M_w}{\vartheta R}\frac{\partial p_{gw}}{\partial p_c}\mathbf{N}_{\mathbf{p}}\mathrm{d}\Omega \qquad (2.5.45)$$

$$P_{\mathrm{gg}}=\int_{\Omega}\mathbf{N}_{\mathbf{p}}^{\mathrm{T}}\frac{\alpha-n}{K_s}\mathrm{S}_g^2\rho_{ga}\mathbf{N}_{\mathbf{p}}\,\mathrm{d}\Omega-\int_{\Omega}\mathbf{N}_{\mathbf{p}}^{\mathrm{T}}\left[\left(\frac{\alpha-n}{K_s}\mathrm{S}_{\mathrm{g}}p_c+n\right)\rho_{ga}\frac{\partial S_{\mathrm{w}}}{\partial p_c}\mathbf{N}_{\mathbf{p}}\right]\mathrm{d}\Omega$$
$$+\int_{\Omega}\mathbf{N}_{\mathbf{p}}^{\mathrm{T}}\mathrm{S}_{\mathrm{g}}\,n\frac{M_a}{\vartheta R}\mathbf{N}_{\mathbf{p}}\mathrm{d}\Omega-\int_{\Omega}\mathbf{N}_{\mathbf{p}}^{\mathrm{T}}\left(\mathrm{S}_{\mathrm{g}}\,n\frac{M_w}{\vartheta R}\frac{\partial p_{gw}}{\partial p_c}\mathbf{N}_{\mathbf{p}}\right)\mathrm{d}\Omega \tag{2.5.46}$$

$$C_{\mathrm{gt}}=-\int_{\Omega}\mathbf{N}_{\mathbf{p}}^{\mathrm{T}}\rho_{ga}\beta_{sg}\mathbf{N}_{\mathbf{t}}\mathrm{d}\Omega+\int_{\Omega}\mathbf{N}_{\mathbf{p}}^{\mathrm{T}}\left(\frac{\alpha-n}{K_s}\mathrm{S}_{\mathrm{g}}p_c+n\right)\rho_{ga}\frac{\partial S_{\mathrm{w}}}{\partial T}\mathbf{N}_{\mathbf{t}}\mathrm{d}\Omega$$
$$-\int_{\Omega}\mathbf{N}_{\mathbf{p}}^{\mathrm{T}}\left[\mathrm{S}_{\mathrm{g}}\,n\frac{M_a}{\vartheta^2R}\mathbf{N}_{\mathbf{t}}+\mathrm{S}_{\mathrm{g}}\,n\frac{M_w}{\vartheta R}\left(\frac{\partial p_{gw}}{\partial T}-\frac{p_{gw}}{\vartheta}\right)\mathbf{N}_{\mathbf{t}}\right]\mathrm{d}\Omega \tag{2.5.47}$$

$$K_{\mathrm{gw}}=\int_{\Omega}\left(\nabla\mathbf{N}_{\mathbf{p}}\right)^T\rho_g\frac{M_aM_w}{M_{\mathrm{g}}^2}\mathbf{D}_{\mathbf{g}}\frac{1}{p_g}\frac{\partial p_{gw}}{\partial p_c}\nabla\mathbf{N}_{\mathbf{p}}\mathrm{d}\Omega \tag{2.5.48}$$

$$H_{\mathrm{gg}}=\int_{\Omega}\left(\nabla\mathbf{N}_{\mathbf{p}}\right)^T\rho_{ga}\frac{\mathbf{k}k_{rg}}{\mu_g}\nabla\mathbf{N}_{\mathbf{p}}\,\mathrm{d}\Omega$$
$$-\int_{\Omega}\left(\nabla\mathbf{N}_{\mathbf{p}}\right)^T\rho_g\frac{M_aM_w}{M_{\mathrm{g}}^2}\mathbf{D}_{\mathbf{g}}\left(\frac{1}{p_g}\frac{\partial p_{gw}}{\partial p_c}\nabla\mathbf{N}_{\mathbf{p}}-\frac{p_{gw}}{\left(p_g\right)^2}\nabla\mathbf{N}_{\mathbf{p}}\right)\mathrm{d}\Omega \tag{2.5.49}$$

$$C_{\mathrm{ts}}=\int_{\Omega}\mathbf{N}_{\mathbf{t}}^{\mathrm{T}}\Delta H_{vap}\,\alpha\,\rho_w\mathrm{S}_{\mathrm{w}}\mathbf{m}^T\,\mathbf{L}\,\mathbf{N}_{\mathbf{u}}\mathrm{d}\Omega \tag{2.5.50}$$

$$C_{\mathrm{tw}}=\int_{\Omega}\mathbf{N}_{\mathbf{t}}^{\mathrm{T}}\Delta H_{vap}\,\rho_w\left(\frac{\alpha-n}{K_s}\mathrm{S}_{\mathrm{w}}^2+\mathrm{S}_{\mathrm{w}}\frac{n}{K_w}\right)\mathbf{N}_{\mathbf{p}}\mathrm{d}\Omega$$
$$+\int_{\Omega}\mathbf{N}_{\mathbf{p}}^{\mathrm{T}}\Delta H_{vap}\left\{\rho_w\left(\frac{\alpha-n}{K_s}\mathrm{S}_{\mathrm{w}}p_w-\frac{\alpha-n}{K_s}\mathrm{S}_{\mathrm{w}}p_g+n\right)\frac{\partial S_{\mathrm{w}}}{\partial p_c}\mathbf{N}_{\mathbf{p}}\right\}\mathrm{d}\Omega \tag{2.5.51}$$

$$C_{\mathrm{tg}}=\int_{\Omega}\mathbf{N}_{\mathbf{t}}^{\mathrm{T}}\Delta H_{vap}\,\rho_w\frac{\alpha-n}{K_s}\mathrm{S}_{\mathrm{w}}\mathrm{S}_{\mathrm{g}}\mathbf{N}_{\mathbf{p}}\mathrm{d}\Omega$$
$$-\int_{\Omega}\mathbf{N}_{\mathbf{p}}^{\mathrm{T}}\Delta H_{vap}\left\{\rho_w\left(\frac{\alpha-n}{K_s}\mathrm{S}_{\mathrm{w}}p_w-\frac{\alpha-n}{K_s}\mathrm{S}_{\mathrm{w}}p_g+n\right)\frac{\partial S_{\mathrm{w}}}{\partial p_c}\mathbf{N}_{\mathbf{p}}\right\}\mathrm{d}\Omega \tag{2.5.52}$$

$$P_{\mathrm{tt}}=\int_{\Omega}\mathbf{N}_{\mathbf{t}}^{\mathrm{T}}\left(\rho C_p\right)_{eff}\mathbf{N}_{\mathbf{t}}\mathrm{d}\Omega+\int_{\Omega}\mathbf{N}_{\mathbf{t}}^{\mathrm{T}}\Delta H_{vap}\left[\beta_{sw}\mathbf{N}_{\mathbf{t}}-\rho_w\left(\frac{\alpha-n}{K_s}\mathrm{S}_{\mathrm{w}}p_w\right.\right.$$
$$\left.\left.-\frac{\alpha-n}{K_s}\mathrm{S}_{\mathrm{w}}p_g+n\right)\frac{\partial S_{\mathrm{w}}}{\partial T}\mathbf{N}_{\mathbf{t}}\right]\mathrm{d}\Omega \tag{2.5.53}$$

$$K_{\mathrm{tw}} = -\int_{\Omega} \left(\nabla \mathbf{N}_{\mathbf{t}}\right)^{T} \Delta H_{vap}\, \rho_{w} \frac{\mathbf{k} k_{rw}}{\mu_{w}} \nabla \mathbf{N}_{\mathbf{p}} \mathrm{d}\Omega \tag{2.5.54}$$

$$\begin{aligned} H_{\mathrm{tt}} &= \int_{\Omega} \mathbf{N}_{\mathbf{t}}^{\mathbf{T}} \left[n \mathrm{S}_{\mathrm{w}} \rho_{w} C_{p}^{w} \frac{\mathbf{k} k_{rw}}{\mu_{w}} \left(-\nabla p_{w} + \rho_{w} \mathbf{g}\right)^{T} \right] \nabla \mathbf{N}_{\mathbf{t}} \mathrm{d}\Omega \\ &+ \int_{\Omega} \mathbf{N}_{\mathbf{t}}^{\mathbf{T}} \left[n \mathrm{S}_{\mathrm{g}} \rho_{g} C_{p}^{g} \frac{\mathbf{k} k_{rg}}{\mu_{g}} \left(-\nabla p_{g} + \rho_{g} \mathbf{g}\right)^{T} \right] \nabla \mathbf{N}_{\mathbf{t}} \mathrm{d}\Omega + \int_{\Omega} \left(\nabla \mathbf{N}_{\mathbf{t}}\right)^{T} \chi_{eff} \nabla \mathbf{N}_{\mathbf{t}} \mathrm{d}\Omega \end{aligned} \tag{2.5.55}$$

The right hand side terms of the (2.5.23), (2.5.30), (2.5.31) and (2.5.32) are

$$\mathbf{f}_{u} = \int_{\Omega} \mathbf{N}_{u}^{T} \left[\rho_{s} \left(n-1\right) + S_{w} n \rho_{w} + S_{g} n \rho_{g} \right] \mathbf{g}\, d\Omega + \int_{\Gamma} \mathbf{N}_{u}^{T} \overline{\mathbf{t}}\, d\Gamma \tag{2.5.56}$$

$$\begin{aligned} \mathbf{f}_{w} &= -\int_{\Gamma} \mathbf{N}_{p}^{T} \left[q_{w} + q_{gw} + \beta_{c} \left(\rho_{gw} - \rho_{gw}^{\infty}\right) \right] d\Gamma \\ &+ \int_{\Omega} \left(\nabla \mathbf{N}_{p}\right)^{T} \rho_{w} \frac{\mathbf{k}\, k_{rw}}{\mu_{w}} \rho_{w} \mathbf{g}\, d\Omega + \int_{\Omega} \left(\nabla \mathbf{N}_{p}\right)^{T} \rho_{gw} \frac{\mathbf{k}\, k_{rg}}{\mu_{g}} \rho_{g} \mathbf{g}\, d\Omega \end{aligned} \tag{2.5.57}$$

$$\mathbf{f}_{g} = -\int_{\Gamma} \mathbf{N}_{p}^{T} q_{ga}\, d\Gamma \tag{2.5.58}$$

$$\mathbf{f}_{T} = -\int_{\Omega} \left(\nabla \mathbf{N}_{T}\right)^{T} \Delta H_{vap}\, \rho_{w} \frac{\mathbf{k}\, k_{rw}}{\mu_{w}} \rho_{w} \mathbf{g}\, d\Omega - \int_{\Gamma} \mathbf{N}_{t}^{T} \left[q_{T} + \alpha_{c} \left(T - T^{\infty}\right) \right] d\Gamma = 0 \tag{2.5.59}$$

2.6. Isothermal airflow and waterflow in deforming porous medium

This case foreseen two fluids that are moving both and one of these has the capability to displace the other fluid from pores during the deformation process. In most of engineering applications, that involve soils as material for a constructions or granular material is studied in order to model natural phenomena, such landslides or debris flow, the effect of temperature can be neglected and the full formulation presented in the section 2.5 can be simplified. This is not the case of modelling concrete or other construction porous material, subjected to fire o high temperature gradient, because the variation of temperature in time is very high in certain cases and in the same way the temperature gradients. In these cases, the effect of the

phase change from liquid to gas has a paramount role on determining the pore pressure that can reach high levels and can produce spalling effects. In the case of an aquifer used as a storage of air or gas, or for a tunnel or shaft construction below the water table, where seepage towards the opening is prevented by the use of compressed air, the isothermal conditions is accepted.

Dealing with such problems, means that the basic variables involved on the system of equations mentioned a while ago, reduce to the three Cartesian directions u_x, u_y, u_z , the water pressure p_w and the gas pressure p_g .

In order to investigate isothermal process, such the cases discussed above or such isothermal consolidation of unsaturated soil, the system of equations in the form (2.5.23), (2.5.30), (2.5.31) and (2.5.32) has to be changed, due that the dependency of some processes from temperature gradients and thermal energy exchange to one phase to another can be neglected, resulting in a simplification of the set of equations. The temperature doesn't vary during the processes, and so, can be excluded from computation, except of using the reference temperature ϑ when is needed. In the simplified set of equations, now, the mass balance equations that will be used in the following formulation, take into account of the liquid water mass balance, this last and of the gas mass balance equation, considered as a mixture of dry air and water vapour. This assumption holds by the fact that without thermal variations or energy exchanges between the phases, the source term $\dot{m}$ is every time null and the liquid water and the gas mixture, preserve during the processes.

Again the linear momentum balance equation (2.2.1) and the density of the multiphase medium (2.2.3) hold. The mass balance equation for water and gas is obtained from the (1.4.18) and (1.4.22) neglecting the accelerations terms (except gravity), the term that takes into account of any phase change ($\dot{m}=0$), and the gradient of the water and gas density that depends on the temperature. The resulting equations for the water and the gas mixture of air and water vapour are:

$$\begin{aligned}&\left(\frac{\alpha-n}{K_S}S_w^2+\frac{n\,S_w}{K_W}\right)\frac{\partial p_w}{\partial t}+\frac{\alpha-n}{K_S}S_w S_g\frac{\partial p_g}{\partial t}\\&+\alpha\,S_w\,\mathbf{m}^T\boldsymbol{L}\frac{\partial \mathbf{u}}{\partial t}+\left(\frac{\alpha-n}{K_S}p_c\,S_w+n\right)\frac{\partial S_w}{\partial t}+\nabla^T\cdot\left[\frac{\mathbf{k}\,k_{rw}}{\mu_w}\left(-\nabla p_w+\rho_w\mathbf{g}\right)\right]=0\end{aligned}\qquad(2.6.1)$$

$$\frac{\alpha-n}{K_S}S_w S_g\frac{\partial p_w}{\partial t}+\frac{\alpha-n}{K_S}S_g^2\frac{\partial p_g}{\partial t}-\left(\frac{\alpha-n}{K_S}p_c S_g+n\right)\frac{\partial S_w}{\partial t}+$$
$$+\alpha S_g\,\mathbf{m}^T\boldsymbol{L}\frac{\partial \mathbf{u}}{\partial t}+\frac{nS_g}{\rho_g}\frac{\partial}{\partial t}\left(\frac{p_g M_g}{\vartheta R}\right)+\nabla^T\cdot\left[\frac{\mathbf{k}\,k_{rg}}{\mu_g}\left(-\nabla p_g+\rho_g\mathbf{g}\right)\right]=0 \tag{2.6.2}$$

Effective stress principle (2.2.2) and constitutive equation (1.3.13) hold. The capillary pressure relationship (1.2.6) for isothermal conditions can be rewritten as

$$S_w = S_w\left(p_c\right) \tag{2.6.3}$$

All other needed properties hold like the general case.

The initial conditions (2.4.1) and boundary conditions (2.4.2) are valid also in the isothermal case, like the general case, with except for the conditions on initial temperature that now is constant during time and equal to ϑ on whole domain. The traction boundary conditions (2.4.3) for the stress are unchanged. The water flux on boundary Γ_w^q reduces to

$$\rho_w\frac{\mathbf{k}\,k^{rw}}{\mu^r}\left(-\nabla p_w+\rho_w\mathbf{g}\right)^T\cdot\mathbf{n}=q_w \text{ on } \quad \Gamma_w^q \tag{2.6.4}$$

And the gas flux on boundary Γ_g^q reduces to

$$\rho_g\frac{\mathbf{k}\,k_{rg}}{\mu_g}\left(-\nabla p_g+\rho_g\mathbf{g}\right)^T\cdot\mathbf{n}=q_g \quad \text{on} \quad \Gamma_g^q \tag{2.6.5}$$

Displacements and pressures values can be expressed in terms of their nodal values like in (2.5.12):

$$\mathbf{u}=\mathbf{N}_u\bar{\mathbf{u}},\quad p_w=\mathbf{N}_p\bar{\mathbf{p}}_w,\quad p_g=\mathbf{N}_p\bar{\mathbf{p}}_g \tag{2.6.6}$$

Like in the section 2.5 the application of standard finite element discretization procedures, i.e. the weighted residual method and then the Galerkin method [3], and the consequent substitution of weight functions with the approximations (2.6.6) followed by an introduction of the effective stress principle (2.2.2), results in the following expression for the equilibrium equation

$$\int_\Omega\mathbf{B}^T\boldsymbol{\sigma}''\,d\Omega-\int_\Omega\alpha\,\mathbf{m}^T\left(S_w\mathbf{N}_p\bar{\mathbf{p}}_w+S_g\mathbf{N}_p\bar{\mathbf{p}}_g\right)d\Omega=$$
$$\int_\Omega\mathbf{N}_u^T\left(\rho_s\left(n-1\right)+S_w n\rho_w+S_g n\rho_g\right)\mathbf{g}\,d\Omega+\int_{\Gamma_u^q}\mathbf{N}_u^T\bar{\mathbf{t}}\,d\Gamma \tag{2.6.7}$$

That is the same of (2.5.13), but now for a linear elastic solid holds

$$\mathbf{P}(\bar{\mathbf{u}}) = \int_{\Omega} \mathbf{B}^T \sigma'' d\Omega = \mathbf{K}_e \bar{\mathbf{u}} \tag{2.6.8}$$

due that the isothermal conditions allow that thermal contribute have no contribution.

Again for non-linear solid phase behaviour the tangent stiffness matrices has to be taken into account and so the expression (2.5.23), change in

$$\mathrm{K_T} \frac{\partial \bar{\mathbf{u}}}{\partial t} - C_{\mathrm{sw}} \frac{\partial \bar{\mathbf{p}}^w}{\partial t} - C_{\mathrm{sg}} \frac{\partial \bar{\mathbf{p}}^g}{\partial t} = \frac{\partial \mathbf{f}^u}{\partial t} \tag{2.6.9}$$

The matrices $\mathrm{K_T}$, C_{sw} and C_{sg} are defined as the (2.5.24), the (2.5.26) and the (2.5.27), as the $\mathbf{f}^u$ term is defined as the (2.5.56).

The specific moisture content

$$C_S = \frac{\partial S_w}{\partial p_c} \tag{2.6.10}$$

arises from considering in the mass balance equations (2.6.1) and (2.6.2) that

$$n \frac{\partial S_w}{\partial t} = n \frac{\partial S_w}{\partial p_c} \frac{\partial p_c}{\partial t} = C_S \left(\frac{\partial p_g}{\partial t} - \frac{\partial p_w}{\partial t} \right) \tag{2.6.11}$$

The weighted residual method applied to the balance equations gives for the liquid water phase the following expression

$$\begin{aligned}
&\int_{\Omega} \mathbf{w}^{*T} \left[\frac{\alpha - n}{K_S} S_w \left(S_w - p_w \frac{C_S}{n} + p_g \frac{C_S}{n} \right) + \frac{n S_w}{K_W} - C_S \right] \frac{\partial p_w}{\partial t} d\Omega \\
&\int_{\Omega} \mathbf{w}^{*T} \left[\frac{\alpha - n}{K_S} S_w \left(S_g + p_w \frac{C_S}{n} - p_g \frac{C_S}{n} \right) + C_S \right] \frac{\partial p_g}{\partial t} \, d\Omega \\
&+ \int_{\Omega} \mathbf{w}^{*T} \left[+ \alpha S_w \mathbf{m}^T \boldsymbol{L} \frac{\partial \mathbf{u}}{\partial t} \right] d\Omega - \int_{\Omega} \left(\nabla \mathbf{w}^{*T} \right) \left[\rho_w \frac{\mathbf{k} \, k_{rw}}{\mu_w} \left(-\nabla p_w + \rho_w \mathbf{g} \right) \right] d\Omega \\
&+ \int_{\Gamma_w^q} \mathbf{w}^{*T} \left[\frac{q_w}{\rho_w} \right] d\Gamma = 0
\end{aligned} \tag{2.6.12}$$

And for the gas phase

$$\begin{aligned}
&\int_{\Omega} \mathbf{w}^{\bullet T}\left[\frac{\alpha-n}{K_S} S_g\left(S_g - p_g\frac{C_S}{n} + p_w\frac{C_S}{n}\right) + \frac{nS_g M_g}{\rho_g \vartheta R} - C_S\right]\frac{\partial p_g}{\partial t} d\Omega \\
&\int_{\Omega} \mathbf{w}^{\bullet T}\left[\frac{\alpha-n}{K_S} S_g\left(S_w + p_g\frac{C_S}{n} - p_w\frac{C_S}{n}\right) + C_S\right]\frac{\partial p_w}{\partial t}\, d\Omega \\
&+\int_{\Omega} \mathbf{w}^{\bullet T}\left[+\alpha S_g\, \mathbf{m}^T \boldsymbol{L}\frac{\partial \mathbf{u}}{\partial t}\right] d\Omega - \int_{\Omega}\left(\nabla \mathbf{w}^{\bullet T}\right)\left[\rho_w \frac{\mathbf{k}\, k_{rg}}{\mu_g}\left(-\nabla p_w + \rho_w \mathbf{g}\right)\right] d\Omega \\
&+\int_{\Gamma_w^q} \mathbf{w}^{\bullet T}\left[\frac{q_g}{\rho_g}\right] d\Gamma = 0
\end{aligned} \tag{2.6.13}$$

Substituting the weight functions with the approximations (2.6.6), as done in section 2.5 the (2.5.30) and the (2.5.31) change in

$$C_{sw}^T \frac{\partial \overline{\mathbf{u}}}{\partial t} + P_{\mathrm{ww}} \frac{\partial \overline{\mathbf{p}}^w}{\partial t} + C_{\mathrm{wg}} \frac{\partial \overline{\mathbf{p}}^g}{\partial t} + H_{\mathrm{ww}}\, \overline{\mathbf{p}}^w = \mathbf{f}^w \tag{2.6.14}$$

$$C_{sg}^T \frac{\partial \overline{\mathbf{u}}}{\partial t} + C_{\mathrm{gw}} \frac{\partial \overline{\mathbf{p}}^w}{\partial t} + P_{\mathrm{gg}} \frac{\partial \overline{\mathbf{p}}^g}{\partial t} + H_{\mathrm{gg}}\, \overline{\mathbf{p}}^g = \mathbf{f}^g \tag{2.6.15}$$

Again the set of three differential equations (2.6.7), (2.6.14) and (2.6.15) can be written in the synthetic form (2.5.33). The hyper matrix and vector of the system now will be

$$\boldsymbol{S} = \begin{bmatrix} \mathrm{K_T} & -C_{\mathrm{sw}} & -C_{\mathrm{sg}} \\ C_{sw}^T & P_{\mathrm{ww}} & C_{\mathrm{wg}} \\ C_{sg}^T & C_{\mathrm{gw}} & P_{\mathrm{gg}} \end{bmatrix} \tag{2.6.16}$$

$$\boldsymbol{H} = \begin{bmatrix} 0 & 0 & 0 \\ 0 & H_{\mathrm{ww}} & 0 \\ 0 & 0 & H_{\mathrm{gg}} \end{bmatrix} \tag{2.6.17}$$

$$\boldsymbol{X} = \begin{Bmatrix} \overline{\mathbf{u}} \\ \overline{\mathbf{p}}^{\mathrm{w}} \\ \overline{\mathbf{p}}^{\mathrm{g}} \end{Bmatrix} \tag{2.6.18}$$

$$\boldsymbol{F} = \begin{Bmatrix} \dfrac{\partial \mathbf{f}^{\mathrm{u}}}{\partial t} \\ \mathbf{f}^{\mathrm{w}} \\ \mathbf{f}^{\mathrm{g}} \\ \end{Bmatrix} \tag{2.6.19}$$

Others matrices are defined as follows:

$$C_{sw}^{T} = \int_{\Omega} \mathbf{N}_{\mathbf{p}}^{\mathbf{T}} \, \alpha \, S_w \mathbf{m}^{T} \, \mathbf{L} \, \mathbf{N}_{\mathbf{u}} \mathrm{d}\Omega \tag{2.6.20}$$

$$P_{\mathrm{ww}} = \int_{\Omega} \mathbf{N}_{\mathbf{p}}^{\mathbf{T}} \left[\frac{\alpha - n}{K_S} S_w \left(S_w - p_w \frac{C_S}{n} + p_g \frac{C_S}{n} \right) + \frac{n S_w}{K_W} - C_S \right] \mathbf{N}_{\mathbf{p}} \mathrm{d}\Omega \tag{2.6.21}$$

$$C_{\mathrm{wg}} = \int_{\Omega} \mathbf{N}_{\mathbf{p}}^{\mathbf{T}} \left[\frac{\alpha - n}{K_S} S_w \left(S_g + p_w \frac{C_S}{n} - \rho_g \frac{C_S}{n} \right) + C_S \right] \mathbf{N}_{\mathbf{p}} \mathrm{d}\Omega \tag{2.6.22}$$

$$H_{\mathrm{ww}} = \int_{\Omega} \left(\nabla \mathbf{N}_{\mathbf{p}} \right)^{T} \frac{\mathbf{k} k_{rw}}{\mu_w} \nabla \mathbf{N}_{\mathbf{p}} \, \mathrm{d}\Omega \tag{2.6.23}$$

$$C_{\mathrm{gs}} = \int_{\Omega} \mathbf{N}_{\mathbf{p}}^{\mathbf{T}} \, \alpha S_g \mathbf{m}^{T} \, \mathbf{L} \, \mathbf{N}_{\mathbf{u}} \mathrm{d}\Omega \tag{2.6.24}$$

$$C_{\mathrm{gw}} = \int_{\Omega} \mathbf{N}_{\mathbf{p}}^{\mathbf{T}} \left[\frac{\alpha - n}{K_s} S_g \left(S_w + p_g \frac{C_S}{n} - p_w \frac{C_S}{n} \right) + C_S \right] \mathbf{N}_{\mathbf{p}} \mathrm{d}\Omega \tag{2.6.25}$$

$$P_{\mathrm{gg}} = \int_{\Omega} \mathbf{N}_{\mathbf{p}}^{\mathbf{T}} \left[\frac{\alpha - n}{K_S} S_g \left(S_g - p_g \frac{C_S}{n} + p_w \frac{C_S}{n} \right) + \frac{n S_g M_g}{\rho_g \vartheta R} - C_S \right] \mathbf{N}_{\mathbf{p}} \mathrm{d}\Omega \tag{2.6.26}$$

$$H_{\mathrm{gg}} = \int_{\Omega} \left(\nabla \mathbf{N}_{\mathbf{p}} \right)^{T} \frac{\mathbf{k} k_{rg}}{\mu_g} \nabla \mathbf{N}_{\mathbf{p}} \, \mathrm{d}\Omega \tag{2.6.27}$$

The specific moisture content that is present in the (2.6.21), the (2.6.22), the (2.6.25) and the (2.6.26) corresponds to the derivative of the degree of water saturation function (or capillary pressure function) (2.6.3). The expression of C_S depends on the formulation chosen from the ones proposed on section 1.5. In particular for Brooks and Corey [4, 5] relationship (1.5.8) the C_S is defined as:

$$\begin{aligned} C_S &= \frac{\partial S_w}{\partial p_c} = -\left(1 - S_{w,irr} - S_{g,irr} \right) \frac{\lambda}{p_c} \left[\frac{p_b}{p_c} \right]^{\lambda} \quad for \; p_c > p_b \\ C_S &= \frac{\partial S_w}{\partial p_c} = 0 \qquad\qquad for \; p_c < p^b \end{aligned} \tag{2.6.28}$$

For the van Genuchten [6] relationship (1.5.14) the C_S is

$$C_S = \frac{\partial S_w}{\partial p_c} = -\frac{\left(1 - S_{w,irr} - S_{g,irr}\right) m\, n \left(\alpha\, p_c\right)^n \left[\left(\alpha\, p_c\right)^n + 1\right]^{-m-1}}{p_c} \qquad for\ p_c > 0 \tag{2.6.29}$$

For a detailed description of the parameter in the (2.6.28) and (2.6.29) please refer to section 1.5. It has been seen from numerical tests that C_S has to be set equal to 0 before reaching a null value of capillary pressure also using van Genuchten formulation that has not a limiting value like the Brooks and Corey formulation.

The right hand side terms of the (2.5.12), the (2.5.23) and the (2.5.24) are

$$\mathbf{f}_u = \int_\Omega \mathbf{N}_u^T \left[\rho_s \left(n-1\right) + S_w n \rho_w + S_g n \rho_g\right] \mathbf{g}\, d\Omega + \int_\Gamma \mathbf{N}_u^T \bar{\mathbf{t}}\, d\Gamma \tag{2.6.30}$$

$$\mathbf{f}_w = \int_\Omega \left(\nabla \mathbf{N}_p\right)^T \rho_w \frac{\mathbf{k}\, k_{rw}}{\mu_w} \rho_w \mathbf{g}\, d\Omega - \int_\Gamma \mathbf{N}_p^T \frac{q_w}{\rho_w} d\Gamma \tag{2.6.31}$$

$$\mathbf{f}_g = \int_\Omega \left(\nabla \mathbf{N}_p\right)^T \rho_g \frac{\mathbf{k}\, k_{rg}}{\mu_g} \rho_g \mathbf{g}\, d\Omega - \int_\Gamma \mathbf{N}_p^T \frac{q_g}{\rho_g} d\Gamma \tag{2.6.32}$$

Finally, further simplification to the set of equations can be achieved for example considering an isothermal one-phase flow in a partially saturated medium. In this case, instead of having the variation in time of both pressures (p_w and p_g), one of two, usually p_g , is fixed and take for example the value of atmospheric pressure, all along the time span and the whole domain. The degree of water saturation, so, is function only of water pressure, and due to the thermal and gas phase fixed degrees of freedom, the number of terms in the hyper matrices decrease again.

The simplest case is given by water flow in a fully saturated porous medium where the degree of water saturation is always equal to 1. These two cases are widely discussed on [1, 7].

2.7. Solution procedures. Time discretization

The analysis of water and gas flow as well as the heat flow through a partial saturated, deforming porous medium represents a field problem with at maximum

six degrees of freedom. By the way if isothermal processes have to been investigated, the isothermal set of equations can be solved, with relevant benefits on computational economy. Fixing the temperature degree of freedom, i.e. working with a fixed reference temperature, reduces the number of terms that has to been calculated to form the hyper matrices and the overall dimension of them as can see comparing the (2.5.34) and the (2.5.35), with the (2.6.16) and the (2.6.17).

The solution of the system of equations (2.5.33) both in the non-isothermal and isothermal version can be done in two basic ways:

- Monolithic approach
- Partitioned approach

The monolithic argumentation approach [3] first proposed by Incropera *et al.* [8] has the advantage to preserve the full coupling of the set of equations, resulting, however, in a lack of symmetry of the coefficient matrix for the combined equations after the discretization in time has been done. In order to try to preserve the symmetry of the system matrix the partitioned approach performs a partitioning of the combined system of equations after the integration in the time domain. One particular partitioning technique, proposed by Schrefler [9], produces a symmetric coefficient matrix and an effective gain in computing time. Both the monolithic argumentation approach and the partitioned solution procedure refer to the same discretization process for the time domain. The partitioning strategies are often adopted due to the fact that the solution of equations presented in this chapter can be separated and treated in two different steps. Thus, depending on the equations of the phase solved first, only one variable will be independent, and once calculated for the current time step the values will be utilized in the calculations of the others dependent variables, in order to fulfil the equilibrium and continuity equations. Despite the advantages in computational time and the possibility to use different kind or order of elements between the phases, the solution is affected by the fact that the computations for all phases are not contemporary and errors can occur in each phase. Insights on uncoupled solution methods are given by Morris [10].

The monolithic approach is the one selected for the present work, in order to obtain a direct solution and preserve the coupling of the system. The lack of symmetry of the system matrix, along with the lack in performance foreseen, will be treated with the adoption, in the F.E. code, of sparse solvers that are optimized for non-symmetric systems of equations.

The discretization in time can be done with the finite differences in time or with the weighted residual method in time with point collocation [2]. The same equations emanate from the two methods.

Considering the (2.5.33) and the hyper matrices involved in this equation, it can be easily seen that the matrices $\boldsymbol{S}$ (2.5.34) and $\boldsymbol{H}$ (2.5.35) are in general non-symmetric depending strongly by the unknowns vector $\boldsymbol{X}$ (2.5.36). With the generalized midpoint rule (or trapezoidal method) that has an implicit scheme, the unknowns vector and relative derivative can be approximated as

$$\left(\frac{\mathrm{d}\boldsymbol{X}}{\mathrm{d}t}\right)_{n+\theta} = \left(\boldsymbol{X}_{n+1} - \boldsymbol{X}_n\right)/\Delta t \qquad \boldsymbol{X}_{n+\theta} = (1-\theta)\boldsymbol{X}_n + \theta\,\boldsymbol{X}_{n+1} \tag{2.7.1}$$

and from the evaluation of the (2.5.33) at time $t_{n+\theta}$, it can be written

$$\left[\boldsymbol{S} + \theta\Delta t\,\boldsymbol{H}\right]\boldsymbol{X}_{n+1} = \left[\boldsymbol{S} - (1-\theta)\Delta t\,\boldsymbol{H}\right]\boldsymbol{X}_n + \Delta t\,\boldsymbol{F}_{n+\theta} \tag{2.7.2}$$

In the previous equation, Δt is the time step length, $\boldsymbol{X}_{n+1}$ and $\boldsymbol{X}_n$ are the state vectors at times t_{n+1} and t_n, θ is a parameter which has limits $0 \le \theta \le 1$ and its value may be obtained from the numerical properties of the scheme. Rewriting the (2.7.2) for the non-isothermal case gives

$$\begin{bmatrix} \mathrm{K_T} & -C_{\mathrm{sw}} & -C_{\mathrm{sg}} & \mathrm{K_{tT}} \\ C_{\mathrm{ws}} & P_{\mathrm{ww}} + \theta\Delta t H_{\mathrm{ww}} & C_{\mathrm{wg}} + \theta\Delta t K_{\mathrm{wg}} & C_{\mathrm{wt}} \\ C_{\mathrm{gs}} & C_{\mathrm{gw}} + \theta\Delta t K_{\mathrm{gw}} & P_{\mathrm{gg}} + \theta\Delta t H_{\mathrm{gg}} & C_{\mathrm{gt}} \\ C_{\mathrm{ts}} & C_{\mathrm{tw}} + \theta\Delta t K_{\mathrm{tw}} & C_{\mathrm{tg}} & P_{\mathrm{tt}} + \theta\Delta t H_{\mathrm{tt}} \end{bmatrix}_{n+\theta} \begin{Bmatrix} \overline{\mathbf{u}} \\ \overline{\mathbf{p}}^{\mathrm{w}} \\ \overline{\mathbf{p}}^{\mathrm{g}} \\ \overline{\mathbf{T}} \end{Bmatrix}_{n+1} =$$

$$\begin{bmatrix} \mathrm{K_T} & -C_{\mathrm{sw}} & -C_{\mathrm{sg}} & \mathrm{K_{tT}} \\ C_{\mathrm{ws}} & P_{\mathrm{ww}} - (1-\theta)\Delta t H_{\mathrm{ww}} & C_{\mathrm{wg}} - (1-\theta)\Delta t K_{\mathrm{wg}} & C_{\mathrm{wt}} \\ C_{\mathrm{gs}} & C_{\mathrm{gw}} - (1-\theta)\Delta t K_{\mathrm{gw}} & P_{\mathrm{gg}} - (1-\theta)\Delta t H_{\mathrm{gg}} & C_{\mathrm{gt}} \\ C_{\mathrm{ts}} & C_{\mathrm{tw}} - (1-\theta)\Delta t K_{\mathrm{tw}} & C_{\mathrm{tg}} & P_{\mathrm{tt}} - (1-\theta)\Delta t H_{\mathrm{tt}} \end{bmatrix}_{n+\theta} \tag{2.7.3}$$

$$\cdot \begin{Bmatrix} \overline{\mathbf{u}} \\ \overline{\mathbf{p}}^{\mathrm{w}} \\ \overline{\mathbf{p}}^{\mathrm{g}} \\ \overline{\mathbf{T}} \end{Bmatrix}_{n} + \Delta t \begin{Bmatrix} \dfrac{\partial \mathbf{f}^{\mathrm{u}}}{\partial t} \\ \mathbf{f}^{\mathrm{w}} \\ \mathbf{f}^{\mathrm{g}} \\ \mathbf{f}^{\mathrm{t}} \end{Bmatrix}_{n+\theta}$$

For $\theta = 1$ the scheme is fully implicit (forward differences) , with $\theta = 0$ results in a fully explicit scheme (backward differences), with $\theta = 0.5$ it results the Crank-

Nicolson scheme that is the one adopted for the analyses in the present work. For the monolithic approach also the value of $\theta = 0.875$ has been used with good results. Hwang *et al.* and Sandhu [11, 12] proposed different values for θ that lead to different schemes from the above mentioned. The matrices in the (2.7.2) are evaluated at time $t_{n+\theta}$.

For the isothermal case the (2.7.3) educes to

$$\begin{bmatrix} \mathrm{K_T} & -C_{\mathrm{sw}} & -C_{\mathrm{sw}} \\ C_{\mathrm{sw}}^T & P_{\mathrm{ww}} + \theta \Delta t H_{\mathrm{ww}} & C_{\mathrm{wg}} + \theta \Delta t K_{\mathrm{wg}} \\ C_{\mathrm{sg}}^T & C_{\mathrm{gw}} + \theta \Delta t K_{\mathrm{gw}} & P_{\mathrm{gg}} + \theta \Delta t H_{\mathrm{gg}} \end{bmatrix}_{n+\theta} \begin{Bmatrix} \overline{\mathbf{u}} \\ \overline{\mathbf{p}}^{\mathrm{w}} \\ \overline{\mathbf{p}}^{\mathrm{g}} \end{Bmatrix}_{n+1} =$$

$$\begin{bmatrix} \mathrm{K_T} & -C_{\mathrm{sw}} & -C_{\mathrm{sw}} \\ C_{\mathrm{sw}}^T & P_{\mathrm{ww}} - (1-\theta)\Delta t H_{\mathrm{ww}} & C_{\mathrm{wg}} - (1-\theta)\Delta t K_{\mathrm{wg}} \\ C_{\mathrm{sg}}^T & C_{\mathrm{gw}} - (1-\theta)\Delta t K_{\mathrm{gw}} & P_{\mathrm{gg}} - (1-\theta)\Delta t H_{\mathrm{gg}} \end{bmatrix}_{n+\theta} \begin{Bmatrix} \overline{\mathbf{u}} \\ \overline{\mathbf{p}}^{\mathrm{w}} \\ \overline{\mathbf{p}}^{\mathrm{g}} \end{Bmatrix}_{n} + \Delta t \begin{Bmatrix} \dfrac{\partial \mathbf{f}^{\mathrm{u}}}{\partial t} \\ \mathbf{f}^{\mathrm{w}} \\ \mathbf{f}^{\mathrm{g}} \\ \\ \end{Bmatrix}_{n+\theta} \qquad (2.7.4)$$

The components of (2.7.4) are the ones presented in section 2.6. The (2.7.2) can be rewritten in the following concise form and a single step finite difference operator can be obtained

$$\Psi\left(\boldsymbol{X}_{n+1}\right) = \left[\boldsymbol{S} + \theta \Delta t\, \boldsymbol{H}\right]_{n+\theta} \boldsymbol{X}_{n+1} - \left[\boldsymbol{S} - (1-\theta)\Delta t\, \boldsymbol{H}\right]_{n+\theta} \boldsymbol{X}_{n} - \Delta t\, \boldsymbol{F}_{n+\theta} = 0 \qquad (2.7.5)$$

where

$$\boldsymbol{X}_{n+\theta} = (1-\theta)\boldsymbol{X}_{n} + \theta \boldsymbol{X}_{n+1} \qquad (2.7.6)$$

and

$$\Psi\left(\boldsymbol{X}_{n+1}\right) = \left[\Psi^{u}\left(\boldsymbol{X}_{n+1}\right), \Psi^{w}\left(\boldsymbol{X}_{n+1}\right), \Psi^{g}\left(\boldsymbol{X}_{n+1}\right), \Psi^{T}\left(\boldsymbol{X}_{n+1}\right)\right]^{T} \qquad (2.7.7)$$

The coupled equation system (2.7.2), presented in section 2.5 and 2.6 reveals that the system of equations is non-linear and can be linearized by an iterative Newton-Raphson procedure, synthetically recalled as

$$\Psi^{\kappa}\left(\boldsymbol{X}_{n+1}^{i}\right) = -\left.\frac{\partial \Psi^{\kappa}}{\partial \boldsymbol{X}}\right|_{\boldsymbol{X}_{n+1}^{i}} \Delta \boldsymbol{X}_{n+1}^{i} \qquad \kappa = u, w, g, T \qquad (2.7.8)$$

In the previous, the Jacobian matrix takes the following form

$$\left.\frac{\partial \boldsymbol{\Psi}}{\partial \boldsymbol{X}}\right|_{\boldsymbol{X}_{n+1}^{i}} = \left[\begin{array}{cccc} \dfrac{\partial \boldsymbol{\Psi}^{u}}{\partial \overline{\mathbf{u}}} & \dfrac{\partial \boldsymbol{\Psi}^{u}}{\partial \overline{\mathbf{p}}_{w}} & \dfrac{\partial \boldsymbol{\Psi}^{u}}{\partial \overline{\mathbf{p}}_{g}} & \dfrac{\partial \boldsymbol{\Psi}^{u}}{\partial \overline{\overline{\mathbf{T}}}} \\ \dfrac{\partial \boldsymbol{\Psi}^{w}}{\partial \overline{\mathbf{u}}} & \dfrac{\partial \boldsymbol{\Psi}^{w}}{\partial \overline{\mathbf{p}}_{w}} & \dfrac{\partial \boldsymbol{\Psi}^{w}}{\partial \overline{\mathbf{p}}_{g}} & \dfrac{\partial \boldsymbol{\Psi}^{w}}{\partial \overline{\overline{\mathbf{T}}}} \\ \dfrac{\partial \boldsymbol{\Psi}^{g}}{\partial \overline{\mathbf{u}}} & \dfrac{\partial \boldsymbol{\Psi}^{g}}{\partial \overline{\mathbf{p}}_{w}} & \dfrac{\partial \boldsymbol{\Psi}^{g}}{\partial \overline{\mathbf{p}}_{g}} & \dfrac{\partial \boldsymbol{\Psi}^{g}}{\partial \overline{\overline{\mathbf{T}}}} \\ \dfrac{\partial \boldsymbol{\Psi}^{T}}{\partial \overline{\mathbf{u}}} & \dfrac{\partial \boldsymbol{\Psi}^{T}}{\partial \overline{\mathbf{p}}_{w}} & \dfrac{\partial \boldsymbol{\Psi}^{T}}{\partial \overline{\mathbf{p}}_{g}} & \dfrac{\partial \boldsymbol{\Psi}^{T}}{\partial \overline{\overline{\mathbf{T}}}} \end{array}\right]_{\boldsymbol{X}=\boldsymbol{X}_{n+1}^{i}} \tag{2.7.9}$$

with an unknowns increment vector that for the i-th iteration is

$$\Delta \boldsymbol{X}_{n+1}^{i} = \left[\Delta \overline{\mathbf{u}}_{n+1}^{i},\ \left(\Delta \overline{\mathbf{p}}^{w}\right)_{n+1}^{i},\ \left(\Delta \overline{\mathbf{p}}^{g}\right)_{n+1}^{i},\ \Delta \overline{\overline{\mathbf{T}}}_{n+1}^{i}\right]^{T} \tag{2.7.10}$$

The updating equations for the basic variable vector is

$$\boldsymbol{X}_{n+1}^{i+1} = \boldsymbol{X}_{n+1}^{i} + \Delta \boldsymbol{X}_{n+1}^{i} \tag{2.7.11}$$

Jacobian matrix can be updated also after a fixed number of time steps, rather than every time step and in this case the linearization is done by a modified Newton Raphson method. Numerical properties of the time discretization in the non-linear (along with linear) case are deepen in detail in the bibliography at number [1].

2.8. Spatial discretization. Choice of elements

The numerical integration is usually realized using computational techniques, for instance Gauss quadrature, Newton-Cotes quadrature [2], where the integral function is evaluated in a series of specific points inside the domain and on the border of it and then it is weighted and added up.

All the procedure has been developed in local or normalized coordinates ξ, η, ζ which take ad maximum value of 1, positive or negative depending on the reference system adopted, as showed in Figure 2.8.1.

For each element it is possible to write

$$x = N_1' x_1 + N_2' x_2 + \ldots = \mathbf{N}' \begin{Bmatrix} x_1 \\ x_2 \\ \vdots \end{Bmatrix} = \mathbf{N}'\mathbf{x}$$

$$y = N_1' y_1 + N_2' y_2 + \ldots = \mathbf{N}' \begin{Bmatrix} y_1 \\ y_2 \\ \vdots \end{Bmatrix} = \mathbf{N}'\mathbf{y} \qquad (2.8.1)$$

$$z = N_1' z_1 + N_2' z_2 + \ldots = \mathbf{N}' \begin{Bmatrix} z_1 \\ z_2 \\ \vdots \end{Bmatrix} = \mathbf{N}'\mathbf{z}$$

In which $\mathbf{N}'$ are standard shape functions given in terms of local coordinates ξ, η, ζ. The points that have coordinates x_1, y_1, z_1, etc. will lie at appropriate points of the element boundary. These points can establish nodes a priori. The global coordinates are so expressed in terms of nodal coordinates by means of a relation where weight functions depending on the local coordinate system. Figure 2.8.1 shows the 20-node isoparametric element, also called brick element or Hexa20.

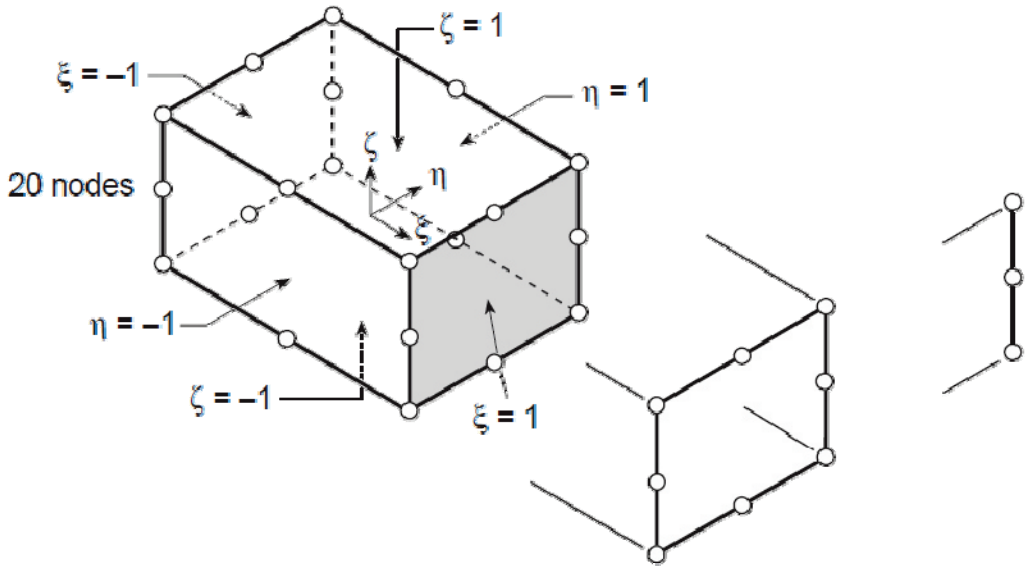

Figure 2.8.1: The 20-node isoparametric element.

The shape functions in terms of local coordinates for this element are for the corner nodes

$$N_i = \frac{1}{8}(1+\xi_0)(1+\eta_0)(1+\zeta_0)(\xi_0+\eta_0+\zeta_0-2) \qquad (2.8.2)$$

And for a typical mid-side node:

$$\xi_i = 0 \quad \eta_i = \pm 1 \quad \zeta_i = \pm 1$$
$$N_i = \frac{1}{4}\left(1+\xi^2\right)\left(1+\eta_0\right)\left(1+\zeta_0\right) \tag{2.8.3}$$

This element has been chosen to perform the discretization of problems in space for the present work and for the F.E. code PLASCON3D and PLASCON3D_PS that will be discussed in chapter 4.

Bibliography

1. Lewis, R.W. and B.A. Schrefler, *The finite element method in the deformation and consolidation of porous media.* 1998.

2. Zienkiewicz, O.C., *The Finite Element Method.* 1989.

3. Galerkin, B.G., *Series solution of some problems of elastic equilibrium of rods and plates.* Vestn. Inzh. Tekh, 1915. **19**: p. 897-908.

4. Brooks, R. and A. Corey, *Hydraulic properties of porous media.* Hydrology Papers, Colorado State University, Fort Collins, 1964. **3**.

5. Brooks, R.H. and A.T. Corey. *Properties of porous media affecting fluid flow*. in *Journal of the Irrigation and Drainage Division, Proceedings of the American Society of Civil Engineers*. 1966.

6. van Genuchten, M.T., *A closed-form equation for predicting the hydraulic conductivity of unsaturated soils.* Soil Science Society of America Journal, 1980. **44**(5): p. 892-898.

7. Lewis, R.W. and B.A. Schrefler, *The finite element method in the deformation and consolidation of porous media.* 1987.

8. Incropera, F.P. and D.P. DeWitt, *Fundamentals of heat and mass transfer*, 1990, Wiley (New York)

9. Richtmyer, R. and K. Morton, *Difference methods for initial-value problems.* New York: Interscience, 1967.

10. Morris, J.L., *Computational methods in elementary numerical analysis*. 1983: Wiley New York.

11. Hwang, C., N. Morgenstern, and D. Murray, *On solutions of plane strain consolidation problems by finite element methods.* Canadian Geotechnical Journal, 1971. **8**(1): p. 109-118.

12. Sandhu, R.S., *Fluid flow in saturated porous elastic media*. 1968: University Microfilms.

3 Implementation of the numerical code PLASCON3D_PS

3.1. Introduction

One of the most time demanding task of the work presented within this thesis and necessary to pursue the final goal of realizing a numerical F.E. code, has been the programming activity related to the numerical implementation of the discretized equations of the previous chapter. The numerical code produced is the result of a rewriting and extension work based on the F.E. “in house” code PLASCON3D. This code will be briefly introduced on next sections.

3.2. Finite Element code PLASCON3D

The code that has been chosen for the implementation of the partial saturated formulation is the fully coupled F.E. research code PLASCON3D that deals with a *u-p-T* formulation (i.e. *u* stands for displacements, *p* for pressure and *T* for temperature). PLASCON3D is based on the fully saturated, eventually non-isothermal, one-phase flow applied to a deformable porous medium. This formulation represents the most simplified set of equations that can be derived from the set of equations presented on chapter 2, at section 2.6. The fully saturated formulation can be obtained once conserving as fluid phase only the liquid phase. In this way is possible to impose the full saturation of voids, i.e. $S_w = 1$ and $S_g = 0$, the liquid pressure will be the only representative pressure basic variable. As result of unitary degree of saturation and a unique pressure variable, the terms related to the gas phase disappear and the dimension of the problem reduces. Furthermore, the system matrices $\mathbf{H}$ and $\mathbf{S}$ are independent from the state vector $\mathbf{X}$ and linearity holds (except that the constitutive relations of the material can even introduce material nonlinearities). The consistency and stability conditions are less strictly and computationally this formulation is less onerous than the one that will be present further.

Together with the assumption of small displacements and neglecting the inertial effects as done in previous chapters when dealing with the acceleration terms (section 1.4), the code has been written taking into account of other simplifying assumptions:

(a) Viscosity of liquid phase will be neglected;

(b) Volume forces and hydraulic pressures are constant and act in the direction of one of global coordinates;

(c) Permeability matrix has null terms out of the diagonal.

The assumption (a) neglecting the viscosity term and its variations in time, has the effect that the permeability coefficients first introduced in chapter 1, and preserved constant during calculations, have to take into account of the eventually initial and constant viscosity, as a factor that affect the permeability itself.

Second assumption (b) says that the volume forces that will be calculated from the average density of the fully saturated medium and the gravity acceleration term as well as the hydrostatic pressure, act in the direction of one of global coordinates, in this case the coordinate z.

Assumption (c), cause that the intrinsic permeability matrix $\mathbf{k}$ as defined in chapter 1, presents only diagonal terms, with null extra-diagonal coefficients. Setting to zero the values of the extra-diagonal coefficients, means that only the direct permeabilities have been taken into account, and the contribute given in each direction (x, y, z) by the permeability characteristics of the medium in the other two directions, has been neglected.

The constitutive model implemented in the original version of PLASCON3D is the elastoplastic model following the formulation proposed by Mohr – Coulomb and Modified Cam-Clay [1].

The complete manual for the first release two-dimensional version named PLASCON as well the descriptions of the variables and routines involved, can be found on bibliography at number [2]. A manual for the three-dimensional implementation named PLASCON 3D can be found in the references [3].

Further developing on the code PLASCON and PLASCON 3D has been done by Majorana C.E., Salomoni V.A. and Zanetti S. [4] and Salomoni V.A and Fincato R. [5-8]. In particular Salomoni, following the work of Bolzon *et al.* [9], introduced the generalized elastoplastic constitutive relation that was developed by Pastor, Zienkiewicz e Chan [10]. Furthermore Salomoni and Fincato introduced an

unconventional plasticity approach based on the subloading surface plasticity model to study the subsidence phenomena above gas reservoir [5-8].

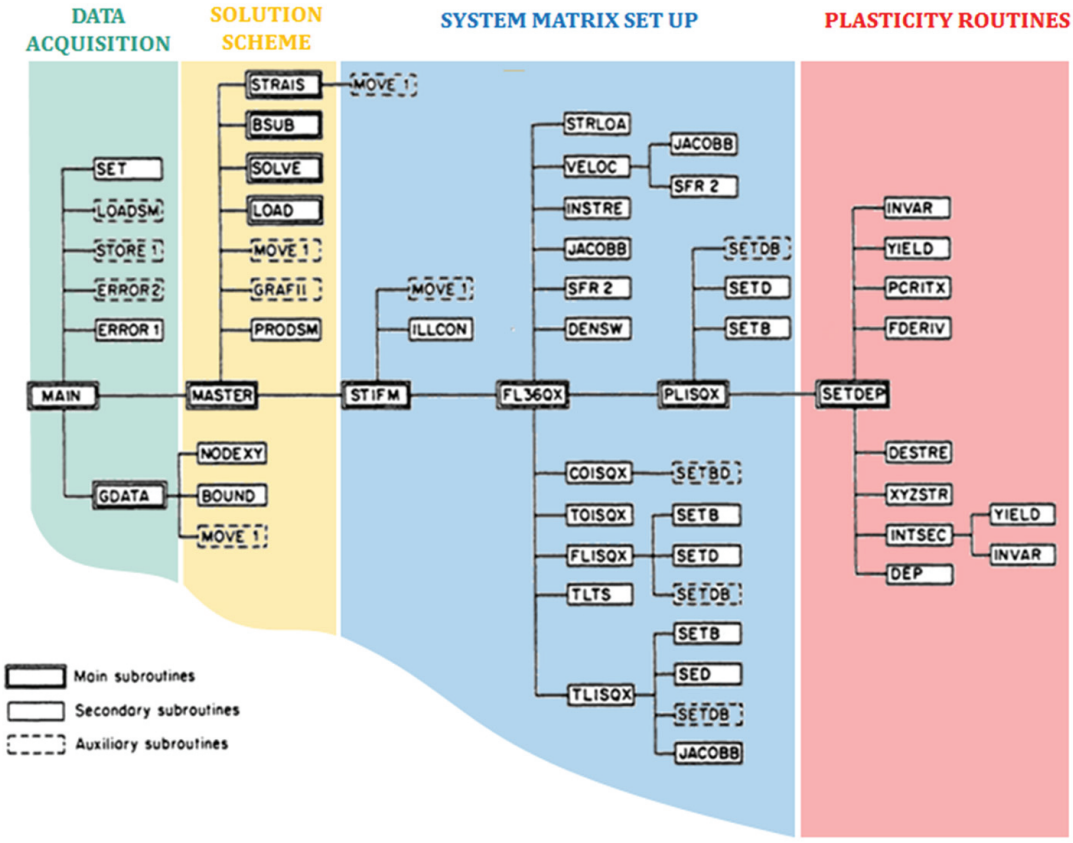

Figure 3.2.1: Simple block schematic of the program PLASCON3D.

Figure 3.2.1 shows a simple schematic of the main program PLASCON in the original version and the mains subroutines. Some minor dependencies has been omitted. In particular the constitutive equations and relative developments that regard the plasticity models are dealt in the routine *SETDEP* recalled by *PLISQX*. The improvements introduced by present work that will be discussed in next section don't interest the plasticity routine *SETDEP* that has been frozen for the moment and will not recalled. Due to this exclusion, the resulting code that has been chosen as starting point for further implementations deals with a pure isotropic and elastic medium.

The finite element used in the PLASCON3D code is the 20-node isoparametric element with quadratic shape functions as described in section 2.8.

3.3. Finite Element code PLASCON3D_PS

In order to implement the discretized set of equations as presented in chapter 2, an important upgrade has been necessary to the fully saturated code presented in section 3.2.

The code has been subjected to various modifications during time since his first release, where the instruction were inputted in Fortran IV language and the results as well as the wide arrays were stored in tape unit. The developing of new standard for Fortran and new compilers along with the substitution of obsolete features like the commons in favour of modules and the possibility of dynamic allocation of variable, allowed have to rewrite in more efficient way the code in order to improve the capabilities and the portability. In the first version, the code was thought to run on VAX calculators, now along with the possibility to run code on dedicated servers the main need is to be sure that the code will compile and run efficiently under Windows systems as well as under UNIX machines.

As explained in section 3.2 the main modifications, that have been already done have been the extension of the analysis capabilities in order to treat two-dimensional domains to three-dimensional domains and the integrations that take into account of better plasticity relations for the solid phase. Such integrations, as the last mentioned, are focused on the constitutive routine and on the routines related to the iterative solving procedure, that has been improved to deal with nonlinearities derived from plasticity [11].

The work that now has been necessary to convert the previous fully saturated version to the new one, comprehensive of a fully coupled partial saturated formulation, has been more extensive if looking at the number of routines that has been subjected even to slight rather than deep modifications. This means only that the rewriting and upgrading work has affected more or less all the standard routines of the previous version, with the introduction of new instructions, with except of constitutive routines that has been deactivated for the part of instructions that involve the plasticity algorithms, taking into account, only for the moment of a linear elastic relation for the solid phase, which calculations are performed in the *PLISQX* routine.

In PLASCON3D_PS the viscosities of gas and water have been considered as factor that affects the hydraulic conductivity of water and gas. Again like the previous version, the intrinsic permeability matrix $\mathbf{k}$ presents non-zero terms only in the diagonal, neglecting thus the cross related effects on directions done by the

other two directions. This means that basically the vertical permeability can be different from the horizontals ones, taking into account of the anisotropy due to the deposition process of sedimentary porous media during the geological formation of the material.

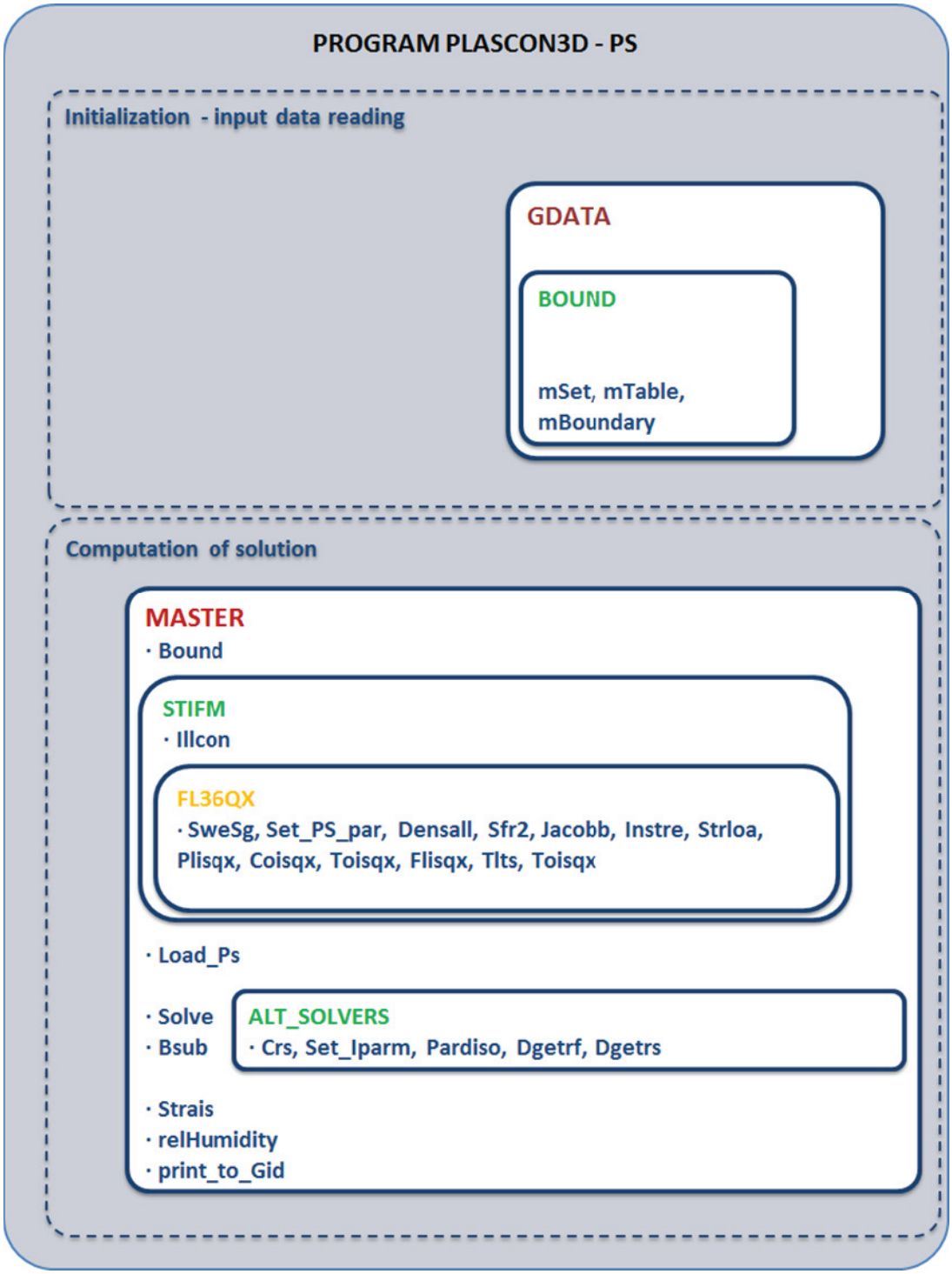

Figure 3.3.1: Simplified schematic of the structure of the code PLASCON3D_PS.

Along with the increase of degrees of freedom of the problem and to the presence now of two pressure terms (one for liquid phase and one for gas phase) the standard skyline solver (subroutines *SOLVE* and *BSUB* on Figure 3.3.1) involved in the solution of the system (2.7.2) with the Gaussian elimination method [12] has been maintained. However, due to the lack of performances of the standard solver, new routines that utilise optimized solvers [13-15] has been written in order to speed up the solving procedures and reduce the computational time. In particular, one of these solvers is able to carry on parallel computation. In this way, the code PLASCON3D_PS that is written in a sequential manner, single thread, can be parallelized during the solving procedures.

The upgrading work has been done using the Fortran 95 language, taking advantage of dynamic allocation of arrays. By the way, the standard routines written in Fortran 77 have been maintained, where possible. Comparing the two program versions, also the semi - dynamic allocation done by the system vector *A* [2], has been dismissed, in favour of a complete declaration of variables.

Concluding, in the current version of PLASCON3D_PS the isothermal formulation presented in section 3.6 has been fully coded and tested. Furthermore the routines involved in the thermal coupling have been implemented in a basic way, but are in a debug stage and due to this have not been used in the present work.

3.4. Description of new routines

With respect of the schematic presented on Figure 3.2.1, some routines and procedures has been added or modified in order to provide the code instructions to calculate new system matrix terms, as already explained in section 3.3. The complete description of the new code as well the complete manual is not intended to be given here. As previously mentioned the manual of the classical PLASCON and PLASCON3D [2, 3] can still cover and explain very well also this version of the code. Hence, only the description of the most important new procedures and the sections of the code that has been modified deeply will be reported.

SWESG

The routine *SWESG* plays a main role on the code framework. In fact it contains all the code that is implied on the calculus of the degrees of saturation S_w and S_g. This routine also calculates the relative permeability coefficients, due to the direct relation with the equivalent saturation S_e. The functions implemented are those given by Lloret and Alonso [16], by Brooks and Corey [17], Liakopoulos [18] and

van Genuchten [19, 20].When a specific expression for the calculus of the relative permeability coefficients isn't supplied with above mentioned relationships, the Brooks and Corey relations have been used by default.

This routine is called before prior to perform the gauss point integration over the single element, that is the main purpose of the *FL36QX* routine. The routine *SWESG* provides as output for each node of the current element the vectors *SW(20), SG(20), KRW(20)* and *KRG(20).* A vector containing the nodal capillary pressure *ELPORECP(20)* is also calculated from the liquid and gas nodal pressure vectors *ELPOREW(20)* and *ELPOREG(20).*

```
    subroutine SWESG (PROP,ELPOREW,ELPOREG,ELPORECP,NODEL)
!---
!---  Description
!---
! *** CALCULATE SW AND SG AS A FUNCTION OF CAPILLARY PRESSURE
!---
!---  Modules included
!---
      use PARSAT
      use DIMPARSAT
      use STORAGE_PS
      use DIMVAR
!---
      implicit none
!---
!---  Variable declaration
!---
      . . .
!---
!---
!---  Saturation initialization
!---
      SW = 0.d0
      SG = 0.d0
      SE = 0.d0

!---  Read from input file initial saturations
      IF (sw_ext .eq. 1) THEN
            READ(46,*) (ext_saturations(J), J=1,4)
            SW = ext_saturations(1)
            SG = ext_saturations(2)
            SWIRR = ext_saturations(3)
            SGIRR = ext_saturations(4)
            DO I = 1, NCN
                SE(I)    =  (SW(I) - SWIRR) / (1-SWIRR)
            END DO
            DO I = 1,NCN
                i_node = NODEL(I)
                SWW (i_node)  =    SW(I)
                SGG (i_node)  =    SG(I)
            END DO
```

```
            DO I = 1,NCN
                ELPORECP(I) = ELPOREG(I) - ELPOREW(I)
            END DO
            DO I = 1, NCN
                SE(I)    =  (SW(I) - SWIRR) / (1-SWIRR)
            END DO
      ENDIF
!---
!--- Read from input file the irreducible saturation
!---
      SWIRR     = PROPPS(MAT,15)
      SGIRR     = PROPPS(MAT,16)
!---
!--- Calculate the capillary pressure for each node
!---
      DO I = 1,NCN
         ELPORECP(I) = ELPOREG(I) - ELPOREW(I)
      END DO
!---
!--- Initialize suction
!---
      SUCTION  =    0.D0
!---
!--- Impose the initial water saturation (optional)
!---
      IF (NSTEP .EQ. 1 .AND. SWINIT .EQ. 1) THEN
              SW     =    SWIN
              SG     =    1.D0 - SW
      ELSE IF (NSTEP .GT. 1 .OR. SWINIT .NE. 1) THEN
!---
!--- Calculus of degree of saturation with the selected function
!---
      SELECT CASE (sw_form)
!---
!--- Alonso et al. (1990) SW function
!---
      CASE (1)
      EMME     =    1.D0 - SWIRR
      ELLE     =    5.D0
      DO I = 1,NCN
       SUCTION = ELPORECP(I)
       IF (PRESSUREPA) THEN
         SUCTION = SUCTION / 1000000.D0
       END IF
!---
       If (SUCTION .GE. 0.d0) then
           SW(I)  = 1.D0 - EMME * TANH (ELLE * SUCTION)
       SG(I)  = 1.D0 - SW(I)
              if (SG(I) .LT. SGIRR) then
                  SG(I) = SGIRR
                  SW(I) = 1.d0 - SGIRR
              end if
       else if (SUCTION .LT. 0.d0) then
              SW(I) = 1.d0 - SGIRR
              SG(I) = SGIRR
       end if
       If (ONE_PHASE_FLOW .EQ. 1 .AND. SG(I) .GT. SGIRR)
```

```
          ELPOREG(I) = PROPPS(MAT,14)
!---
      END DO
!---
!--- Brooks & Corey (1966) SW function
!---
      CASE (2)
      !IF (PRESSUREPA) p_bubbl = p_bubbl / 1000000.D0
      p_bubbl   = PROPPS(MAT,17)
      PSDIND    = PROPPS(MAT,18)
      maxsuct   = PROPPS(MAT,20)
       !IF (PRESSUREPA)  maxsuct = maxsuct /  1000000.D0
       DO I = 1,NCN
       SUCTION = ELPORECP(I)
       !IF (PRESSUREPA) THEN
       !  SUCTION = SUCTION / 1000000.D0
       !END IF
       if (SUCTION .GE. p_bubbl .AND. SUCTION .LE. maxsuct) then
           SW(I) = SWIRR + (1.d0 - SGIRR - SWIRR) *
                    (p_bubbl/SUCTION)**PSDIND
           SG(I) = 1.D0 - SW(I)
       else if (SUCTION .GT. maxsuct) then
           SW(I) = SWIRR + (1.d0 - SWIRR) *
                   (p_bubbl/maxsuct)**PSDIND
           SG(I) = 1.D0 - SW(I)
       else if (SUCTION .LT. p_bubbl) then
              SW(I) = 1.d0 - SGIRR
              SG(I) = SGIRR
       end if
!---
      If (ONE_PHASE_FLOW .EQ. 1 .AND. SG(I) .GT. SGIRR)
      ELPOREG(I) = PROPPS(MAT,14)
!---
!--- Liakopoulos SW function
!---
     CASE (4)
       DO I = 1,NCN

       If (ELPORECP(I) .GE. 0.d0) then
       SW(I)  = 1.D0 - 1.9722D-11 * (ELPORECP(I)**2.4279D0) !Questa
funzione restituisce Sw = 0 a Pc = 25555 Pa
       SG(I)  = 1.D0 - SW(I)
              if (SG(I) .LT. SGIRR) then
                  SG(I) = SGIRR
                  SW(I) = 1.d0 - SGIRR
              end if
       else if (ELPORECP(I) .LT. 0.d0) then
              SW(I) = 1.d0 - SGIRR
              SG(I) = SGIRR
       end if
       If (ONE_PHASE_FLOW .EQ. 1 .AND. SG(I) .GT. SGIRR)
       ELPOREG(I) = PROPPS(MAT,14)
!---
      END DO
!---
!--- van Genuchten (1978, 1980) SW function
!---
```

```
      CASE (5)
      AVG  = PROPPS(MAT,21)
      NVG  = PROPPS(MAT,22)
      MVG  = PROPPS(MAT,23)
!---
       DO I = 1,NCN
       SUCTION = ELPORECP(I)
       if (SUCTION .GT. 0.d0) then
           SW(I) = SWIRR + (1.d0 - SGIRR - SWIRR) *
                   (1/(1+(AVG*SUCTION)**NVG))**MVG
           SG(I) = 1.D0 - SW(I)
       else if (SUCTION .LE. 0.d0) then
              SW(I) = 1.d0 - SGIRR
              SG(I) = SGIRR
       end if
!---
       If (ONE_PHASE_FLOW .EQ. 1 .AND. SG(I) .GT. SGIRR)
       ELPOREG(I) = PROPPS(MAT,14)
!---
      END DO
      END SELECT
      ENDIF
!---
!--- Copying the saturation values on global vectors
!---
      DO I = 1,NCN
        i_node = NODEL(I)
        SWW (i_node)  =    SW(I)
        SGG (i_node)  =    SG(I)
      END DO
!!-----------------------------------------------------------------
!---
!--- Calculus of equivalent saturation
!---
     DO I = 1, NCN
            i_node = NODEL(I)
            SE(I)    =  (SW(I) - SWIRR) / (1-SWIRR)
!---
!--- Calculus of relative permeability coefficient
!---
            SELECT CASE (sw_form)
!---
!---
!--- Liakopoulos
!---
            CASE (4)
            !--- Wetting Phase
            KRW(I) = 1.d0 - 2.207d0 * (1.d0 - SW(I)) ** 1.0121d0
            !--- Non-Wetting Phase
            KRG(I) = ((1.d0 - SE(I))**2.D0) *
                     (1.D0 - SE(I) ** ((2.d0 + PSDIND)/PSDIND))
            IF (KRG(I) .LT. PROPPS(MAT,19)) KRG(I) = PROPPS(MAT,19)
!---
!--- van Genuchten (1978 - 1980)
!--- Mualem        (m = 1-1/n)
!--- Burdine       (m = 1-2/n)
!---
```

```
            IF (INT(NVG*(1.d0-MVG)) .EQ. 1) THEN
            KRW(I) = (SE(I) ** 0.5d0) * (1.d0 - (1.d0 -SE(I) **
                     (1/MVG)) ** MVG) ** 2.d0
            KRG(I) = (1.d0 -SE(I)) ** 0.5d0 * (1.d0 -SE(I) **
                     (1/MVG)) ** (2.d0 * MVG)
            ELSE IF (INT(NVG*(1.d0-MVG)) .EQ. 2) THEN
            KRW(I) = (SE(I) ** 2.d0) * (1.d0 - (1.d0 -SE(I) **
                     (1/MVG)) ** MVG)
            KRG(I) = (1.d0 -SE(I)) ** (1.d0/3.d0) * (1.d0 -SE(I) **
                     (1/MVG)) ** (2.d0 * MVG)
            ELSE
            write(*,*) ' Not Mualem or Burdine for van Genutchen
                         permeability'
            pause
            END IF
            IF (KRG(I) .LT. PROPPS(MAT,19)) KRG(I) = PROPPS(MAT,19)
!---
!--- Standard Brooks & Corey (1966) relative permeability
!--- coefficients
!---
            CASE DEFAULT
            !--- Wetting Phase
            KRW(I) = SE(I) ** ((2.d0 + 3.d0 * PSDIND) / PSDIND)
            !--- Non-Wetting Phase
            KRG(I) = ((1.d0 - SE(I))**2.D0) * (1.D0 - SE(I) **
            ((2.d0 + PSDIND)/PSDIND))
            IF (KRG(I) .LT. PROPPS(MAT,19)) KRG(I) = PROPPS(MAT,19)
!---
            END SELECT
!---
!--- Check for krw and krg  not on 0-1 range
!---
            IF (KRW(I) .LT. 0.d0 .OR. KRW(I) .GT. 1.d0) THEN
                write (IOUT, *) "WARNING: Rel. permeabil. (w) out
                                 of range! node:", i_node
            END IF
!---
            IF (KRG(I) .LT. 0.d0 .OR. KRG(I) .GT. 1.d0) THEN
                write (IOUT, *) "WARNING: Rel. permeabil. (g) out
                                 of range! node:", i_node
            END IF
!---
!--- Copying the relative permeability coefficients on global
!--- vectors
!---
      KRWW (i_node)  =    KRW(I)
      KRGG (i_node)  =    KRG(I)

      END DO

      END IF
!---
!--- End of Subroutine
!---
      RETURN
    END
```

The routine selects the proper saturation function by mean of the *sw_form* parameter that has been set on the input file of the program. Then calculates the degree of saturation eventually swapping the existence domain depending on the capillary pressure, i.e. for negative capillary pressure values or that approaches to bubbling pressure the code sets automatically the value of saturations to the limits value (except the irreducible values set on the input file). The equivalent saturation is calculated for each node of the element considered and relative permeability coefficients are calculated so on, in order to be utilized in the *FLISQX* routine.

At each time step the global vector provides the full storage of saturations and permeabilities for printing purposes.

SET_PSAT_PARAMETER

This routine is a minor one and is implied for very few purposes when performing isothermal analyses. The main role of this subroutine is to set values for useful parameters from the values given in the input files.

```
    subroutine SET_PSAT_PARAMETER (PROP,ELTEMP)
!---
!--- Description
!---
!---  Calculate some of partially saturated parameters needed
!---
!--- Modules included
!---
      use DIMPARSAT
      use PARSAT
      use STORAGE_PS
      use DIMVAR
!---
      implicit none
!---
!---  Variable Declaration
!---
      . . .
!---
      POR       =    PROP(MAT,16)
      THREF     =    PROPPS(MAT,1)
      MW        =    PROPPS(MAT,2)  !Molar Mass of Liquid
      MA        =    PROPPS(MAT,3)  !Molar Mass of Gas
      RCONST    =    PROPPS(MAT,4)  !Universal gas constant
      GVECT     =    PROPPS(MAT,13) !Gravity vector
      !KW        =    1.0d0 / PROP(MAT,6)
      !KA        =    PROPPS(MAT,14)
!---
!---  Computing the Molar Mass of Gas
!---
      MG      =   ((DENS_GW / DENS_G) * (1.d0 / MW) +
```

```
                  (DENS_GA / DENS_G) * (1.d0 / MA))
!---
!---  Setting the reference temperature
!---
      TH = THREF
!---
!---  Calculating the relative pressure of air and water vapour
!--- (optional in the isothermal analysis)
!---
      KINDPRESS = 1
      SELECT CASE (KINDPRESS)
!
!     CASE (1)
        PGW     =   DENS_GW * TH * RCONST / MW
        PGA = PG - PGW
      CASE (2)
        PGA     =   DENS_GA * TH * RCONST / MA
        PGW     = PG - PGA
      END SELECT
!---
!--- End of subroutine
!---
      return
      end subroutine
```

Optionally it calculates the relative gas pressure of air and water vapour (if the gas is not dry air).

DENSALL

Routine *DENSALL* is involved on the calculation of the various densities utilized in the general formulation.

```
    subroutine DENSALL(PROP,P,NEA1,ELTEMP,ELPOREW,ELPOREG)
!---
!--- Description
!---
!--- This routine calculates the medium, water, air and water vapour
!--- density.
!---
!--- Modules included
!---
      use MTMTB
      use DIM
      use SPC
      use SPC1
      use SPC3
      use SPC5
      use CTR1
      use VAR
      use PLAST
      use PARSAT
```

```
      use DIMPARSAT
      use STORAGE_PS
      use DIMVAR
!---
      implicit none
!---
!---  Variable Declaration
!---
      . . .
!---
!--- Reading from PROP array
!---

         ROW  = PROP   (MAT,18)
         ROGA = PROPPS (MAT,5)
         ROGW = PROPPS (MAT,6)
         ROG  = ROGA + ROGW
         ROS  = PROPPS (MAT,7)
!---
!--- Isothermal case
!---

      IF (NTHERM .EQ. 0) THEN
         DENS_W    = ROW
         DENS_GA   = ROGA
         DENS_GW   = ROGW
         DENS_G    = ROG
         DO I = 1,NCN
            DENS      =  (1.D0 - POR) * ROS + POR * SW(I) * DENS_W +
                          POR * SG(I) * DENS_G
         END DO
            DENS = DENS / 20.d0
!---
!--- Non- isothermal case
!---

      ELSE IF (NTHERM .EQ. 1) THEN
!---
!--- Reading from PROP array
!---

      ALPHA    =    PROP(MAT,20)
      WCOMP    =    PROP(MAT,6) / PROP(MAT,16)  !(n/K_W) / (1/K_S
      DENSIN   =    PROP(MAT,18)
      AIN2     =    0.D0
      BIN2     =    0.D0
      CIN2     =    0.D0
!---
!--- Computes  nodal contributes
!---
      DO I = 1,NCN
!--- Water (Fernandez 1972)
           AIN2     =    AIN2 + P(I) * ELTEMP(I)  * ALPHA
                         - P(I) * ELPOREW(I) * WCOMP
!--- Water Vapour
           BIN2     =    BIN2 + P(I) * (- P(I) * ELPOREG(I)) * MW /
                         (RCONST * P(I) * ELTEMP(I))
```

```
!--- Air  (ARIA)
           CIN2     =    CIN2 + P(I)* ROGAIR(ELTEMP(I))
!---
      END DO
!---
!--- Storage of updated values on g.p.
!---
      DENSWW (2,IGJG,NEL) =    AIN2
      DENSGW (2,IGJG,NEL) =    BIN2
      DENSGA (2,IGJG,NEL) =    CIN2
!---
!--- Computes  densities at g.p.
!---

      IF (NSTEP .EQ. 1) THEN
!---  Water density
          DENS_W    = ROW
!---  Water vapour density
          DENS_GW   = ROGW   !@20°C
!---  Air density
          DENS_GA = 0.d0
          DO I =1,NCN
                  DENS_GA   = DENS_GA +P(I)*ROGAIR(ELTEMP(I))
          END DO
          ROGA      = DENS_GA   !@20°C - 293 K
!---  Gas density
          ROG       = ROGA + ROGW
          DENS_G    = ROG
!---  Multiphase medium
          DO I = 1,NCN
              DENS      =  (1.D0 - POR) * ROS + POR * SW(I) * DENS_W
                         + POR * SG(I) * DENS_G
          END DO
!---
         DENS = DENS / 20.d0 !Densità media
!---
       ELSE
!--- Water density (Fernandez 1972)
         DENS_W    = ROW  + ROW * (DENSWW(1,IGJG,NEL)-
                     DENSWW(2,IGJG,NEL))
!--- Water vapour density
         DENS_GW   = ROGW + ROGW * (DENSGW(1,IGJG,NEL)-
                     DENSGW(2,IGJG,NEL))
!--- Air density
         DENS_GA   = ROGA + ROGA * (DENSGA(1,IGJG,NEL)-
                     DENSGA(2,IGJG,NEL))
!--- Gas density
         DENS_G    =  DENS_GW + DENS_GA
!--- Multiphase medium
        DO I = 1,NCN
             DENS      =  (1.D0 - POR) * ROS + POR * SW(I) * DENS_W
                        + POR * SG(I) * DENS_G
        END DO
!---
        DENS = DENS / 20.d0 !Densità media
!---
      ENDIF
```

```
!---
!---  Storage of old g.p. contribution
!---

      DENSWW (1,IGJG,NEL)  =    AIN2
      DENSGW (1,IGJG,NEL)  =    BIN2
      DENSGA (1,IGJG,NEL)  =    CIN2
!---
!--- End of subroutine
!---
      END IF
      RETURN
      END
```

In the case of isothermal analysis, the routine set the various densities to the values given in the input files for the reference temperature. The density of the multiphase medium is calculated with the equation (3.2.3) using the degrees of saturation computed with the routine *SWESG*.

The variation of the density of the phases due to variation of mere pressure fields, in the isothermal case, is neglected here, by the fact that the water compressibility has been taken into account with water bulk modulus in the equation that form the P_{ww} component of matrix $\mathbf{S}$ (2.6.21). The change in volume for the gas, instead, has been taken into account in the (2.6.26) with the term that involves the universal gas constant R at reference temperature ϑ.

In the non-isothermal case a specific formulation for densities depending on temperature must be provided, and this has been done with the formulation of Fernandez [21, 22] for the water, with the curves provided with the function *ROGAIR* that computes the change in volume, and so in density of dry air, and with the state equation (1.3.28) for the water vapour or for a more accurate prevision of dry air density. Here the densities for water, dry air and water vapour are stored for the actual time step and for each gauss point in an array, in order to compute at each time step the density variations.

FLISQX

The routine *FLISQX* plays a main role on computations of matrix coefficients that form the hyper matrix of the system. First the routine computes the diagonal terms relative to water and gas phase named PWW and PGG and the corresponding extra diagonal terms CWG and CGW that assure the fully coupling of the two phases. Secondly the routine *SETD* and *SETD_PS* are recalled in order to compute

the flux terms HWW and HGG respectively of water phase and gas phase. The moisture content CS is calculated calling the *PDERIV_SW_PC_ND*.

```
    subroutine FLISQX(PROP,SLOAD, B, D,DB,P,HWW, KWG, HGG, KGW, HTT,
         KTW, PWW, CWG, CGW, PGG, ELPOREW,ELPOREG,ELLPORECP,DEL,CEL,
                                                QLOADW,QLOADG,FGW,FGG)
!---
!--- Description
!---
!--- This routine perform the computations relative to the
!--- components of hyper matrix H (HWW, KWG, KGW, HGG, KTW, HTT)
!--- and the routine SETD_PS is recalled to calculate the
!--- contributions of this term
!--- This routines perform also the calculations relative the
!--- components of hyper matrix S (PWW, PGG, CWG and CGW)
!--- and some load vectors as  SLOAD, QLOADW, QLOADG
!---
!--- Modules included
!---
      . . .
      . . .
      use DIMPARSAT
      use PARSAT
      use DIMVAR
!
      implicit real(REAL_KIND) (a-h,o-z)
!---
!---  Variable Declaration
!---
      . . .
!---
!---  Set Some parameters
!---  n / K_w
      ROWC    =    PROP(MAT,16) * PROP(MAT,6)
!---  n * M_g /(rog * t_ref * R)
      ROGC    =    PROP(MAT,16) * MG / (ROG * TH * RCONST)
!---  Specific weight of material
      BODYF   =    PROP(MAT,7)
!---  1 / (3 * K_s)
      ROCKC   =    PROP(MAT,17) / 3.d0
!---  (n - 1) / K_s
      ROCKCN  =   (PROP(MAT,16) - 1.d0) * PROP(MAT,17)
!---  Gravity vector
      GVECT1  =    0.d0
      GVECT2  =    0.d0
      GVECT3  =    GVECT

!---  ROCKCN2 =   (ALFACMP-POR)/KS
!---
!---  Calculation of stiffness matrix D
!---
      CALL    SETD  (PROP,P,D,DEL,ICS1,0)
!---
      DSUM    =    D(1,1) + D(1,2) + D(1,3) + D(2,1) + D(2,2) +
                   D(2,3)+ D(3,1) + D(3,2) + D(3,3)
!---  [(alpha - n) / K_s + n / K_w ]
      CONC    =    ROWC - ROCKCN - (ROCKC * ROCKC * DSUM) / DAREA
```

```
!---  (alpha - n) / K_s
      CONCX   =         - ROCKCN - (ROCKC * ROCKC * DSUM) / DAREA
!---
      DO I = 1,KSIZE2
           AIT     =    P(I) * DAREA
           CONC1   =    0.d0
           CONC2   =    0.d0
           CONC3   =    0.d0
!---
!---  Calculation of moisture content with PDERIV_SW_PC_ND
!---
                CS = PDERIV_SW_PC_ND (ELPORECP(I))
!---
!---  Calculation of contributes for PWW when isothermal case is
!---  considered
!---

                CONC1 = CONCX * SW(I) * (SW(I) - ELPOREW(I) * CS/POR
                        + ELPOREG(I) * CS/POR) - CS + SW(I) * ROWC
!---
!---  Calculation of contributes for CWG when isothermal case is
!---  considered
!---
                CONC2 = CONCX * SW(I) * (SG(I) + ELPOREW(I) * CS/POR
                       - ELPOREG(I) * CS/POR) + CS
!---
!---  Calculation of contributes for CGW when isothermal case is
!---  considered
!---
                CONC3 = CONCX * SG(I) * (SW(I) - ELPOREW(I) * CS/POR
                       + ELPOREG(I) * CS/POR) + CS
!---
!---  Calculation of contributes for PGG when isothermal case is
!---  considered
!---
                CONC4 = CONCX * SG(I) * (SG(I) - ELPOREG(I) * CS/POR
                        + ELPOREW(I) * CS/POR) - CS + SG(I) * ROGC
!---
!---  Loop through nodes to calculate HWW and HGG contributions
!---
           DO J = 1,KSIZE2
                BIT1   =    0.D0
                BIT2   =    0.D0
                BIT3   =    0.D0
                BIT4   =    0.D0
                BIT5   =    0.D0
                BIT6   =    0.D0
                BIT61  =    0.D0
                BIT7   =    0.D0
                DIT1   =    0.D0
                FIT1   =    0.D0
                GIT1   =    0.D0
!---
!---  Calculation of contributes for HWW (isothermal)
!---
                KRX = KRW(I)
                CALL    SETB  (B,CEL,P, ICS2)
```

```
                CALL    SETD  (PROP,P,D,DEL,ICS2,1)
                CALL    SETDB (B,D,DB,KSIZE2,ICS2)
                DO K = 1,ICS2
                     BIT2     =    BIT2 + B(K,I) * DB(K,J)
                END DO
!--- FGW
                IF (J .EQ. I) BIT2F     =   (B(1,I) * D(1,1) *
GVECT1 + B(2,I) * D(2,2) * GVECT2 + B(3,I) * D(3,3) * GVECT3) *
DENS_W
!---
!---  Calculation of contributes for HGG (isothermal)
!---
                KRX = KRG(I)
                CALL    SETB  (B,CEL,P, ICS2)
                CALL    SETD  (PROP,P,D,DEL,ICS2,3)
                CALL    SETDB (B,D,DB,KSIZE2,ICS2)
                DO K = 1,ICS2
                     BIT4     =    BIT4 + B(K,I) * DB(K,J)
                ENDDO
!---
!---  Assembly of contributes of hyper matrices H
!---
             HWW(I,J) = HWW(I,J) + BIT2
!---
             HGG(I,J) = HGG(I,J) + BIT4
!---
!---  Assembly of contributes of hyper matrices S
!---
             BIT1 = PWW (I,J) + AIT * P(J) * CONC1
             PWW (I,J) = BIT1
!---
             DIT1 = CWG (I,J) + AIT * P(J) * CONC2
             CWG(I,J) = DIT1
!---
             FIT1 = CGW (I,J) + AIT * P(J) * CONC3
             CGW(I,J) = FIT1
!---
             GIT1 = PGG (I,J) + AIT * P(J) * CONC4
             PGG(I,J) = GIT1

           ENDDO
           II      =    I * 3
!---
!---  Calculations of flux vectors due to sources elements
!---
          QLOADW(I)    =    QLOADW(I)  +  AIT * ELFLOWW
          QLOADG(I)    =    QLOADG(I)  +  AIT * ELFLOWG
!---
!---  Calculations of body forces - alternative 1 (now disabled)
!---
!           SLOAD(II)    =    SLOAD(II)  -  AIT * BODYF
!---
!---  Calculations of body forces - alternative 2
!---
          SLOAD(II)    =    SLOAD(II)  -  AIT * DENS * GVECT3
      END DO
!---
```

```
!--- End of subroutine
!---
      RETURN
      END
```

FUNCTION PDERIV_SW_PC_ND

This function has been created to perform the partial derivative of degree of water saturation over the capillary pressure. In the isothermal formulation, this derivative has been alternatively expressed by the term (2.6.10) that represents the moisture content. The derivative depends on the water saturation function chosen during the analysis from those discussed on section 1.5 and an section 2.6. This function is recalled in the subroutine FLISQX and is computed for each node.

```
     real(REAL_KIND) function PDERIV_SW_PC_ND (CP)
!---
!--- Description
!---
!---  Evaluate DESW / DEPC
!---
!--- Modules included
!---
      use PARSAT
      use CTR1
      use DIMVAR
!---
      implicit none
!---
!---  Variable Declaration
!---
      . . .
!---
      parameter(TOLL = -0.0006d0)

!---
!--- Select the SW formulation
!---
       SELECT CASE (sw_form)
!--- Lloret and Alonso formulation
       CASE (1)
       IF (PRESSUREPA) THEN
         CP = CP / 1000000.D0
       END IF
       PDERIV_SW_PC_ND = - (EMME * ELLE * 1.d0) /
                         ((COSH(ELLE*CP))**2.d0)
!--- Brooks & Corey
       CASE (2)
       maxsuct = PROPPS(MAT,20)
       p_bubbl   = PROPPS(MAT,17)
       IF (CP .LT. p_bubbl) THEN
            PDERIV_SW_PC_ND = 0.d0
```

```
       ELSE IF (CP .GT. maxsuct) THEN
            PDERIV_SW_PC_ND = -((1.d0 - SGIRR - SWIRR) * PSDIND *
                        (p_bubbl/maxsuct) ** PSDIND)  / maxsuct
       ELSE
            PDERIV_SW_PC_ND = -((1.d0 - SGIRR - SWIRR) * PSDIND *
                        (p_bubbl/CP) ** PSDIND)  / CP
       END IF
!--- Liakopoulos
       CASE (4)
       PDERIV_SW_PC_ND = - 1.9722D-11 * 2.4279D0 *
                          (CP **(2.4279D0 - 1.D0))
!--- Van Genutchen
       CASE (5)
       AVG  = PROPPS(MAT,21)
       NVG  = PROPPS(MAT,22)
       MVG  = PROPPS(MAT,23)
       IF (CP .LE. 0.d0) THEN
            PDERIV_SW_PC_ND = 0.d0
       ELSE
            PDERIV_SW_PC_ND = -(1.d0/CP)*(1.d0-SWIRR-SGIRR)* MVG *
                              NVG * ((AVG*CP)**NVG)
                              * ((AVG*CP)**NVG + 1.d0)**(-MVG-1.d0)
       END IF
       CASE  DEFAULT
       write (*,*) 'Error in PDERIV_SW_PC_ND'
       END SELECT
!---
!--- End of function
!---
      return
      end function
```

SETD_PS

The *SETD_PS* routine is implied on determining the terms that enter in the HWW, HGG, KGW and KWG matrix coefficients. This routine use the intrinsic permeability coefficients in each direction (x, y and z) and pre multiply them by the relative permeability coefficients k_{rw} and k_{rg}.

```
    subroutine SETD_PS (PROP,P,D,DEL,MPARSAT)
!---
!--- Description
!---
!---  CALCULUS OF COEFFICENTS FOR THE MATRIX HWW, HGG, KGW and KWG
!---
!--- Modules included
!---
      . . .
      . . .
      use DIMPARSAT
```

```
      use PARSAT
      use DIMVAR
!---
      implicit none
!---
!--- Variable declaration
!---
     . . .
!---
!--- Setting viscosities and other parameters
!---
       MUW    = PROPPS(MAT,8)
       MUG    = PROPPS(MAT,9)
       GPFAC = 1.d0
!---
!--- Setting intrinsic permeabilities
!---

      IF (PERMPS .EQ. 1) THEN
            KABS1   = PROPPS(MAT,10) ! x-direction
            KABS2   = PROPPS(MAT,11) ! y-direction
            KABS3   = PROPPS(MAT,12) ! z-direction
      ELSE
            KABS1   = PROP(MAT,3) ! x-direction
            KABS2   = PROP(MAT,4) ! y-direction
            KABS3   = PROP(MAT,5) ! z-direction
      END IF
!---
!--- Setting the amplification factor for one-phase flow
!---

      IF (ONE_PHASE_FLOW .EQ. 1) GPFAC = 1.0D+00
!---
!--- Selecting the matrix calculation recalled from FLISQX
!---
      SELECT CASE (MPARSAT)
!---
      CASE(1)
!---
!---  HWW (EQ. 3.126)
!---
      IF (PERMPS .EQ. 1) THEN
        DD1 = KABS1 * KRX/MUW
        DD2 = KABS2 * KRX/MUW
        DD3 = KABS3 * KRX/MUW
!---
        DDD1 = 0.d0
        DDD2 = 0.d0
        DDD3 = 0.d0
!---
        D(1,1)  =    DD1 * DAREA + DDD1 * DAREA
        D(2,2)  =    DD2 * DAREA + DDD2 * DAREA
        D(3,3)  =    DD3 * DAREA + DDD3 * DAREA
!---
      ELSE IF (PERMPS .EQ. 0) THEN
!---
        DD1 =  KABS1 * KRX *  (1.d0 / ROW)
```

```
        DD2 =  KABS2 * KRX *  (1.d0 / ROW)
        DD3 =  KABS3 * KRX *  (1.d0 / ROW)
!---
        D(1,1)  =    DD1 * DAREA
        D(2,2)  =    DD2 * DAREA
        D(3,3)  =    DD3 * DAREA
      END IF
!---
!---  HGG (EQ. 10B.13)
!---
      CASE(3)
!---
      IF (PERMPS .EQ. 1) THEN
      DDD1 = KABS1 * KRX * GPFAC /MUG
      DDD2 = KABS2 * KRX * GPFAC /MUG
      DDD3 = KABS3 * KRX * GPFAC /MUG
!---
      D(1,1)  =    DDD1 * DAREA
      D(2,2)  =    DDD2 * DAREA
      D(3,3)  =    DDD3 * DAREA
!---
      ELSE IF (PERMPS .EQ. 0) THEN
!---
        DD1 =  KABS1 * KRX * GPFAC * (MUW/MUG) *    (1.d0 / ROG)
        DD2 =  KABS2 * KRX * GPFAC * (MUW/MUG) *    (1.d0 / ROG)
        DD3 =  KABS3 * KRX * GPFAC * (MUW/MUG) *    (1.d0 / ROG)
!---
        D(1,1)  =    DD1 * DAREA
        D(2,2)  =    DD2 * DAREA
        D(3,3)  =    DD3 * DAREA
      END IF
!
      CASE DEFAULT
      write (IOUT,*) 'WRONG MPARSAT CODE IN SETD_PS'
!---
      CONTINUE
      END SELECT
!---
!---  End of subroutine
!---

      return
      end subroutine
```

The routine is called together the *SETD* routine in *FLISQX*. In the fully saturated version of the code *PLASCON3D* the permeability matrix is calculated directly in *SETD*. A dedicated routine has been now created in order to access to keep distinguished the calculations done for the mechanical contribution (that uses *SETD* as well for the mechanical part), from those performed for the permeability contribution for both gas and liquid. The right calculation procedure is selected by the parameter *MPARSAT* that for isothermal analysis can assume the values 0 for

stiffness matrix coefficient calculations, 3 for the liquid permeability matrix coefficients (*HWW*) and 6 for the gas permeability matrix coefficients (*HGG*). In the standard version of the code, the permeability coefficient is not given by the product of intrinsic permeability times the relative permeability of the phase, but is given directly in the form K_w/γ_w that holds for the only liquid phase. In order to maintain the older representation for the permeability coefficients, due to the fact that sometimes intrinsic permeability for the medium is not available, different calculations are performed varying the parameter *PERMPS* from the integer value of 0 to 1. When *PERMPS* is equal to 0 the older permeability coefficient is used and adapted with the viscosities ratio. This is not an exact procedure but help to carry on calculation when leak of parameter occurs. The value of the permeability coefficients for the three directions is stored in the *KASB1*, *KASB2*, *KASB3* variables. The value of these coefficients are so multiplied by the volume afferent to the gauss point (*DAREA*) and the stored in the diagonal components of the matrix D. *SETD_PS* exchanges here the diagonal components of the array *D* (that is used also for the mechanical stiffness calculations in *PLISQX*), to the routine *FLISQX* that evaluates them by multiplying with the shape functions contained in the array P.

ALTERNATIVE_SOLVERS

The subroutine *ALTERNATIVE_SOLVERS* has been written to put beside to the standard skyline solver implemented originally on *PLASCON* a set of sparse solving tools. This routine provides four different types of solution procedures that are based on two kinds of solver libraries. These solvers, basically, perform the solution of system (2.7.2).

This routine implement solver routines contained in the “Linear Algebra PACKage” (LAPACK 3.3) libraries [15, 23] and the PARDISO [13, 24] solver that is optimized for multithread processors in order to perform eventually parallel computation. Manuals as well further insights, relative to the nature of these solvers, can be found on literature at the [25].

For each of this two solving techniques, the user can choose between two criteria to apply the boundary conditions on fixed node. This can allow four different way of solve the linear system. The first criterion for the imposition of boundary conditions

on certain fixed degrees of freedom, use the so called “row and column elimination” and the second the so called “penalty coefficient”.

The first, represents the clean way of impose the Dirichlet boundary conditions and reduce the dimension of the system matrix to solve, eliminating the equations that correspond to the know value (solution) imposed. This method however, is not very cheap because force to do recursive reallocations of global system matrix in memory and this costs several operations. The second one is faster, but the resolution process is influenced by proper choice of the penalty coefficient value that multiplies the diagonal terms corresponding to the degree of freedom that has to be fixed. This method maintains the original dimensions of the global system matrix that had before the imposition of boundary conditions, due to the fact that only scalar multiplications are involved in this operation. A careful reading of the source code attached below can explains how these methods work.

In order to preserve the possibility to use the original solvers of previous version of PLASCON all the operations, such local element to global system matrix assembly, set up of boundary conditions and compact row storing has been implemented or recalled in this subroutine. This is not an efficient way to perform these operations due to the fact that they can be done simultaneously to the local matrix computation operations (subroutine *FL36QX*), but is more suitable in order to maintain compatibility with older routines.

```
      subroutine ALTERNATIVE_SOLVERS (FIX,NOP,R1,U,NBC,GASHT,
                                      IGS,MDF1,SOLVER_METHOD)

!---  Description

!--- ASSEMBLE THE WHOLE SYSTEM MATRIX AND SOLVE THE SYSTEM
!--- LAPACK SOLVERS AND PARDISO PARALLEL SOLVER IMPLEMENTED

!---  Modules included

      . . .
      . . .
      use PARSAT
!---
      implicit none

!---  Variable declaration

      . . .
      . . .
      . . .
      integer(INT_KIND)                              :: SOLVER_METHOD

!--- 0 = Standard Skyline Gaussian Elimination,
!--- 1 = Lapack Non - Symm Solver with PENALTY,
!--- 2 = Lapack Non - Symm Solver with 0 -1,
```

```
!--- 3 = PARDISO with PENALTY,
!--- 4 = Lapack with row/column elimination,
!--- 5 = PARDISO with row/column elimination

!---  Initialization of main parameters

      parameter(PENALTY_COEFF = 10.0D+20)
      parameter(TRANS = 'N')
      parameter(UPLO  = 'U')
      parameter(msglvl = 0)

!---  Initialization right hand side term


      allocate(b(MRHS))
      b = R1

!---  Global matrix allocation

      msize = NP * NDF
      allocate(SYSMAT(msize,msize))
      SYSMAT = 0.d0


!---  Looping on local element matrix to form global matrix


      DO EL_COUNT = 1,NE
      ESTIFM  = 0.d0

!---  Reading the local stiffness matrix

      READ    (ITP2)    N,((ESTIFM(I,J), J=1,KSIZE),I=1,KSIZE)
      . . .
      . . .
      . . .
      END DO

!---  Setting auxiliary system array

      omsize = msize
      allocate(SYSMAT2(omsize,omsize))
      SYSMAT2 = SYSMAT

!---  Setting up the d.o.f fixity vector

      FIXVECTOR = 0
      J = 0
            DO I = 1, NBN
              nbound_index = NBC(I)
              IZ = 10**(NDF-1)
              FIXCODE = NFIX(nbound_index)
              DO L = 1,NDF
                     bccode = 1
                     IF (L .EQ. 4 .OR. L .EQ. 5) bccode = 2
                     J = nbound_index*NDF - NDF + L
                     IF (FIXCODE .LT. IZ) THEN
```

```
                      FIXVECTOR(J) = 0
                      ELSE IF (FIXCODE .GE. IZ) THEN
                      FIXVECTOR(J) = bccode
                      FIXCODE = FIXCODE - IZ
                      END IF
!                      J = J+1
                      IZ = IZ / 10
              END DO
            END DO
!-----------------------------------------------------------------------

!---  SETTING UP THE BOUNDARY CONDITIONS (SOLVERS 1, 4, 5)

IF (SOLVER_METHOD .EQ. 1 .OR. SOLVER_METHOD .GE. 4) THEN

    SELECT CASE (SOLVER_METHOD)

!--- with penalty coefficient (SOLVER 1)

    CASE(1)
               J = 1
               DO I = 1, NBN
                      nbound_index = NBC(I)
                      c = nbound_index * NDF + 1 - NDF
                      d = nbound_index * NDF
                      DO L = c, d
                      IF (FIXVECTOR(J) .NE. 0) THEN
                          SYSMAT(L,L) = PENALTY_COEFF
                          b(L)        = PENALTY_COEFF * U(L)
                      IF (FIXVECTOR(J) .EQ. 2) b(L)= b(L) / CURILL
                      END IF
                      J = J + 1
                      END DO
               END DO
    msize2 = msize

!--- with row and column elimination (SOLVER 4 and 5)

    CASE DEFAULT
    allocate(SYSMAT_dummy(msize,msize))
    allocate(b_dummy(msize))
    x = 0.d0
    count = 0
    SYSMAT_dummy = SYSMAT
    b_dummy      = b

!--- deallocation

    deallocate(SYSMAT)
    deallocate(b)

    DO I = 1, msize
        IF (FIXVECTOR(I) .NE. 0) THEN
           count = count + 1
           x(I) =  U(I)
           SYSMAT_dummy (I,I) = 0.d0
           IF (FIXVECTOR(I) .EQ. 2) x(I) = x(I) / CURILL
```

```
            b_dummy(:) = b_dummy(:) - SYSMAT_dummy(:,I) * x(I)
            SYSMAT_dummy (:,I) = 0.d0
            SYSMAT_dummy (I,:) = 0.d0
         ENDIF
    END DO

!--- reduced allocation

    allocate(SYSMAT(msize2,msize2))
    allocate(b(msize2))
    SYSMAT = 0.d0

!--- copying on reduced system array

      . . .
      . . .
      . . .

!--- Final deallocation of dummy arrays

    deallocate(SYSMAT_dummy)
    deallocate(b_dummy)
    END SELECT
!---

    SELECT CASE (SOLVER_METHOD)

!--- *************** SOLUTION WITH PARDISO **********************

    CASE (5)

!--- COMPACT SPARSE ROW STORAGE

      . . .
      . . .
      . . .
           CALL CSRS_ (SYSMAT,msize2,count,A,ia,ja)

!--- SET UP PARDISO PARAMETER

           maxfct = 1
           mnum   = 1
           mtype  = 11
           perm   = 0
           xs = 0.d0

           call SET_IPARM(iparm)

           pt = 0

!--- set optimal core number

                 call mkl_set_num_threads(iparm(3))

!--- Calling the pardiso routine

           phase  = 11
```

```
                  call pardiso (pt, maxfct, mnum, mtype, phase,
                                msize2, A, ia, ja, perm, 1, iparm,
                                msglvl, b, xs, error)
           phase  = 22
                  call pardiso (pt, maxfct, mnum, mtype, phase,
                                msize2, A, ia, ja, perm, 1, iparm,
                                msglvl, b, xs, error
           phase  = 33
                  call pardiso (pt, maxfct, mnum, mtype, phase,
                                msize2, A, ia, ja, perm, 1, iparm,
                                msglvl, b, xs, error

    CASE DEFAULT

!--- SET UP LAPACK ROUTINES PARAMETER

               allocate(ipiv(msize2))
               ipiv = 0

!--- *************** SOLUTION WITH LAPACK **********************

               call dgetrf(msize2, msize2, SYSMAT, msize2, ipiv,
                           info1)
!
               call dgetrs(TRANS,msize2,1,SYSMAT,msize2,ipiv,b,
                           msize2,info2)
!
               deallocate(ipiv)
    END SELECT
!---------------------------------------------------------------------
ELSE IF (SOLVER_METHOD .EQ. 2) THEN

!---  SETTING UP THE BOUNDARY CONDITIONS (SOLVERS 2)

               J = 1
               DO I = 1, NBN
                      nbound_index = NBC(I)
                      c = nbound_index * NDF + 1 - NDF
                      d = nbound_index * NDF
                      DO L = c, d
                      IF (FIXVECTOR(J) .NE. 0) THEN
                          SYSMAT(L,:) = 0.d0
                          SYSMAT(L,L) = 1.d0
                          b(L)        =  U(L)
                          IF (FIXVECTOR(J) .EQ. 2) b(L) = b(L) /
                                                                CURILL
                      END IF
                      J = J + 1
                      END DO
               END DO

           ISYMM = 0

!--- SET UP LAPACK ROUTINES PARAMETER

               allocate(ipiv(msize))
               ipiv = 0
```

```
!--- *************** SOLUTION WITH LAPACK **********************


               call dgetrf(msize,msize,SYSMAT,msize,ipiv,info1)
!
               call dgetrs(TRANS,msize,1,SYSMAT,msize,ipiv,b,MRHS,
                                                              info2)
!
               deallocate(ipiv)
!---------------------------------------------------------------------
ELSE IF (SOLVER_METHOD .EQ. 3) THEN

!---  SETTING UP THE BOUNDARY CONDITIONS (SOLVERS 3)

!--- Application of penalty
               J = 1
               DO I = 1, NBN
                      nbound_index = NBC(I)
                      c = nbound_index * NDF + 1 - NDF
                      d = nbound_index * NDF
                      DO L = c, d
                      IF (FIXVECTOR(J) .NE. 0) THEN
                          SYSMAT(L,L) = PENALTY_COEFF
                          b(L)        = PENALTY_COEFF * U(L)
                          IF (FIXVECTOR(J) .EQ. 2) b(L) = b(L) /
                                                          CURILL
                      END IF
                      J = J + 1
                      END DO
               END DO

!--- COMPACT SPARSE ROW STORAGE

      . . .
      . . .
      . . .
           CALL CSRS_ (SYSMAT,msize2,count,A,ia,ja)

!--- SET UP PARDISO PARAMETER

maxfct = 1
mnum   = 1
mtype  = 11
perm   = 0
xs = 0.d0
call SET_IPARM(iparm)
pt = 0

!--- set optimal core number

                  call mkl_set_num_threads(iparm(3))

!--- Calling the pardiso routine

phase  = 11
       call pardiso (pt, maxfct, mnum, mtype, phase, msize, A, ia,
```

```
                            ja, perm, 1, iparm, msglvl, b, xs, error)
phase  = 22
       call pardiso (pt, maxfct, mnum, mtype, phase, msize, A, ia,
                            ja, perm, 1, iparm, msglvl, b, xs, error)
phase  = 33
       call pardiso (pt, maxfct, mnum, mtype, phase, msize, A, ia,
                            ja, perm, 1, iparm, msglvl, b, xs, error)

!---------------------------------------------------------------------

END IF

!--- Copying the solution to GASHT array

     . . .
     . . .
     . . .

!--- Rewind output binary units


      REWIND       ITP2
      REWIND       ITP21

!--- Dismantle all pardiso allocations in memory

          phase  = - 1
          call pardiso (pt, maxfct, mnum, mtype, phase, msize, A,
                      ia, ja, perm, 1, iparm, msglvl, b, xs, error)
      deallocate(A)
      deallocate(ja)
      deallocate(ia)
      deallocate(SYSMAT)
      deallocate(b)

!--- Creating an update R1 vector for updated fluxes

      allocate(b(omsize))
      b = 0.d0
      R1 = 0.d0
      J = 1
      DO I = 1, NP
          DO L = 1, NDF
              b(J) = GASHT(2,L,I)
              J = J + 1
          END DO
      END DO
 !---
      xs = 0.d0
      DO L = 1 ,MRHS
        DO J = 1 ,MRHS
            xs(L) = xs(L) + SYSMAT2(L,J) * b(J)
        END DO
      END DO
            R1 = xs - R1

      END IF
```

```
      deallocate(SYSMAT2)
      deallocate(b)

!--- Conditioning the results with CURILL FACTOR

     GASHT (2,4,:) = GASHT (2,4,:) * CURILL
     GASHT (2,5,:) = GASHT (2,5,:) * CURILL

!--- End of subroutine

    RETURN
    END subroutine ALTERNATIVE_SOLVERS
```

The term *CURILL* that appear in this routine, is set in the routine *ILLCON* (System Matrix Set Up in Figure 3.2.1). This coefficient rescales the terms that correspond to the fluid phases, in this way the solution at each time step, of the linear system of equations (2.7.4)

$$\begin{bmatrix} \mathrm{K_T} & -C_{\mathrm{sw}} & -C_{\mathrm{sw}} \\ C_{\mathrm{sw}}^T & P_{\mathrm{ww}}+\theta\Delta t H_{\mathrm{ww}} & C_{\mathrm{wg}}+\theta\Delta t K_{\mathrm{wg}} \\ C_{\mathrm{sg}}^T & C_{\mathrm{gw}}+\theta\Delta t K_{\mathrm{gw}} & P_{\mathrm{gg}}+\theta\Delta t H_{\mathrm{gg}} \end{bmatrix}_{n+\theta} \begin{Bmatrix} \bar{\mathbf{u}} \\ \bar{\mathbf{p}}^{\mathrm{w}} \\ \bar{\mathbf{p}}^{\mathrm{g}} \end{Bmatrix}_{n+1} =$$

$$\begin{bmatrix} \mathrm{K_T} & -C_{\mathrm{sw}} & -C_{\mathrm{sw}} \\ C_{\mathrm{sw}}^T & P_{\mathrm{ww}}-(1-\theta)\Delta t H_{\mathrm{ww}} & C_{\mathrm{wg}}-(1-\theta)\Delta t K_{\mathrm{wg}} \\ C_{\mathrm{sg}}^T & C_{\mathrm{gw}}-(1-\theta)\Delta t K_{\mathrm{gw}} & P_{\mathrm{gg}}-(1-\theta)\Delta t H_{\mathrm{gg}} \end{bmatrix}_{n+\theta} \begin{Bmatrix} \bar{\mathbf{u}} \\ \bar{\mathbf{p}}^{\mathrm{w}} \\ \bar{\mathbf{p}}^{\mathrm{g}} \end{Bmatrix}_{n} + \Delta t \begin{Bmatrix} \dfrac{\partial \mathbf{f}^{\mathrm{u}}}{\partial t} \\ \mathbf{f}^{\mathrm{w}} \\ \mathbf{f}^{\mathrm{g}} \\ \end{Bmatrix}_{n+\theta} \qquad (3.4.1)$$

is equal to the solution of this system

$$\begin{bmatrix} \mathrm{K_T} & -C_{\mathrm{sw}}\,\omega & -C_{\mathrm{s}}\omega \\ C_{\mathrm{sw}}^T\omega & \left(P_{\mathrm{ww}}+\theta\Delta t H_{\mathrm{ww}}\right)\omega^2 & \left(C_{\mathrm{wg}}+\theta\Delta t K_{\mathrm{wg}}\right)\omega^2 \\ C_{\mathrm{sg}}^T\omega & \left(C_{\mathrm{gw}}+\theta\Delta t K_{\mathrm{gw}}\right)\omega^2 & \left(P_{\mathrm{gg}}+\theta\Delta t H_{\mathrm{gg}}\right)\omega^2 \end{bmatrix}_{n+\theta} \begin{Bmatrix} \bar{\mathbf{u}} \\ \bar{\mathbf{p}}^{\mathrm{w}}/\omega \\ \bar{\mathbf{p}}^{\mathrm{g}}/\omega \end{Bmatrix}_{n+1} =$$

$$\begin{Bmatrix} 1 \\ \omega \\ \omega \end{Bmatrix}^T \begin{bmatrix} \mathrm{K_T} & -C_{\mathrm{sw}} & -C_{\mathrm{sw}} \\ C_{\mathrm{sw}}^T & P_{\mathrm{ww}}-(1-\theta)\Delta t H_{\mathrm{ww}} & C_{\mathrm{wg}}-(1-\theta)\Delta t K_{\mathrm{wg}} \\ C_{\mathrm{sg}}^T & C_{\mathrm{gw}}-(1-\theta)\Delta t K_{\mathrm{gw}} & P_{\mathrm{gg}}-(1-\theta)\Delta t H_{\mathrm{gg}} \end{bmatrix}_{n+\theta} \begin{Bmatrix} \bar{\mathbf{u}} \\ \bar{\mathbf{p}}^{\mathrm{w}} \\ \bar{\mathbf{p}}^{\mathrm{g}} \end{Bmatrix}_{n} + \qquad (3.4.2)$$

$$+\Delta t \begin{Bmatrix} \dfrac{\partial \mathbf{f}^{\mathrm{u}}}{\partial t} \\ \omega \mathbf{f}^{\mathrm{w}} \\ \omega \mathbf{f}^{\mathrm{g}} \\ \end{Bmatrix}_{n+\theta}$$

where ω is equal to the *CURILL* value. This technique has the purpose to normalize the orders of magnitude of the components of the global system matrix. Sometimes discrepancies of several orders of magnitude between the stiffness values and the permeability coefficients, of solid and liquid phases produce a malconditioned system and the impossibility to obtain good results. With a prudent choice of the value of *CURILL* factor, discrepancies can be reduced and an equivalent system can be solved. Also the boundary conditions values imposed by row and column elimination technique or by penalty coefficient have to be resized by the *CURILL* value in order to proper conditioning the system. At the end the array *GASHT* that contains the updated solution for each node has to be multiplied by the conditioning term for the fluid phase in order to obtain the right results.

ROUTINE CSRS

This short routines perform the assembly of a generic square matrix, not necessary symmetric, with the compact row storage algorithm [26, 27] as requested by the *PARDISO* solver [13, 24, 25]. More details on the *CSRS* algorithm and on the format of input arrays for *PARDISO* are available on suggested literature.

```
      subroutine CSRS (SYSMAT,msize,count,A,IA,JA)

!--- Description

!---  Assembly of CSRS storing arrays

!--- Modules included

      . . .
      . . .
      use DIMVAR
!---
      implicit none

!--- Variable declaration


      . . .
      . . .

!--- Creation of sysmat, ia and ja


count2 = 1
count3 = 0

do i = 1,msize
   count3 = count3 + 1
   first = 0
   do j = 1,msize
      if (SYSMAT(i,j) .NE. 0.d0) then
```

```
         A (count2)  = SYSMAT(i,j)
         ja(count2) = j
         if (first .EQ. 0) ia(count3) = count2
         first = 1
         count2 = count2+1
      end if
   end do
   if (first .EQ. 0) count3 = count3 - 1
end do

!--- End of routine

return
end
```

Bibliography

1. Roscoe, K.H. and J. Burland, *On the generalized stress-strain behaviour of wet clay.* 1968.

2. Majorana, C., R. Lewis, and B. Schrefler, *Two-dimensional non-linear thermo-elastoplastic consolidation program Plascon.* The Finite Element Method in the Deformation and Consolidation of Porous Media, Lewis RW, Schrefler BA (eds), 1987.

3. Befi, M., *Modelli tridimensionali per l'analisi termomeccanica di geomateriali* Department of Civil, Environmental and Architectural Engineering, 1993: p. 271.

4. Zanetti, S., *Analisi tridimensionale di problemi di subsidenza per estrazione di fluidi.* Master Thesis, Departement of Civili, Environmental and Architectural Engineering, Padua, 1995-1996: p. 133.

5. Salomoni, V.A. and R.L. Fincato. *Subloading surface plasticity model algorithm for 3D subsidence analyses above gas reservoirs*. 2011.

6. Salomoni, V.A. and R. Fincato, *3D subsidence analyses above gas reservoirs accounting for an unconventional plasticity model.* International Journal for Numerical and Analytical Methods in Geomechanics, 2012. **36**(8): p. 959-976.

7. Salomoni, V.A. and R. Fincato, *Subloading surface plasticity model algorithm for 3D subsidence analyses above gas reservoirs.* International Journal of Geomechanics, 2012. **12**(4): p. 414-427.

8. Salomoni, V.A. and R. Fincato. *3D modelling of geomaterials accounting for an unconventional plasticity approach*. 2011.

9. Bolzon, G., B. Schrefler, and O. Zienkiewicz, *Elastoplastic soil constitutive laws generalized to partially saturated states.* Géotechnique, 1996. **46**(2): p. 279-289.

10. Pastor, M., O. Zienkiewicz, and A. Chan, *Generalized plasticity and the modelling of soil behaviour.* International Journal for Numerical and Analytical Methods in Geomechanics, 1990. **14**(3): p. 151-190.

11. Fincato, R., *3D nonlinear coupled modelling of geomaterials using the unconventional Subloading Surface approach*, 2013.http://paduaresearch.cab.unipd.it/5567/

12. Strassen, V., *Gaussian elimination is not optimal.* Numerische Mathematik, 1969. **13**(4): p. 354-356.

13. Schenk, O. and K. Gärtner, *Solving unsymmetric sparse systems of linear equations with PARDISO.* Future Generation Computer Systems, 2004. **20**(3): p. 475-487.

14. Anderson, E., *LAPACK Users' guide*. Vol. 9. 1999: Siam.

15. Anderson, E., et al., *LAPACK Users' guide*. 1995: Society for Industrial and Applied Mathematics Philadelphia.

16. Lloret, A. and E.E. Alonso, *State surfaces for partially saturated soils.* Proceedings of the 11th International Conference on Soil Mechanics and Foundation Engineering, San Francisco, 12-16 august 1985. Publication of Balkema, 1985.

17. Brooks, R.H. and A.T. Corey. *Properties of porous media affecting fluid flow*. in *Journal of the Irrigation and Drainage Division, Proceedings of the American Society of Civil Engineers*. 1966.

18. Liakopoulos, A.C., *Transient flow through unsaturated porous media*, 1964, University of California, Berkeley

19. van Genuchten, M.T., *A closed-form equation for predicting the hydraulic conductivity of unsaturated soils.* Soil Science Society of America Journal, 1980. **44**(5): p. 892-898.

20. van Genuchten, R., *Calculating the unsaturated hydraulic conductivity with a new closed-form analytical model*. 1978: International Ground Water Modeling Center.

21. Fernandez, R. and V. Schrock. *Natural convection from cylinders buried in a liquid-saturated porous medium*. in *Proceedings of the 7th International Heat Transfer Conference*. 1982.

22. Fernandez, R.T., *Natural convection from cylinders buried in porous media*, 1972, University of California, Berkeley

23. E. Anderson, Z.B., C. Bischof, S. Blackford, J. Demmel, J. Dongarra, J. Du Croz, A. Greenbaum, S. Hammarling, A. McKenney, and D. Sorensen, *Linear Algebra PACKage (LAPACK).* 1991, 1992, and 1998.

24. Schenk, O., et al., *PARDISO: a high-performance serial and parallel sparse linear solver in semiconductor device simulation.* Future Generation Computer Systems, 2001. **18**(1): p. 69-78.

25. *Intel Corporation - Intel® Math Kernel Library 11.0.3 Reference Manual*, 2011

26. Jennings, A., *A compact storage scheme for the solution of symmetric linear simultaneous equations.* The Computer Journal, 1966. **9**(3): p. 281-285.

27. Liu, J.W., *A compact row storage scheme for Cholesky factors using elimination trees.* ACM Transactions on Mathematical Software (TOMS), 1986. **12**(2): p. 127-148.

4 Numerical analyses

4.1. Introduction

In this chapter some numerical tests are presented. First of all, the results of analyses on test problems obtained with the code PLASCON3D_PS and a commercial code has been compared, in order to check the reliability of mechanical phase and fluid phases computations.

Further, a drainage by gravity test that reproduce the Liakopoulos experiment [1] on a sand column, will be discussed. Along with the presentation of this case, numerical strategies adopted to avoid numerical problems that can arise from the transition between states with different degrees of saturation (in particular from the fully saturation with water to the partially saturated conditions).

Comparison between two different water retention functions will be done in a case of flexible footing resting in a partially saturated soil, while a portion of aquifer will be analysed in the case of gas injection.

Finally, a comparison based on computing performances of the different implemented solvers will be given.

4.2. Phases tests

Solid phase

This first series of tests has been performed in order to check the mechanical solution and to compare the results obtained with the code with the commercial F.E. code Straus7. The test problem, involves one 20-nodes brick element with 27 gauss points, fully restrained at the bottom base and restrained horizontally on lateral surface, in the way that only vertical displacements are allowed (Figure 4.2.1a). The porosity of the medium is $n \cong 0$, the degrees of saturation are $S_w = 0$ and $S_g = 0$ as well as null pressure fields $p_w = 0$ and $p_g = 0$ are set on all nodes. The solid phase is loaded with a unitary pressure $p^* = 1$ on top surface, and null water and gas flux was imposed. The reference temperature was set to be

$\vartheta = 293.15\,\mathrm{K}$. The Young's modulus was set to $E = 4.0 \cdot 10^4\,\mathrm{MPa}$ with a null Poisson's coefficient. The boundary conditions are summarized in Figure 4.2.1a while the comparison of results in terms of displacements has been reported in Figure 4.2.2. As it can be seen the agreement between results is perfect. The test on solid phase has been done also for a column mesh of ten elements with identical material properties and boundary conditions (Figure 4.2.1b), in order to check the global assembling procedure of the local matrix contributes. The results in terms of vertical displacements are reported on Figure 4.2.3. As before the agreement is very good.

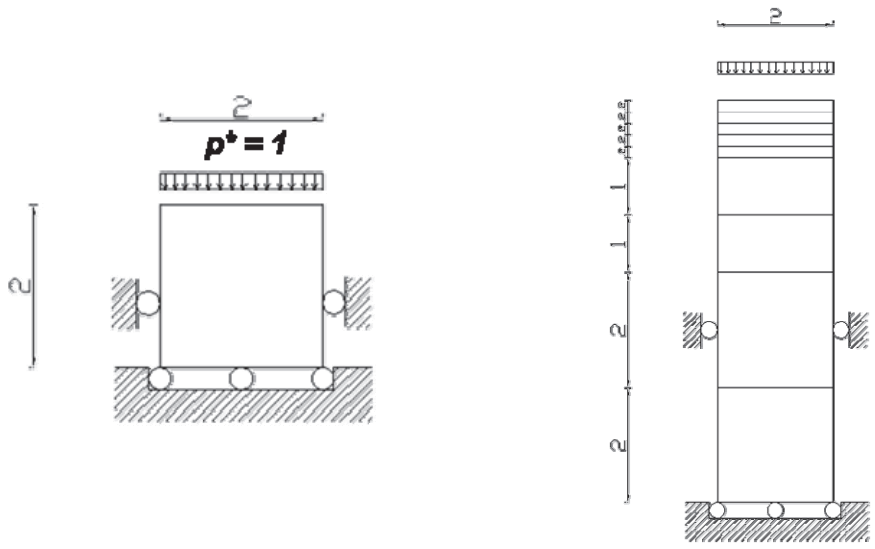

(a) (b)

Figure 4.2.1: Schematics of test problems for the solid phase. One brick element (a); ten brick elements (b).

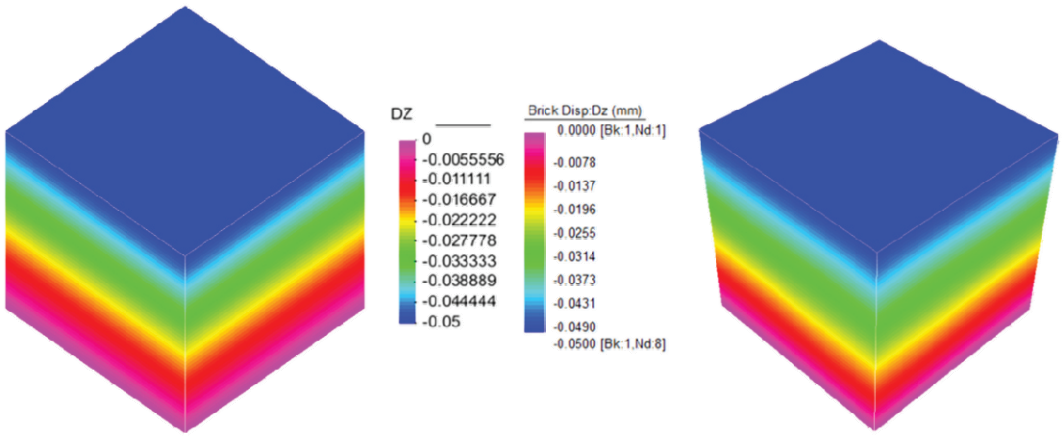

(a) (b)

Figure 4.2.2: Displacements along z direction obtained with PLASCON3D_PS (a); results obtained with Straus7 (b).

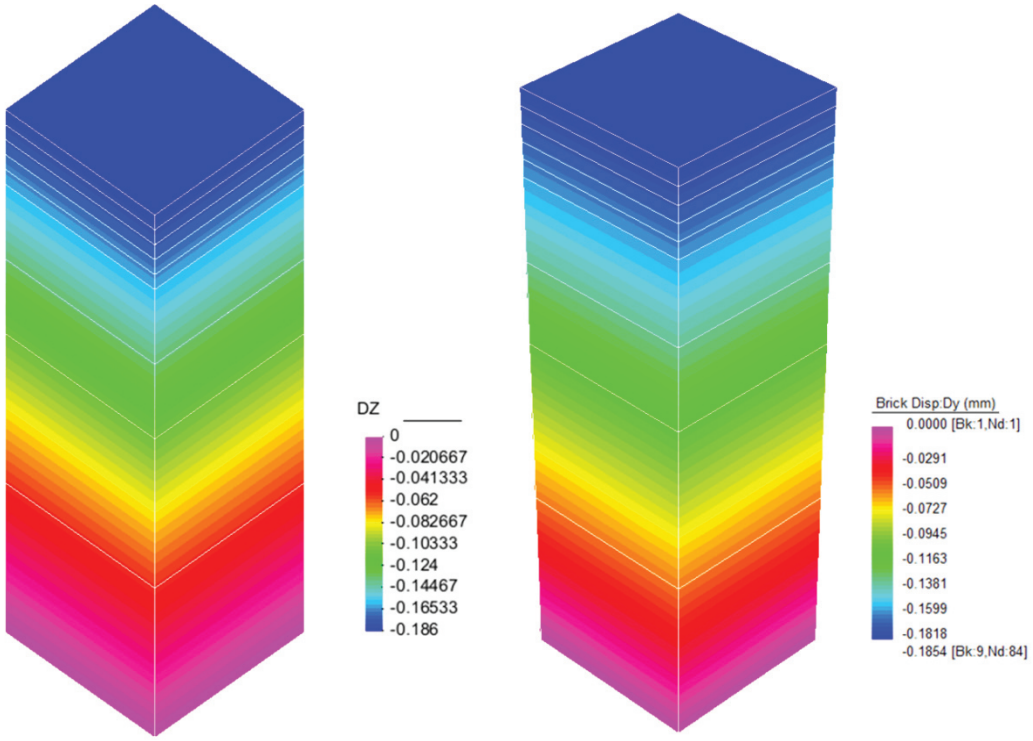

(a) (b)

Figure 4.2.3: Displacements along z direction obtained with PLASCON3D_PS (a); results obtained with Straus7 (b).

Liquid and gas phases

The liquid and gas phases have been checked comparing the results of one phase at once with the results obtained with the classical PLASCON3D where alternatively the properties of water and gas were set. Again, two meshes, one with one brick element and another with ten brick elements, have been tested. The boundary conditions consist on a full restrain of displacements at the base, then on the nodes at the base and on top surfaces the pressure of the phase that has to be checked is set to zero. Other nodes have the pressure degree of freedom free to vary, while the other phase has null value on all nodes. The degree of saturation of the phase that has to be checked is set to 1. The top surface nodes on the two mesh are subjected to a increasing vertical displacement that evolves linearly to a final value of 5 mm. The boundary conditions are summarized in Figure 4.2.4a-b while the comparison of results in terms of liquid pressures has been reported in Figure 4.2.5 and for the mesh with ten elements on Figure 4.2.6. As can be seen, again, the agreement between the two codes is perfect and the results obtained for the gas phase where saturations are set to $S_w = 0$ and $S_g = 1$ are similar to the one obtained for the liquid phase, and denoted perfect matching as well.

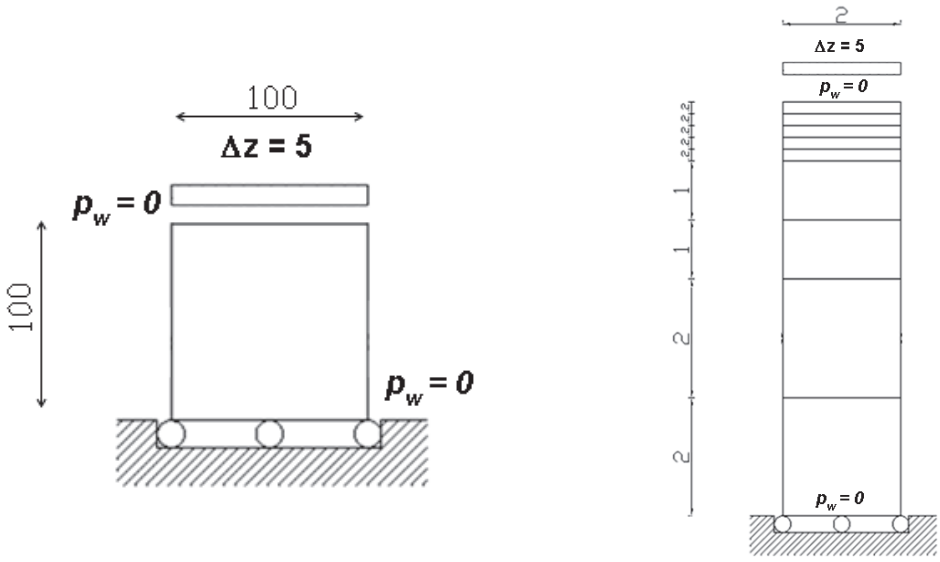

(a) (b)

Figure 4.2.4: Schematic of test problem for the liquid phase. One brick element (a); ten brick elements (b).

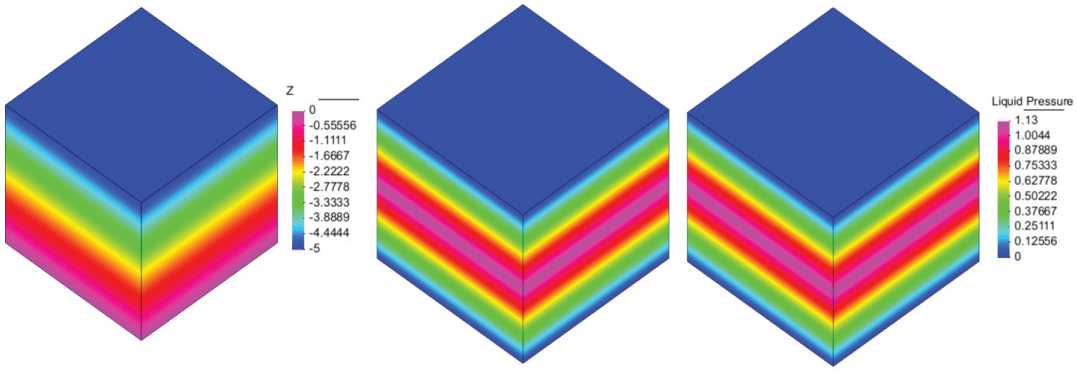

(a) (b) (c)

Figure 4.2.5: Displacements obtained at the end of load process of a brick element (a); liquid pressure obtained with PLASCON3D_PS (b); liquid pressure obtained with PLASCON3D (b).

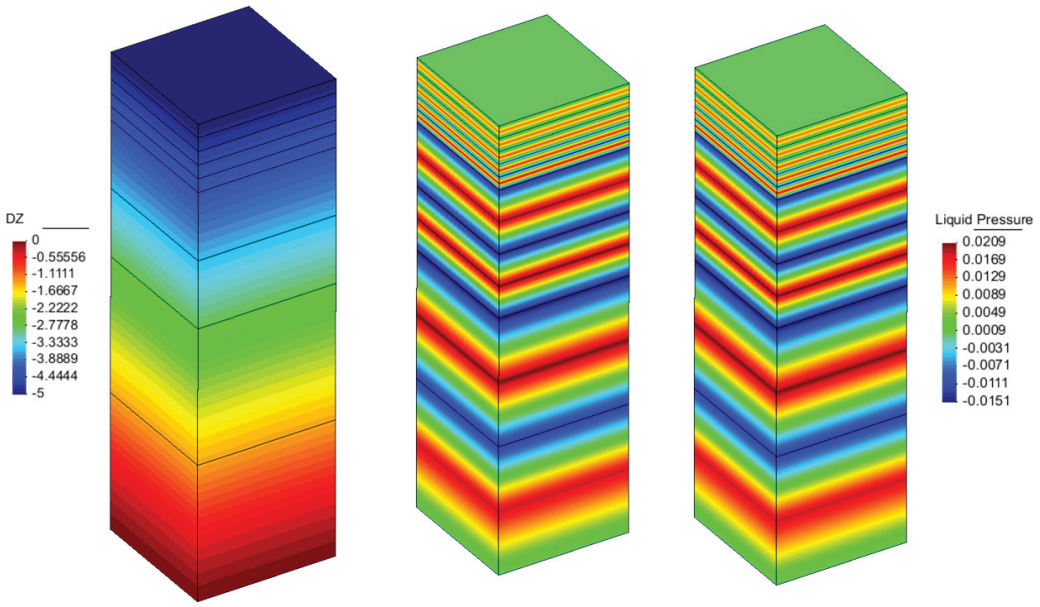

(a) (b) (c)

Figure 4.2.6: Displacements obtained at the end of load process of a ten elements mesh (a); liquid pressure obtained with PLASCON3D_PS (b); liquid pressure obtained with PLASCON3D (b).

4.3. Drainage test

The case presented in the following is used quite often as validation test of numerical codes that implement the partial saturated formulation. This benchmark is based on the experimental test that Liakopoulos [1] carried out in laboratory on an instrumented sand column, to observe the desaturation of a material sample subjected to only gravitational effects.

Experimental test

In the experiment of Liakopoulos [1] a 1.0 m column of Del Monte sand was packed into a Perspex box having a square base with edge length of 0.1 m. The column was instrumented with a sufficient number of tensiometers to measure the moisture tension at several points along the column. Before the starting of the experiment, at $t < 0$, the sand sample was continuously wetted by addition of water from top surface and was allowed to drain freely at the bottom through a micro pore filter, until uniform flow conditions were established. At starting of the experiment ($t = 0$) the wetting from the top of the column was ceased and the tensiometers readings were recorded.

For the degree of water saturation vs. capillary pressure relationship, an approximated Brooks and Corey function, given by of Liakopoulos [1], can applied (Figure 4.3.1):

$$S_w = 1.0 - 1.9722 \cdot 10^{-11}\, p_c^{2.4279} \tag{4.3.1}$$

$$k_{rw} = 1.0 - 2.207\left(1 - S_w\right)^{1.0121} \tag{4.3.2}$$

While for gas relative permeability holds again the relation given by Brooks and Corey:

$$k_{rg} = \left(1 - S_e\right)^2 \left(1 - S_e^{5/3}\right) \tag{4.3.3}$$

With

$$S_e = \left(S_w - 0.2\right) / \left(1 - 0.2\right) \tag{4.3.4}$$

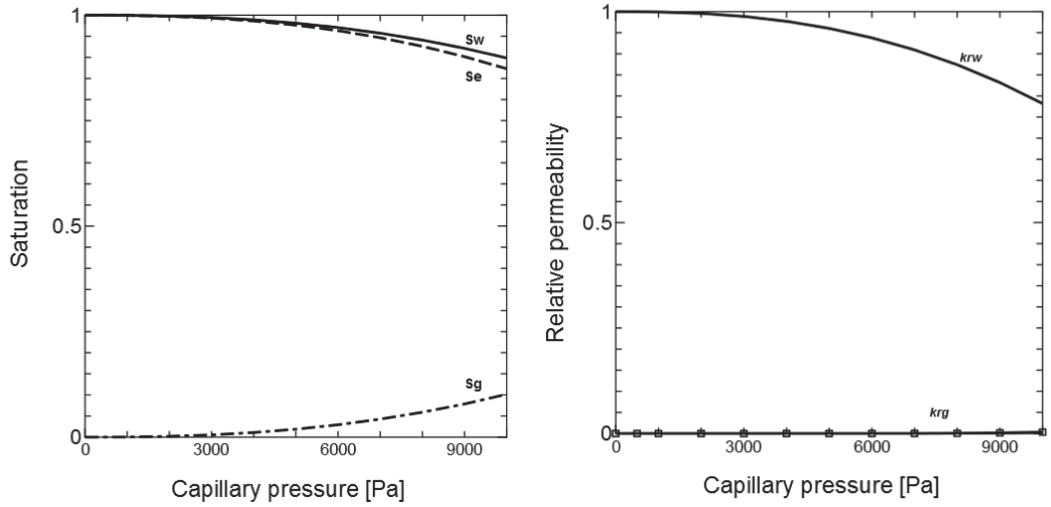

Figure 4.3.1: Evolution with capillary pressure of the degrees of saturation and relative permeabilities for the Liakopoulos [1] suggested law.

Boundary conditions and mesh discretization

The test problem was solved numerically by Liakopoulos [1], Narashiman and Whitherspoon [2], Schrefler and Simoni [3], Zienkiewicz *et al.* [4], Schrefler and Zhan [5], Gawin *et al.* [6], as well as by Gawin and Schrefler [7] to check their numerical models.

In particular [8] adopted the following initial and boundary conditions (also reported in Figure 4.3.2). The initial conditions on all the nodes are:

$$p_c = 0 \;\Rightarrow S_w = 1 \tag{4.3.5}$$

A Steady vertical flow of water, as well as a state of mechanical equilibrium was assumed. For the lateral surfaces the boundary conditions are:

$$\begin{aligned} &q_T = 0,\ q_w = 0,\ q_g = 0 \\ &u_h = 0 \end{aligned} \tag{4.3.6}$$

Where u_h are the horizontal displacements of soil. For the top surface:

$$p_g = p_{atm} \tag{4.3.7}$$

while for the bottom surface

$$\begin{aligned} &p_g = p_{atm},\ p_c = 0 \\ &u_v = u_h = 0 \end{aligned} \tag{4.3.8}$$

Where u_v are the horizontal displacements of soil.

The properties of the Del Monte sand sample are reported on Table 4.3.1.

Table 4.3.1: Property of Del Monte sand used in the Liakopoulos experiment

Young's modulus	$E = 1.3\ \mathrm{MPa}$
Poisson's ratio	$\nu = 0.4$
Solid grain density	$\rho_s = 2000\,\mathrm{kg \cdot m^{-2}}$
Liquid density	$\rho_w = 1000\,\mathrm{kg \cdot m^{-2}}$
Porosity	$n = 0.2975$
Intrinsic permeability	$\mathrm{k} = 4.5 \cdot 10^{-13}\ \mathrm{m^2}$
Water viscosity	$\mu_w = 1 \cdot 10^{-3}\ \mathrm{Pa \cdot s}$
Air viscosity	$\mu_a = 1.8 \cdot 10^{-5}\ \mathrm{Pa \cdot s}$
Gravitational acceleration	$g = 9.806\,\mathrm{m \cdot s^{-2}}$
Atmospheric pressure	$p_{atm} = 101325\,\mathrm{Pa}$

Due to the fact that an isothermal analysis was carried out, a reference temperature on the whole domain was taken ($\vartheta = 293.15\,\mathrm{K}$). Furthermore, the Biot's constants was taken $\alpha = 1$ denoting non deformable solid grains, i.e. all displacements

involved on the process are given by a rearrangements of soil skeletons and voids volume.

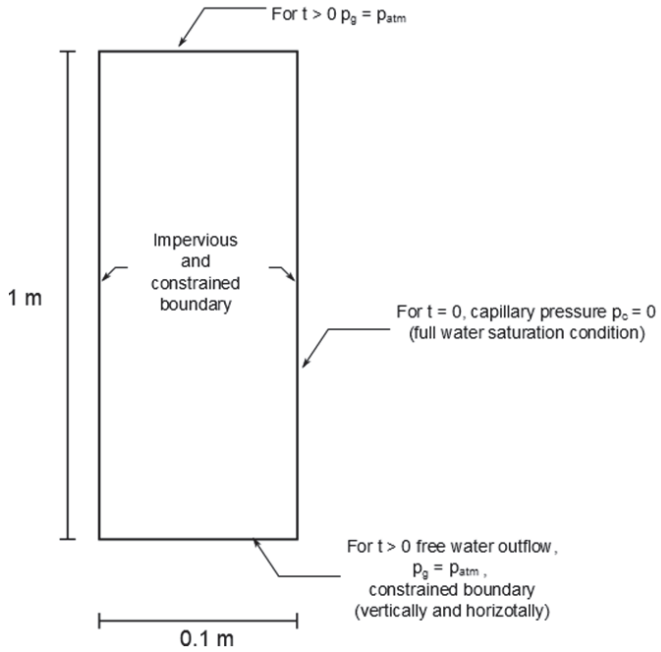

Figure 4.3.2: Boundary conditions for the test performed by Liakopoulos.

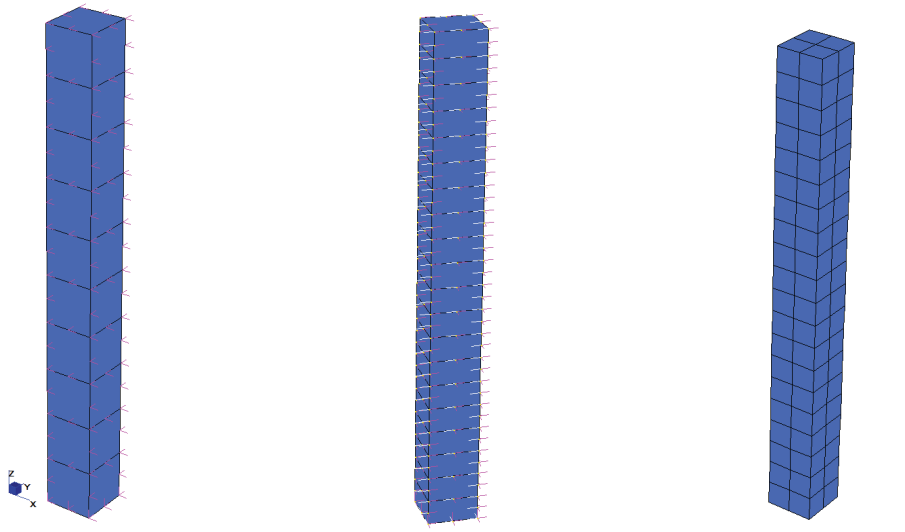

Figure 4.3.3: Three-dimensional meshes of the Del Monte sand column from Liakopoulos experiment.

In order to compare the two-dimensional analyses in the above mentioned works with a three-dimensional one, the mesh geometry tested with PLASCON3D_PS follows the two-dimensional mesh adopted in [8]. The mesh has been simply extruded over the plane by 0.1 meter. In this way, the domain that was subdivided in ten 8-nodes isoparametric elements in [8], here is subdivided in ten 20-nodes

isoparametric brick elements (details about the element that has been adopted can be found in the Section 2.8). Furthermore, all the initial and boundary conditions has been maintained as given in (4.3.6), (4.3.7) and (4.3.8), with the addition that now horizontal displacements are u_x , u_y and the vertical one is u_z. Now to maintain as in [8] the axial symmetry given by the horizontal constraints, both the degrees of freedom relative to u_x and u_y have been fixed.

The gravity flux has been implemented with the following equation

$$\mathbf{f}_{\mathrm{w}} = \int_{\Omega} \left(\nabla \mathbf{N}_{\mathrm{p}} \right)^{T} \rho_{w} \frac{\mathbf{k} k_{rw}}{\mu_{w}} \mathbf{g} \, d\Omega \tag{4.3.9}$$

Where only the vertical component of the gravity vector $\mathbf{g}$, is different from zero.

For the analyses, the domain has been discretized in 10, 20 and 80 brick elements. The resulting three-dimensional meshes have been reported on Figure 4.3.3.

Transition from fully saturated to partial saturated state

This test has been solved in the past by the different authors in three different ways, in order to manage the numerical complexities that arise when the transition from fully saturated state to the partially saturated state take place. They are:

a. The gas pressure value in the partially saturated zone is assumed to be equal to the atmospheric pressure (one phase-flow approach), which implies a infinite, not physically realistic, value of gas relative permeability. This assumption was used by Schrefler and Simoni [3], Schrefler and Zhan [5] and Gawin *et al.* [6, 7] ;

b. A very small, but finite, value of gas relative permeability exists even for the fully saturated state. This physically implies that a flow of gas exists for the fully saturated state and can be obtained by appropriate modification to the capillary pressure-saturation relationship [5] and/or the relative permeability curve [7]. With this approach the gas-phase continuity equation is always maintained;

c. A so called “switching” between the one-phase, saturated flow and full two-phase solutions could occur at a certain value of the saturation, e.g. at the value corresponding to the bubbling pressure, which has a physical justification. Also, the application of and additional lower limit for the gas relative permeability is usually necessary in order to avoid oscillations in the pressure solution. This approach was proposed by Gawin *et al.* [6] and Gawin and Schrefler [7].

In the present work, the problem of the changing in the saturation state, has been solved pursuing the method a) and b). The first implies that even for small degrees of gas saturation the pressure of the gas phase is always at standard atmospheric pressure and the gas relative permeability, that usually depends as well as the one for the water, on the degree of saturation S_w , is set to higher values. The second method allows, rather than the third, that the gas phase continuity equation last also for degrees of saturation very close to the full saturation. To achieve this goal, both the degrees of saturation, have not to reach null values in every point of capillary pressure range, otherwise the corresponding equations will be multiplied by a null value leading very soon to singularities in the global system matrix, with the impossibility to solve the whole system of equations that will be malconditioned with respect to every solving scheme.

In PLASCON3D_PS, as presented within the discussion of this case and the ones that will follow, two strategies can be adopted to avoid this numerical problem.

The first numerical strategy is to add a positive term to the water retention function as evidenced for example comparing the (1.5.7) with the (1.5.8). The additional term $S_{g,irr}$ has the same physical meaning of the irreducible degree of water saturation $S_{w,irr}$, that take into account of the presence, even little, of one phase into the other. This is the method adopted in the solution with PLASCON3D_PS of this test case. After that the assumption of the existence of a small but positive value of irreducible degree of gas saturation has been made during the developing of the present work, it has been discovered that a very similar strategy has been adopted also by Laloui *et al.* [9]. In order to avoid numerical problems, Laloui *et al.* make some assumption on the maximum degree of saturation, set to the value of $S_w = 0.99$ and the minimal gas relative permeability set to $k_{rg} = 0.01$. In addition they fixed the maximal change in relative permeability to a maximum of 5% each step from the previous step of the analysis.

The second numerical strategy, is to set a small but positive value of initial capillary pressure that allows, with respect to the retention curve adopted, a small but positive, initial value of degree of water saturation. While this last strategy affects only the initial conditions and guess a good numerical path at the onset, for the solution of the initial time steps, the first strategy acts during all the analysis and prevents null values of gas saturation at each time step. In practice, while the first is a compulsory assumption, the second is recommended where initial conditions involve fully saturation of a part of the domain. In most of cases, the two strategies have to be used simultaneously.

The method c) that is not implemented in PLASCON3D_PS can be regarded as alternative to method b), with the difference that the one-phase, fully saturated, formulation coexists with the partial one, and holds on that nodes that reach the full saturation $S_w = 1$. The "switch" is performed monitoring the capillary pressure on nodes, and with this method, a single finite element can have nodes on which is applied one formulation and nodes in which holds the partially formulation. Without such switch or the assumption done with method b) and above mentioned, the presence of a null degree of saturation induces to a mal conditioned problem. The method c) despite its correctness introduces the need of locating the isobar that may cross an element and requires a dedicated implementation of the switch procedure that affect deeply the code structure and need of an evaluation of optimal time step to avoid pressure oscillation [6, 10]. The switching procedure well explained in [10].

Numerical results

Numerical results will be given for the 10 elements mesh and the finest mesh with 80 elements in order to test sensitivity of the results with the mesh refinement. The results presented regard both the method with only one phase flow (water flow) in partially saturated state, with pressure of the gas phase at atmospheric pressure and the method that take into account of airflow and water flow in the porous medium. Results are given plotting the variation of pressures, degree of water saturation and vertical displacements vs. the column height (1 m) for 0, 5, 10, 20, 30, 60 and 120 minutes. Contour maps for water pressure, gas pressure, capillary pressure, degree of water saturation and displacements are reported for the mesh with 10 elements (Figure 4.3.9 to Figure 4.3.17).

The results in terms of gas pressure has been reported only for the second method of analysis due to the fact that in the first method gas pressure reaches immediately the atmospheric pressure value in the partial saturated zone. This can be done setting the relative permeability of the gas a finite but very high value.

As can be seen from graphs reported on Figure 4.3.4 to Figure 4.3.8, where two methods are compared, the final water pressures and displacements have the same distribution along the height of the column (Figure 4.3.4 and Figure 4.3.8). Despite capillary pressure values on top are very similar between two cases (Figure 4.3.6) the first case presents higher values at each height, and generally this values are reached before in time than the second case. This result is achieved by effect of the higher relative permeability of the gas that allows that in each point of the partial saturated zone the pressure of the gas is equal to the atmospheric one. This fact influences directly the degree of water saturation along height that for the first case

shows a desaturation effects pretty homogeneous along all the height, in the other hand, the second case shows that desaturation effects occurs principally on the first 30 cm from the top of the column where the air entry effect, as well as gas relative permeability are higher (Figure 4.3.7). Water pressure decrease by effect of gravity forces more rapidly in the second case, where the capillary effects are less than the first case (Figure 4.3.4).

Displacements behave in the same way, denoting that values of vertical displacements close to final value at 120 minutes are reached faster than the case where one phase water flow is considered (Figure 4.3.8).

Finally the suction effects induced on the gas phase by the gravity water flow are higher, as expected, during the firsts 20 minutes of analysis (second method), denoting during this time span the lowest values of gas pressure (less than 98000 Pa at 10 minutes).

Graph results of the one-phase water flow case compared with two-phase flow results for the 10 elements mesh

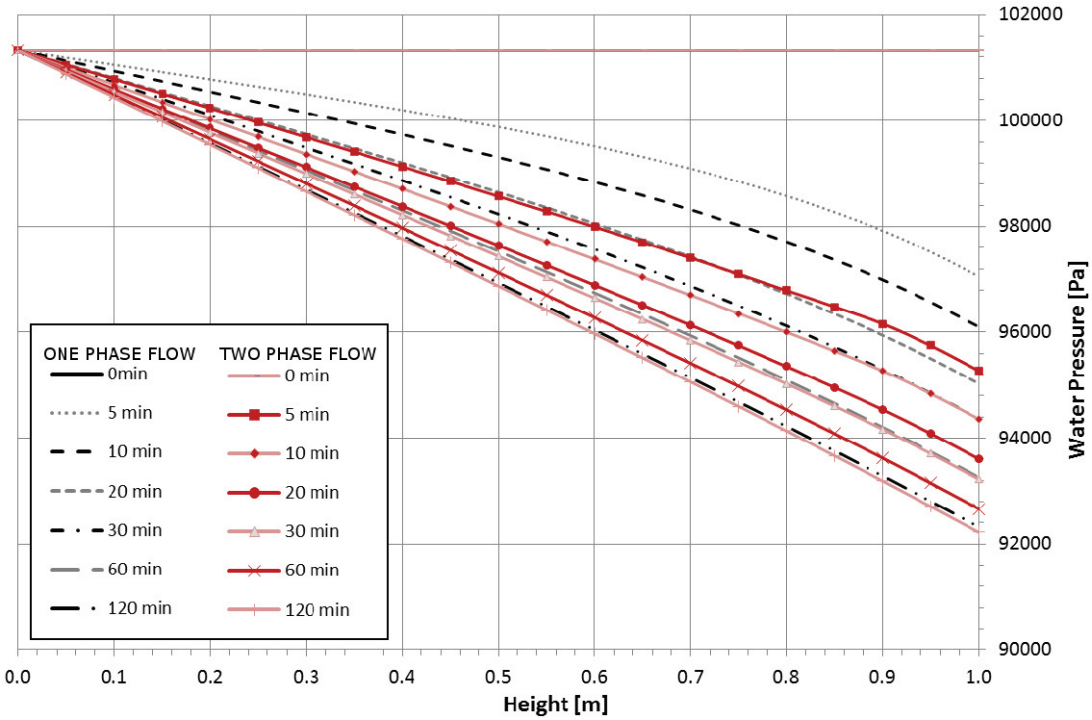

Figure 4.3.4: Water pressure [Pa] vs. height [m] for the one phase water flow case (black lines) and two-phase flow case (red lines with indicators), for the 10 element mesh.

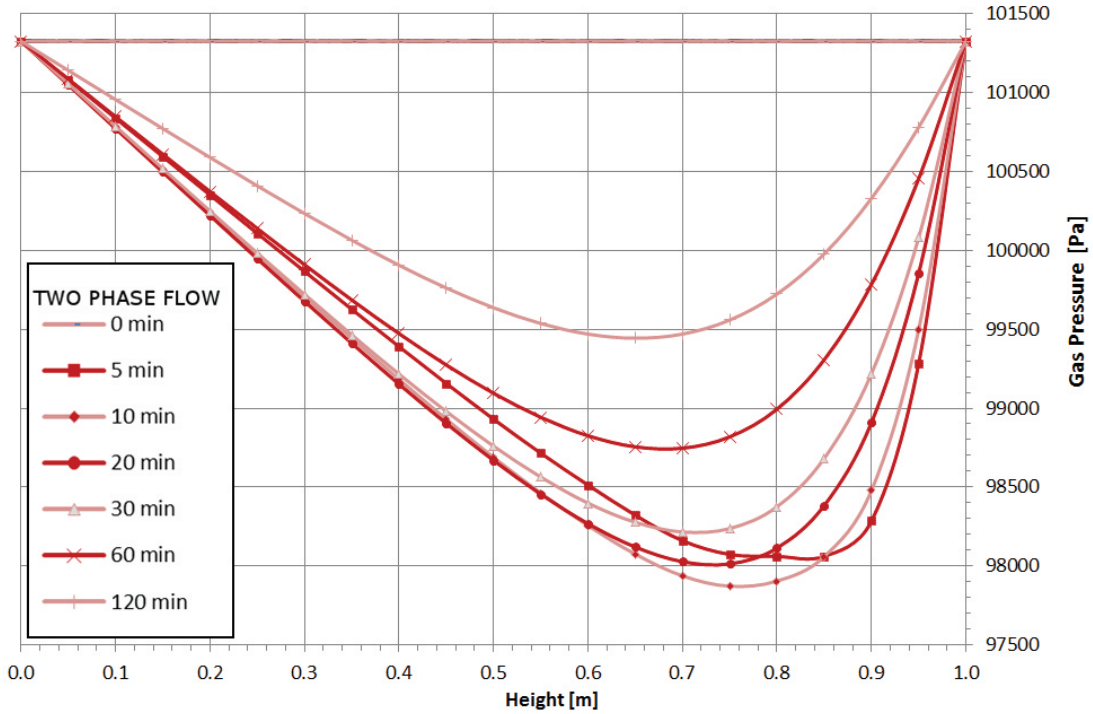

Figure 4.3.5: Gas Pressure [Pa] vs. height [m] for two-phase flow case (red lines with indicators), for the 10 element mesh.

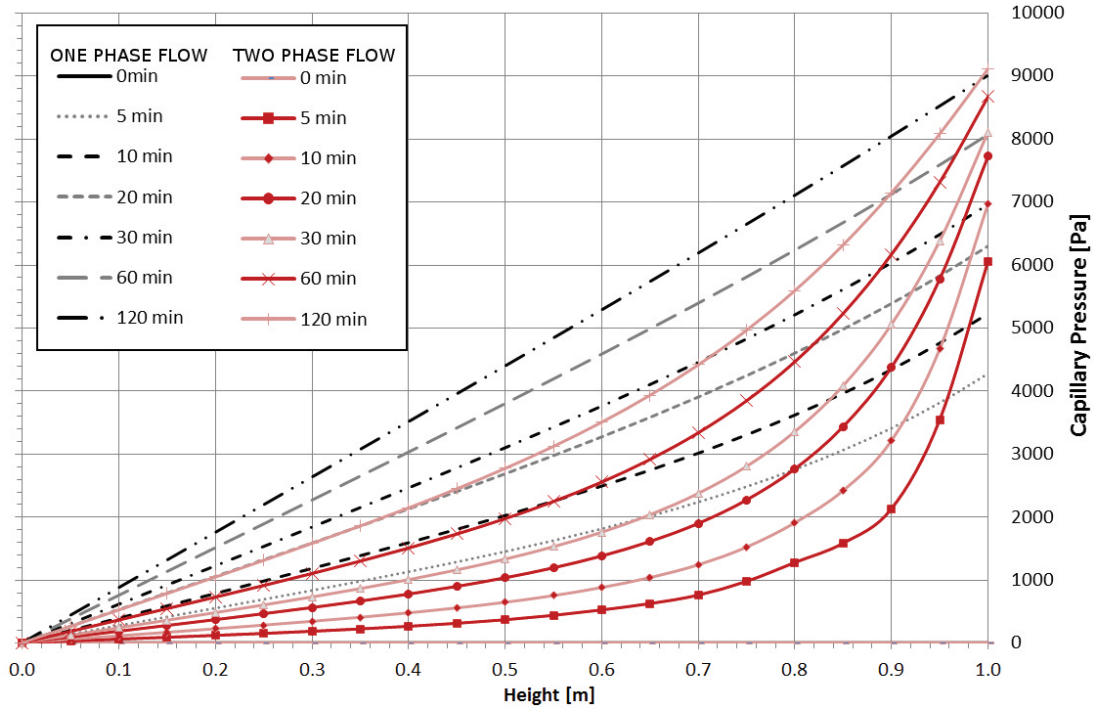

Figure 4.3.6: Capillary Pressure [Pa] vs. height [m] for the one phase water flow case (black lines) and two-phase flow case (red lines with indicators), for the 10 element mesh.

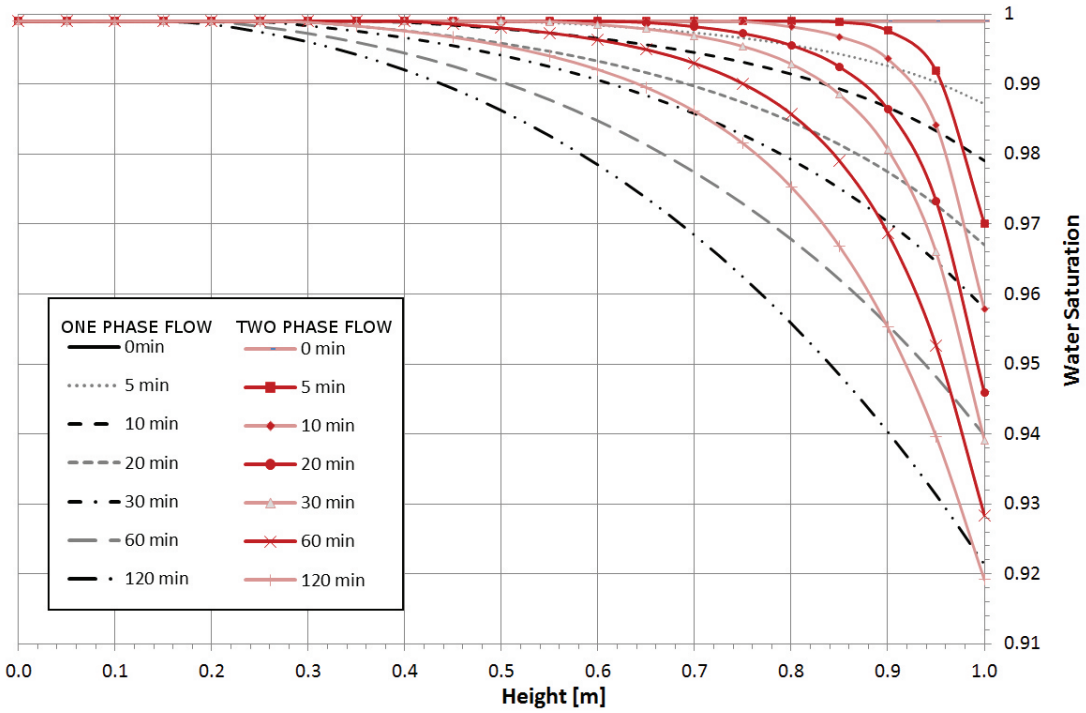

Figure 4.3.7: Water Saturation vs. height [m] for the one phase water flow case (black lines) and two-phase flow case (red lines with indicators), for the 10 element mesh.

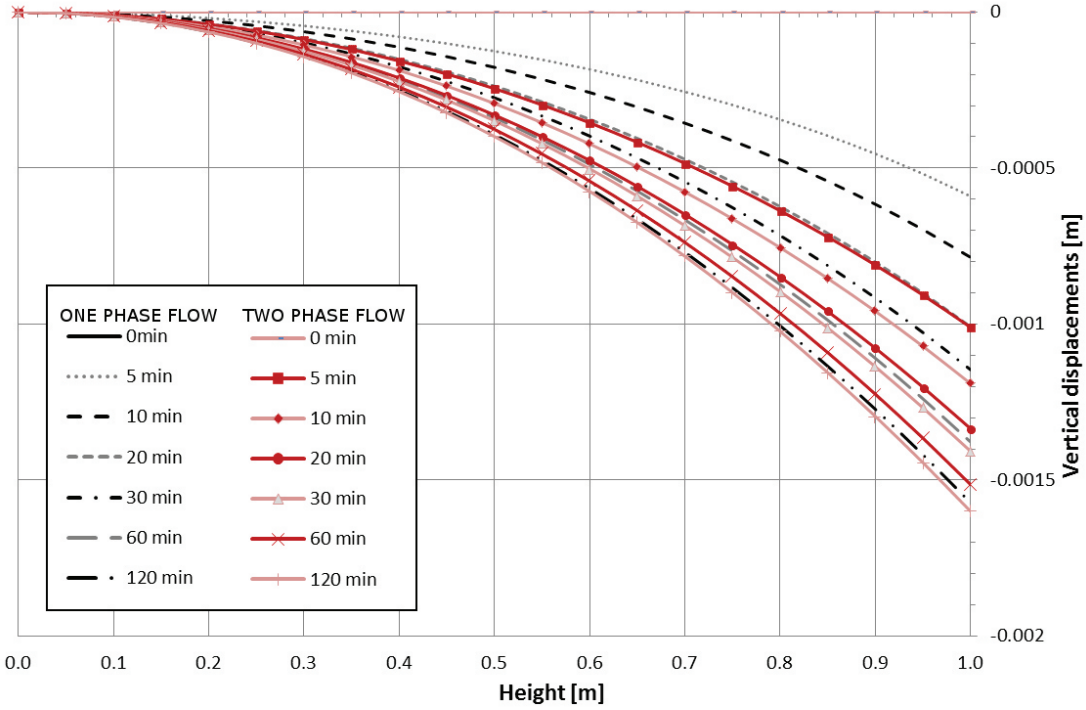

Figure 4.3.8: Vertical displacements [m] vs. height [m] for the one phase water flow case (black lines) and two-phase flow case (red lines with indicators), for the 10 element mesh.

Contour maps for the one-phase water flow results

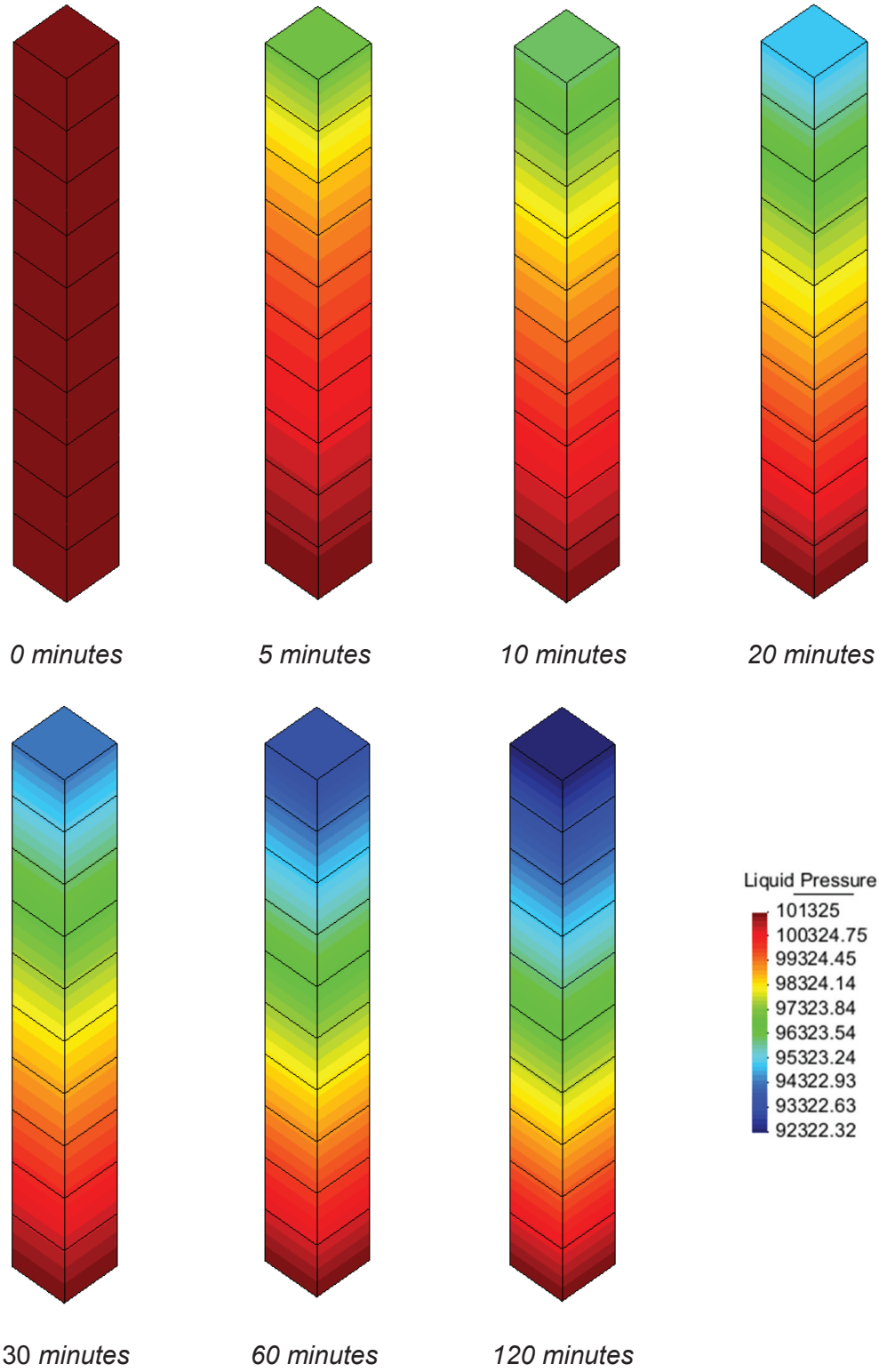

Figure 4.3.9: Water Pressure [Pa] for the one-phase water flow case, for the 10 element mesh.

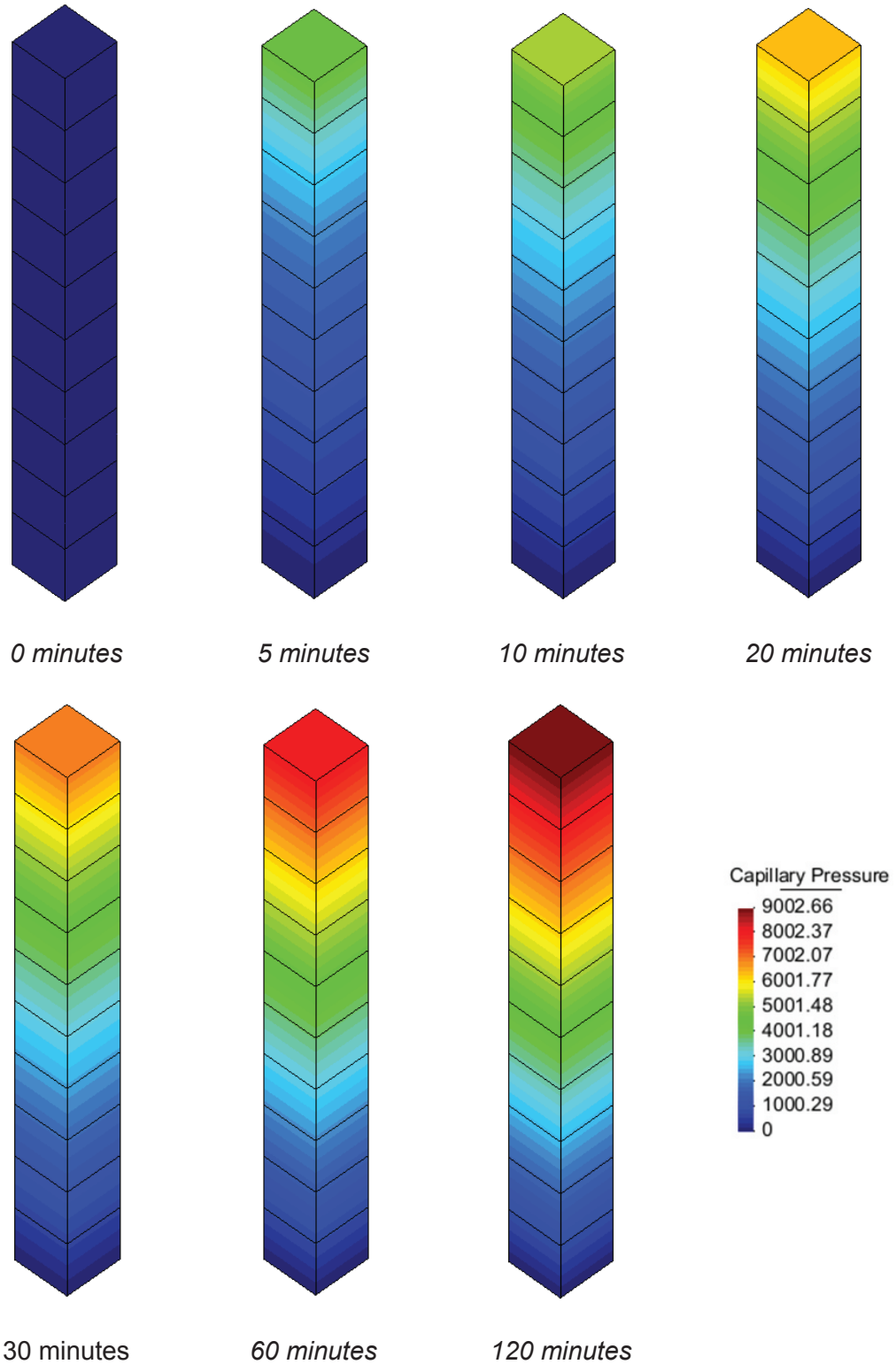

Figure 4.3.10: Capillary pressure [Pa] for the one-phase water flow case, for the 10 element mesh.

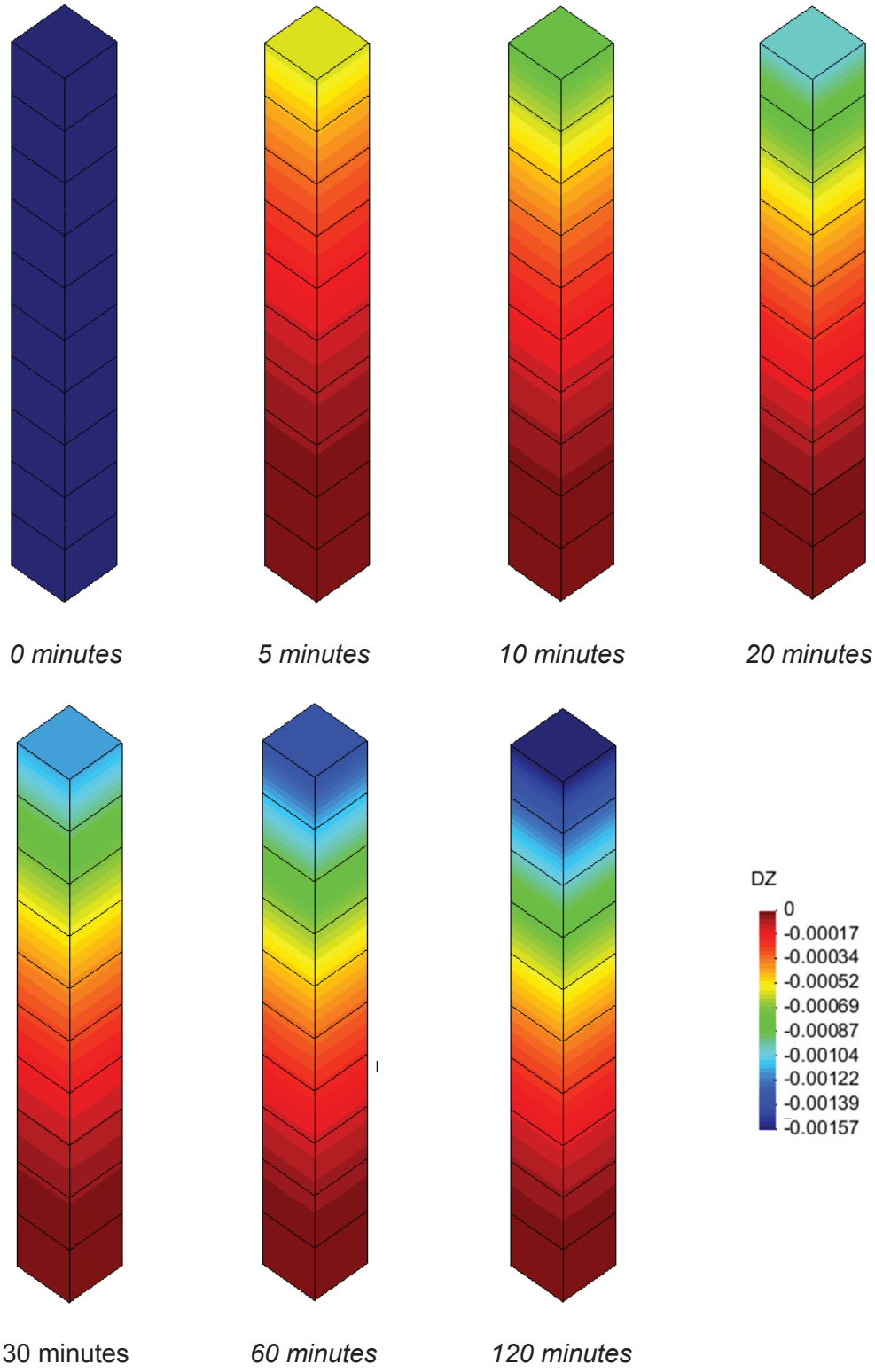

Figure 4.3.11: Displacements [m] for the one-phase water flow case, for the 10 element mesh.

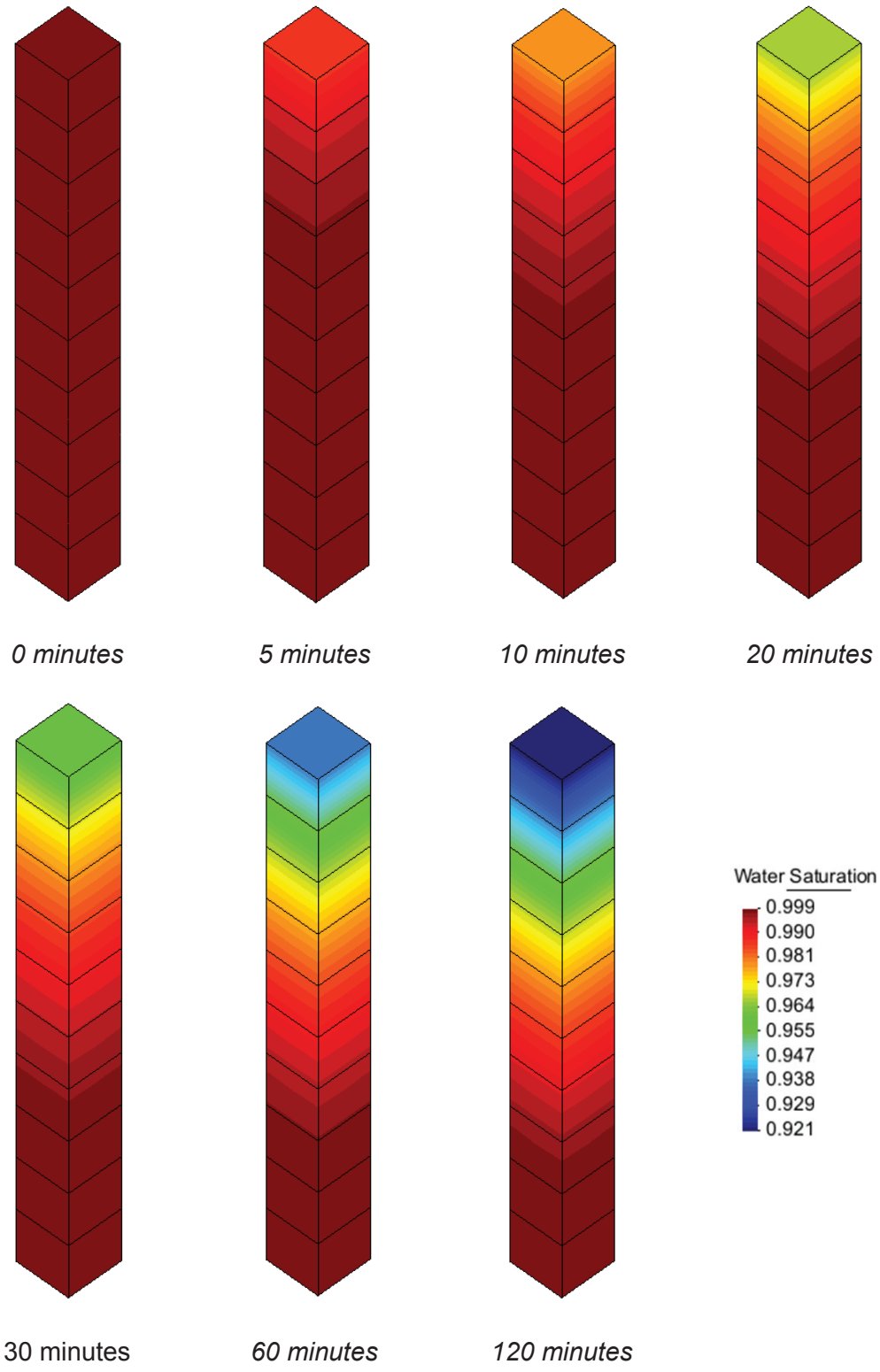

Figure 4.3.12: Degree of water saturation for the one-phase water flow case, for the 10 element mesh.

Contour maps for the two-phase flow results

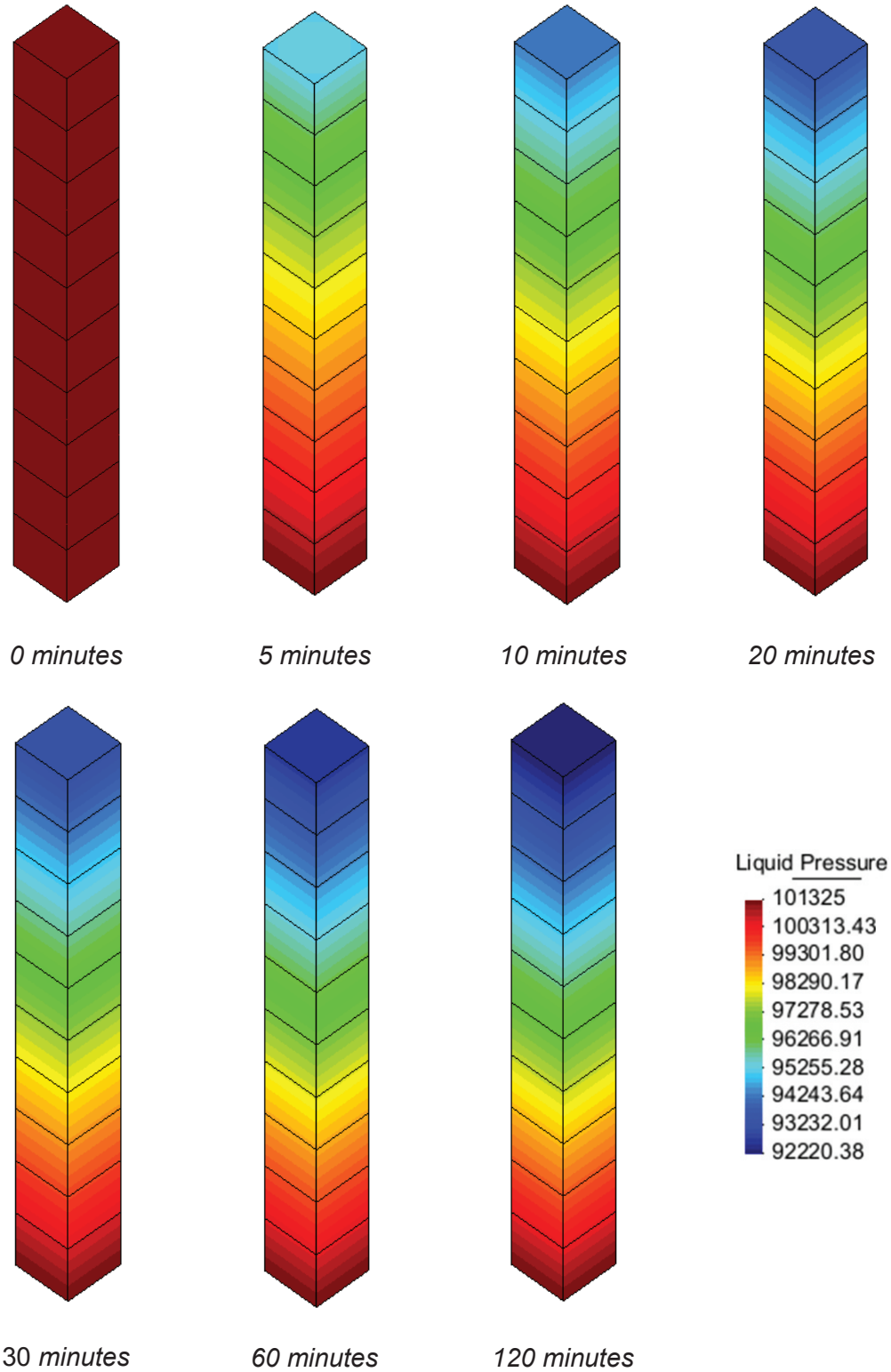

Figure 4.3.13: Water Pressure [Pa] for the two-phase flow case, for the 10 element mesh.

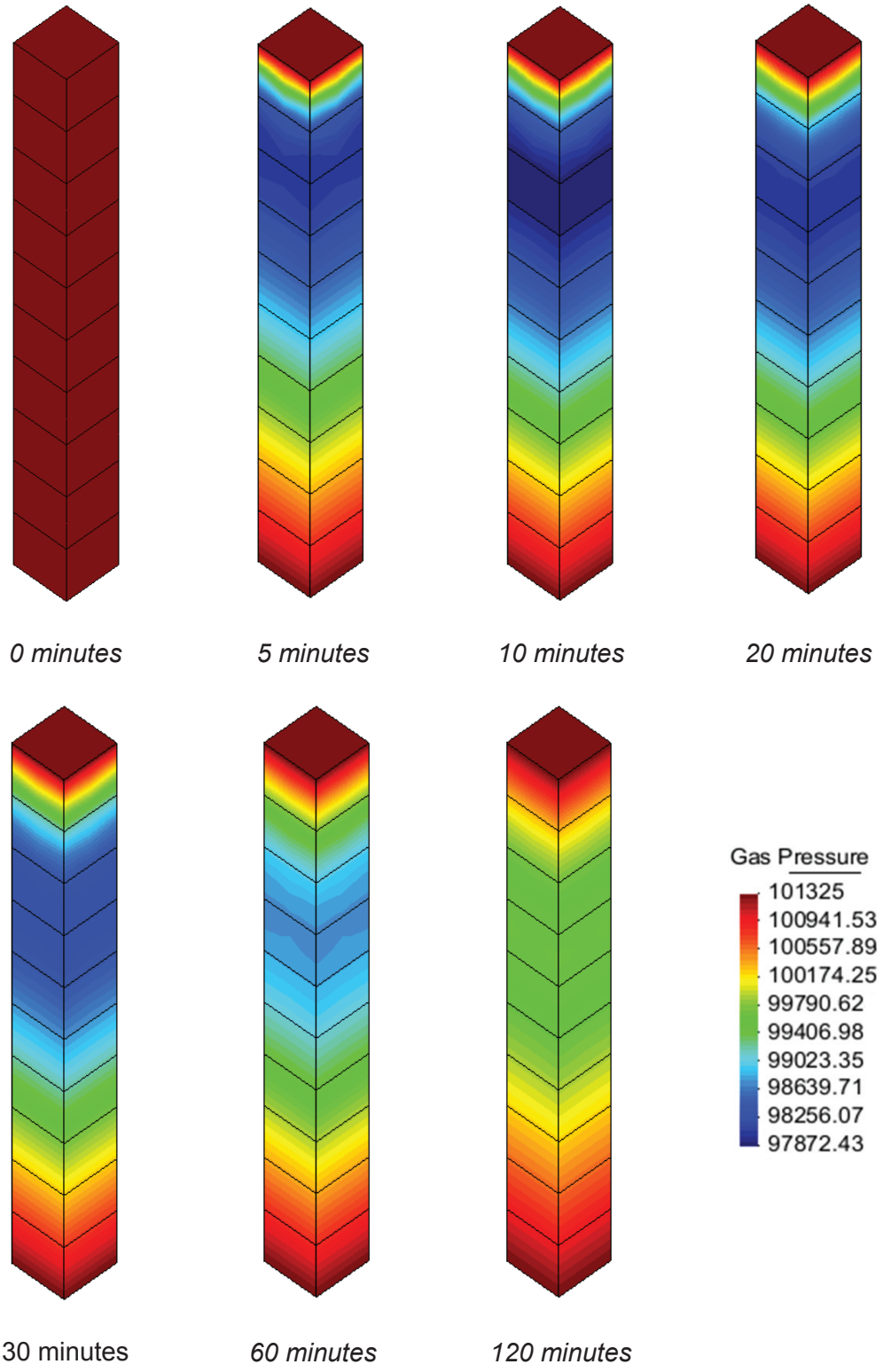

Figure 4.3.14: Gas Pressure [Pa] for the two-phase flow case, for the 10 element mesh.

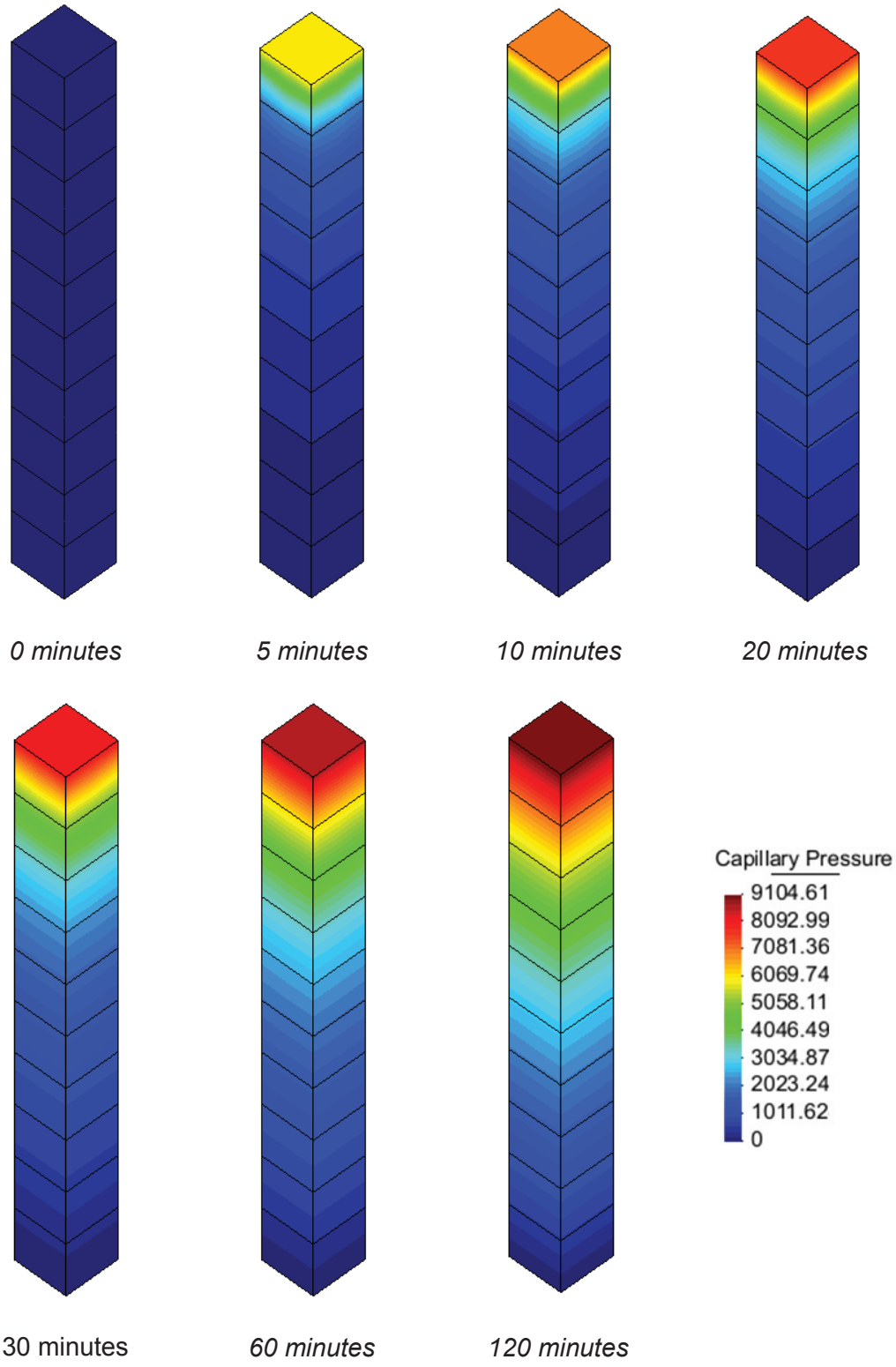

Figure 4.3.15: Capillary pressure [Pa] for the two-phase flow case, for the 10 element mesh.

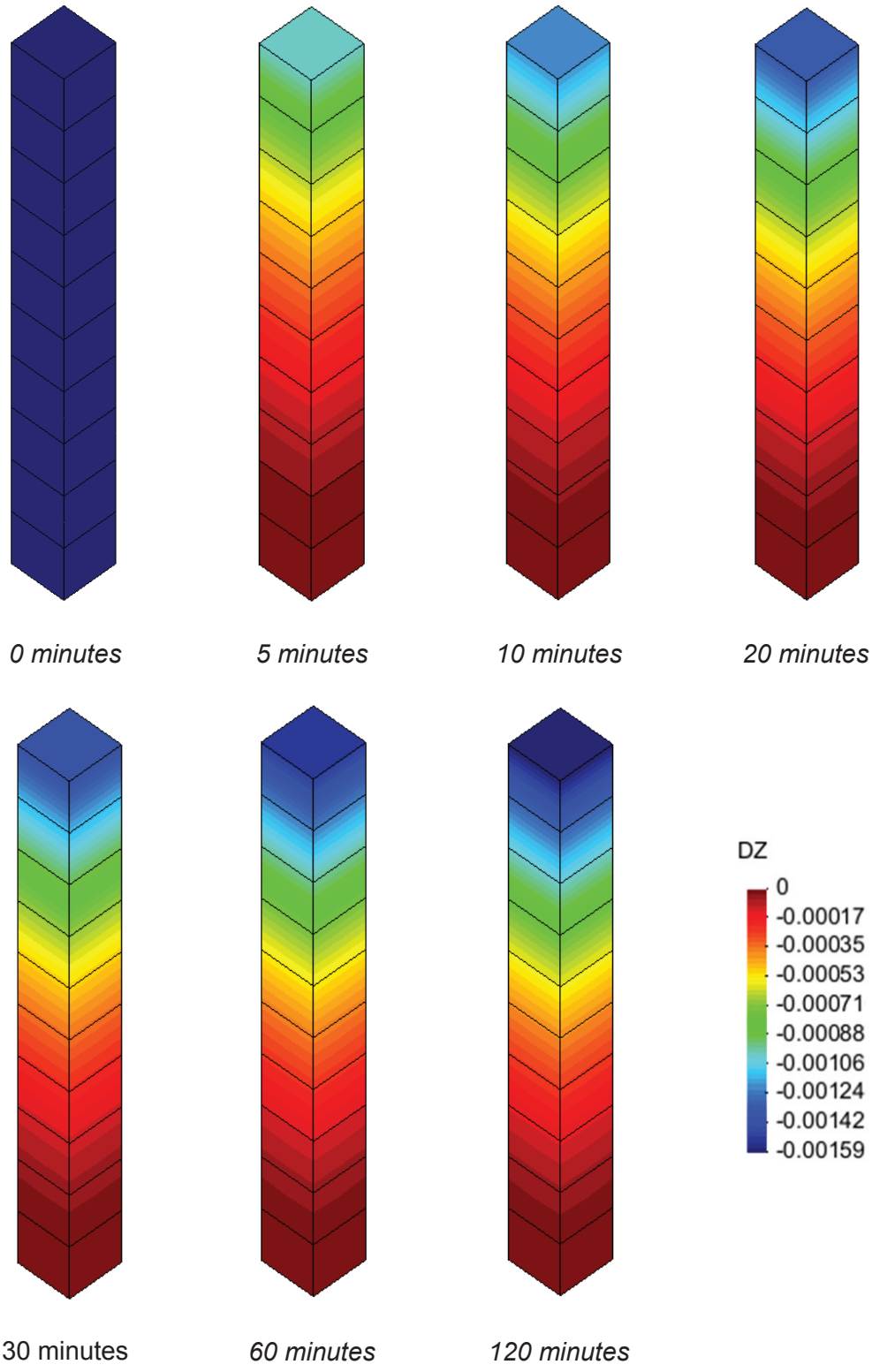

Figure 4.3.16: Displacements [m] for the two-phase flow case, for the 10 element mesh.

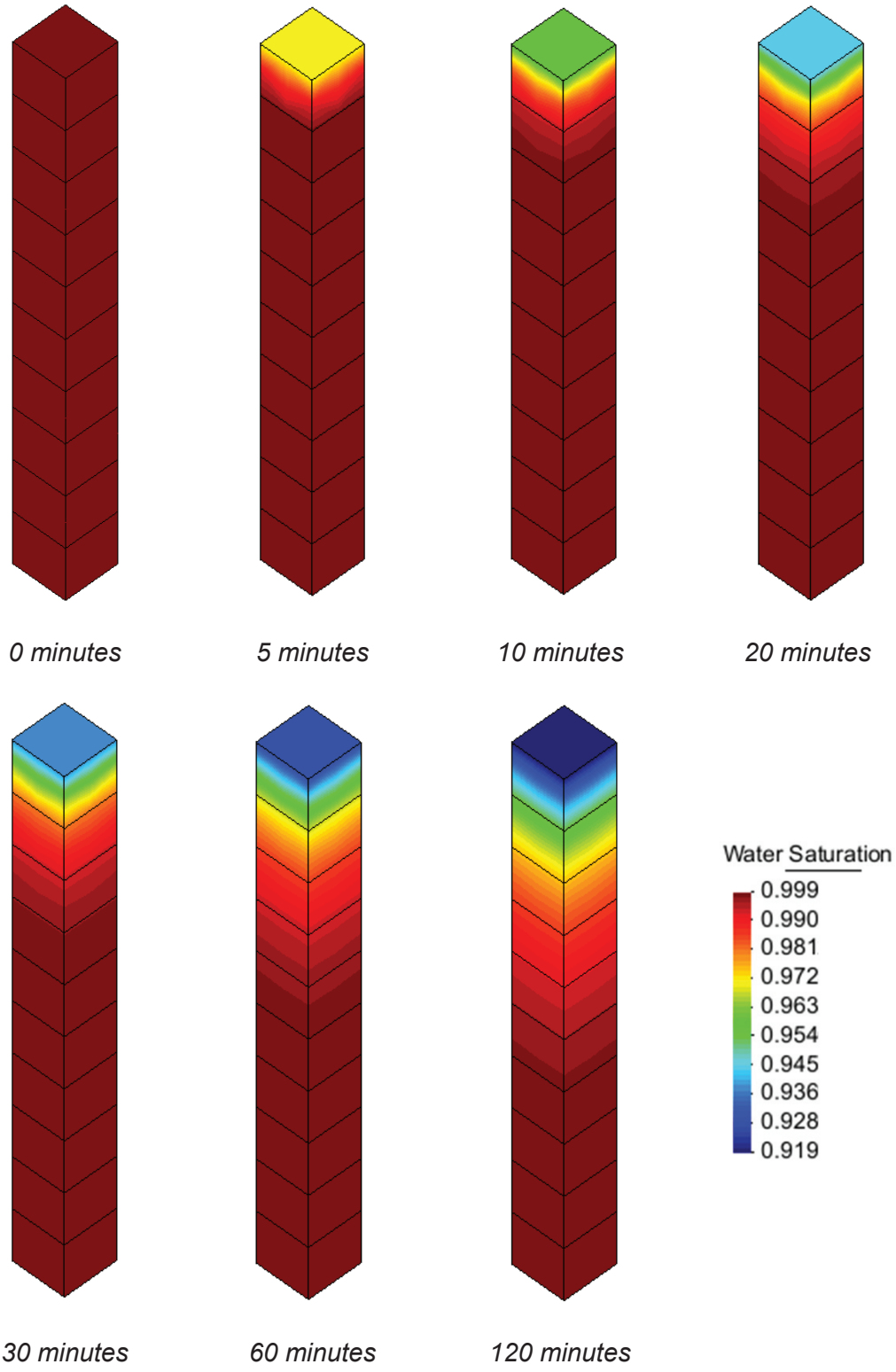

Figure 4.3.17: Degree of water saturation for the two-phase flow case, for the 10 element mesh.

For completeness the graph results relative to the analyses with the fine mesh (80 elements) are here reported (Figure 4.3.18 to Figure 4.3.22). The same considerations that have been done for the mesh with 10 elements are valid.

Figure 4.3.23 to Figure 4.3.27 show results in terms of capillary pressure, vertical displacements and degree of water saturation for the two phase flow case, only. Furthermore, as can be seen, a comparison between 10 elements mesh and 80 elements mesh is done and the results from these sensitivity analyses are very similar among two space discretization, i.e. mesh refining doesn't affect the results significantly. However, limited differences can be noticed, in particular for gas pressure, for the capillary pressure and for the degree of water saturation for the initial times of 5 and 10 minutes. This limited gap between results disappears for time higher than 30 minutes.

Graph results of the one-phase water flow case compared with two-phase flow results for the 80 elements mesh.

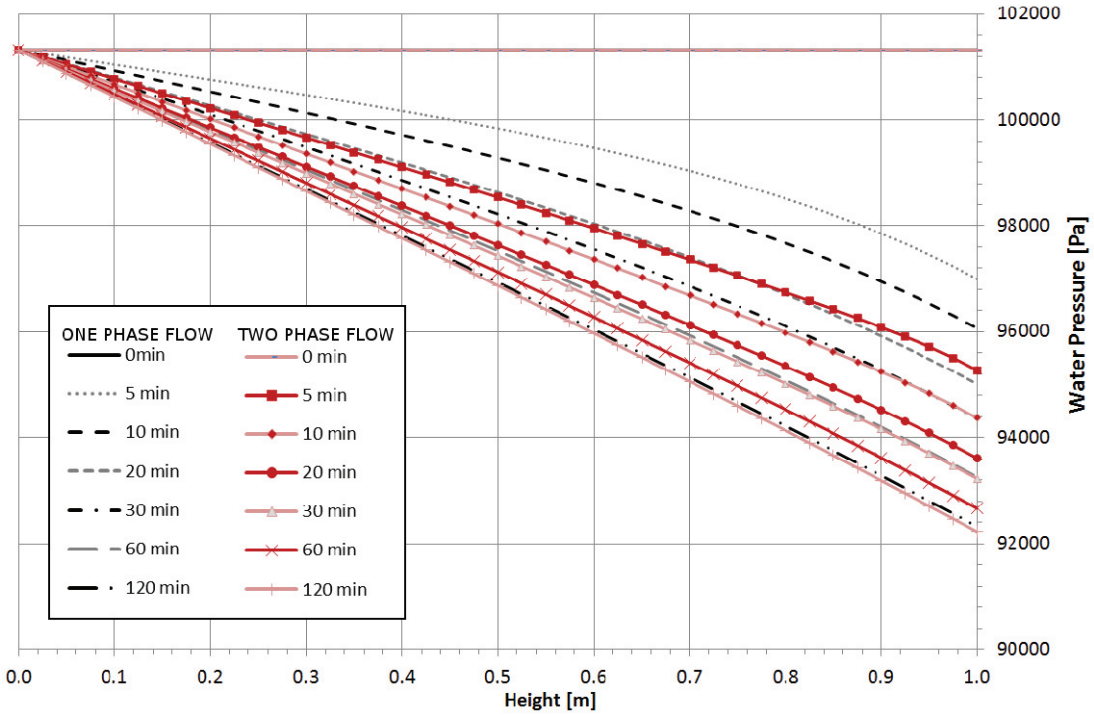

Figure 4.3.18: Water pressure [Pa] vs. height [m] for the one phase water flow case (black lines) and two-phase flow case (red lines with indicators), for the 80 element mesh.

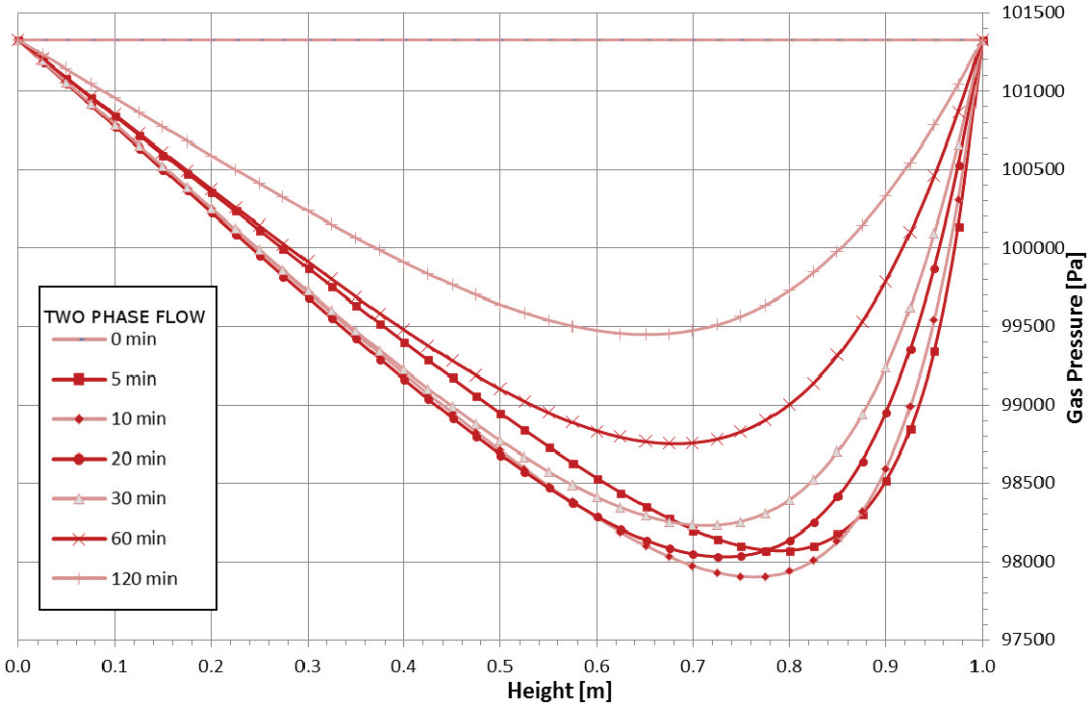

Figure 4.3.19: Gas Pressure [Pa] vs. height [m] for the two-phase flow case (red lines with indicators), for the 80 element mesh.

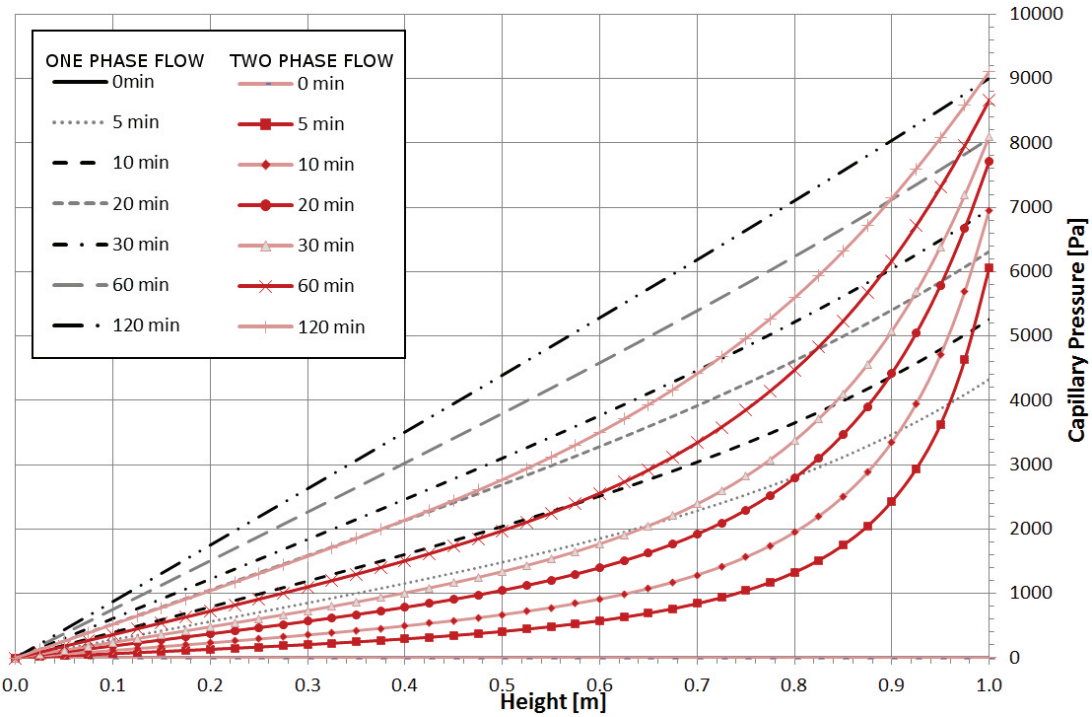

Figure 4.3.20: Capillary Pressure [Pa] vs. height [m] for the one phase water flow case (black lines) and two-phase flow case (red lines with indicators), for the 80 element mesh.

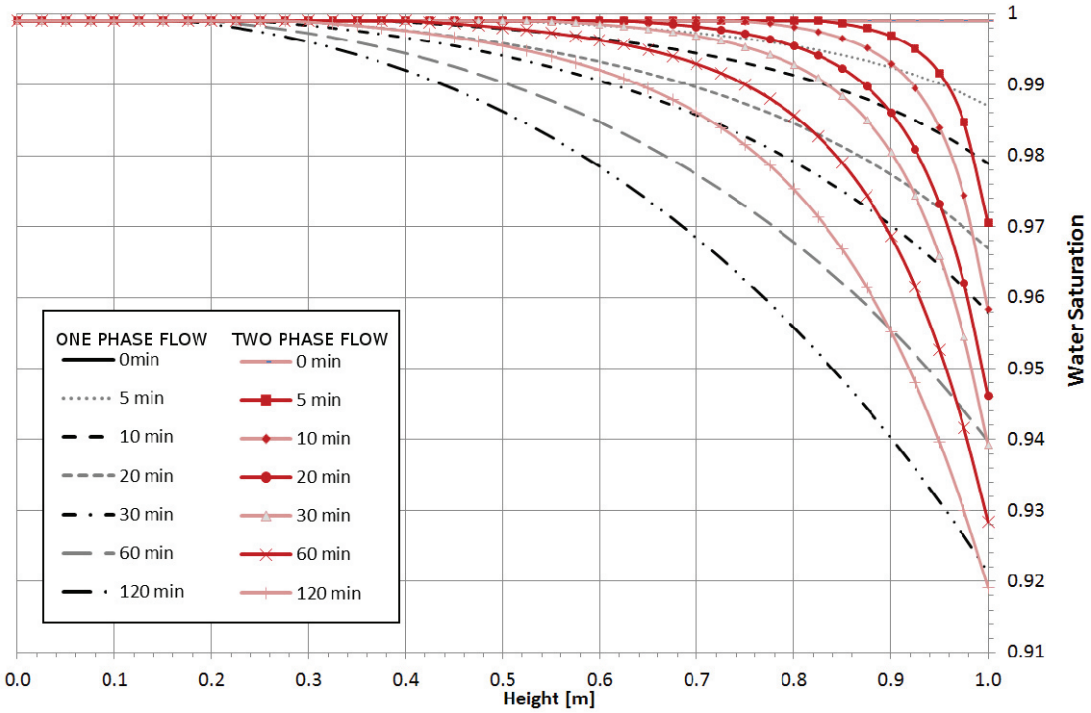

Figure 4.3.21: Water Saturation vs. height [m] for the one phase water flow case (black lines) and two-phase flow case (red lines with indicators), for the 10 element mesh.

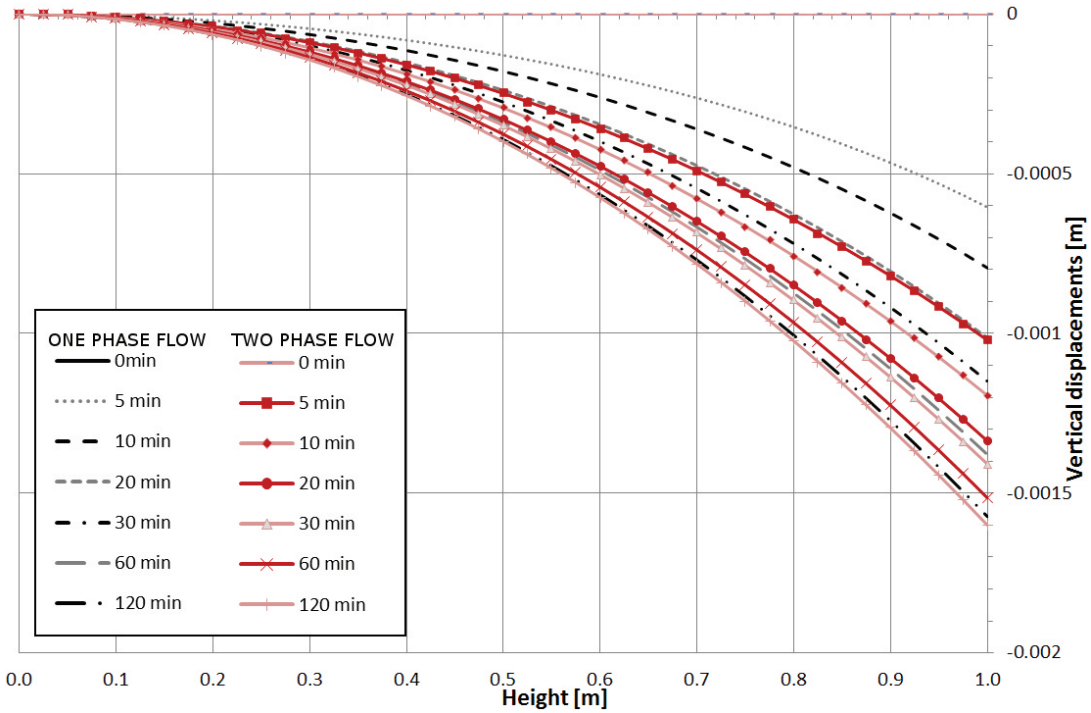

Figure 4.3.22: Vertical displacements [m] vs. height [m] for the one phase water flow case (black lines) and two-phase flow case (red lines with indicators), for the 80 element mesh.

Comparison between the 10 elements mesh results and 80 mesh results

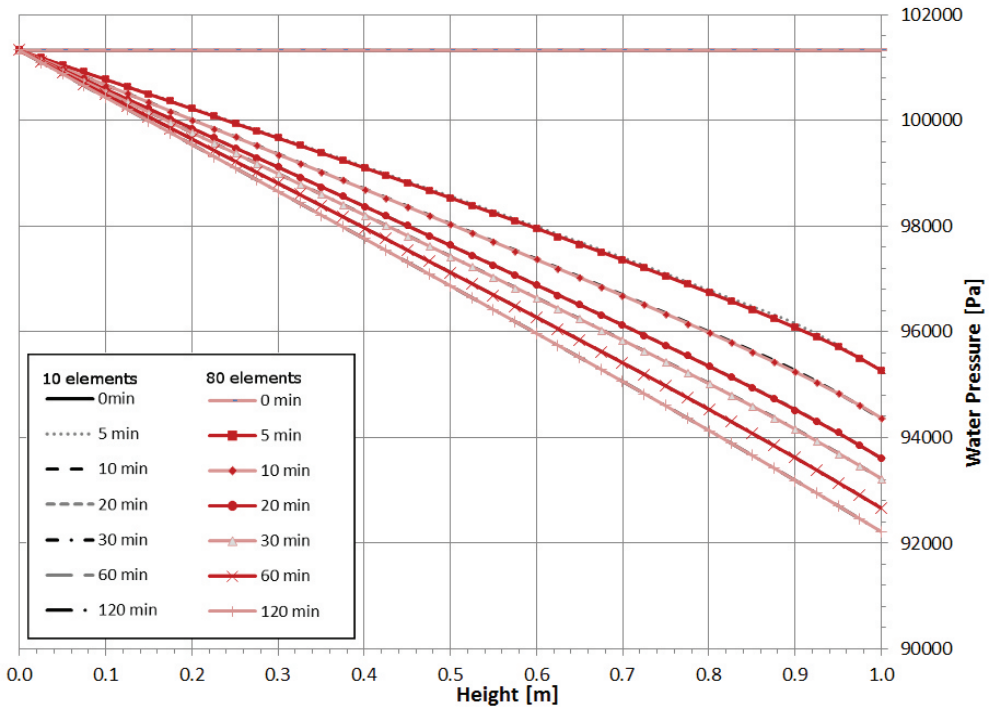

Figure 4.3.23: Water pressure [Pa] vs. height [m] result comparison between 10 elements mesh (black lines) and 80 element mesh (red lines with indicators).

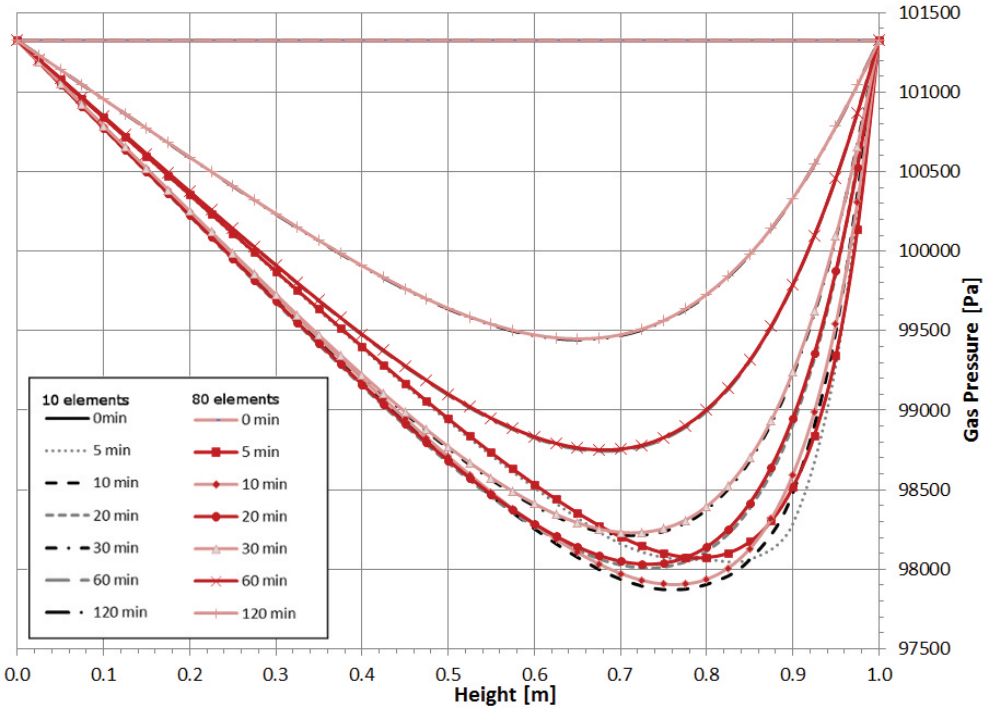

Figure 4.3.24: Gas pressure [Pa] vs. height [m] result comparison between 10 elements mesh (black lines) and 80 element mesh (red lines with indicators).

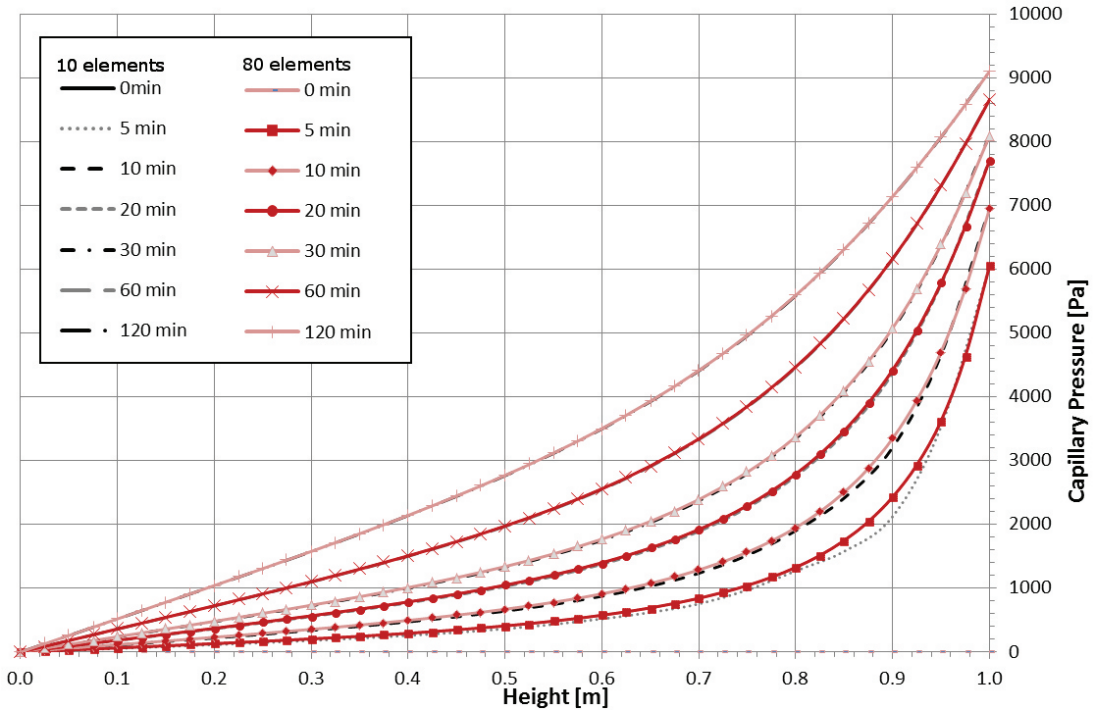

Figure 4.3.25: Capillary pressure [Pa] vs. height [m] result comparison between 10 elements mesh (black lines) and 80 element mesh (red lines with indicators).

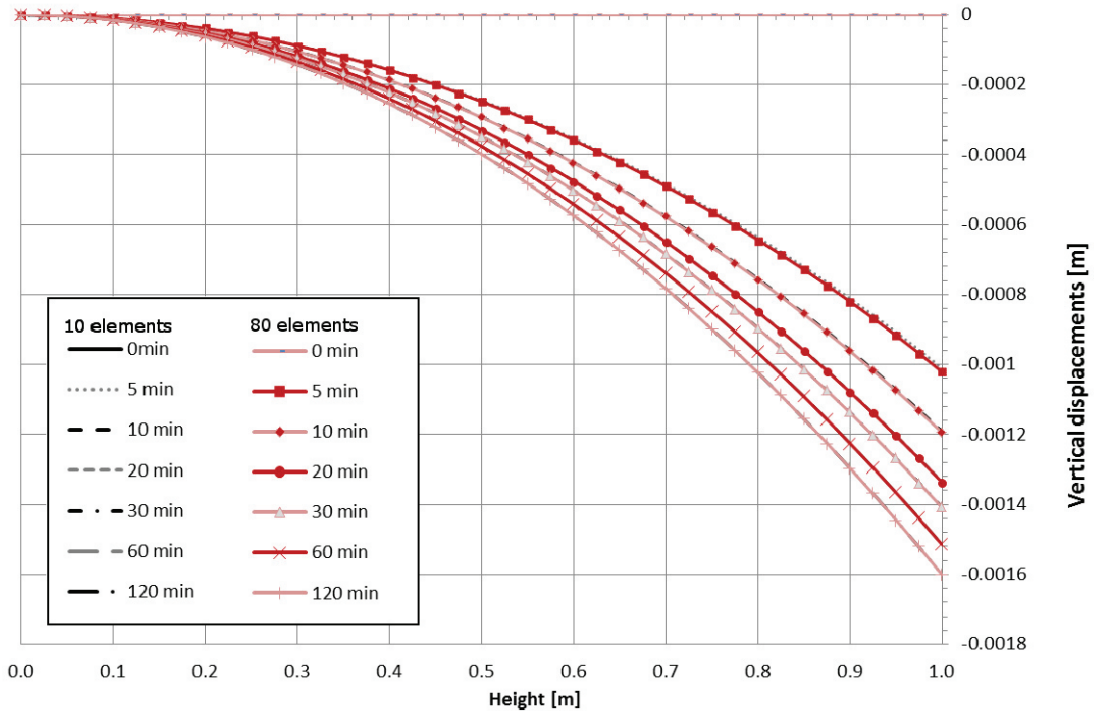

Figure 4.3.26: Vertical displacements [m] vs. height [m] result comparison between 10 elements mesh (black lines) and 80 element mesh (red lines with indicators).

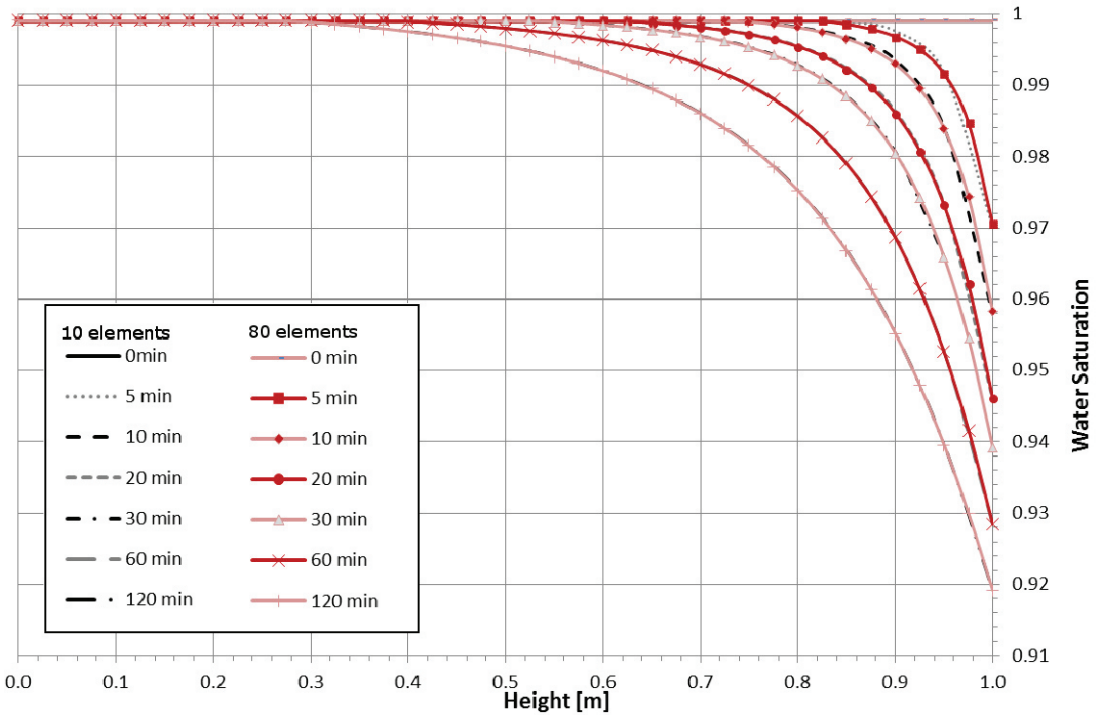

Figure 4.3.27: Water Saturation vs. height [m] result comparison between 10 elements mesh (black lines) and 80 element mesh (red lines with indicators).

The last three graphs (Figure 4.3.28 to Figure 4.3.30) show the comparison in terms of vertical displacements and water outflows between the results obtained with PLASCON3D_PS with a three-dimensional model and those obtained by Gawin and Schrefler [11] with a two-dimensional model, in both cases with the 10 element mesh.

While the results for the case of one phase flow are the same in terms of vertical displacements, the same is not for the case of two phase, water and air flow. Results obtained by Gawin and Schrefler [11] approach to the final value of vertical displacement more rapidly in the first hour of analysis than the results obtained with the PLASCON3D_PS. Conversely, results with PLASCON3D_PS are faster in the second hour of analysis with respect to the two-dimensional model. However the final value of displacements is the same. These differences are given by the different approach used in [11] with respect to the one used in this work, to treat the transition between full saturated states to partial saturated states. While in [11] the transition is performed with a switch from a $\boldsymbol{u - p}$, fully saturated formulation to a $\boldsymbol{u - p_w - p_g}$ partial saturated formulation, in PLASCON3D_PS, as explained before, the formulation used is always the $\boldsymbol{u - p_w - p_g}$ partially saturated maintaining also for states near the unitary degree of water saturation the coupling with the balance gas equation.

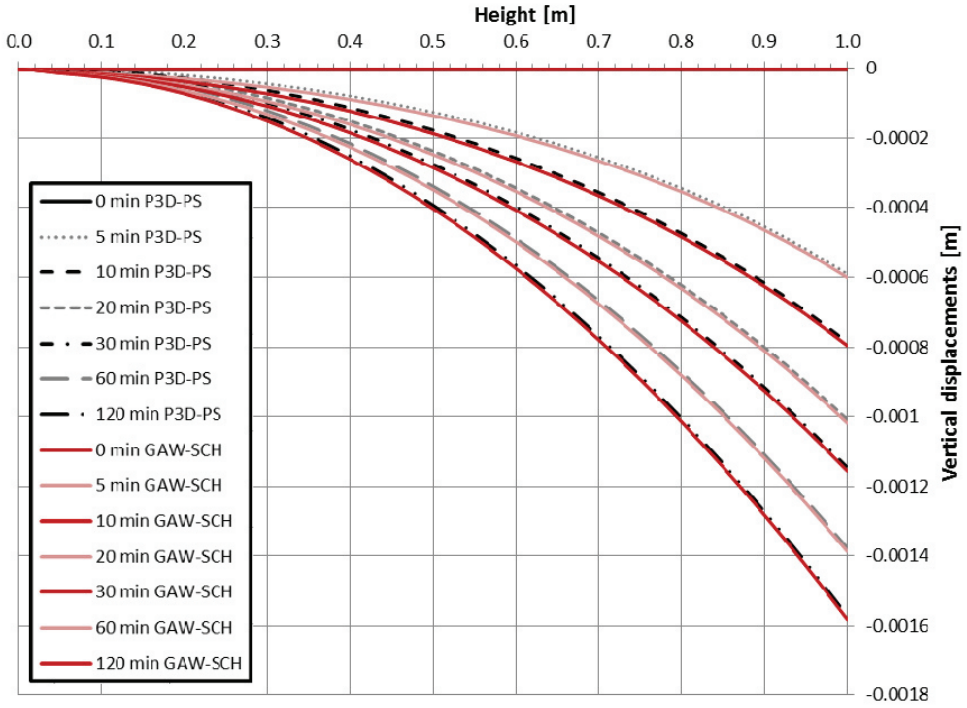

Figure 4.3.28: Vertical displacements vs. height [m] result comparison, between the solution obtained with PLASCON3D_PS (black discontinued lines) and results obtained by Gawin and Schrefler [11] (red solid lines), in the case of one-phase water flow.

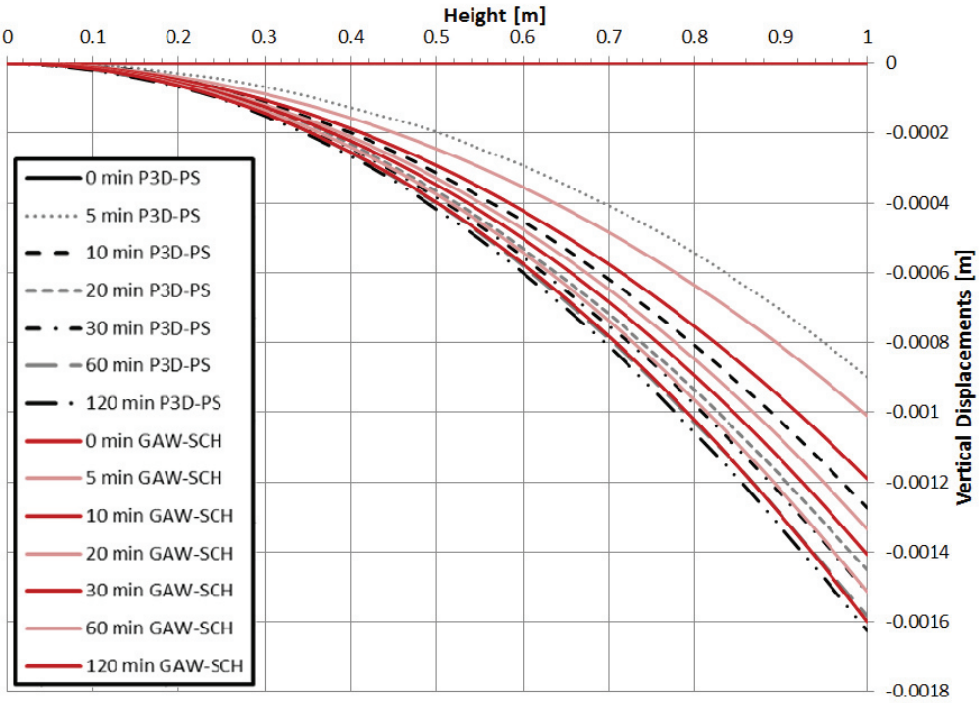

Figure 4.3.29: Vertical displacements vs. height [m] result comparison between the solution obtained with PLASCON3D_PS (black discontinued lines) and results obtained by Gawin and Schrefler [11] (red solid lines), in the case of two-phase flow.

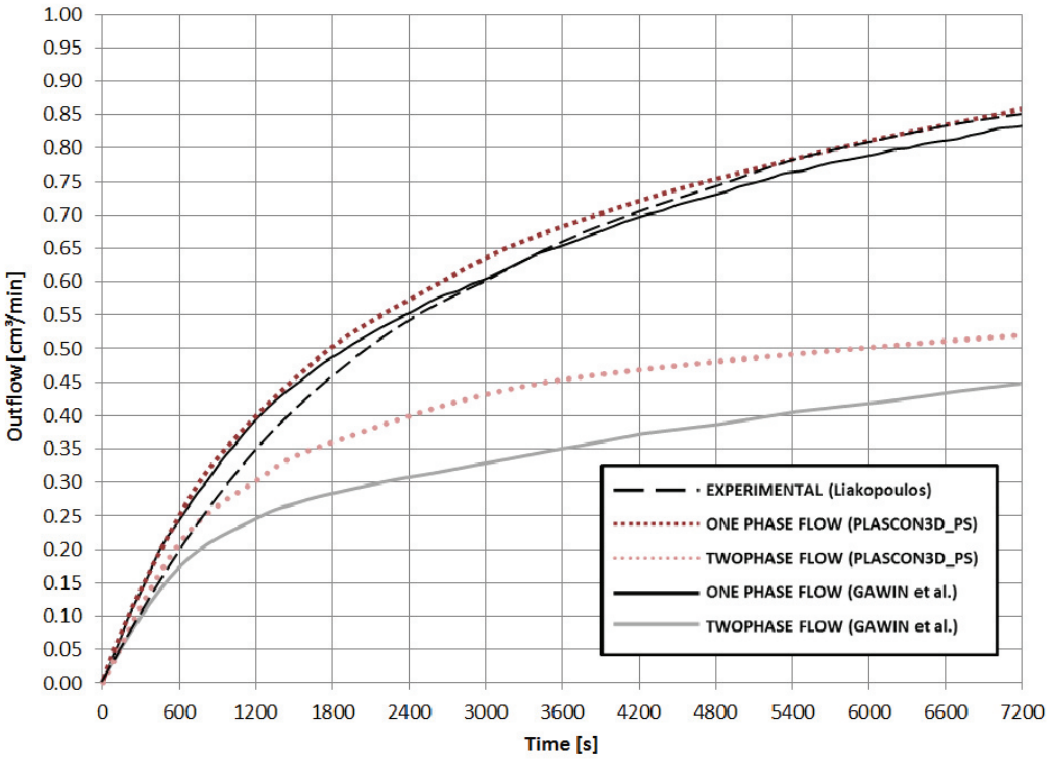

Figure 4.3.30: Outflows comparison. Dashed line is the experimental outflow (Liakopoulos); Dotted lines are from numerical computation with PLASCON3D_PS; Solid lines are from numerical computations performed by Gawin and Schrefler [11].

Finally, comparing the water outflows from the bottom of the column, a good achievement with the experimental data and the previous simulations found in [11], has been obtained with the numerical computations performed with PLASCON3D_PS with the first method and this means that the one phase water flow method gives a more realistic forecast of the real behaviour found with the experiment of Liakopoulos and the real material characteristics.

4.4. Flexible footing in a partially saturated soil

The numerical analyses presented here deal with a flexible footing that rests on a partial saturated soil. The main cross section of the domain is a rectangular which dimensions are 12 m height and 19 m length. This problem was first solved by Lloret *et al.* [12] using two computer programs, the ICFEP (Imperial College) that is a general stress-strain computer code and a program named NOSAT that solves the flow stage. From these information is not clear how far the coupling was preserved with this partitioned procedure. To model the relation between capillary pressure and degree of saturation, the state surface approach [13] were used in [12] by the authors, in order to obtain a valid expression for (2.6.3). The first of

(1.5.10) was used but no information about the parameters was given. Despite the lack of information regarding the material parameter and the load conditions, at least, contours of degree of saturation and vertical displacement evolution in time are available from [12].

Schrefler and Zhan [5] solved the problem using the Brooks and Corey relation (1.5.7), but again they didn't give any information on the material properties and on the parameter used in the water retention curve relation (1.5.7). Due to this fact, only qualitative comparison can be done between the original results presented in [12], the ones presented in [5] and the ones presented in this work.

Boundary conditions and mesh discretization

The two-dimensional mesh used by Lloret *et al.* [12] and Schrefler and Zhan [5], with the pressure load over the footing, can be seen in Figure 4.4.1, as well as the three points where authors gave results. The dimension of this discretization of the domain has been adopted also for the three-dimensional meshes, obtained by a 1 meter extrusion along the y direction of the rectangular domain. As results the three-dimensional mesh of Figure 4.4.2a has been created, while Figure 4.4.2b shows the fine mesh that has been done carrying out a refinement of the first mesh. The coarse mesh of Figure 4.4.2a has 40 elements for a total of 348 nodes, while the fine one has 440 elements for a total of 2681 nodes (details about the element that has been adopted can be found in the Section 2.8).

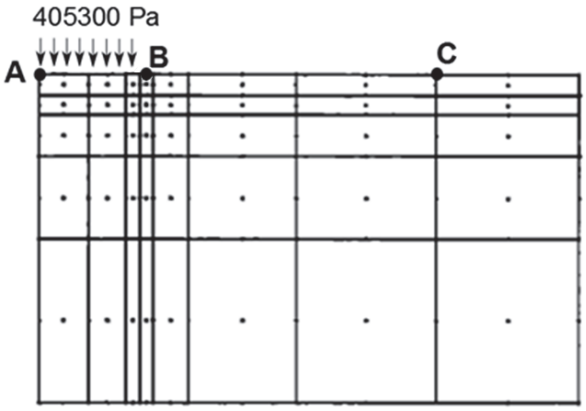

Figure 4.4.1: Mesh utilized by Lloret et al. [12] and Schrefler and Zhan [5] to discretize the flexible footing problem. Results in terms of displacements are given by authors for the points A, B and C.

The boundary conditions applied to the two meshes are the following:

- For $t < 0$, the saturation on bottom surface is $S_w = 1$, while for top surface $S_w = 0.75$. The capillary pressure is assumed to vary linearly from bottom to top

surface, while the degree of water saturation varies accordingly with the water saturation – capillary pressure relation adopted;

- For t > 0, the lateral surfaces are impervious and constrained to horizontal displacements. The nodes on the bottom surface are all constrained with respect to vertical and horizontal displacements. The top surface outside the footing (that is supposed to lay over the first three elements of top surface as showed in Figure 4.4.1) has S_w = 1, while under the footing a load of 405300 N/m² insist on the soil for all the time of the simulation.

For the water saturation – capillary pressure relation the Brooks & Corey [14, 15] relation has been used

$$\begin{aligned} S_w &= S_{w,irr} + \left(1 - S_{w,irr}\right)\left[\frac{p_b}{s}\right]^{\lambda} \quad for\ s > p_b \\ S_w &= 1 - S_{g,irr} \qquad\qquad for\ s < p_b \end{aligned} \tag{4.4.1}$$

Where the relative permeabilities are expressed as

$$\begin{aligned} k_{rw} &= S_e^{(2+3\lambda)/\lambda} \\ k_{rg} &= \left(1 - S_e\right)^2 \left(1 - S_e^{(2+\lambda)/\lambda}\right) \end{aligned} \tag{4.4.2}$$

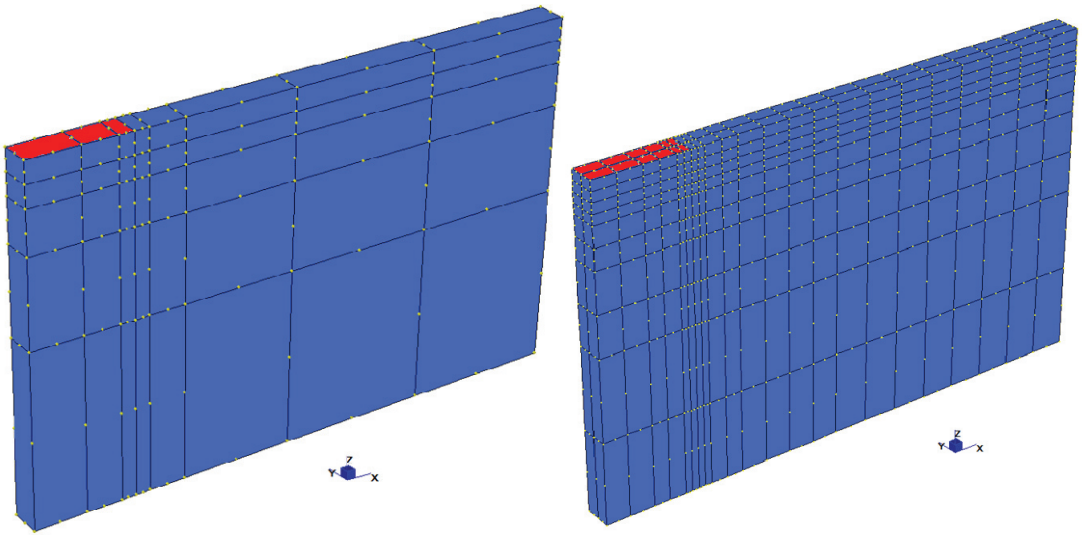

(a) (b)

Figure 4.4.2: Discretization of the domain for the flexible footing problem. Coarse (a) and fine (b) mesh. The red surface represents the loaded footing.

In the same way, the van Genuchten relationship has been also considered in the final analyses, in order to compare results

$$S_e = \left[\frac{1}{1+\left(\bar{\alpha}\, p_c\right)^n} \right]^m \tag{4.4.3}$$

For Mualem [16], the relationship $m = 1 - 1/n$ holds. The two relationships are showed in Figure 4.4.3.

The (1.5.21) has been adopted for the relative permeability for the liquid phase

$$k_{rw} = S_e^{1/2} \left(1 - \left(1 - S_e^{1/m}\right)^m\right)^2 \quad \left(m = 1 - 1/n\right) \tag{4.4.4}$$

while for the gas phase holds the relation proposed by Parker *et al.*[17, 18]

$$k_{rg} = \left(1 - S_e\right)^{1/2} \left(1 - S_e^{1/m}\right)^{2m} \tag{4.4.5}$$

Figure 4.4.4 plots the relative permeability functions for water and gas (dry air) for the Brooks and Corey relationship and the van Genuchten relationship.

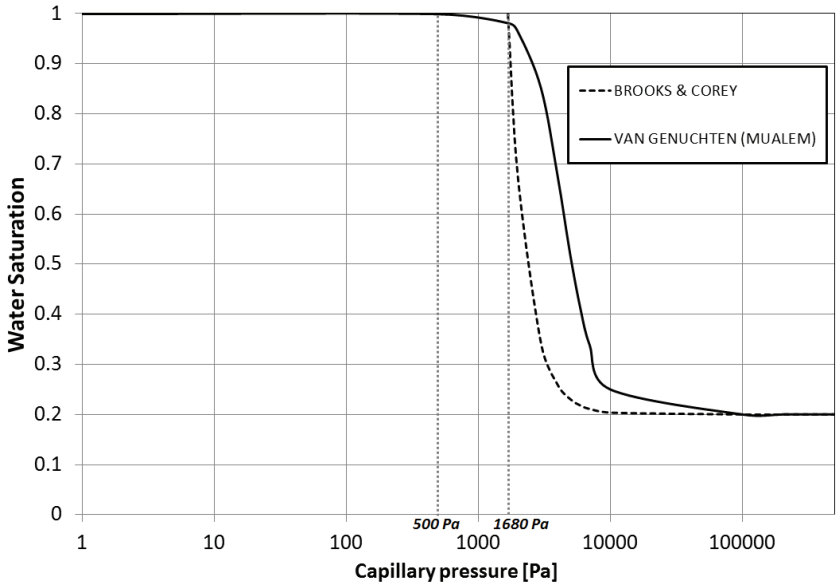

Figure 4.4.3: Comparison of Brooks-Corey vs. van Genuchten water saturation functions.

As widely discussed in the previous section 4.3, in order to better achieve the convergence of the solution and avoid numerical problems for the initial steps a minimum capillary pressure at the time t=0 has been set to the value of $p_{c,i} = p_b$ when using the Brooks and Corey relation and $p_{c,i} = p_c(S_w \cong 1.0)$ when using the

van Genuchten expression, where unitary degree of water saturation is required by the initial conditions and boundary conditions (Figure 4.4.5 and

Table 4.4.2). Together with this assumption on initial capillary pressure a minimum degree of gas saturation has been set equal to $S_{g,irr} = 0.001$ (see also equation (1.5.8)). Finally, a condition on the minimum relative permeability for the gas phase has also done, fixing the inferior limit value to $k_{rg} = 0.0005$. Varying this parameter with values not far from the curves (Figure 4.4.4) can allow a better calculation of the permeability contributions (in particular when the Brooks and Corey relation is used), with a sensible smoothing effects on pressure results over the domain. However, varying this limiting parameter of some degree of magnitude (e.g. setting it to a hundred times greater) can affect considerably the results. Here a careful choice of this parameter has been done in order to prevent excessive influence on the final results.

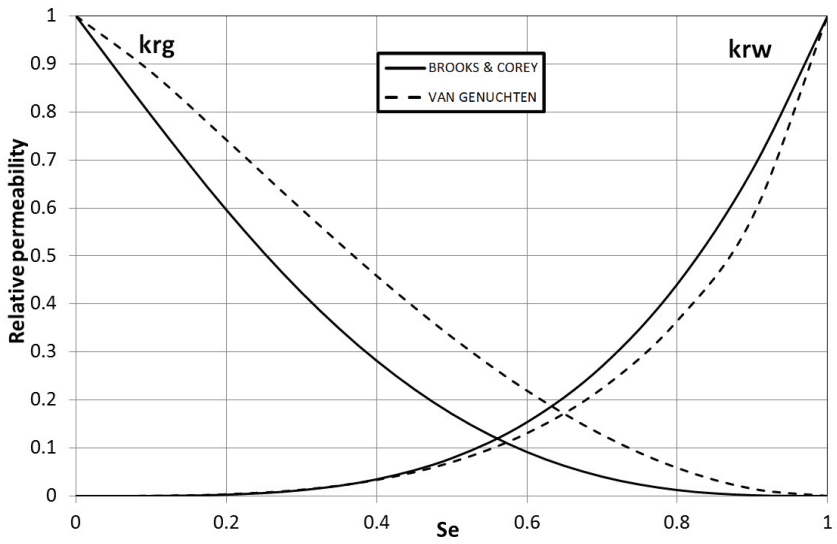

Figure 4.4.4: Comparison of Brooks-Corey vs. van Genuchten water saturation functions.

Numerical Results

Several sets of material characteristics have been tested in order to find a qualitative matching with the results presented in literature [5, 12]. The characteristics of the material that allow a good average fitting with the displacements results presents in literature at [5] are reported in Table 4.4.1 and

Table 4.4.2 , is plausible with a silty sand moderately dense. The initial state for the following analyses is the one given by the initial conditions described above and the initial conditions capillary pressure and saturations profile can be seen in Figure 4.4.5a-b.

While for the coarse mesh the choice of the time interval for the single time steps doesn't have effects on the convergence to a solution, for the fine mesh an initial time step of 10 s has been chosen to carry out the analyses and allow a better computation at initial time steps.

Table 4.4.1: Material characteristics of a silty sand moderately densed.

Young's modulus	$E = 8.5\ \text{MPa}$
Poisson's ratio	$\nu = 0.35$
Solid grain density	$\rho_s = 2000\,\text{kg/m}^3$
Liquid density (STC)	$\rho_w = 1000\,\text{kg/m}^3$
Air density (STC)	$\rho_g = 1.22\,\text{kg/m}^3$
Porosity	$n = 0.2$
Intrinsic permeability	$\text{k} = 5.0 \cdot 10^{-14}\ \text{m}^2$
Water viscosity	$\mu_w = 3 \cdot 10^{-4}\ \text{Pa} \cdot \text{s}$
Air viscosity	$\mu_a = 2.4 \cdot 10^{-5}\ \text{Pa} \cdot \text{s}$
Atmospheric pressure	$p_{atm} = 101325\,\text{Pa}$

Table 4.4.2: Degree of water saturation vs. capillary pressure curve parameters for a silty sand. Brooks and Corey (B.C.) and van Genuchten (V.G.).

Bubbling pressure (B.C.)	$p_b = 1680\,\text{Pa}$
Pore size distribution index (B.C.)	$\lambda = 3.0$
Irriducible degree of water saturation (B.C.)	$S_{w,irr} = 0.2$
Capillary pressure at fully saturated conditions (B.C.)	$p_{c,i} = 1680\,Pa$
alpha (V.G.)	$\bar{\alpha} = 2.50 \times 10^{-4}\ \text{Pa}^{-1}$
m (V.G.)	0.75
n (V.G.)	4
Capillary pressure at fully saturated conditions (V.G.)	$p_{c,i} = 500\,Pa$

Results are here presented for both the two meshes with coarse and fine discretizations, for an intermediate time of t = 10^5 s and for the later time of t = $5 \cdot 10^8$

s. In the last contours maps (the ones that refer to a time of t = $5 \cdot 10^8$ s) the precision on the legends has been increased in some cases in order to better appreciate slight differences on the contours.

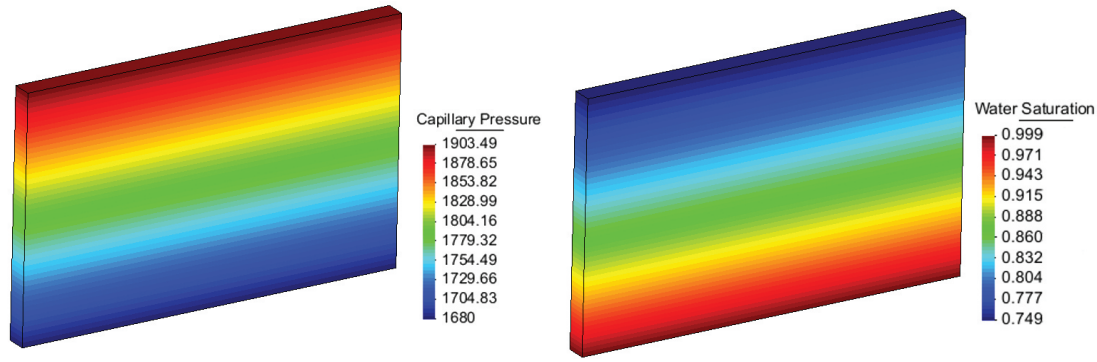

(a)

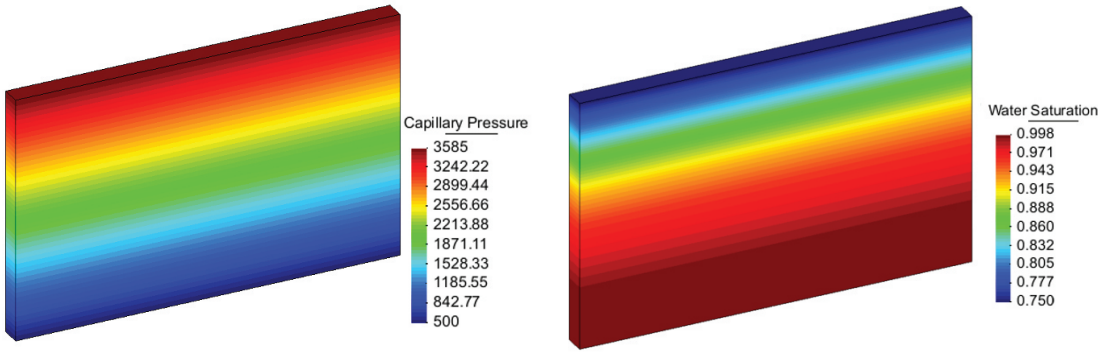

(b)

Figure 4.4.5: Capillary pressure [Pa] and degree of water saturation for t = 0. With Brook and Corey function (a) and van Genuchten – Mualem function (b).

The two relationship relative to the degree of water saturation vs. capillary pressure presented before has been used for the analyses. C*ase 1* refers to the analyses where Brooks and Corey relationship has been used, C*ase2* a where van Genuchten relationship has been used.

Figure 4.4.18 shows the deformed mesh, magnified five times than the normal values, compared with the underformed one. In order to plot the graphs, the point A (on the left, under the footing), the point B (outside the footing) and the point C (far from the footing) on the top surface have been taken as reference point (Figure 4.4.1).

Results with the Brooks and Corey relationship (Case 1). Results for t = 10^5 s

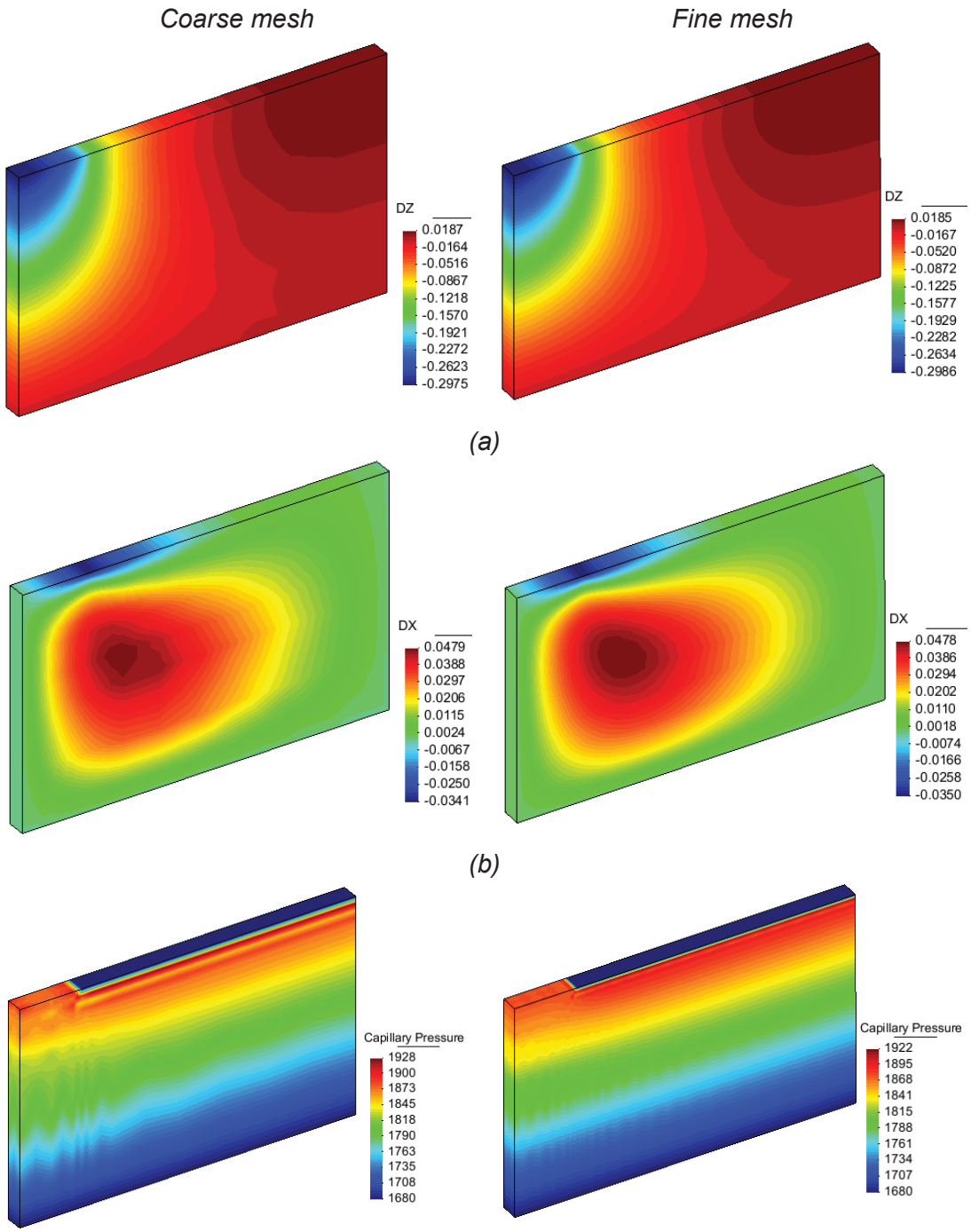

Figure 4.4.6: Vertical displacements [m] (a); Horizontal displacements [m] (b); Capillary pressure (c); for the Case 1 at t = 10^5 s.

Results with the Brooks and Corey relationship (Case 1). Results for t = 10^5 s

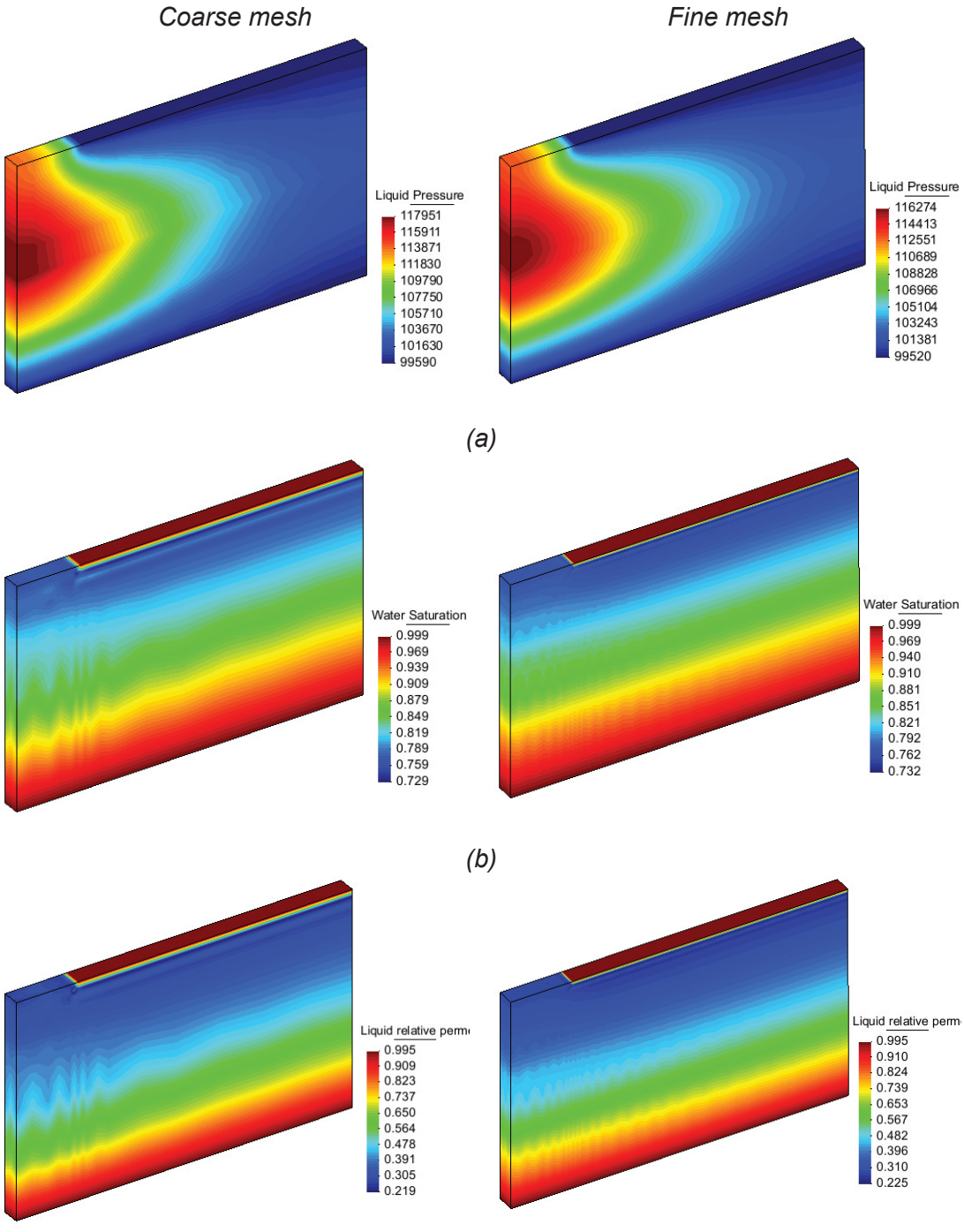

Figure 4.4.7: Water Pressure [Pa] (a); Water saturation (b); Relative water permeability(c); for the Case 1 at t = 10^5 s.

Results with the Brooks and Corey relationship (Case 1). Results for t = 10^5 s

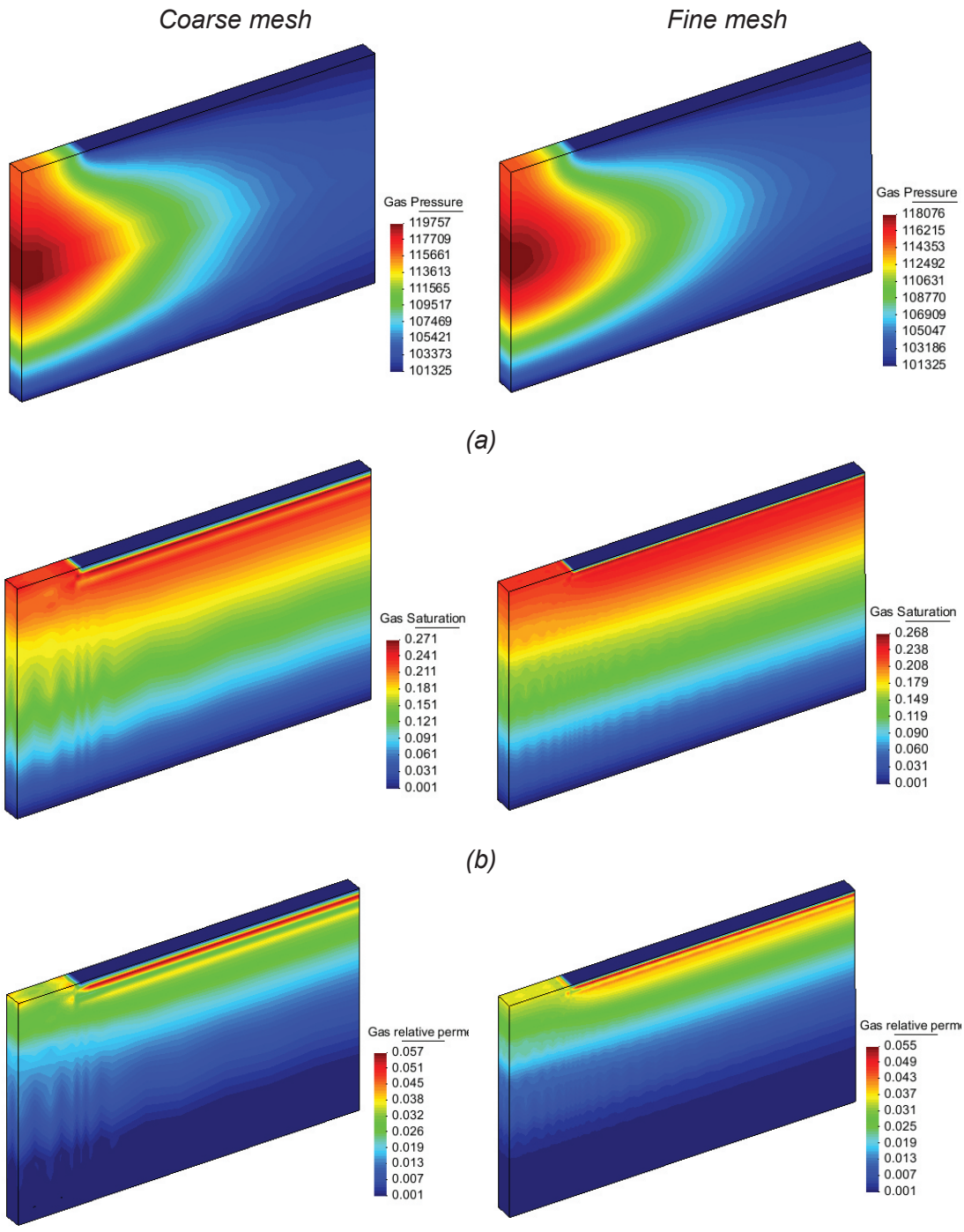

Figure 4.4.8: Gas Pressure [Pa] (a); Gas saturation (b); Relative gas permeability(c); for the Case 1 at t = 10^5 s.

Results with the van Genuchten relationship (Case 2). Results for t = 10^5 s

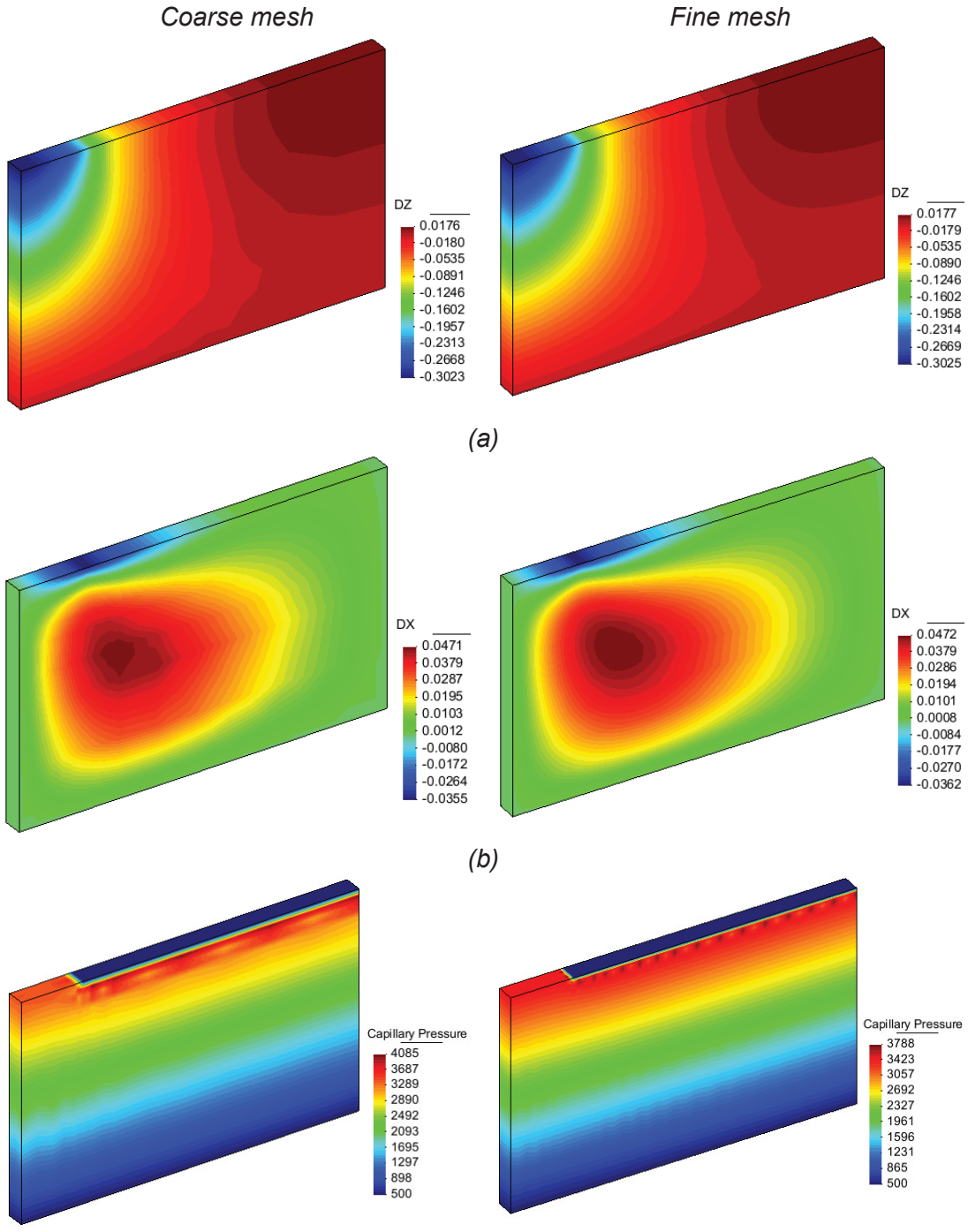

Figure 4.4.9: Vertical displacements [m] (a); Horizontal displacements [m] (b); Capillary pressure (c); for the Case 2 at t = 10^5 s.

Results with the van Genuchten relationship (Case 2). Results for t = 10^5 s

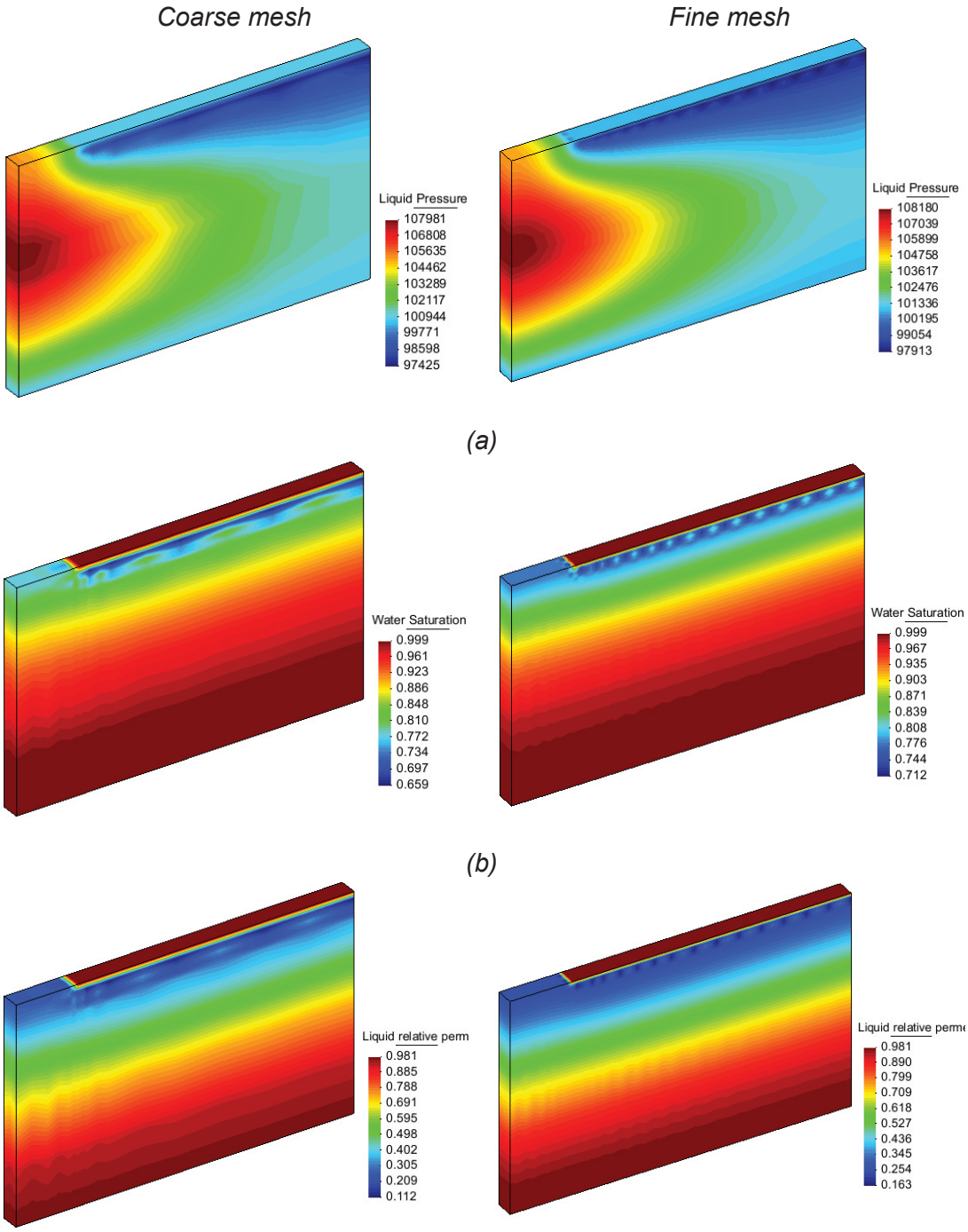

Figure 4.4.10: Water Pressure [Pa] (a); Water saturation (b); Relative water permeability(c); for the Case 2 at t = 10^5 s.

Results with the van Genuchten relationship (Case 2). Results for t = 10^5 s

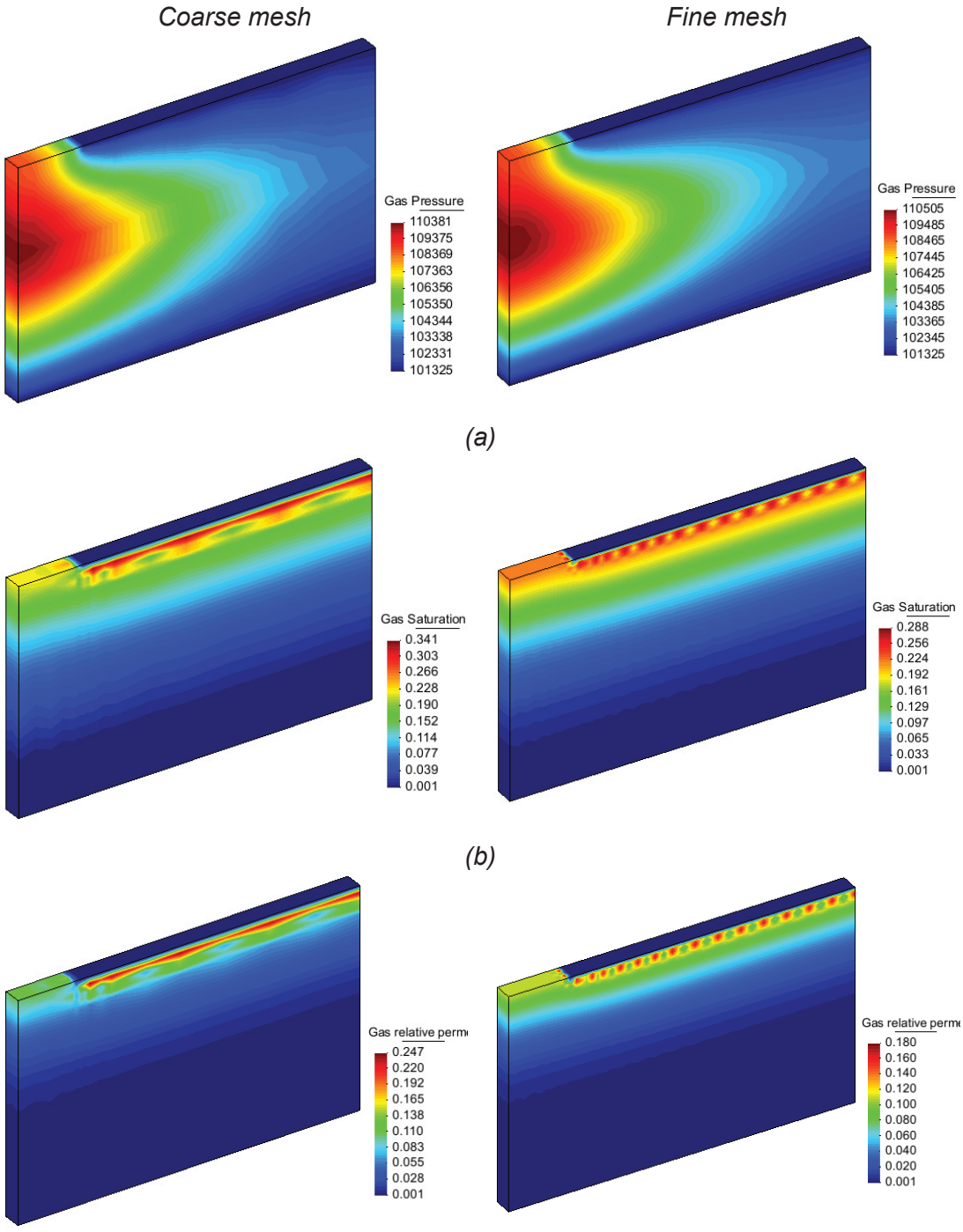

Figure 4.4.11: Gas Pressure [Pa] (a); Gas saturation (b); Relative gas permeability(c); for the Case 2 at t = 10^5 s.

Results with the Brooks and Corey relationship (Case 1). Results for t = 5·10^8 s

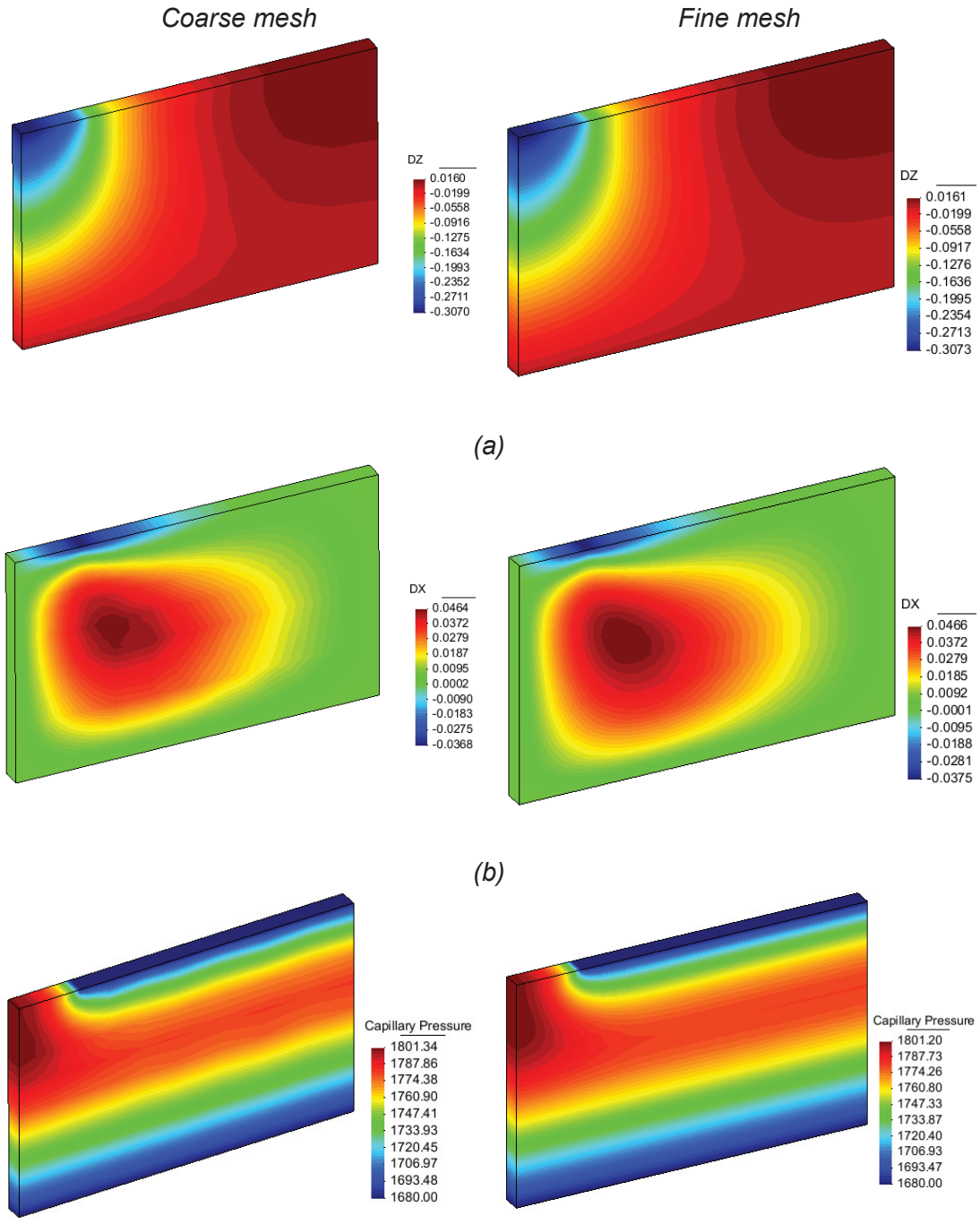

Figure 4.4.12: Vertical displacements [m] (a); Horizontal displacements [m] (b); Capillary pressure (c); for the Case 1 at t = 5·10^8 s.

Results with the Brooks and Corey relationship (Case 1). Results for t = 5·10^8 s

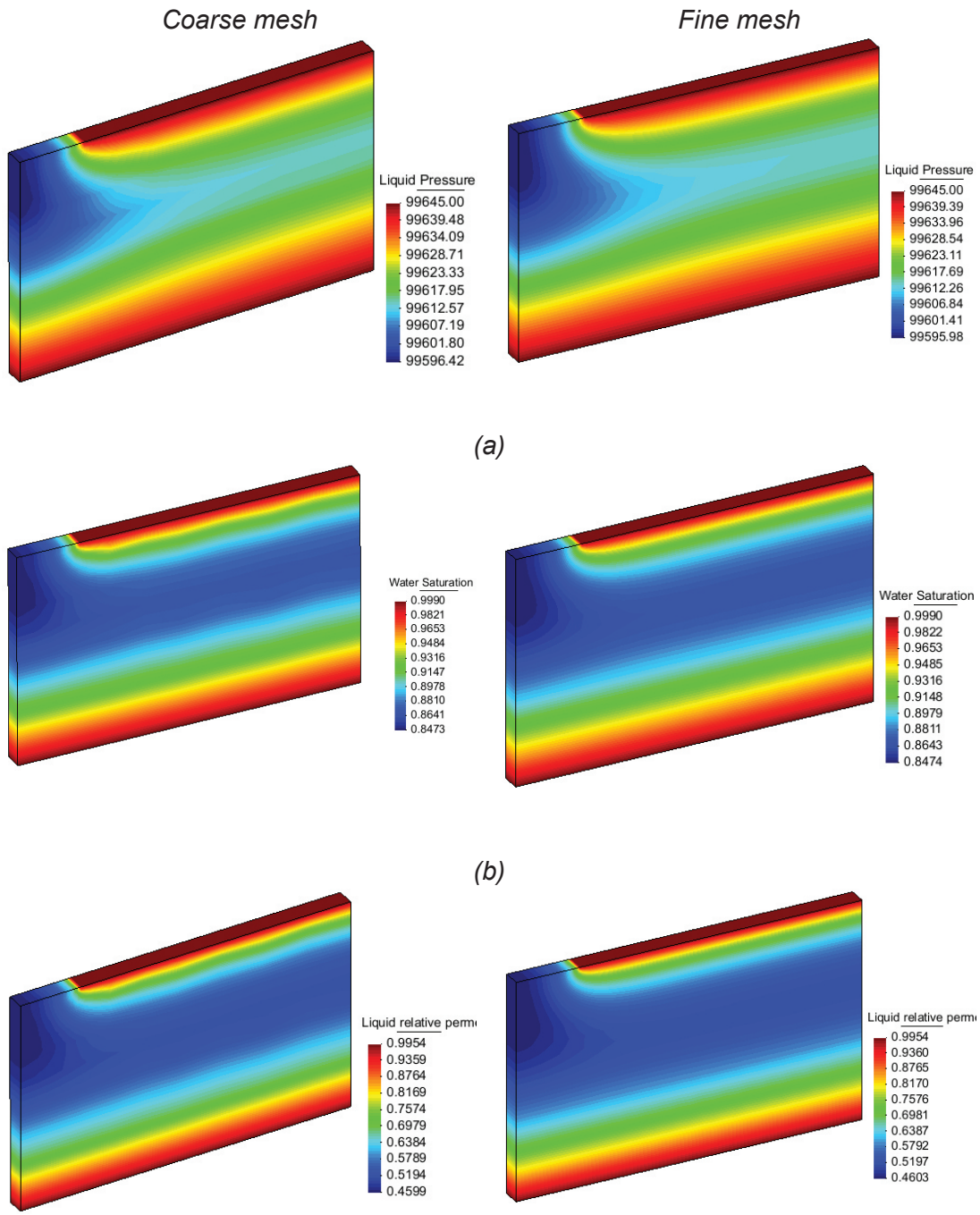

Figure 4.4.13: Water Pressure [Pa] (a); Water saturation (b); Relative water permeability(c); for the Case 1 at t = 5·10^8 s.

Results with the Brooks and Corey relationship (Case 1). Results for t = 5·10^8 s

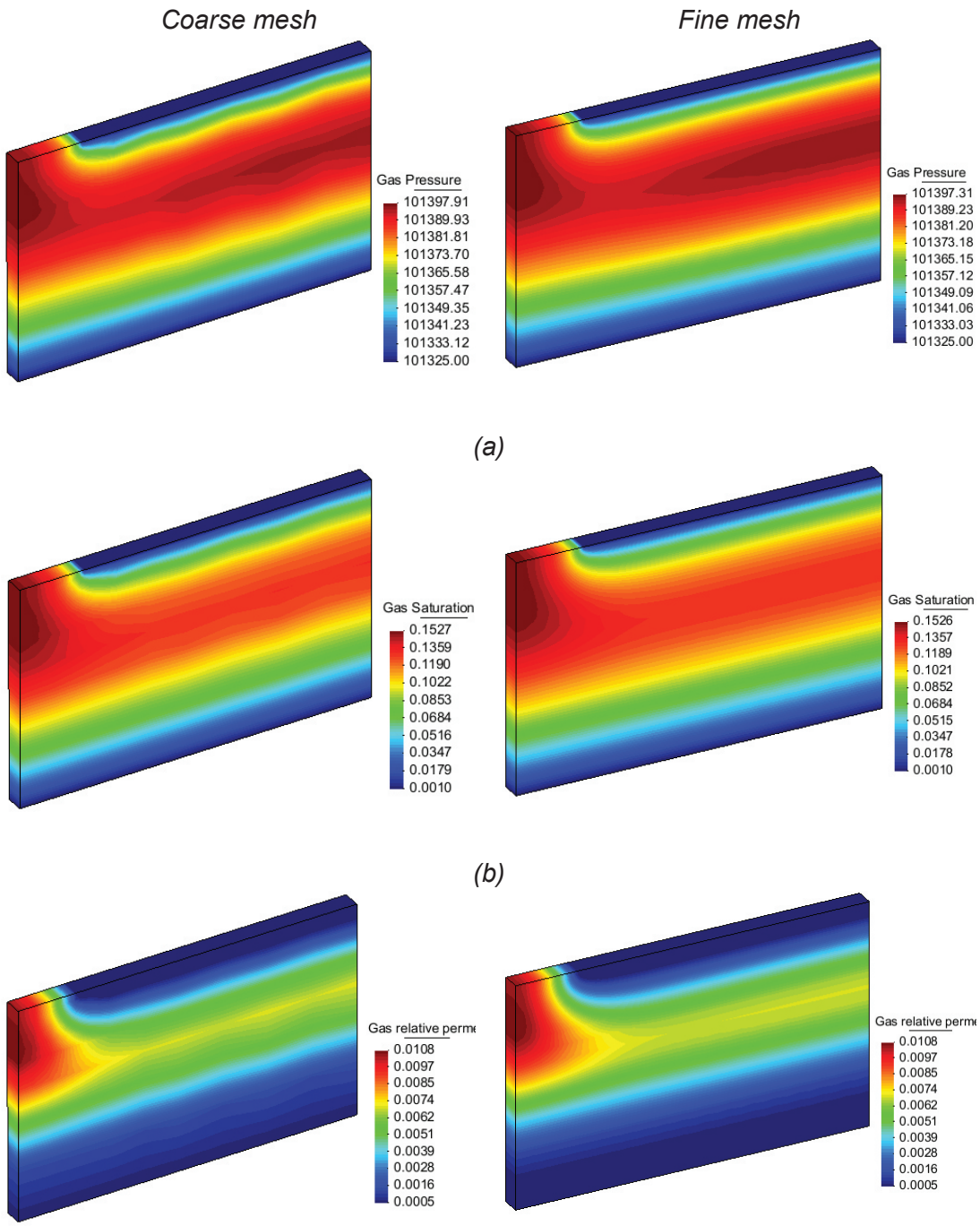

Figure 4.4.14: Gas Pressure [Pa] (a); Gas saturation (b); Relative gas permeability(c); for the Case 1 at t = 5·10^8 s.

Results with the van Genuchten relationship (Case 2). Results for t = 5·10^8 s

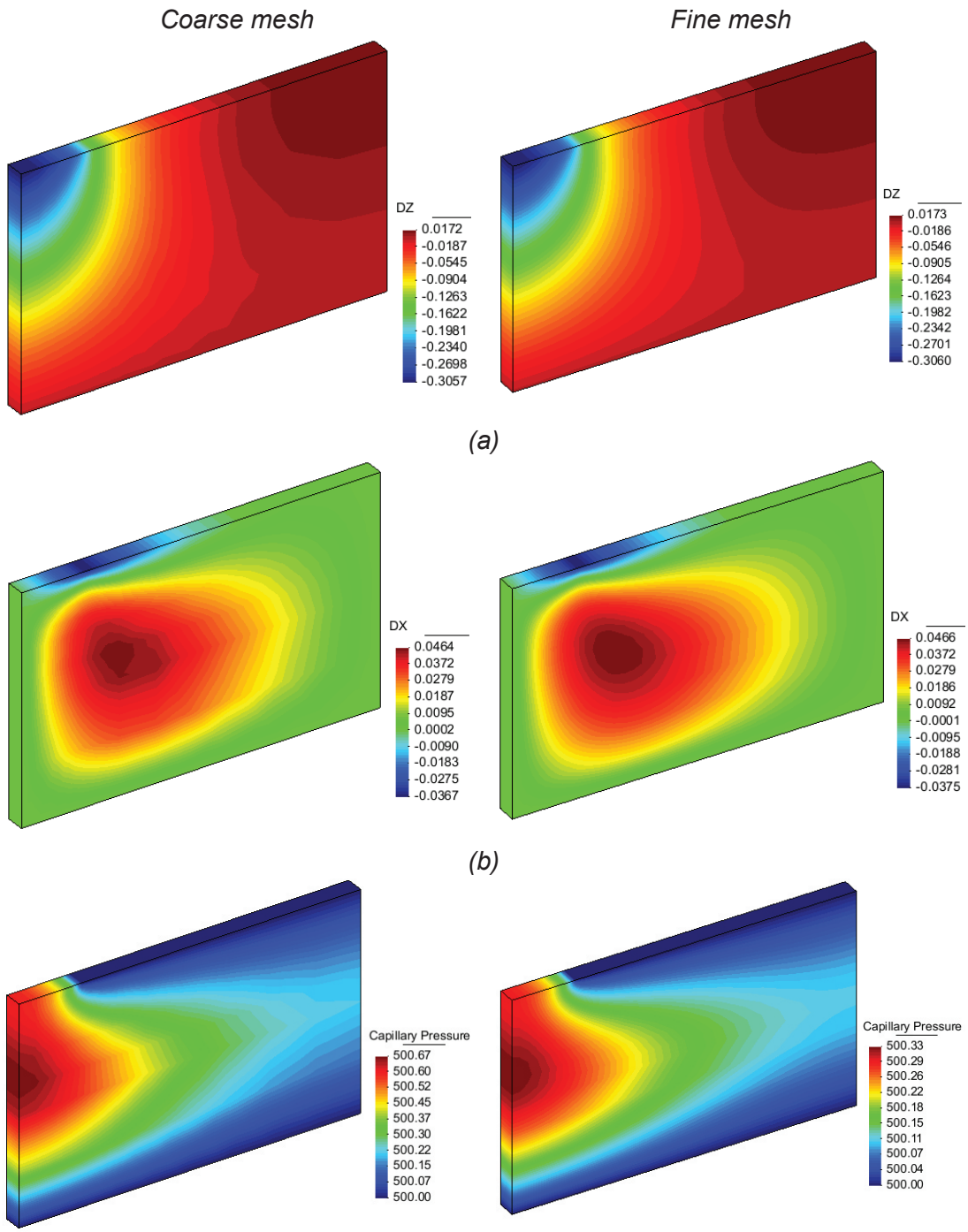

Figure 4.4.15: Vertical displacements [m] (a); Horizontal displacements [m] (b); Capillary pressure (c); for the Case 2 at t = 5·10^8 s.

Results with the van Genuchten relationship (Case 2). Results for t = 5·10^8 s

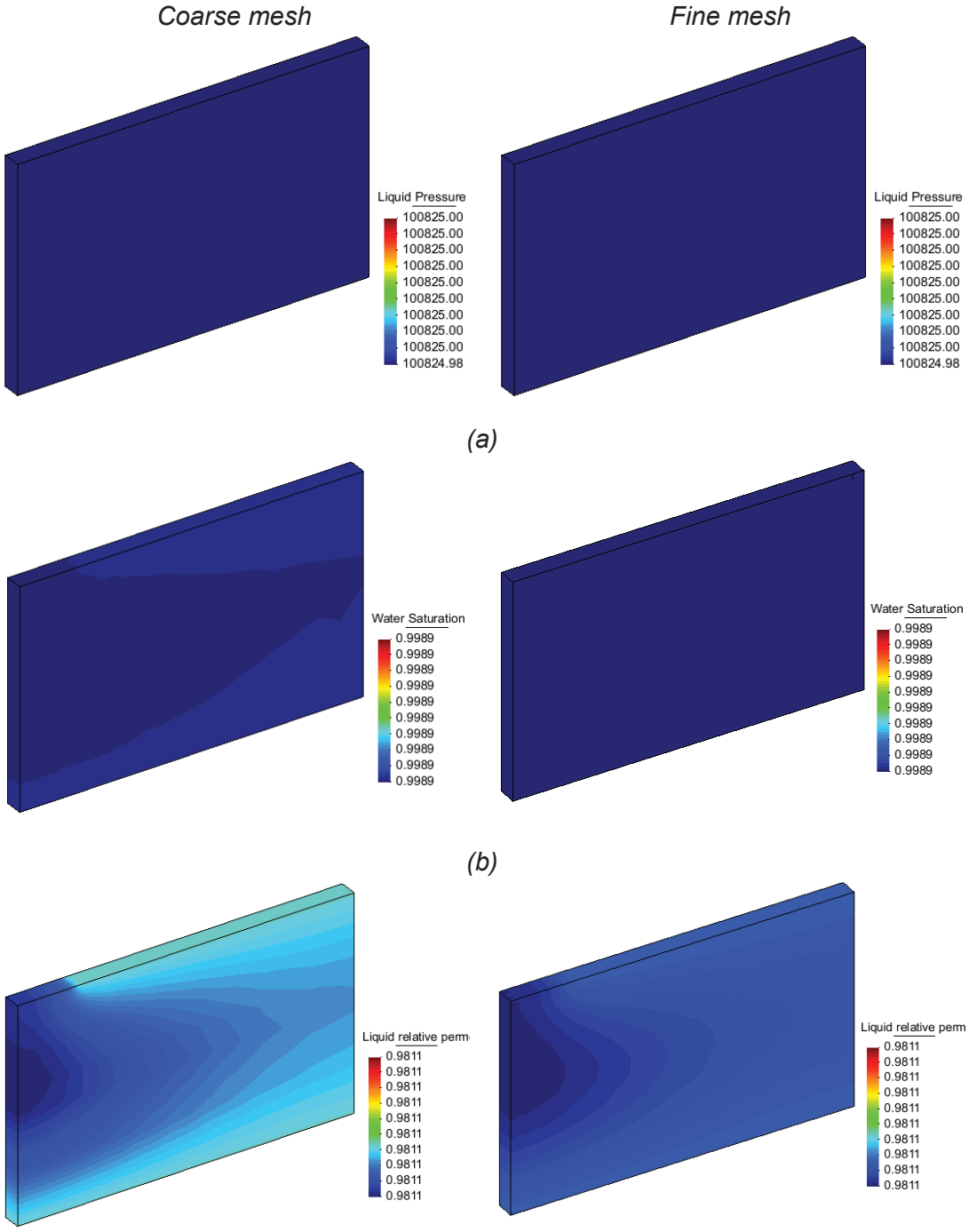

Figure 4.4.16: Water Pressure [Pa] (a); Water saturation (b); Relative water permeability(c); for the Case 2 at t = 5·10^8 s.

Results with the van Genuchten relationship (Case 2). Results for t = 5·10^8 s

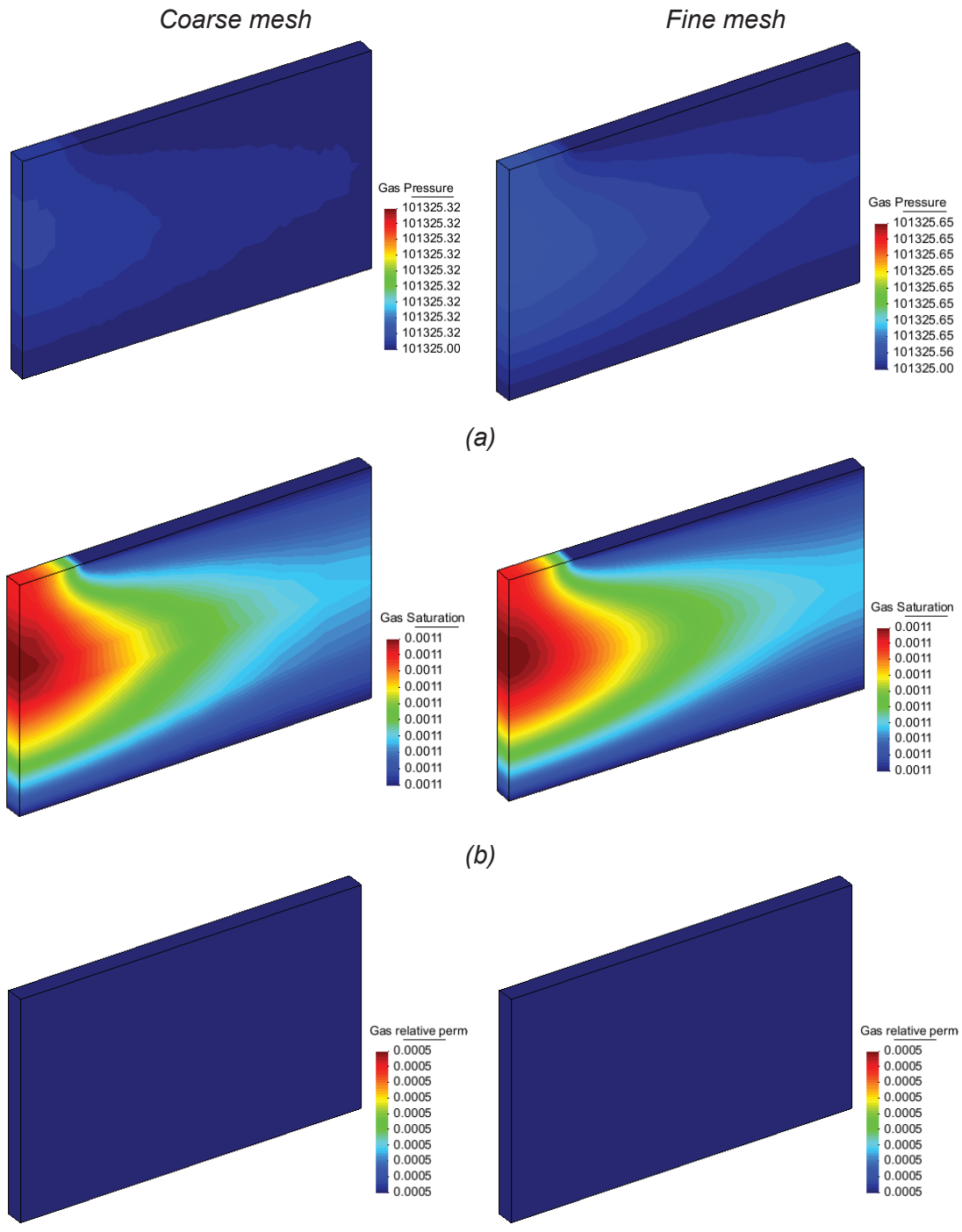

Figure 4.4.17: Gas Pressure [Pa] (a); Gas saturation (b); Relative gas permeability(c); for the Case 2 at t = 5·10^8 s.

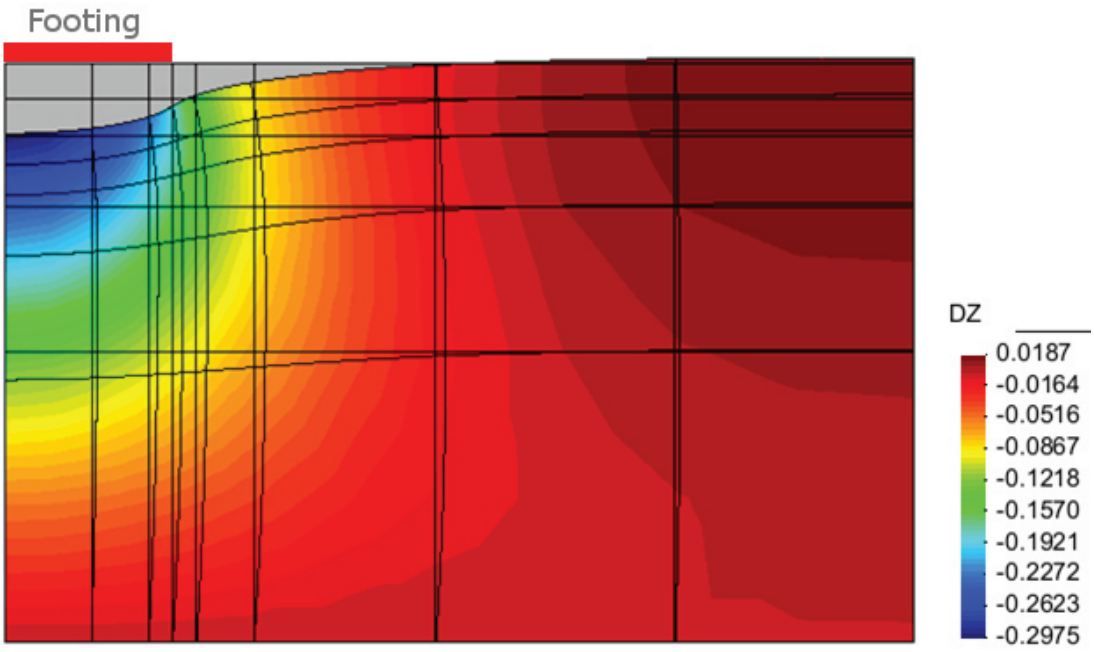

Figure 4.4.18: 2D visualization of the vertical displacements for t = 10^5 s (Brooks and Corey relationship) with the coarse mesh. Results are plotted on the deformed mesh (5 x). Grey mesh is at initial undeformed conditions.

Generally speaking, the results obtained with the fine mesh are smoother than those obtained with the coarse mesh, due to the higher number of nodes in which results are calculated, and so the results displaying as well as the calculations over the domain are more precise.

The displacements distributions on the domain for the solid phase are pretty similar and values are very close comparing the *Case 1* with the *Case 2*. The same can be said comparing results achieved with the two mesh discretizations, here differences are very slight. By effect of Poisson's coefficient of the material, the vertical load induces horizontal displacements that consequently provoke a short of expansion effect that rise the portion of top surface farthest from the load.

While the displacements fields among the two cases are matching quite well the same doesn't occur for the others fields. In particular, if qualitatively the shapes of the pressures distribution are quite identical, denoting high pressure values right under the footing, as expected, the limit values reached in the *Case 1* for water and gas pressure are higher that the *Case 2* (Figure 4.4.7 and Figure 4.4.8 compared with Figure 4.4.10 and Figure 4.4.11). Despite that higher values for pressures have been obtained in the *Case 1*, the capillary pressure values, that denote the difference between the fluid phases pressures, are higher in the *Case 2*, as can be seen also from Figure 4.4.19, where capillary pressure evolutions have been plotted for the reference point A (the one under the footing). Figure 4.4.20 shows

instead the evolution in time of the degree of water saturation for the same point, in both cases. As expected, differents values of capillary pressure doesn't mean great differences of degrees of saturation, at least for lower times (see also Figure 4.4.3). Due to these considerations, together with the fact that the same material properties and general parameter configurations have been adopted, it can be clear that the difference between cases, in value of the capillary pressure for the initial times, influences also the initial vertical displacement observed at the reference point A (the same occurs at the point B and C). As can be seen from the graphs plotted in Figure 4.4.21 to Figure 4.4.23, the maximum negative value of vertical displacement is observed for the point A for the *Case 1*, that records lower values of capillary pressure at a relative initial time of 10^3 s. This displacement value is higher than the one obtained by the *Case 2*. The entity of capillary pressure, as well as its variation in time, directly affects the response of the medium to the constant load. In fact, the *Case 1* shows very slow variation in time of capillary pressure and water saturation in the point A, with a quasi horizontal plateau for the most of the simulation time (Figure 4.4.19 and Figure 4.4.20), while steeper profiles can be obtained for *Case 2*. In the *Case 2*, the higher negative value of vertical displacement is reached more rapidly than in the *Case 1*.

Around time of 10^6 seconds, the value of capillary pressure for the *Case 2* decreases first moderately then more rapidly towards the inferior limit of 500 Pa that has been taken as boundary condition of fully saturation. As can be seen from contour maps for the highest time presented, the full saturation by water of the whole domain, occurs for the *Case 2*, around the time of $5 \cdot 10^8$ seconds, that correspond to the initial steady value of capillary pressure of 500 Pa. The capillary pressure of the *Case 1*, decreases appreciably later, at the time of 10^8 seconds towards the initial steady value that coincides with the bubbling pressure (1680 Pa), neverthless, the fully saturated condition is reached only for a time greater than 10^{10} s. Despite that the fully saturated conditions are not reached in *Case 1*, whitin the simulation time set for the analyses, from contour maps relative to *Case 1* (Figure 4.4.13 and Figure 4.4.14), it can be seen that ranges of pressures are very close to the one imposed at the boundaries and so the system is going to approach slowly to the steady conditions.

Finally, comparing the vertical displacements for the point A, B and C with those obtained by Schrefler and Zhan [5], for a closer span of simulation time, it can be seen, from Figure 4.4.21 to Figure 4.4.23, that no perfect matching of the results has been obtained with the supposed parameters for the water retention relationships (Table 4.4.2), however, the average displacements correspond at

each reference point, and this mean that a satisfactory achivement of mechanical charachteristics of soil has been obtained.

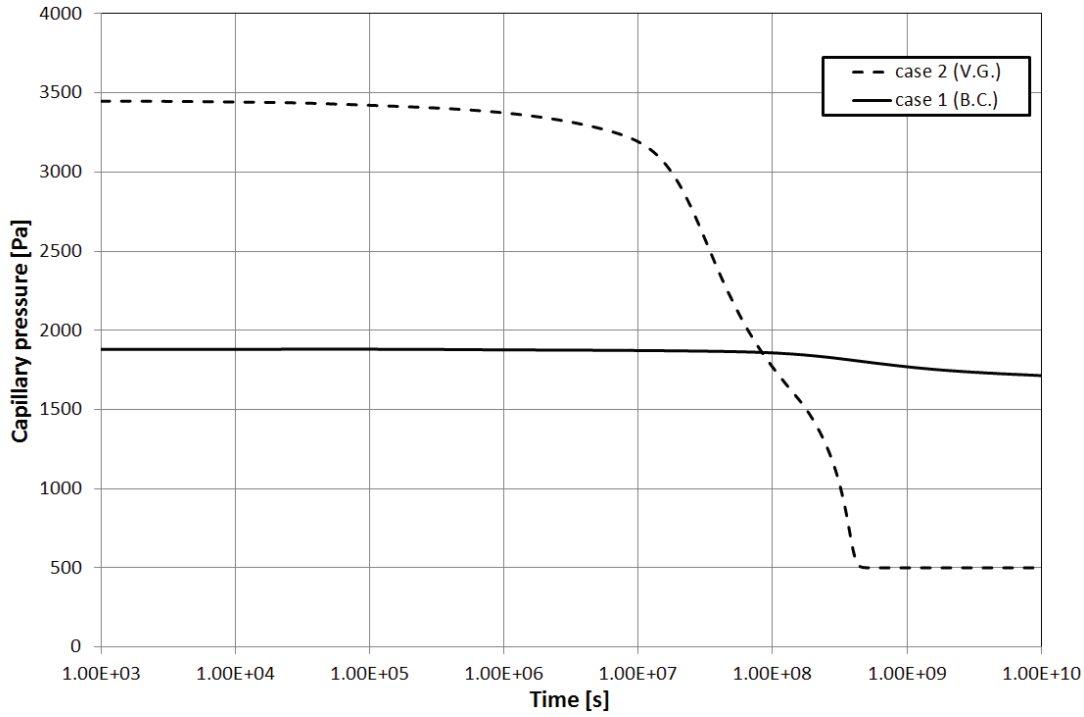

Figure 4.4.19: Capillary pressure evolution in time for the point A on top surface of the domain. Comparison between Case 1 and Case 2 results obtained with PLASCON3D_PS.

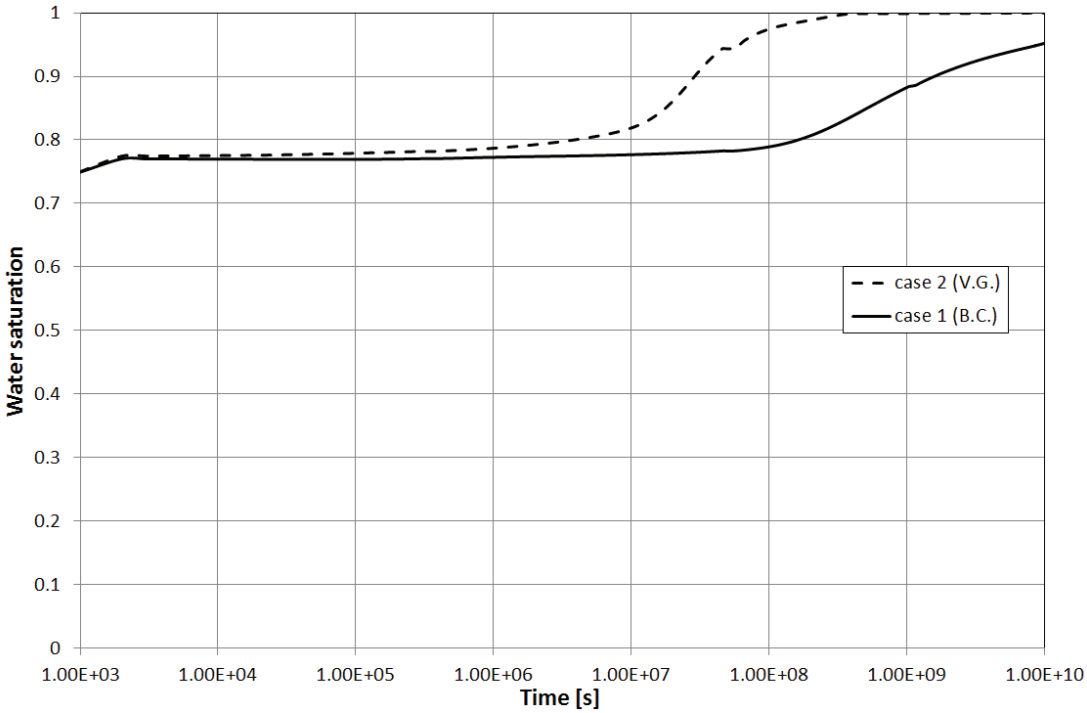

Figure 4.4.20: Water saturation evolution in time for the point A on top surface of the domain. Comparison between Case 1 and Case 2 results obtained with PLASCON3D_PS.

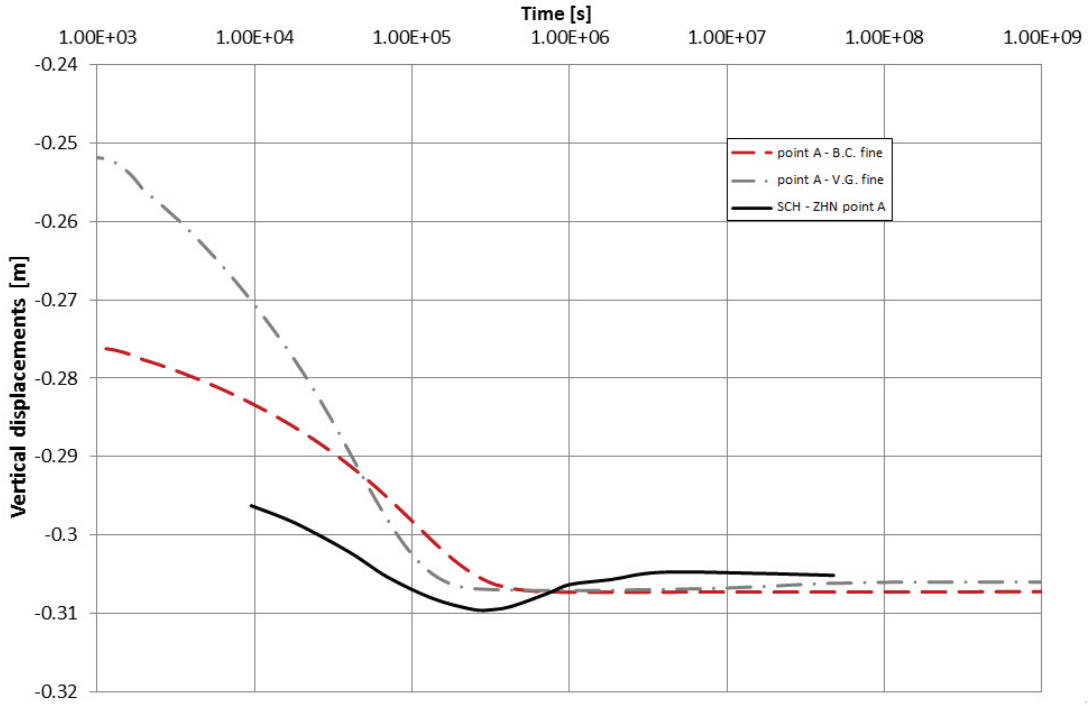

Figure 4.4.21: Vertical displacements evolution in time for the point A on top surface of the domain. Comparison between results obtained with PLASCON3D_PS (with Brooks and Corey and van Genuchten relationships) and results given by Schrefler and Zhan [5].

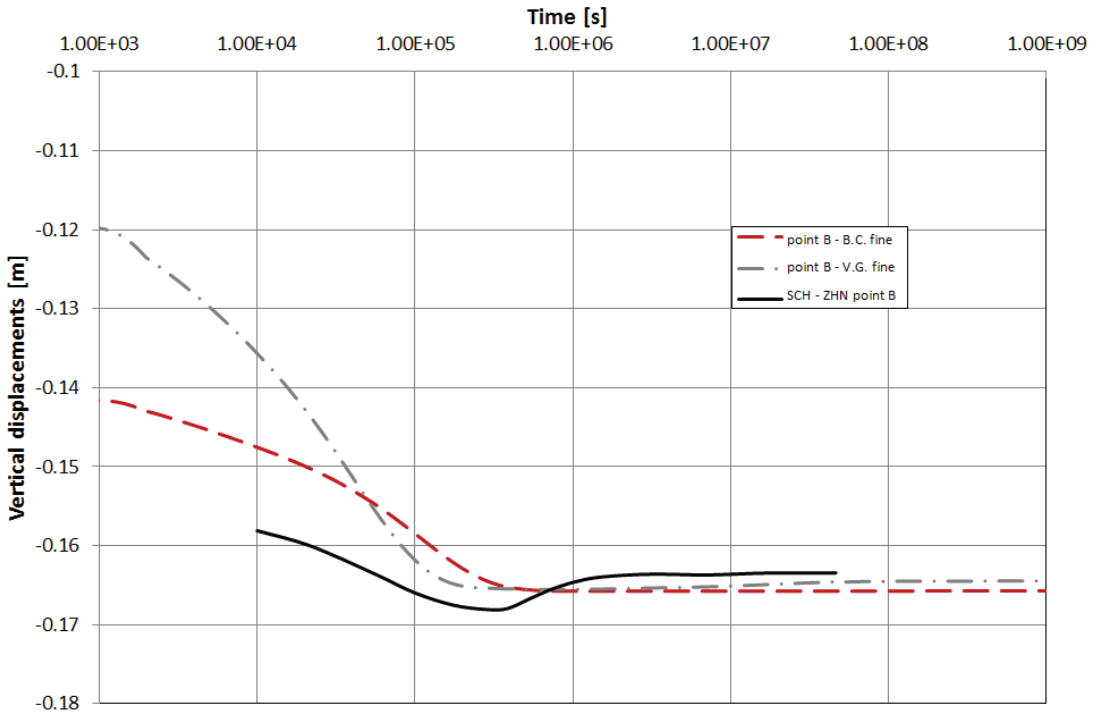

Figure 4.4.22: Vertical displacements evolution in time for the point B on top surface of the domain. Comparison between results obtained with PLASCON3D_PS (with Brooks and Corey and van Genuchten relationships) and results given by Schrefler and Zhan [5].

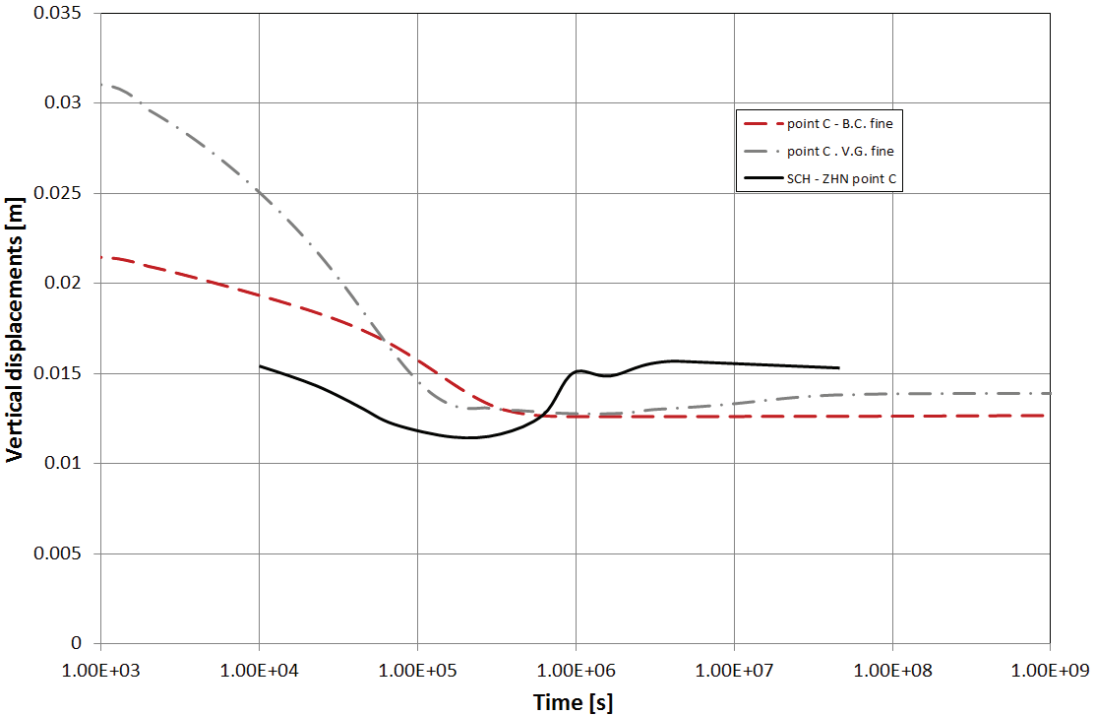

Figure 4.4.23: Vertical displacements evolution in time for the point C on top surface of the domain. Comparison between results obtained with PLASCON3D_PS (with Brooks and Corey and van Genuchten relationships) and results given by Schrefler and Zhan [5].

Schrefler and Zhan observed, for increasing times, a swelling (or expansion) of the top cross section, that is typical of clay soils. What that can be observed from the results obtained with the PLASCOND3D_PS is that a very similar recovery of the vertical displacements occurs, after the time of 10^6 second, for the *Case 2*. The recover of the vertical displacements are greater for the reference point A, and coincides with the change of slope in the capillary pressure vs. time diagram (Figure 4.4.19), i.e. when capillary pressure decreases rapidly. This recover is not appreciable in the *Case* 1, even if it is present, due to the restricted range of variation of capillary pressure from the maximum value to the one set by the bonduary conditions. Comparing the two water saturation vs. capillary pressure relations, the one given by Brooks and Corey (4.4.1) and the one given by van Genutchen (4.4.3) it can be said that for the first part of the simulation. i.e. before the maximum vertical settlement value for each reference point has been reached, the *Case* 1 that adopt the (4.4.1) shows the same slope that the results presented in [5], but with shifted values. The (4.4.3) behaves better at greater times, when is able to reproduce a vertical displacements recovery as observed by Schrefler and Zhan [5].

All the alternative solvers introduced in the chapter 4, have been successful employed. PARDISO, running in multi threads (parallel) mode, with row and column

elimination method for the imposition of boundary conditions, has proved to be the most efficient solver for the resolution of the fine mesh, while for the coarse mesh LAPACK routines with rows and columns elimination running in single thread (sequential) mode has proved to be the most computationally efficient. Results about the performances of the solvers are discussed on section 4.6.

4.5. Air injection into an aquifer in air storage aquifer model: Media Gallesville Acquifer

This numerical example has the aim to analyse a greater domain, with respect to the ones presented in the sections before, like and aquifer, located at a certain deep, subjected to gas injection operations. This case study has been already performed by Meiri [19], Meiri and Karadi [20], assuming a crushproof solid skeleton, and so, no results for the displacements field were produced. By the way, the deformability of the solid phase has been take into account by Schrefler *et al.* [5].

The dimensions and parameters that describe the aquifer reservoir are similar to the Media Gallesville Aquifer studied by Katz *et al.* [21]. The aquifer has 110 m of diameter and the height is 20 m and the homogeneous material which it is made is sand.

Boundary conditions and mesh discretization

The material specifications, as well the other model parameters are reported in Table 4.5.1 and a schematization of the aquifer model is given in Figure 4.5.1.

The medium of which the aquifer is made, is assumed to be at the beginning fully saturated of water, with relative permeability of $\mathbf{k} = 5 \times 10^{-13} \mathrm{m}^2$, a porosity $n = 0.2$ and the aquifer is subjected to a constant temperature of 149°C. The initial aquifer pressure is 5.066 x 10^6 Pa ($\cong$ 50 atm).

Due to the fully saturated initial conditions, the formulation implemented in the PLASCON3D_PS requires initial values for the water and gas pressure that correspond to the saturated state. The saturation state transition from the full saturation to the partial saturation of the medium is again performed maintaining the full coupling of the gas balance equation with other balancing equations, also in the case that the degree of water saturation reaches the unitary value (as previously done in the cases presented in the sections 4.3 and 4.4). This means that even if the fully saturated state is reached, the value of the degree of water saturation will

assume a value very close to 1, allowing that a residual, but small (<1%), degree of gas saturation always exists. This assumption was made similarly in the work of Laloui *et al.* [9]. As consequence to this approach the value of the water pressure has been set in order to obtain a small positive value of capillary pressure, while the gas pressure has been maintained at the aquifer initial pressure, that is also been taken as average gas injection pressure in the following. The value of the initial capillary pressure, that match with the above mentioned requirement is $p_{c,i} = 1680\,\text{Pa}$. Following, also an initial capillary pressure $p_{c,i} = 500\,\text{Pa}$ has been set, in order to compare the solution when values less than the bubbling pressure, are chosen as initial values for the capillary pressure.

Table 4.5.1: Aquifer model characteristics.

Young's modulus	$E = 0.692\ \text{MPa}$
Poisson's ratio	$\nu = 0.27$
Solid grain density	$\rho_s = 2000\,\text{kg}/\text{m}^3$
Liquid density (STC)	$\rho_w = 1000\,\text{kg}/\text{m}^3$
Air density (STC)	$\rho_g = 1.22\,\text{kg}/\text{m}^3$
Porosity	$n = 0.2$
Intrinsic permeability	$\text{k} = 5.0 \cdot 10^{-13}\ \text{m}^2$
Water viscosity	$\mu_w = 3 \cdot 10^{-4}\ \text{Pa} \cdot \text{s}$
Air viscosity	$\mu_a = 2.4 \cdot 10^{-5}\ \text{Pa} \cdot \text{s}$
Gravitational acceleration	$g = 9.806\,\text{m} \cdot \text{s}^{-2}$
Aquifer confinement pressure	$p_{atm} \simeq 50\ \text{atm}$

The boundary conditions for t > 0 are: impervious lateral surfaces ($q_w = 0,\ q_a = 0$) and fixed horizontal displacements ($u_h = 0$). On bottom surface both horizontal and vertical displacements are not allowed ($u_h = 0$ and $u_v = 0$), as well the gas flux ($q_a = 0$). The water pressure is equal to the initial pressure of the aquifer minus the value of bubbling pressure discussed in the following ($p_w = 5.06432 \times 10^6\ \text{Pa}$). Top surface is subjected to a constant gas flux and zero water flux. All nodes that don't belong to the bottom surface are free to move vertically.

In order to provide a correct boundary condition for the gas flux that is injected homogeneously on the top surface of the aquifer, the constant flux in terms of mass of gas injected per seconds per unit area ($q_a = 2.44 \times 10^{-4}\ \mathrm{kg/s} \times \mathrm{m}^2$) must be translated to a volumetric value that depends on the gas density.

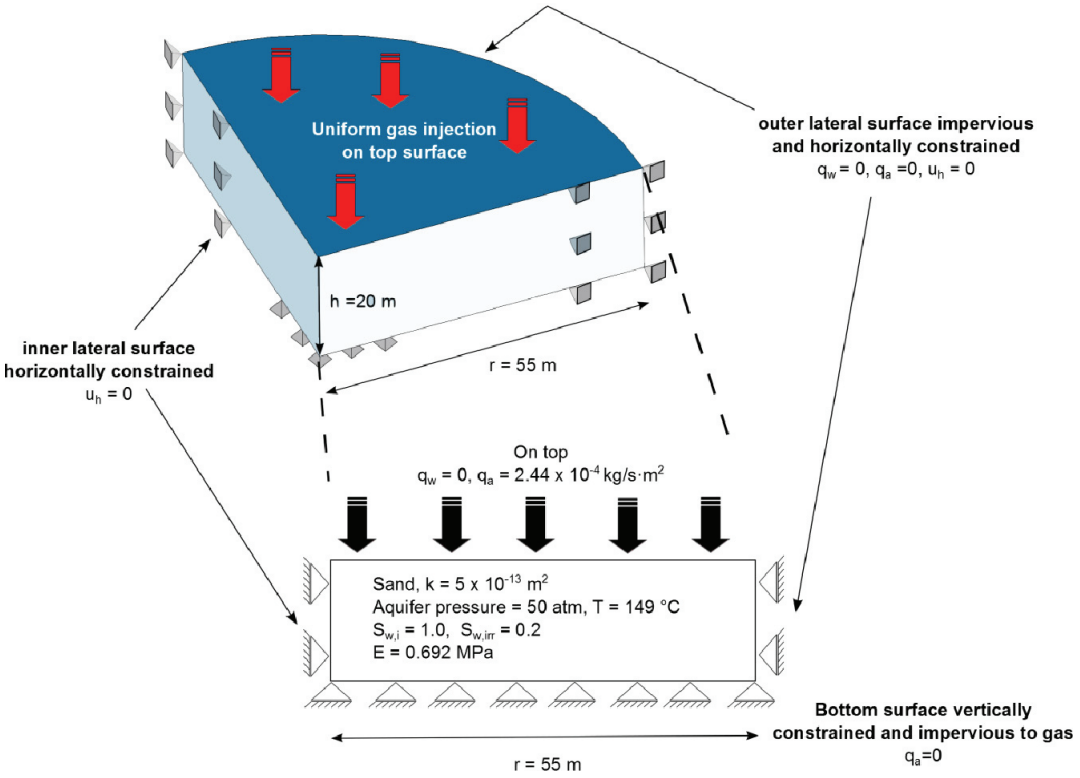

Figure 4.5.1: Schematics of a quart of aquifer and main boundary conditions.

Due to the dramatically different conditions prevailing at the deep where reservoir is located, compared with the conditions at the surface, it must be kept in mind that the same quantity of gas mass occupies different volumes depending on conditions considered. At the ground surface where deep is equal to zero, the air is at standard tank conditions (STC). In other words, the air density value of 1.22 kg/m³ that correspond to a specific volume for the air of about 0.82 m³/kg must be recalculated at the reservoir conditions.

Assuming that air behaves as an ideal gas, Meiri [22] provided a suitable relation for the formation volume factor of air at the reservoir temperature

$$\beta_a(p_a) = 1.46/p_a \tag{4.5.1}$$

The formation volume factor of a gas is defined as the ratio of the volume of the gas at the reservoir temperature and pressure to the volume at the standard or surface temperature and pressure. This coefficient relates the volume of fluids that are

obtained at the surface (stock tank) to the volume that the fluid actually occupied when it was compressed in the reservoir.

This relation can be easily written as

$$\beta_a = \frac{V_{a,RES}}{V_{a,STC}} \tag{4.5.2}$$

With $p_a = 50\,\mathrm{atm}$ the formation volume factor is $\beta_a \simeq 0.03$. Thus, the gas flux expressed in terms of mass can be calculated in terms of volume at standard conditions and then calculated in terms of volumetric flux at reservoir conditions, at least for the discovery initial pressure.

For the water saturation – capillary pressure relation the Brooks & Corey [14, 15] relation has been used

$$\begin{aligned} S_w &= S_{w,irr} + \left(1 - S_{w,irr}\right)\left[\frac{p_b}{s}\right]^{\lambda} \quad for\ s > p_b \\ S_w &= 1 - S_{g,irr} \qquad\qquad for\ s < p_b \end{aligned} \tag{4.5.3}$$

and

$$\begin{aligned} k_{rw} &= S_e^{(2+3\lambda)/\lambda} \\ k_{rg} &= \left(1 - S_e\right)^2 \left(1 - S_e^{(2+\lambda)/\lambda}\right) \end{aligned} \tag{4.5.4}$$

The values of $S_{w,irr}$, p_b and λ are respectively 0.2, 1680 Pa and 3.0. The relationship is the one presented in the previous section in Figure 4.4.3.

As schematized in Figure 4.5.1 the domain that has been tested, consists in a quart of the whole aquifer. The domain has been subdivided with 270 20-node iso-parametric elements (details about the element that has been adopted can be found in the Section 2.8) , for a total of 1438 nodes. The height has been subdivided by ten elements. The final mesh has been reported on Figure 4.5.2.

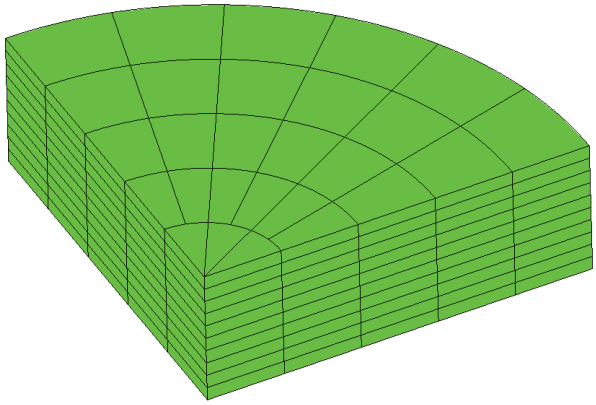

Figure 4.5.2: Discretization of a quart of the circular aquifer.

Numerical results

The simulated injection takes place during a time span of 80 hours. A time step of 1800 s (0.5 hour) and of 180 (0.05 hour) has been used, with no appreciable differences on final results. Results have been plotted in graph for 0, 10, 20, 30, 40, 50, 60, 70 and 80 hours.

Contour maps for water and gas pressures and for displacements and water saturation have been reported at 10 and 80 hours of simulation (Figure 4.5.3 to Figure 4.5.6). The results for the other simulation times are qualitatively similar.

Graphical results are reported for water and gas pressures and for displacements and water saturation (Figure 4.5.7 to Figure 4.5.11). Comparisons with the results of other authors have been done in Figure 4.5.10 to Figure 4.5.12.

With reference to the graphs reported in Figure 4.5.7 to Figure 4.5.9 can be seen that, in the first part of the simulation that takes about 40 hours, the aquifer is compacting, with a decreasing trend in terms of pressure values both for water and gas. The gas displaces the water present in the aquifer and with time occupies the voids volume released by water. This fact can be observed also in the graph relative to the degree of water saturation vs. height (Figure 4.5.10). For later times than 40 hours the aquifer reverses its trend and starts progressively to expand. As long as the storage of gas volume at higher height levels increases, the pressures, initially decreasing, start to recover progressively. The pressure has a minimum at the interface of two fluids and as can be seen from Figure 4.5.7 and Figure 4.5.8. the minimum value of pressure, both for water and gas, is more or less constant with time, however, the corresponding height where it can be observed, decreases, moving with time towards the bottom of the aquifer, i.e. the aquifer is storing gas progressively.

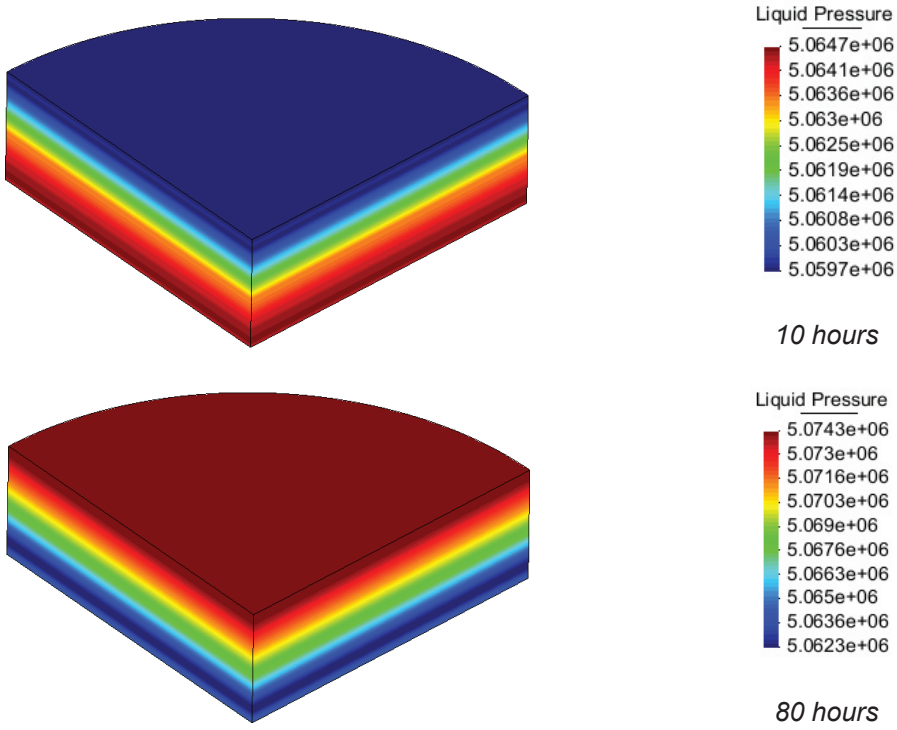

Figure 4.5.3: Contour maps obtained with PLASCON3D_PS for the water pressure [Pa] for 10 and 80 hours.

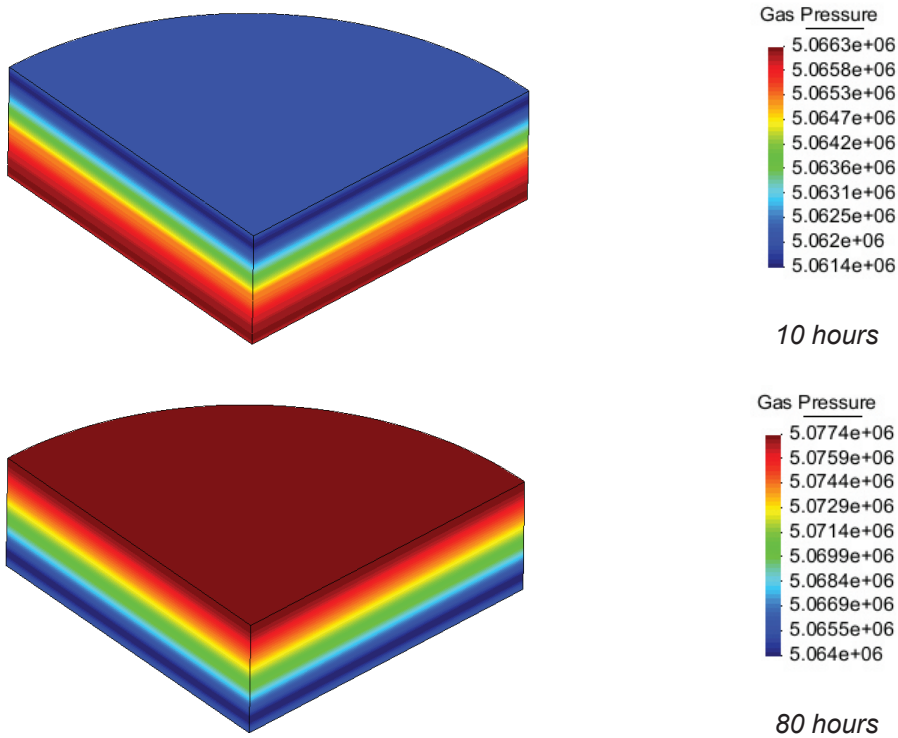

Figure 4.5.4: Contour maps obtained with PLASCON3D_PS for the gas pressure [Pa] for 10 and 80 hours.

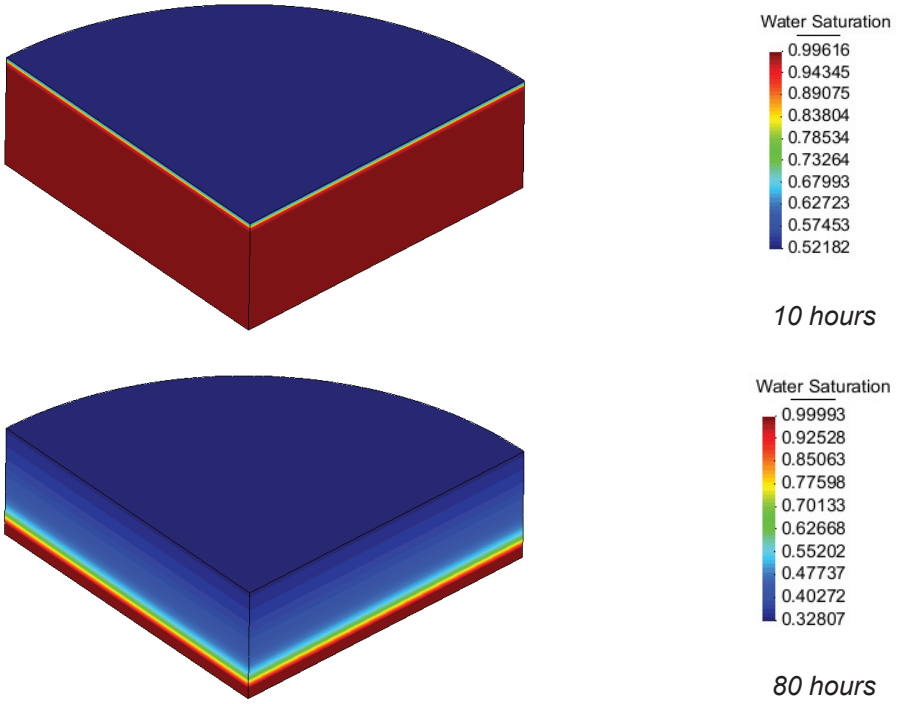

Figure 4.5.5: Contour maps obtained with PLASCON3D_PS for the degree of water saturation for 10 and 80 hours.

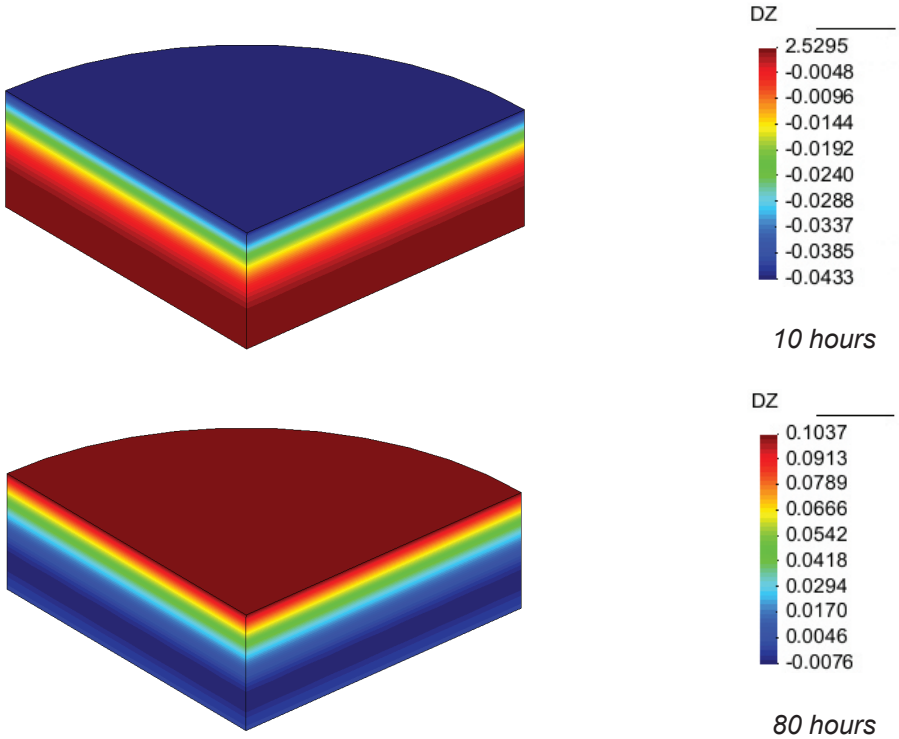

Figure 4.5.6: Contour maps obtained with PLASCON3D_PS for vertical displacements [m] for 10 and 80 hours.

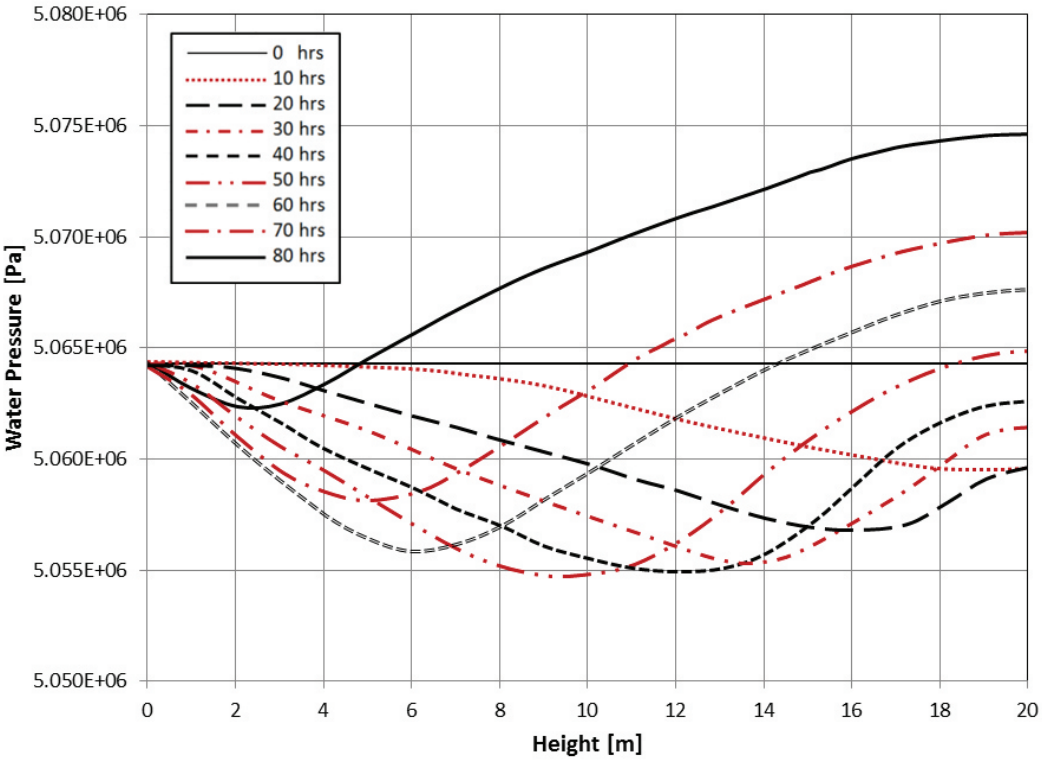

Figure 4.5.7: Water pressure vs. height [m] results obtained with PLASCON3D_PS.

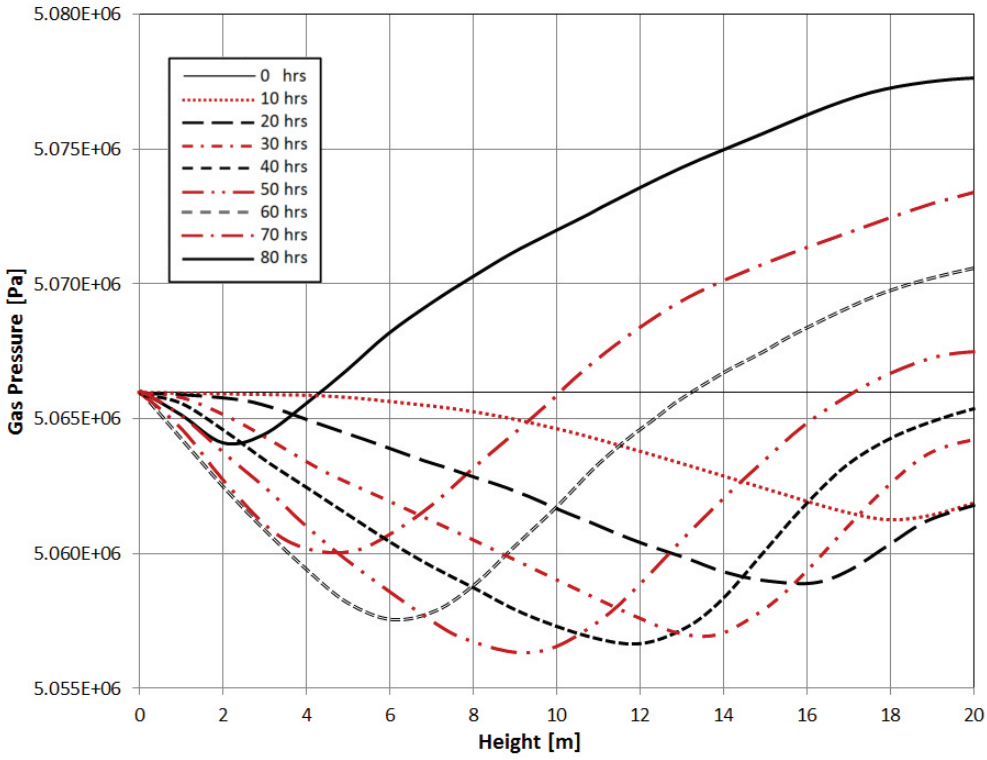

Figure 4.5.8: Gas pressure vs. height [m] results obtained with PLASCON3D_PS.

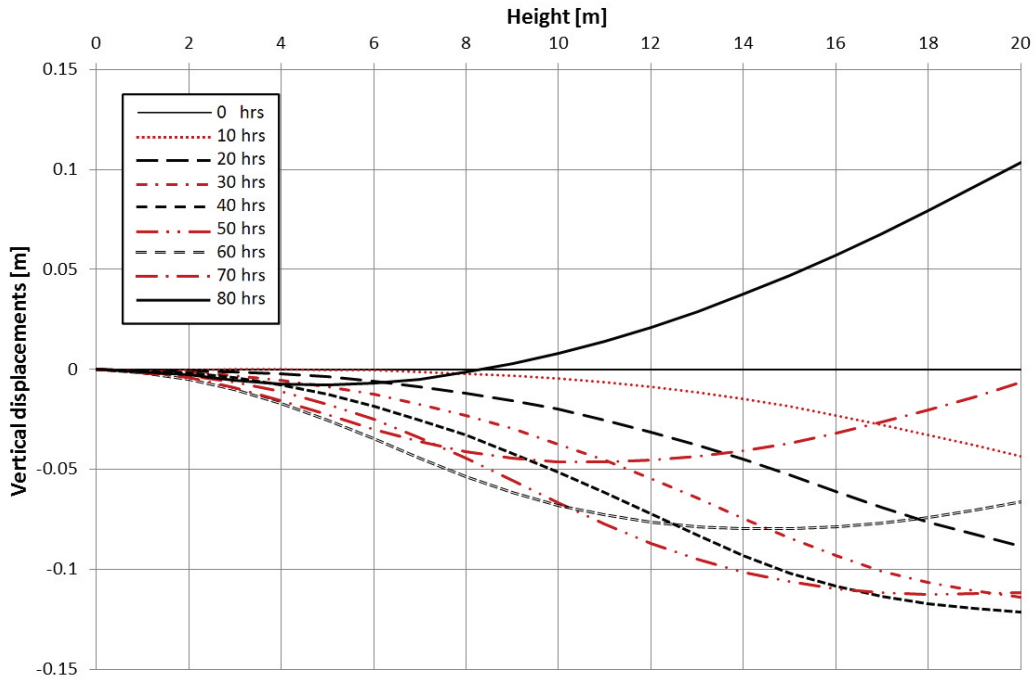

Figure 4.5.9: Vertical displacements [m] vs. height [m] results obtained with PLASCON3D_PS.

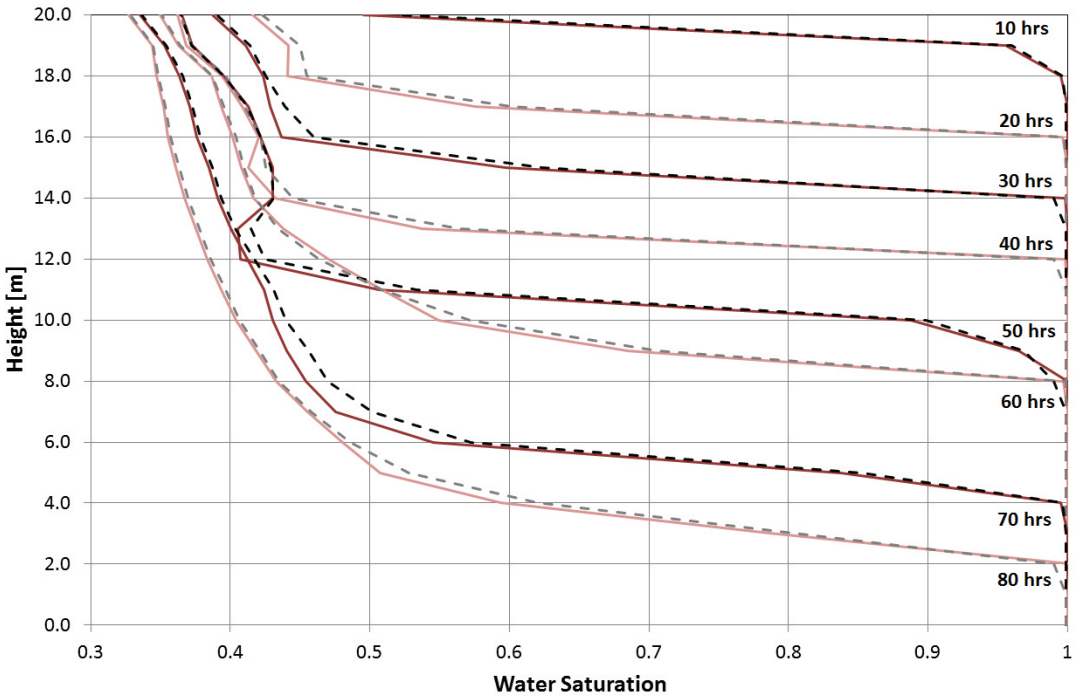

Figure 4.5.10: Degree of water saturation vs. height [m] results obtained with PLASCON3D_PS (dashed lines) compared with those obtained by Schrefler and Zhan [5] (continuous lines).

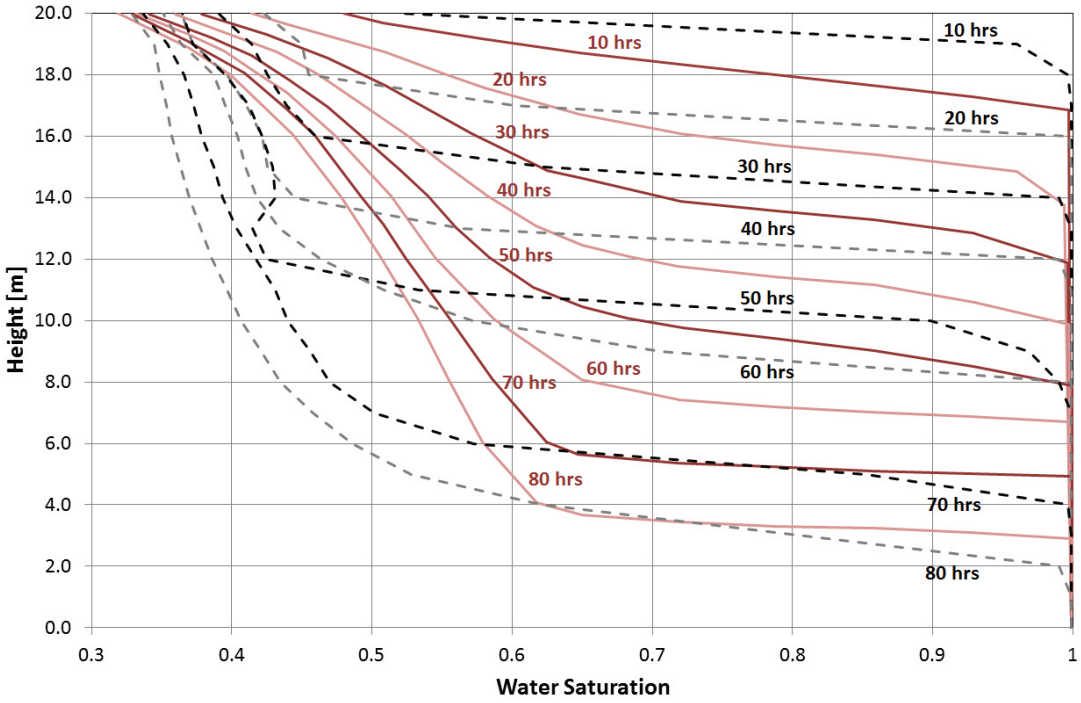

Figure 4.5.11: Degree of water saturation vs. height [m] results obtained with PLASCON3D_PS (dashed lines) compared with those obtained by Meiri and Karadi [20] (continuous lines).

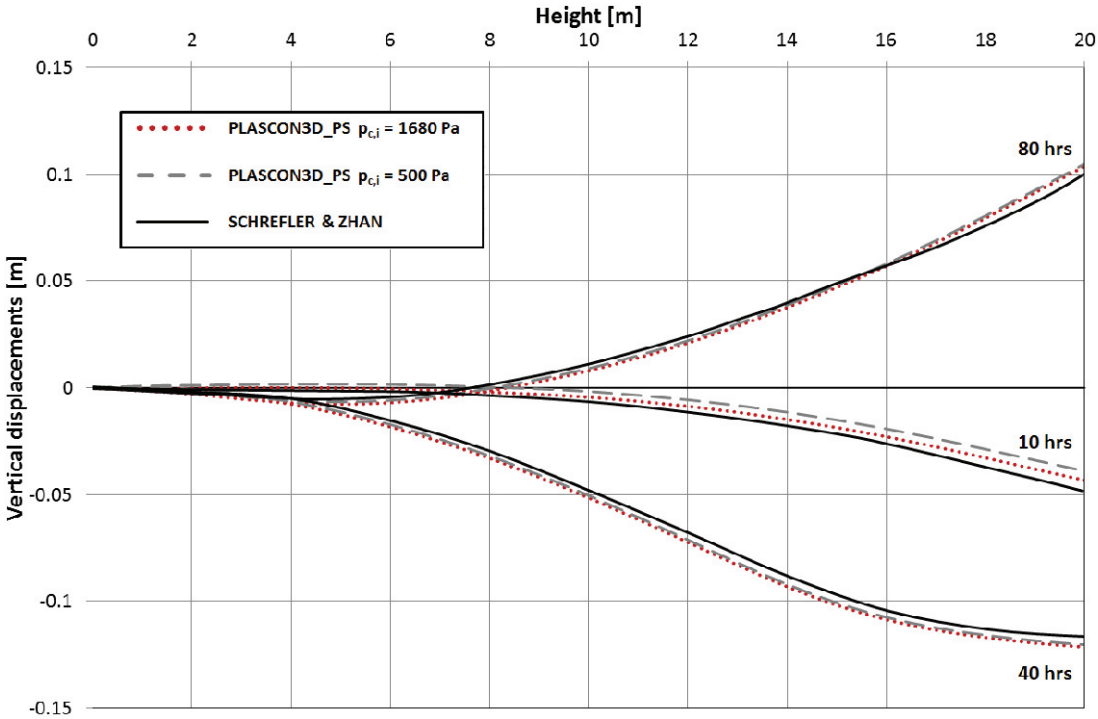

Figure 4.5.12: Vertical displacements [m] vs. height [m] results obtained with PLASCON3D_PS (dotted lines for $p_{c,i}$ = 1680 Pa and dashed lines for $p_{c,i}$ = 500 Pa) compared with those obtained by Schrefler and Zhan [5] (continuous lines).

Schrefler and Zhan [5], solved the problem with a coupled formulation, using a two-dimensional domain similar to the two-dimensional column adopted to treat the Liakopoulos test case by the same authors (obviously with the dimensions of the central cross section of the aquifer), which is solved here in the section 4.3. Here the one-dimensional problem for the solid phase has been solved adopting a three-dimensional domain that corresponds to the quart of aquifer. The agreement with the results obtained by the above mentioned authors is very good in terms of degree of water saturation and displacements (Figure 4.5.10 and Figure 4.5.12). With respect to the Meiri [19] and Meiri and Karadi [20] works, a proper Young's modulus and Poisson's coefficients for the material has been used and the effects a of the deformable solid skeleton on the degree of water saturation profiles on can be seen in Figure 4.5.11, where a comparison with the original authors has been done. While for a rigid skeleton the desaturation on the domain is larger at the beginning of the simulation, for a deformable material present larger desaturation effects for later times of simulation.

As explained before the initial conditions for gas and pressure are different and values are shifted by a small positive value of capillary pressure in order to ensure a proper correspondence of the initial state on the water saturation vs. capillary pressure curve (Figure 4.4.3). In fact for values above the bubbling pressure p_b , the entry of the air/gas into the porous matrix occurs (see also section 1.5) and so a positive value for the degree of gas saturation can be achieved, as required by the approach, in order to ensure full coupling between the phases. However, the modification to the (1.5.8), along with a proper setting of initial conditions has important consequences as described in the section 4.3.

Here, as result of the introduction of the residual gas saturation, the solution of the problem is possible also for initial values of capillary pressure less than the bubbling pressure. This can be done ensuring a residual gas saturation of 0.1% also for value of $p_{c,i} = 500\,\mathrm{Pa}$. In particular, as showed by Figure 4.5.12, at the onset results in terms of vertical displacements adhere more to the results obtained in [5] for $p_{c,i} = p_b$,although results with $p_{c,i} = 500\,\mathrm{Pa}$ are good. Later the influence of the initial conditions disappears and the results in two cases are identical, as expected.

All the alternative solvers introduced in the chapter 4 have been successful employed, however LAPACK routines running in sequential mode, with row and column elimination method used for the imposition of boundary conditions, has proved to be the computationally most efficient solver for the resolution of the problem. Results about the performances of the solvers are discussed on section 4.6.

4.6. Analysis of the solvers performances

In the following, the computational performances in terms of CPU time spent into the block of code relative to solution procedures have been reported. Results refer to the average time, in seconds, that has been spent for a singular time step. The computations have been performed on multi core UNIX servers named Antares. Table 4.6.1 summarizes the dimension of the problems that have been analysed in the present work.

Table 4.6.1: Summary of problems dimension considered in the present work.

	Elements	Nodes
Liakopoulos 10 el. mesh	10	128
Liakopoulos 80 el. mesh	80	621
Footing coarse mesh	40	348
Footing fine mesh	440	2681
Aquifer mesh	270	1438

All the analyses presented, have been carried out with all the solvers implemented in the code. The alternative solvers presented, that are put by side of the standard skyline solver, are based on the LAPACK routines [23] and on the PARDISO solver [24]. Two different way of imposing the boundary conditions have been tested, as first, the method that uses the penalty coefficient has been considered. The second method uses the row and column elimination (section 3.4). An average value of the time spent to solve the linear system of equations for a single time step has been calculated and reported in Table 4.6.2 for the computations done in single-thread mode, while in Table 4.6.3 for the computations done in parallel model (the value is the sum of time over all cores).

Table 4.6.2: Performances in terms of CPU time [s] spent into the solver routines when running on sequential mode (one thread). Values in bold are the best for the relative mesh.

	Standard Skyline	LAPACK w. penalty coeff.	PARDISO w. penalty coeff.	LAPACK w. row / col. elim.	PARDISO w. row / col. elim.
Liakopoulos 10 el.	0.36	0.02	0.0240	0.0120	**0.008**
Liakopoulos 80 el.	230	1.25	0.52	0.44	**0.41**
Footing coarse	35	0.25	0.18	**0.12**	0.13
Footing fine	-	90.4	10.7	33.8	**9.2**
Aquifer	-	13.8	3	**1.6**	2

As can be seen comparing the two tables, the multi-thread mode doesn't affect the CPU time needed to standard skyline solver to achieve the solution of the problems. This was expected, due to the fact that the standard solver routine is made by a code block of sequential instructions that don't allow a parallelization, thus, the solver uses only a CPU core even the parallelization of the code is allowed by the compiler settings. However, this solver has a great lack of efficiency when is employed to solve meshes larger than a certain number of elements, such the fine mesh used in the flexible footing problem (section 4.4) or the mesh related to the gas injection in aquifer (section 4.5).

Table 4.6.3: Performances in terms of CPU time [s] spent into the solver routines when running on parallel mode (multi thread). Values in bold are the best for the relative mesh.

	Standard Skyline	LAPACK w. penalty coeff.	PARDISO w. penalty coeff	LAPACK w. row / col elim.	PARDISO w. row / col. elim.
Liakopoulos 10 el.	0.36	0.22	0.5	**0.19**	0.23
Liakopoulos 80 el.	230	4	1.5	1.17	**0.84**
Footing coarse	35	0.78	0.61	0.4	**0.38**
Footing fine	-	91.1	10.8	34.1	**8.2**
Aquifer	-	23.3	8	3.5	**3.4**

PARDISO has been proved to be the best solver, denoting a considerable saving in computational time and a good choice in every situation. However, also LAPACK routines work very well.

The time take into account of the global system matrix assembly, followed by the imposition of boundary conditions and the by the solution of the system of equations. With reference to the dimension of the problems that have been treated within this work, the row and column method is the best method to impose the boundary conditions and preparing the linear system to the solving operations. In fact, this method reduces the dimension of the global matrix that is attempt to being solved, resulting in less computational cost and a gain in CPU time. The penalty coefficient, instead, despite is faster than the first, preserve the global system dimension with a consequently larger computational cost and CPU time in order to obtain solution.

Concluding the best choice for a mesh of small dimension is PARDISO running in sequential, single-thread mode, with row and column elimination method. However, also the use of LAPACK routines with the same configurations obtains good results. For larger mesh (e.g. 400 elements and 2500 nodes) best results are obtained with PARDISO running in parallel mode.

Bibliography

1. Liakopoulos, A.C., *Transient flow through unsaturated porous media*, 1964, University of California, Berkeley

2. Narasimhan, T. and P. Witherspoon, *Numerical model for saturated-unsaturated flow in deformable porous media: 3. Applications.* Water Resources Research, 1978. **14**(6): p. 1017-1034.

3. Schrefler, B. and L. Simoni, *A unified approach to the analysis of saturated-unsaturated elastoplastic porous media.* Numerical Methods in Geomechanics, 1988: p. 205-212.

4. Zienkiewicz, O.C., et al., *Static and dynamic behaviour of soils: a rational approach to quantitative solutions. II. Semi-saturated problems.* Proceedings of the Royal Society of London. A. Mathematical and Physical Sciences, 1990. **429**(1877): p. 311-321.

5. Schrefler, B. and Z. Xiaoyong, *A fully coupled model for water flow and airflow in deformable porous media.* Water Resources Research, 1993. **29**(1): p. 155-167.

6. Gawin, D., P. Baggio, and B.A. Schrefler, *Coupled heat, water and gas flow in deformable porous media.* International Journal for numerical methods in fluids, 1995. **20**(8-9): p. 969-987.

7. Gawin, D., B.A. Schrefler, and M. Galindo, *Thermo-hydro-mechanical analysis of partially saturated porous materials.* Engineering Computations, 1996. **13**(7): p. 113-143.

8. Lewis, R.W. and B.A. Schrefler, *The finite element method in the deformation and consolidation of porous media.* 1998.

9. Laloui, L., G. Klubertanz, and L. Vulliet, *Solid–liquid–air coupling in multiphase porous media.* International journal for numerical and analytical methods in geomechanics, 2003. **27**(3): p. 183-206.

10. Gabriele, G., *Modellazione numerica di problemi idro-termo-meccanici nei mezzi porosi parzialmente saturi.* Department of Civil, Environmental and Architectural Engineering, DICEA, Padua, 2010-2011.

11. Gawin, D. and B.A. Schrefler, *Modelling of saturated-unsaturated transition in porous media.* Proceedings of the GIMC-AMC Conference, Padua, 1996.

12. Lloret, A., et al. *Flow and deformation analysis of partially saturated soils*. in *European conference on soil mechanics and foundation engineering. 9*. 1987.

13. Lloret, A. and E.E. Alonso, *State surfaces for partially saturated soils.* Proceedings of the 11th International Conference on Soil Mechanics and Foundation Engineering, San Francisco, 12-16 august 1985. Publication of Balkema, 1985.

14. Brooks, R. and A. Corey, *Hydraulic Properties of Porous Media, of Colorado State University Hydrology Paper, 3.* Colorado State University, 1964.

15. Brooks, R.H. and A.T. Corey. *Properties of porous media affecting fluid flow*. in *Journal of the Irrigation and Drainage Division, Proceedings of the American Society of Civil Engineers*. 1966.

16. Mualem, Y., *A new model for predicting the hydraulic conductivity of unsaturated porous media.* Water resources research, 1976. **12**(3): p. 513-522.

17. Parker, J. and R. Lenhard, *A model for hysteretic constitutive relations governing multiphase flow: 1. Saturation-pressure relations.* Water Resources Research, 1987. **23**(12): p. 2187-2196.

18. Parker, J., R. Lenhard, and T. Kuppusamy, *A parametric model for constitutive properties governing multiphase flow in porous media.* Water Resources Research, 1987. **23**(4): p. 618-624.

19. Meiri, D., *Two-phase flow simulation of air storage in an aquifer.* Water Resources Research, 1981. **17**(5): p. 1360-1366.

20. Meiri, D. and G.M. Karadi, *Simulation of air storage aquifer by finite element model.* International Journal for Numerical and Analytical Methods in Geomechanics, 1982. **6**(3): p. 339-351.

21. Katz, D.L.V. and E.R. Lady, *Compressed air storage for electric power generation*. 1976: May be ordered from Ulrich's Books.

22. Meiri, D., *Analysis of compressed air aquifer storage by finite element method*, 1979, University of Wisconsin-Milwaukee.

23. Anderson, E., *LAPACK Users' guide*. Vol. 9. 1999: Siam.

24. Schenk, O. and K. Gärtner, *Solving unsymmetric sparse systems of linear equations with PARDISO.* Future Generation Computer Systems, 2004. **20**(3): p. 475-487.

5 Conclusions

The present work can be inserted in the framework of the Solid Mechanics, applied to the porous media theories. The model for the saturated and unsaturated medium presented here in the chapter 1, is a macro scale, physical approach characterization of the continuum presented in the more complex hybrid mixture theory developed first by Hassanizadeh and Gray [1, 2] and then by Lewis and Schrefler [3] and Zienkiewicz *et al.* [4, 5]. Along with the equations that govern the porous medium, a set of constitutive equations, able to describe all the mechanical, hydraulic and thermodynamic aspects were needed to complete the multiphase formulation.

The principal goal of this work has been to achieve a numerical tool, that was able to solve finite elements (F.E.) numerical problems, in order to foresight the behaviour of different geomaterials, such soils, in partial saturated states, where capillarity effects play a paramount role on the determination of mechanical quantities.

Due to this challenging purpose, it has been determinant understanding the physic processes related to the saturation and desaturation of the solid skeleton and to find some mathematical relations [6-8], suitable for the numerical implementation into the three-dimensional research F.E. code PLASCON3D [9].

To numerically solve the new initial and boundary value problem presented in the Chapter 2, the basic pressure variable (*p)* considered as representative of the saturated fluid phase in previous works [10-14] has been split, in order to take into account of the two separated fluid phases. Thus, with respect to the formulation used in the past, it has been necessary to specify a new set of discretized equations that refers to the non-isothermal and isothermal airflow and water flow. Along with this set of equations, the finite element method applied to system equations and the solution procedures needed have been presented.

The finite element numerical code PLASCON3D_PS, that implement a coupled hydro-thermo-mechanical formulation has been obtained at the end of an intensive programming activity, basically targeted to update and extend the previous releases of the research code already in use. Most relevant differences between the two codes and the major modifications have been discussed in Chapter 3, where most important routines of the code have been listed.

In order to check the functionality of the code during and at the end of the programming activity, several benchmark tests have been carried out with previous version and commercial software.

The research of suitable test cases for the validation and the fruition of the code has not been an easy task, due to the lack of three-dimensional coupled solutions for partially saturated problems for soil, as well for other geomaterials. However, some two-dimensional coupled problems dealing with unsaturated soils were solved in literature and an experimental test was available to perform a validation of the code.

Chapter 4 resumes the numerical analyses that followed the numerical implementation of PLASCON3D_PS, first of all the code has been employed to solve the Liakopoulos test case [15] that deals with the desaturation processes that occurs to a sand column subjected to gravity water flux and natural air flow from the top.

This first test, put the attention on how was possible to manage the transition to the initial fully saturated state, where the degree of saturation of water is unitary and only the water pressure has meaning, to the partial saturated state, where the degrees of saturation depends strictly from the capillarity effects of the soil. As explained in section 1.5 and 4.3, null values of degree of gas saturation cause severe numerical problems or the impossibility to solve the linear system of equation, due to the null determinant of the linear system that is being attempted to solve.

With respect to most of approaches that can be found in literature, and summarized in [16], the approach followed maintains the gas balance equation also for states very close or that coincide to the full saturation with water, introducing a small irreducible degree of gas saturation that avoid the cancellation of the gas phase terms. This approach was also followed by Laloui *et al.* [17] putting some limitations on the maximum value of the degree of water saturation.

Solutions for the Liakopoulos test case have been obtained, both for one phase water flow, considering the air at the atmospheric conditions that for the case of a two phase fluid flow. The partially saturated formulation implemented in the code, has evidenced the ability to well reproduce the distributions in the domain of pressures, degrees of saturation, vertical displacements and outflow that can be found in literature results [18] and experimental results.

This goal, as well the procedures to manage the transition between different saturation states, have been confirmed when flexible footing on partially saturated

soil [19, 20] and the simulation of a gas injection into aquifer problem [20-22] have been approached and solved with good results.

In particular, with respect to the previous works, two different three-dimensional mesh refinement and two different relationships, able to model the degree of water saturation vs. capillary pressure relation [6, 8], have been compared when dealing with the flexible footing problem. The comparison denotes the capabilities of the code to manage different water retention models for the soil and the numerical efficiency and accuracy of the code approaching to different mesh discretization. The full set of results in terms of displacements, water, gas and capillary pressures, water and gas saturations and relative permeabilities have been computed, for a wide time span, necessary to follow the evolution of the above mentioned quantities from the initial state to the final, fully saturated state.

With the need to obtain computationally efficient solutions of the problems presented in the sections 4.4 and 4.5 , that were difficult to obtain with the standard solver implemented in the original code, a set of optimized and parallelizable sparse solvers [23, 24] have been interfaced with PLASCON3D_PS, obtaining as results a gain in memory and processor performance and reducing drastically the computational time both on local machines that on the “Antares” research server.

The work presented in this thesis, along with the first and new three-dimensional coupled F.E. code PLASCON3D_PS, are only the starting point of several research developments, that concern the study of partially saturated porous media, in the more general framework of coupled problems. Further possible activities, just to give some examples, can deal with the test and validation of non-isothermal numerical problems, as well as the numerical analysis parallel to experimental works on real domains, such embankments or heart dams. But also the implementation of new constitutive models for the solid phase such plasticity, unconventional plasticity or creep such the ones that has been recently developed [10-14] or those under developing and the study of the influence of the stress of the solid phase on the expressions that aim to model the degree of water saturation vs. capillary pressure relation, as evidenced by [7]. Finally, the extension of this work to other geomaterials different from soils, such concrete, is foreseen to be one of the closest goals to achieve.

Bibliography

1. Hassanizadeh, M. and W.G. Gray, *General conservation equations for multi-phase systems: 1. Averaging procedure.* Advances in Water Resources, 1979. **2**: p. 131-144.

2. Hassanizadeh, M. and W.G. Gray, *General conservation equations for multi-phase systems: 2. Mass, momenta, energy, and entropy equations.* Advances in Water Resources, 1979. **2**: p. 191-203.

3. Lewis, R.W. and B.A. Schrefler, *The finite element method in the deformation and consolidation of porous media.* 1987.

4. Zienkiewicz, O.C., et al., *Static and dynamic behaviour of soils: a rational approach to quantitative solutions. I. Fully saturated problems.* Proceedings of the Royal Society of London. A. Mathematical and Physical Sciences, 1990. **429**(1877): p. 285-309.

5. Zienkiewicz, O.C., et al., *Static and dynamic behaviour of soils: a rational approach to quantitative solutions. II. Semi-saturated problems.* Proceedings of the Royal Society of London. A. Mathematical and Physical Sciences, 1990. **429**(1877): p. 311-321.

6. Brooks, R.H. and A.T. Corey. *Properties of porous media affecting fluid flow*. in *Journal of the Irrigation and Drainage Division, Proceedings of the American Society of Civil Engineers*. 1966.

7. Lloret, A. and E.E. Alonso, *State surfaces for partially saturated soils.* Proceedings of the 11th International Conference on Soil Mechanics and Foundation Engineering, San Francisco, 12-16 august 1985. Publication of Balkema, 1985.

8. van Genuchten, M.T., *A closed-form equation for predicting the hydraulic conductivity of unsaturated soils.* Soil Science Society of America Journal, 1980. **44**(5): p. 892-898.

9. Majorana, C., R. Lewis, and B. Schrefler, *Two-dimensional non-linear thermo-elastoplastic consolidation program Plascon.* The Finite Element Method in the Deformation and Consolidation of Porous Media, Lewis RW, Schrefler BA (eds), 1987.

10. Salomoni, V.A. and R. Fincato. *3D modelling of geomaterials accounting for an unconventional plasticity approach*. 2011.

11. Salomoni, V.A. and R. Fincato, *Subloading surface plasticity model algorithm for 3D subsidence analyses above gas reservoirs.* International Journal of Geomechanics, 2012. **12**(4): p. 414-427.

12. Salomoni, V.A. and R. Fincato, *3D subsidence analyses above gas reservoirs accounting for an unconventional plasticity model.* International Journal for Numerical and Analytical Methods in Geomechanics, 2012. **36**(8): p. 959-976.

13. Salomoni, V.A. and R.L. Fincato. *Subloading surface plasticity model algorithm for 3D subsidence analyses above gas reservoirs*. 2011.

14. Zanetti, S., *Analisi tridimensionale di problemi di subsidenza per estrazione di fluidi.* Master Thesis, Departement of Civili, Environmental and Architectural Engineering, Padua, 1995-1996: p. 133.

15. Liakopoulos, A.C., *Transient flow through unsaturated porous media*, 1964, University of California, Berkeley

16. Lewis, R.W. and B.A. Schrefler, *The finite element method in the deformation and consolidation of porous media.* 1998.

17. Laloui, L., G. Klubertanz, and L. Vulliet, *Solid–liquid–air coupling in multiphase porous media.* International journal for numerical and analytical methods in geomechanics, 2003. **27**(3): p. 183-206.

18. Gawin, D. and B.A. Schrefler, *Modelling of saturated-unsaturated transition in porous media.* Proceedings of the GIMC-AMC Conference, Padua, 1996.

19. Lloret, A., et al. *Flow and deformation analysis of partially saturated soils*. in *European conference on soil mechanics and foundation engineering. 9*. 1987.

20. Schrefler, B. and Z. Xiaoyong, *A fully coupled model for water flow and airflow in deformable porous media.* Water Resources Research, 1993. **29**(1): p. 155-167.

21. Meiri, D., *Analysis of compressed air aquifer storage by finite element method*, 1979, University of Wisconsin-Milwaukee.

22. Meiri, D., *Two-phase flow simulation of air storage in an aquifer.* Water Resources Research, 1981. **17**(5): p. 1360-1366.

23. Anderson, E., *LAPACK Users' guide*. Vol. 9. 1999: Siam.

24. Schenk, O., et al., *PARDISO: a high-performance serial and parallel sparse linear solver in semiconductor device simulation.* Future Generation Computer Systems, 2001. **18**(1): p. 69-78.

6 Appendix: Structural analyses and integrated design of the MITICA Injector assembly

6.1. Introduction

In the framework of the activities foreseen for PRIMA (Padova Research on Injector Megavolt Accelerated) the MITICA neutral beam injector plays the role of main experiment, aiming to build, operate, test and optimize a full power and full scale prototype of the ITER Heating Neutral Beam Injector [1-3].

The entire MITICA system will be housed in special buildings, suitably designed to provide all the necessary supports, interfaces and shielding walls for nuclear radiation safety. Therefore, an integrated design of the MITICA system and relevant buildings shall be developed and verified carefully, considering all the different configurations, operational modes and load combinations.

This contribution explains in detail the set of finite elements numerical models and results presented in [4] about the MITICA assembly integrated analyses. The model takes into account properly constraints to ground and surrounding buildings, to study and verify the static and seismic response of the whole assembly.

The load cases are defined and the numerical analyses described. Load definition and analyses have been performed considering the requirements of both the ASME [5, 6] and the National Standard N.T.C. 2008 [7] for the seismic verification of structures subject to design response spectra.

The obtained results are finally shown in detail and discussed, also comparing some different design options for design optimization.

Section 6.2 is dedicated to the description of the geometry of the different parts of the system such the transmission line, the vessels, and the high voltage bushing and the modelling choices are presented, with respect to the employed numerical tool: ANSYS (Release 13.0).

Section 6.3 is about the modelling of the three bellows elements. The theoretical considerations made to assign the three different design shear stiffness to the bellow devices are here shown and the benchmark tests for validation are reported, as well.

Section 6.4 focuses on the modelling of the supports of the transmission line, with respect to the element choice, the degree of restraint and their assumed position along the transmission line.

6.2. Geometry of the structures and equipment

Transmission line geometry

The following references to the subdivision of the whole transmission line, reported in the numbered scheme below in Figure 6.2.1, will be considered, in order to better define the geometrical properties of the pipes. The same scheme will be used also in section 6.4, to assign the design mass weight at each discrete piece of the pipeline.

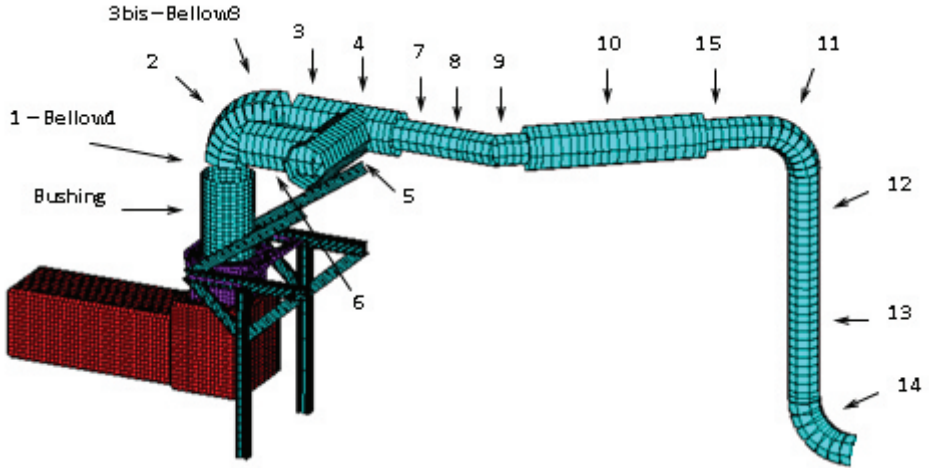

Figure 6.2.1: Schematic subdivision of the transmission line.

In Table 6.2.1 the length of the single pieces of line are reported. The modelling of the transmission line has been extended until the last elbow pipe element, the presence of the remaining pipes being negligible from the point of view of the dynamic analysis of the global model, if they are properly supported. The transmission line is characterized by three different diameters; the thickness of the pipes has been assumed constant equal to 20 mm. The assigned geometry is reported in Table 6.2.2.

Table 6.2.1: Length of the single parts of transmission line as in Figure 6.2.1.

Pipe number	Length [mm]	Pipe number	Length [mm]
1	775	8	1570
2	4773	9	2837
3-bis	1000	10	9282
3	1225	15	2922
4	4485	11	3770
5	6425	12	6621
6	4173	13	5859
7	2710	14	3770

The modelling of the transmission line has been extended until the last elbow pipe element, the presence of the remaining pipes being negligible from the point of view of the dynamic analysis of the global model, if they are properly supported.

The transmission line is characterized by three different diameters; the thickness of the pipes has been assumed constant equal to 20 mm. The assigned geometry is reported in Table 6.2.2.

Table 6.2.2: Section assignment.

Pipe number	**Section ID**
2-3-4-5-6	1
7-8-9 15 - 11-12-13-14	2
10	3

Section 1 comprises parts from 2 to 6 of the whole transmission line (excluding part 3-bis, which stand for bellow 3, which will be illustrated in section 6.3. Section 2 comprises two continuous parts of the transmission line: from 7 to 9 and from 15 to 14. Finally, section 3 is assigned to pipe 10. The section of the bushing is characterized by the parameters reported in the last column of Table 6.2.3, where *I* is the moment of inertia and *J* the torsion constant of the circular sections.

Table 6.2.3: Geometry of transmission line sections.

	Section 1	*Section 2*	*Section 3*	*Bushing*
External radius [mm]	1236	857	1220	1400
Thickness [mm]	20	20	20	20
Area [mm^2]	153944	106354	151935	174673
I [mm^4]	$0.116 \cdot 10^{12}$	$0.381 \cdot 10^{11}$	$0.111 \cdot 10^{12}$	$0.169 \cdot 10^{12}$
J [mm^4]	$0.231 \cdot 10^{12}$	$0.762 \cdot 10^{11}$	$0.222 \cdot 10^{12}$	$0.169 \cdot 10^{12}$

For the numerical analyses the model has been discretized through BEAM188 elements.

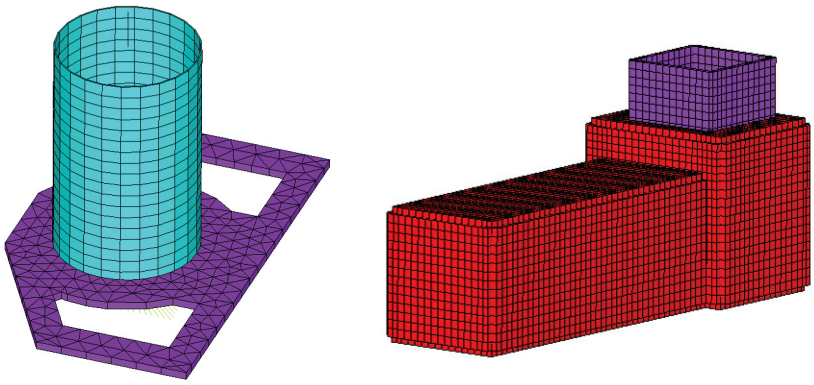

(a) (b)

Figure 6.2.2: Bushing support slab model (a); Vessel and Source model (b).

Bushing support geometry

The frame structure supporting the bushing has been implemented according to the geometry and the structural considerations that lead to an optimization with respect to the stress and displacement field under the seismic load case. In the global model the bushing support frame has been meshed with BEAM188 elements.

The bushing support slab, instead, has been modelled with SHELL281 elements, which are assigned thickness 150 mm (Figure 6.2.2a).

Beam line vessel and beam source vessel

The beam line and the beam source vessels geometry have following dimensions respectively: 3550 x 3454 x 9550 mm and 4550 x 4495 x 3765 mm. For sake of simplicity the connection element of the Vessel to the Source has been assimilated to the first one and assigned its cross-sectional area and properties. The Dome has dimensions: 2800 x 1820 x 2800 mm (Figure 6.2.2b).

The beam line vessel and the beam source vessel, as well as the Dome, have been meshed with SHELL281 elements. The Dome and also the high voltage bushing support slab have been endowed of one series of in-plane rigid links each, in addition, as illustrated in Figure 6.2.3a, in order to guarantee a sufficient rigid behaviour of these components.

The beam line and the beam source vessels have been assigned thickness 147 mm, i.e. an average equivalent value, not considering the stiffening bars on the surface of the two components; the Dome has thickness 50 mm. The use of an equivalent thickness guarantees that the real stiffness, coming from the real

thickness of the vessel (20 mm) plus the stiffening ribs, is actually applied to the model.

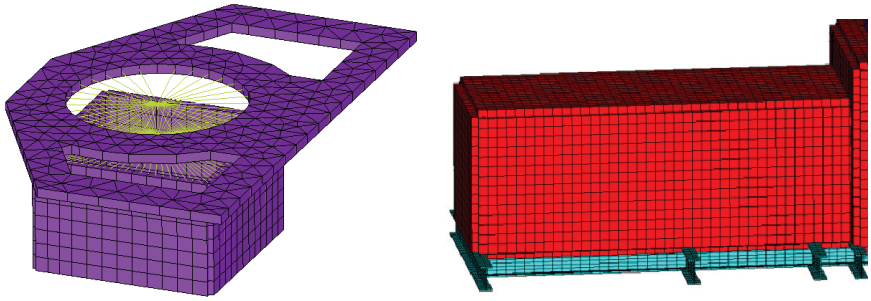

(a) (b)

Figure 6.2.3: Rigid links detail (a); Vessel support beams model (b).

The support structure for the beam line vessel consists in BEAM188 elements with the IPE600 cross-section of properties reported in Table 6.2.4.

Table 6.2.4: Geometry of the support beam of the Vessel.

h [mm]	600
b [mm]	300
Area [mm^2]	15600
I_{11} [mm^4]	$9.208 \cdot 10^8$
I_{22} [mm^4]	$3.387 \cdot 10^7$
J [mm^4]	$1.330 \cdot 10^6$

Truss Structure

For the truss structure reinforcing the line against horizontal displacements, when outside from the MITICA building, elements LINK180 are adopted; they are uniaxial tension-compression elements, which do not consider bending transmission, as required for pin-jointed structures (Figure 6.2.4).

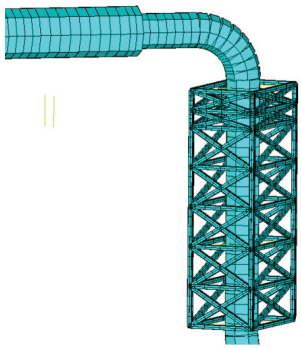

Figure 6.2.4: Truss structure model.

The cross-sectional area of these elements has been set to 3900 mm^2.

6.3. Shear stiffness of bellows

Three bellows are placed in the transmission line. The lengths are reported in Table 6.3.1.

Table 6.3.1: Length of the bellows.

Bellow number	Length [mm]
1	775
2	550
3	1000

Bellow 1 and 3 are localized along the transmission line as reported in Figure 6.2.1; bellow 2 is between the Dome and the High Voltage Bushing.

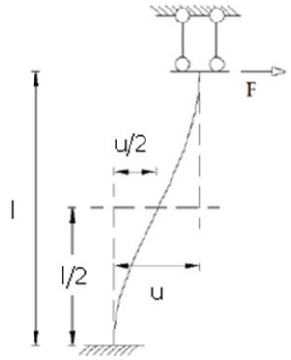

Figure 6.3.1: Static scheme for bellows.

The design shear stiffness of 1.5-3-4.5 t/mm has been assigned to the bellow elements, according to the static scheme in Figure 6.3.1, describing the bending of a beam restrained as it is the bellow along the transmission line (i.e. preventing axial displacement and rotations), under a shear force F :

$$u = \frac{Fl^3}{12\,EI} \qquad (6.3.1)$$

where u is the maximum displacement at the end free to translate, l is length of the beam, F the external shear force and EI the bending stiffness.

Imposing the bellow to resist 1.5-3-4.5 t/mm against shear forces, requires to assign a proper moment of inertia I to the bellow section, according to (6.3.1), provided the material is known (stainless steel 316L, E = 193000 MPa).

At the same time, for the axial stiffness EA of the bellow, with A resistant cross-section area, the axial stiffness of the pipes contiguous to the bellows is assigned.

The finite elements chosen for meshing the bellows are BEAM4; this kind of beam requires the definition of A and I, not necessarily imposing the geometry of the section, which is not known in fact.

These are the imposed quantities for the three bellows, for each design shear stiffness:

Table 6.3.2: Parameters for shear stiffness assignment of each bellow configuration

Bellow number	1	2	3
Area [mm^2]	174673	153944	153944
	Shear stiffness = 1.5t/mm		
$I_{11} = I_{22}$ [mm^4]	2770741	990328	5952383
	Shear stiffness = 3t/mm		
$I_{11} = I_{22}$ [mm^4]	5541482	1980655	11904765
	Shear stiffness = 4.5t/mm		
$I_{11} = I_{22}$ [mm^4]	8312223	2970983	17857148

In Figure 6.3.2 results in terms of transversal displacements of one of the benchmark tests, held to model the behaviour of the bellows under shear forces, are reported; nodal displacements of bellow 3 are here shown, under a shear force of 1.5 t; the maximum displacement, compatibly with the restraints, is on top and equal to 1 mm, as required. Similar tests have been made for the other configurations.

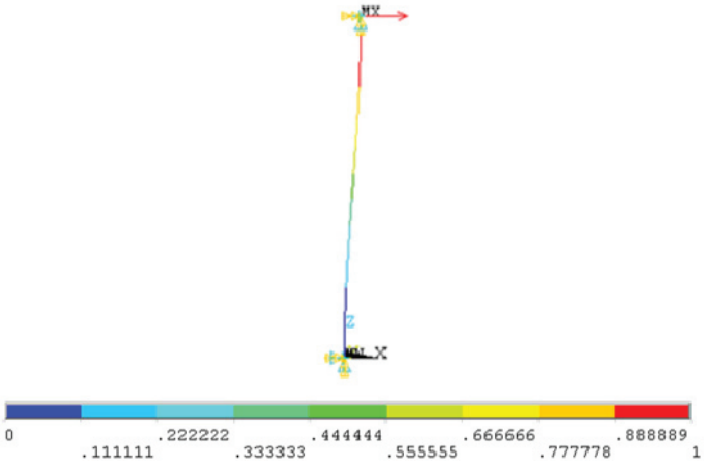

Figure 6.3.2: Displacements for bellow 3 under a shear force of 1.5 t [mm].

6.4. Transmission line supports modelling

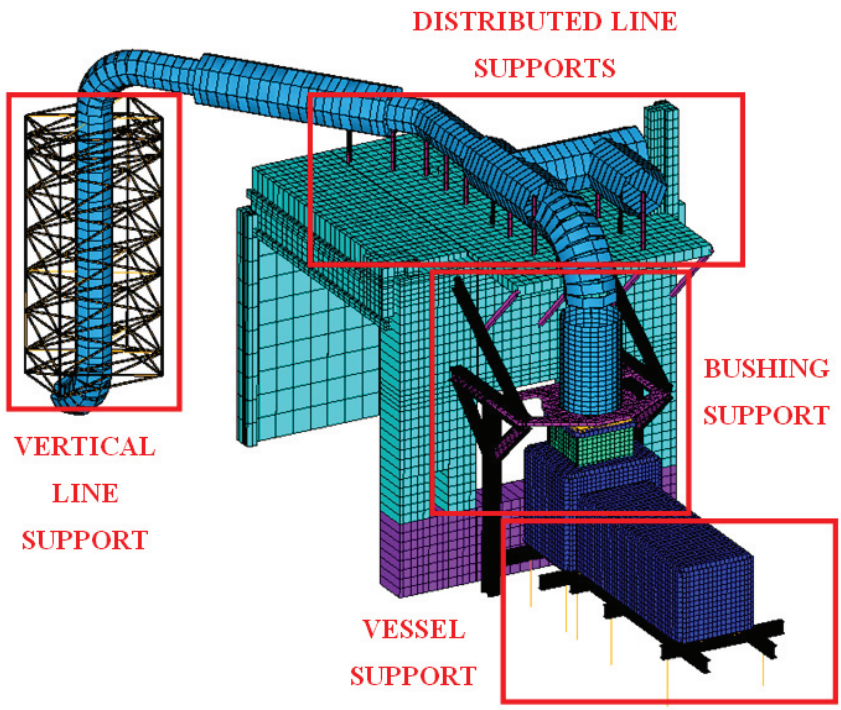

Figure 6.4.1: Supporting system.

Support devices constraint in several ways the pipeline to the ground and to the MITICA building. They can fix all the degrees of freedom (displacements and rotations) or partially restrain the model at the points of interest.
Four different supporting systems can be identified along the transmission line, as shown in Figure 6.4.1, and they are described in the following paragraphs.

Beam line and beam source vessels supports

The beam line and the beam source vessels are supported by a frame made of an IPE shape section as previously described in paragraph 1.3 and showed in Figure 6.4.2a. The support frame is restrained to the ground with un-deformable beams, modelled with rigid links MPC184, so that, when the seismic load case occurs, they can totally transmit the seismic acceleration to the IPE beams, without contributing with local displacements to the global vessel's displacements.

The support frame to the beam line vessel and the beam source vessel is modelled with BEAM188 elements of assigned section. The density of the support can be neglected in the analysis, in order to consider only the beam line vessel and the beam source vessel modes in the natural frequency analyses.

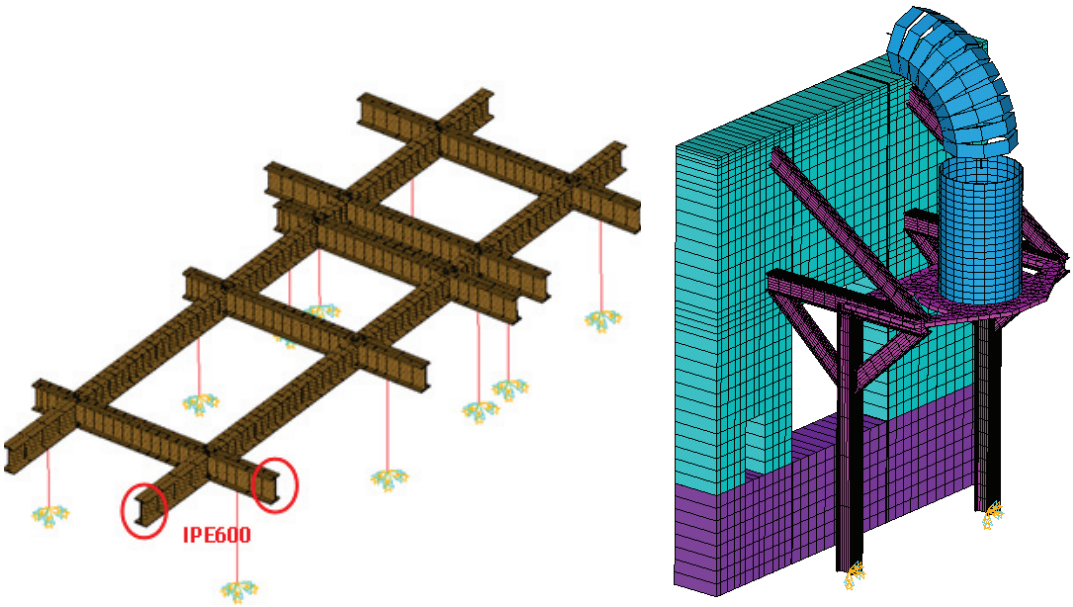

(a) (b)

Figure 6.4.2: Beam line and beam source vessel frame. F.E model with elements BEAM188 and rigid beam - MPC184 (a); Bushing support structure. F.E. model with elements SHELL281 for the slab and monolithic wall, BEAM188 for the bushing support (b).

High voltage bushing supports

This sub-structure is addressed to support the bushing and the attached parts of the transmission line. The high voltage bushing is one of the most heavy and sensitive device of the whole pipeline. Its weight is entirely transmitted to the support slab and the support frame structure, which enable to transfer the load finally to the ground and to the vertical monolithic wall of the surrounding building.
The bushing support structure has been constrained to the ground at the two columns ends and to the wall of the MITICA. Figure 6.4.2b shows more in detail the support structure in relations to the high voltage bushing, bellows and the first elbow of the transmission line.

Transmission line supports

The transmission line has been subdivided in four parts named: TL2, HVD, HV and TL3. The horizontal part of the transmission line is supposed to be constrained to the top floor of MITICA with a system of restraints, which have been modelled with BEAM188 elements of suitable cross-section area ad stiffness, in order to obtain a rigid behaviour in all directions and to perform, this way, the most severe transmission of the dynamic load to the structure.

Beams highlighted with red boxes (Figure 6.4.3) are “end-realeased”.

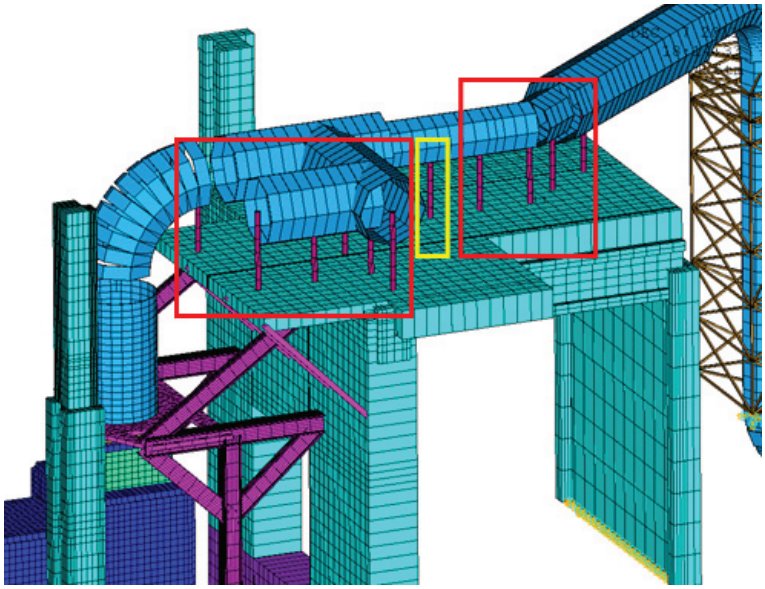

Figure 6.4.3: Detail of the slider beam constraint device along the transmission line.

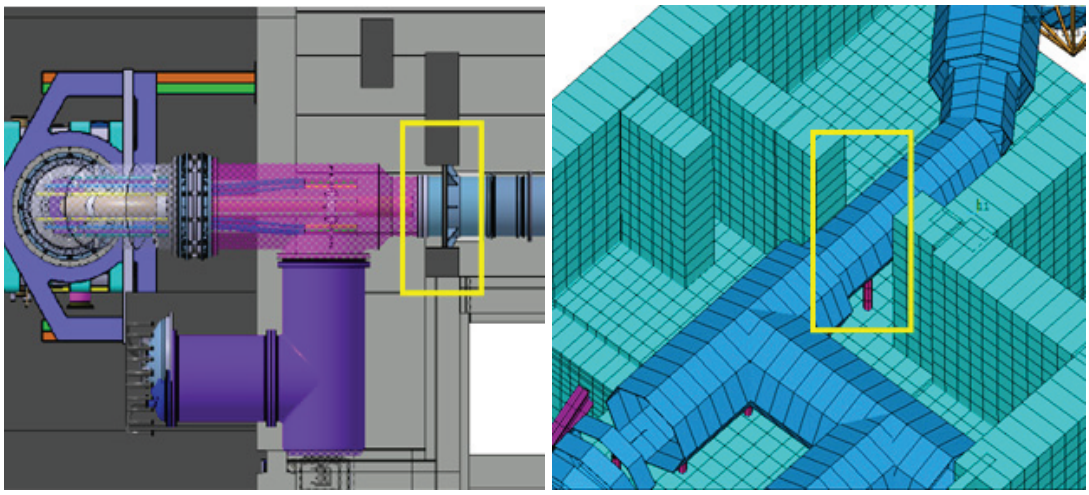

(a) (b)

Figure 6.4.4: CAD drawing of transmission line fixing device detail (a); Detail of the axial constraint device along the transmission line (b).

Traslational displacements along the direction of the pipeline are allowed. All the remaining degrees of freedom are fixed, so that the constraints act as slider elements during the dynamic load, uncoupling the displacements of the line in its longitudinal direction, from the building displacements along the same direction. The support spacing is approximately 2m.

The yellow boxed beam in the same figure is totally restrained both in translational and rotational displacementents, to accomplish the RFX request to simulate an axial costraint after the transmission line, part TL3 (see Figure 6.4.4a-b).

Vertical line support

To support the part of the transmission line located outside the MITICA building, a truss structure has been modelled, which the vertical line is restrained to, at the three points marked with red arrows in Figure 6.4.5. The truss structure is fixed at the base corner nodes.

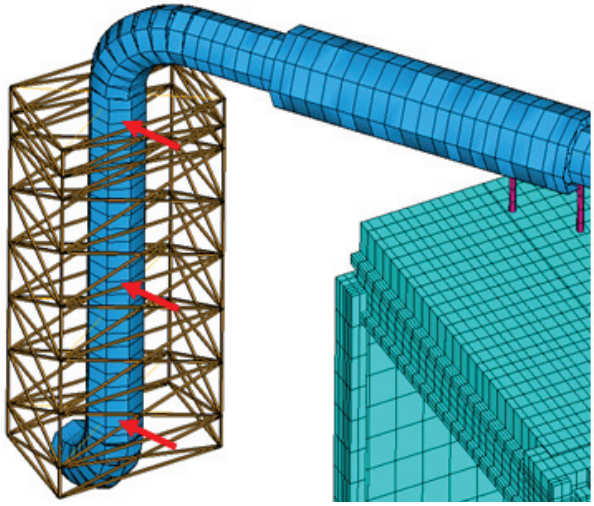

Figure 6.4.5: Vertical line restraints to the truss structure support.

6.5. Load cases on the transmission line

Static loads

The static analysis evaluates the stress and the displacement field on the structure, subject to the gravity loads, also referred to as “dead loads”, both structural and non-structural (e.g. equipment devices), and the pressure load inside the line. The static loads to be combined with the dynamic action of the design earthquake are:

- self-weight of the structural elements given by manufacturer specifications;
- weight of the non-structural mass flowing inside the pipes;
- internal pressure on the pipeline (6bar).

Seismic load case evaluation. Modal and response spectrum analysis

Seismic design and verification is performed through linear combinations of effects, involving permanent and variable actions on the structure. According to the ASME approach, static and dynamic actions combine linearly to give the global design load case combination. The seismic load case is evaluated by means of the modal analysis and subsequent response spectrum analysis.

As regards the modal analysis, 150 eigenvalues are sought, in order to reach over 90% of mass participation factor in all three directions, X, Y and Z. Despite the number of eigenvalue extracted, only few vibrational modes contribute with an important mass participation factor.

With the spectral response analysis is possible to calculate the response of a structure subjected seismic (dynamic) load given as base excitation in almost one of directions (X, Y or Z). The base excitation spectrum is applied as a translational excitation at the base, equally at all fixed degrees of freedom. The excitation may act in any arbitrary direction in the global X-Y-Z system and defined in terms of acceleration. The typical input spectra used for these analyses are the ones provided by N.T.C. 2008 [7] (Figure 6.5.1 and Figure 6.5.2).

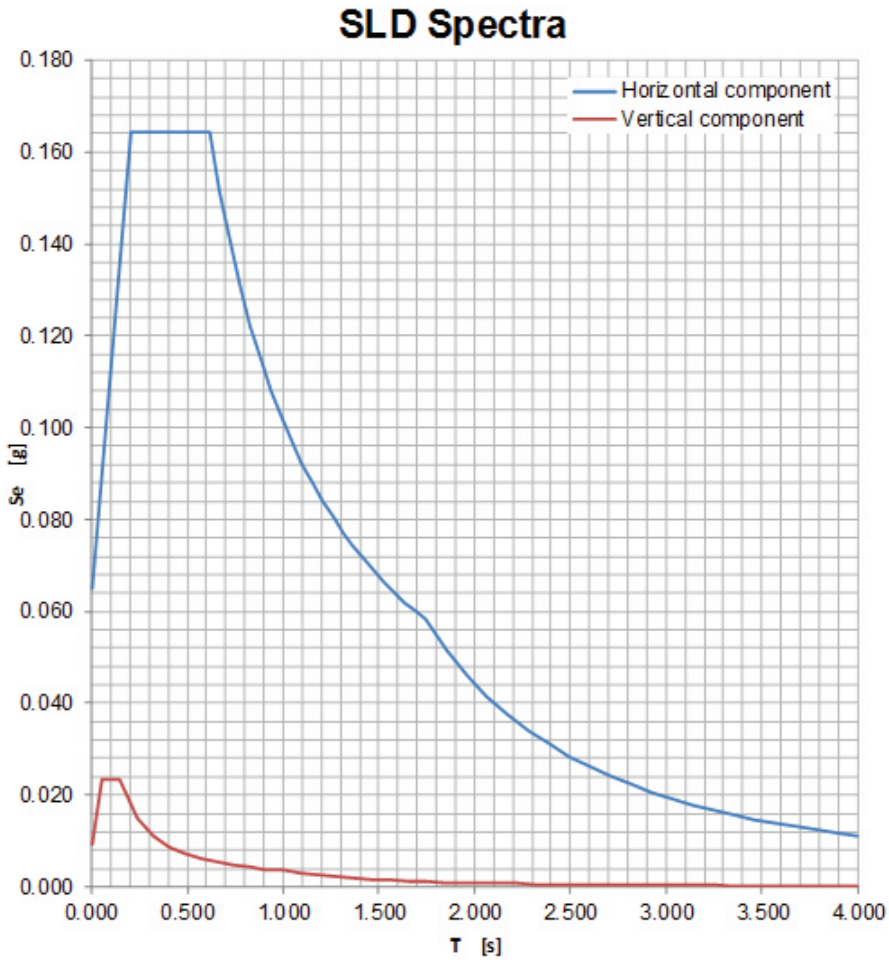

Figure 6.5.1: Damage limit state as provided by [7] for the MITICA site.

The results of a spectral analysis are given as envelopes of maximum values of nodal displacements, element stresses, and element strains, recovered reactions at

constrained nodes and elastic forces at unconstrained nodes. The maximum response values are calculated by combining the maximum response of all modes included in the analysis. Contributions from individual modes are available as well as the combined maximum values.

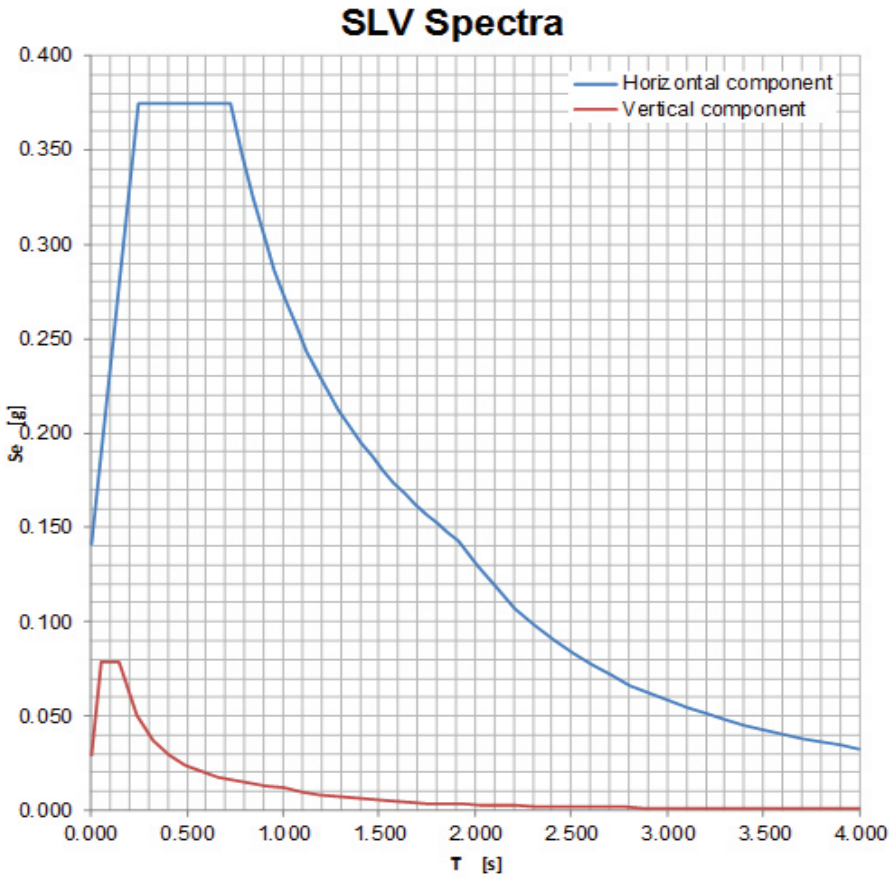

Figure 6.5.2: Life safeguard limit state as provided by [7] for the MITICA site.

A single-point response spectrum analysis (SPRS) has been applied. The solver is based on the mode superposition technique and, basically, studies the structure when excited by a spectrum of known direction and frequency components, acting uniformly on all supports.

The damping of the structure is taken into account by setting the structural damping ratio to 0.05 (5%). This damping ratio is independent from Rayleigh damping, material damping and modal damping.

The combination of modes is made applying the CQC method. The total mode response is given by:

$$R_a = \left(\sum_{i=1}^{N} \sum_{j=1}^{N} \varepsilon_{ij} R_i R_j \right)^{1/2} \qquad \textbf{(6.5.1)}$$

where:

- R_a = total modal response
- N = total number of expanded modes
- ε_{ij}= coupling coefficient (the value of ε_{ij} = 0.0 implies modes i and j are independent and approaches 1.0 as the dependency increases)
- $R_i = A_i\Psi_i$ = modal response in the i-th mode
- $R_j = A_j\Psi_j$ = modal response in the j-th mode
- A_i = mode coefficient for the i-th mode
- A_j = mode coefficient for the j-th mode
- Ψ_i = the i-th mode shape
- Ψ_j = the j-th mode shape

Ψ_i and Ψ_j may be the degree of freedom response, reactions, or stresses.

Finally, the N.T.C. 2008 [7] provides the seismic load case combinations that take into account of the seismic loads adding then the static loads:

- **FOR A SEISMIC LOAD ON X DIRECTION (LOAD CASE 1) :**

$$1.0\ E_X + 0.3E_Y + 0.3\ E_Z + G_1 + G_2 \qquad \textbf{(6.5.2)}$$

- **FOR A SEISMIC LOAD ON Y DIRECTION (LOAD CASE 2) :**

$$0.3E_X + 1.0E_Y + 0.3\ E_Z + G_1 + G_2 \qquad \textbf{(6.5.3)}$$

- **FOR A SEISMIC LOAD ON Z DIRECTION (LOAD CASE 3) :**

$$0.3E_X + 0.3E_Y + 1.0E_Z + G_1 + G_2 \qquad \textbf{(6.5.4)}$$

where G_1 stands for the load of the structural Mass, G_2 for the load of the non-structural mass (equipment), E_Y, E_X, E_Z for the seismic action along X, Y and Z directions, respectively.

6.6. Analyses overview

The reference system for the model is shown in the following:

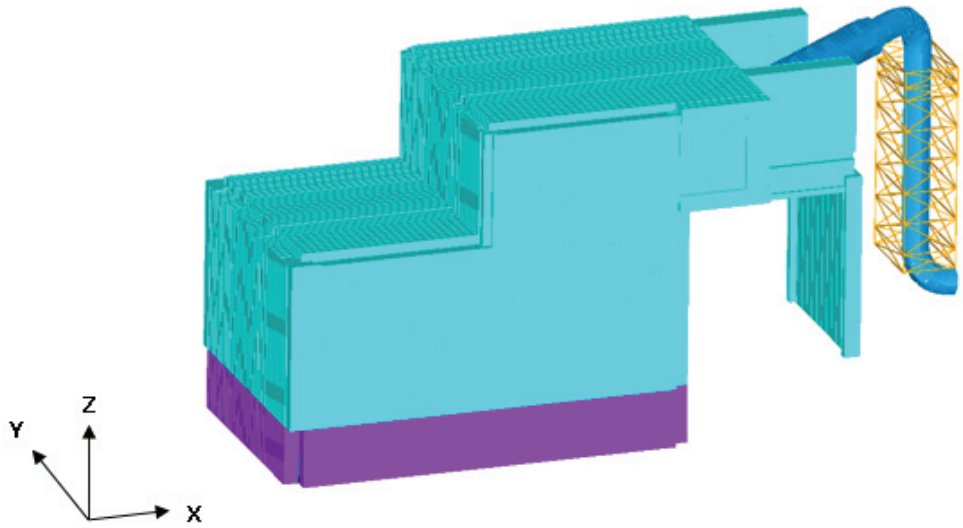

Figure 6.6.1: Global Reference System adopted for the model.

In the following a brief description of the numerical analyses is given. The most relevant numerical results are reported for each kind of analysis; in particular three configurations have been studied, due to the different characterization of the transverse stiffness of bellows.

Table 6.6.1: Configurations studied.

Configuration	Bellows shear stiffness [t/mm]
1	1.5
2	3.0
3	4.5

A further configuration (configuration 4) has been taken into account, considering set 1 (bellows with 1.5 t/mm shear stiffness) and no constraint point along the horizontal part of the line (see Figure 6.4.4), so that the line is free to slide along the longitudinal direction (X direction of the model), and only the outer truss structure is meant to restrain the transmission line.

Displacement results summary

Table 6.6.2 summarizes the total displacements D_{XYZ} [mm] for the global model (transmission line and components) and for the reduced model (bushing-bellows system), for each configuration of bellows (1, 2, 3, 4) and each seismic loading direction (X, Y, Z) or seismic combination. The red values are the highest and correspond to configuration 4, as expected, for any seismic combination. The green values are the best results in terms of displacements, for each seismic combination.

Table 6.6.2: Displacement field (D_{XYZ}) [mm]. Results summary for SLV Limit State.

	Seismic load direction	Configuration 1 (1.5 t/mm)	Configuration 2 (3 t/mm)	Configuration 3 (4.5 t/mm)	Configuration 4 (1.5 t/mm – free sliding)
Whole transmission line	X	6.094	6.125	6.097	24.384
	Y	5.871	5.847	5.801	8.770
	Z	3.773	3.774	3.756	6.947
Bushing - bellows	X	4.336	3.532	3.491	23.823
	Y	4.182	3.601	3.656	5.928
	Z	1.809	1.498	1.522	5.556

Finally , Table 6.6.3 compares static results (gravity loads + pressure loads), again for each configuration of bellows and each seismic loading direction. The red values are the worst, the green ones, instead, the best both for the global model and the model limited to the bushing-bellows system.

Table 6.6.3: Displacement field (D_{XYZ}) [mm]. Results summary for static loads.

	Configuration 1 (1.5 t/mm)	Configuration 2 (3 t/mm)	Configuration 3 (4.5 t/mm)	Configuration 4 (1.5 t/mm – free sliding)
Whole transmission line	1.986	1.988	1.989	3.857
Bushing - bellows	1.024	1.007	0.999	3.857

With reference to Table 6.6.2 and Table 6.6.3, the contour maps of most relevant results (the highest for the configuration 4 and the best results for the other configurations) in terms of displacements are following reported.

Static analysis and Results

Configuration 1

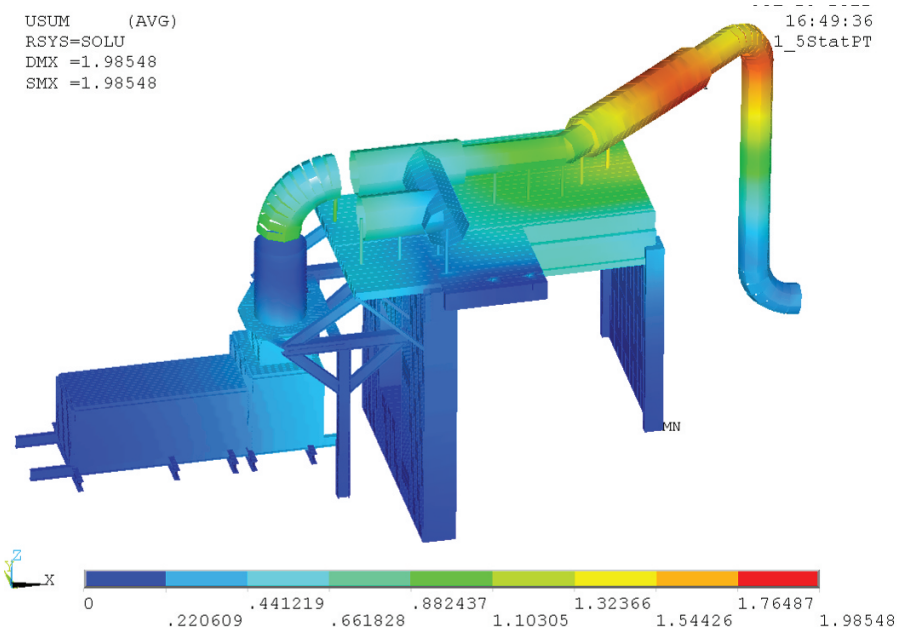

Figure 6.6.2: Displacement Results (D_{XYZ}) for gravity + pressure loads [mm].

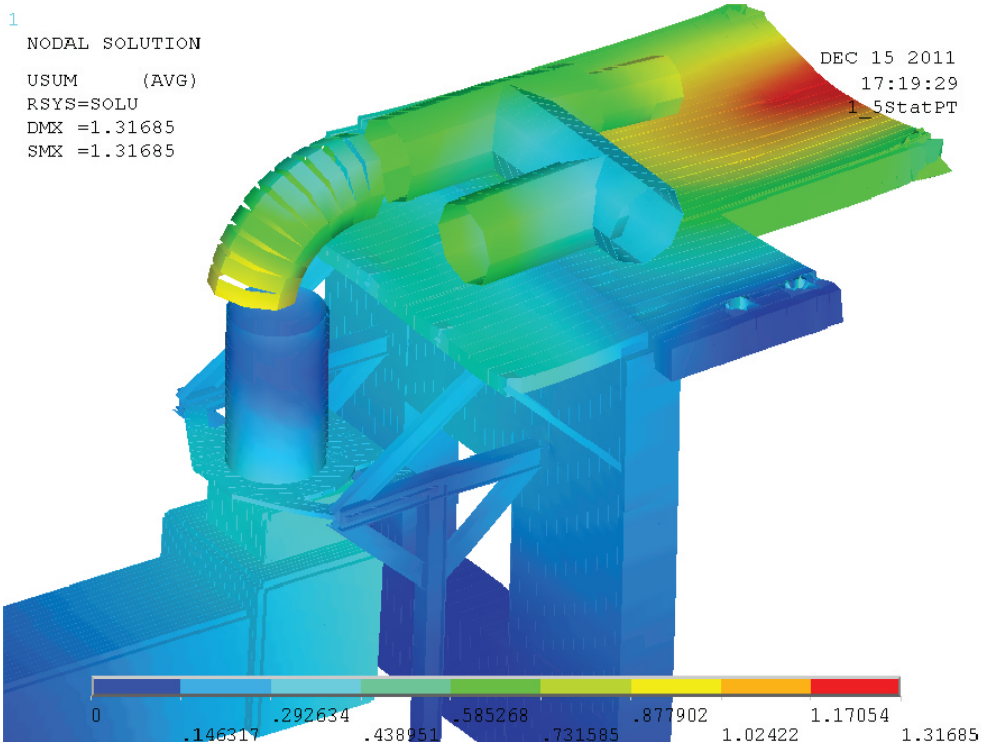

Figure 6.6.3: Displacement Results (D_{XYZ}) for gravity + pressure loads [mm]. Detail of Bushing, TL3, and HVD.

Configuration 4

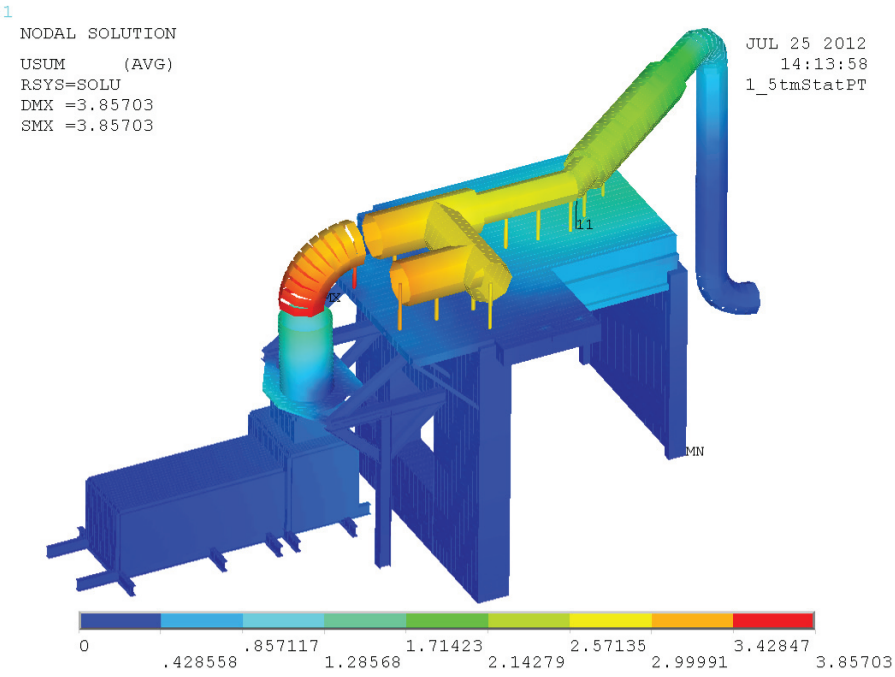

Figure 6.6.4: Displacement Results (D_{XYZ}) for gravity + pressure loads [mm].

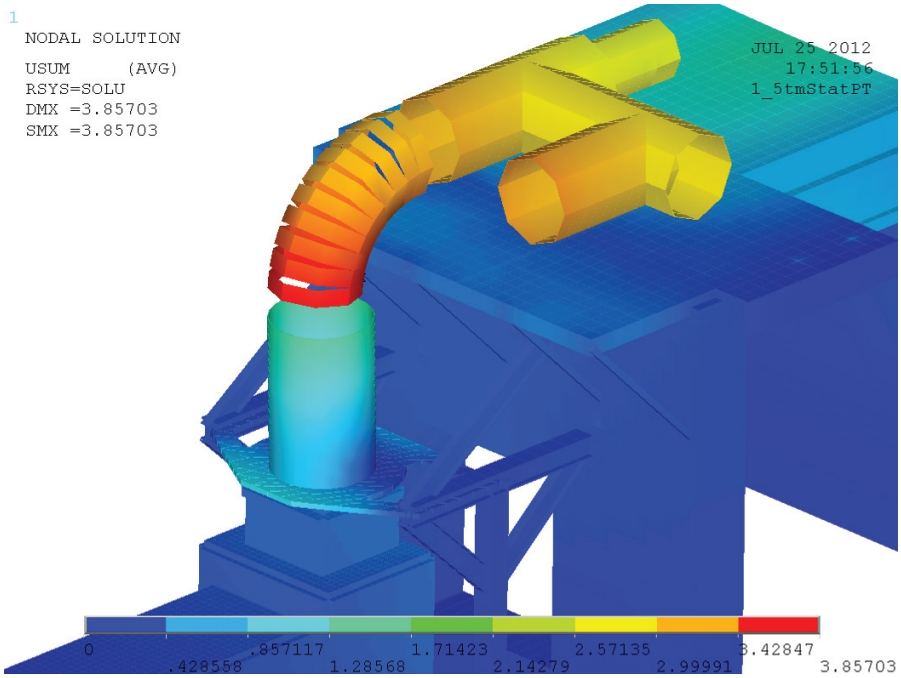

Figure 6.6.5: Displacement Results (D_{XYZ}) for gravity + pressure loads [mm]. Detail of Bushing, TL3, and HVD.

Modal analysis and Results

Numerical results are shown below for each configuration, in terms of natural frequencies of the global model. Participation factors must be intended as percentage fraction of total mass. The first 4 values in descending order of magnitude, with respect to the mass participation, are reported, for X and Y direction. The modal shapes corresponding to the 3 most relevant frequencies (highlighted in yellow in the table) are then plotted.

Configuration 1

Table 6.6.4: First four modal results (natural frequencies and relative participation factors)

X - Direction			Y - Direction		
Mode No.	Frequency [Hz]	Mass Participation Factor [%]	Mode No.	Frequency [Hz]	Mass Participation Factor [%]
15	17.4929	12.65	4	10.4827	44.25
14	16.3751	11.28	6	11.5722	10.40

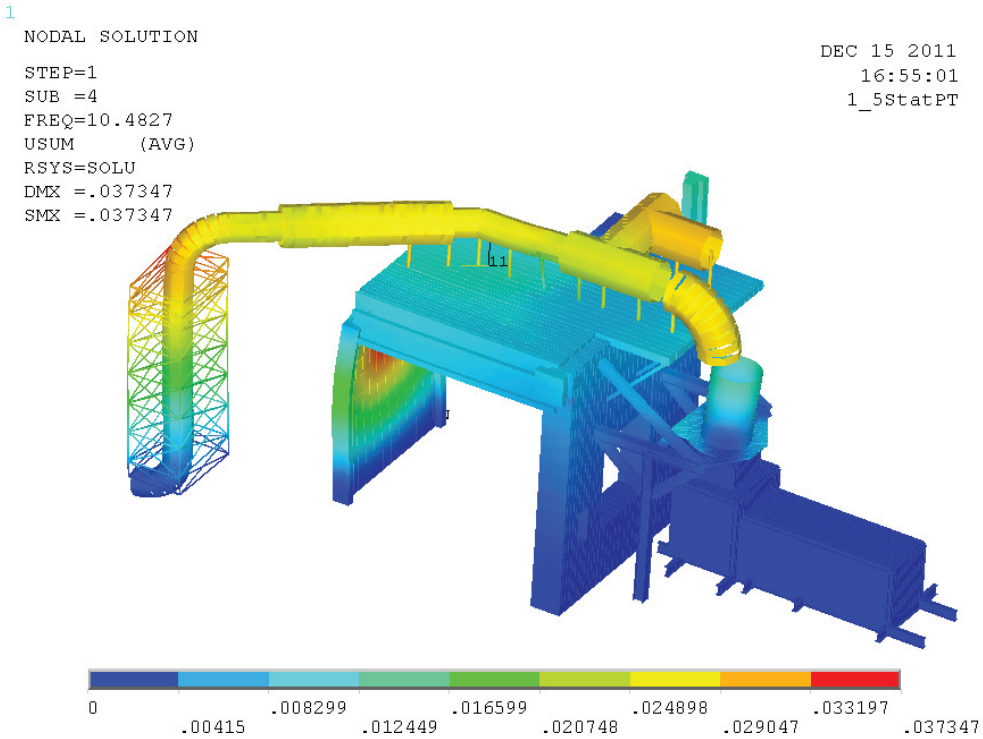

Figure 6.6.6: Vibrational mode corresponding to 10.4827 Hz (Y).

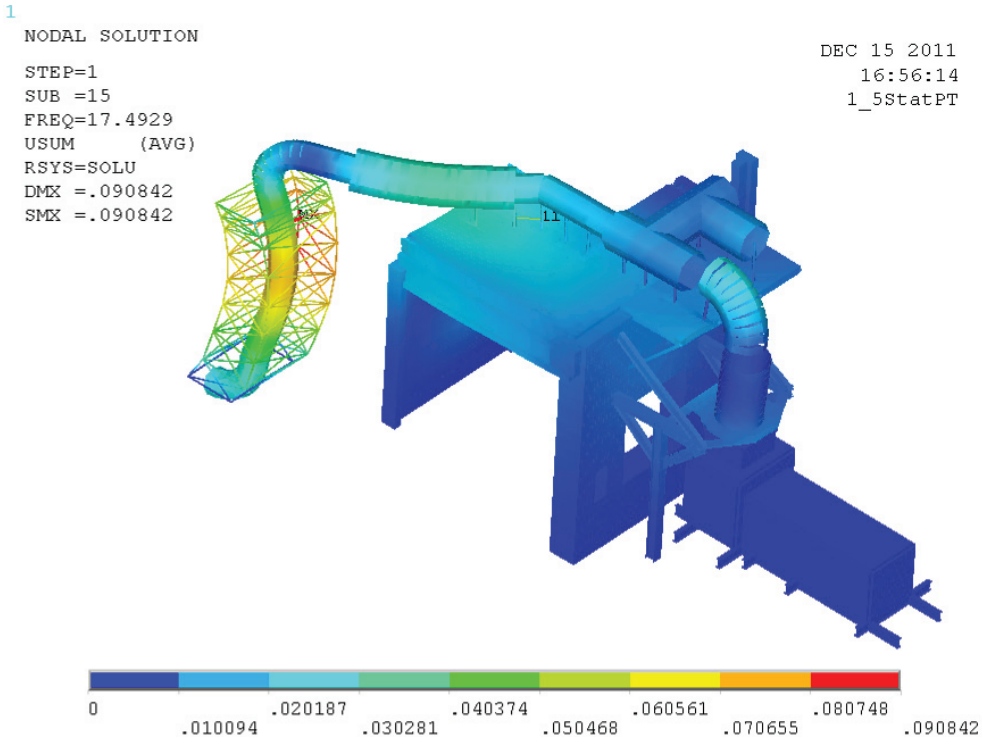

Figure 6.6.7: Vibrational mode corresponding to 17.4929 Hz (X).

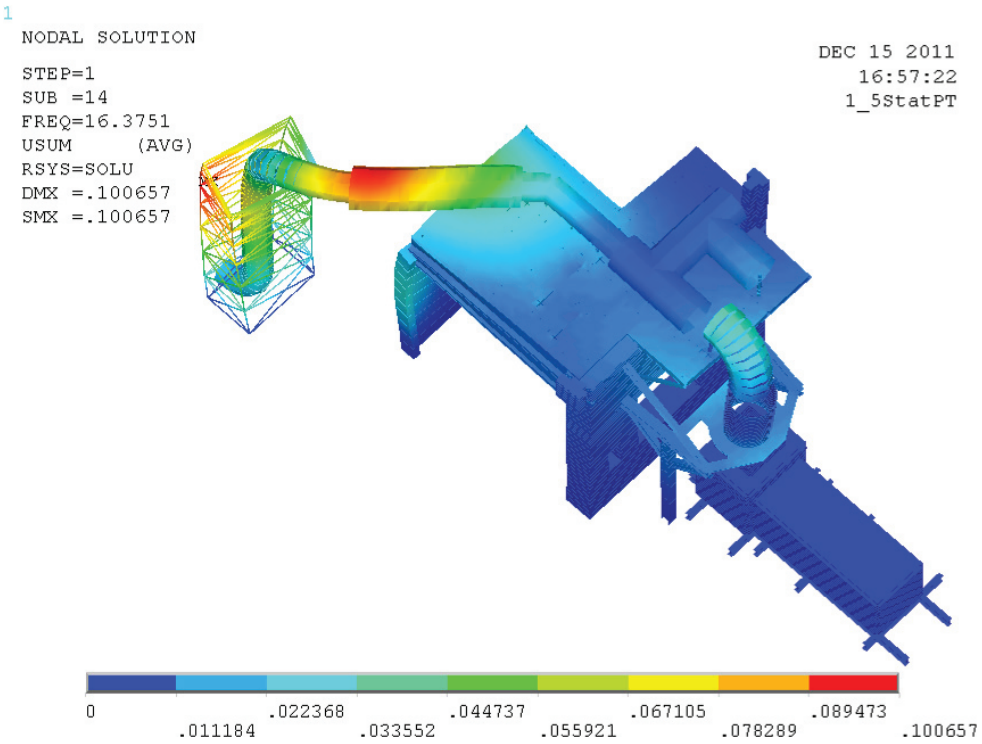

Figure 6.6.8: Vibrational mode corresponding to 16.3751 Hz (X).

Configuration 4

Table 6.6.5: First four modal results (natural frequencies and relative participation factors).

X - Direction			Y - Direction		
Mode No.	Frequency [Hz]	Mass Participation Factor [%]	Mode No.	Frequency [Hz]	Mass Participation Factor [%]
15	17.3129	18.71	5	10.6581	50.13
12	14.6731	12.58	6	10.9493	8.90

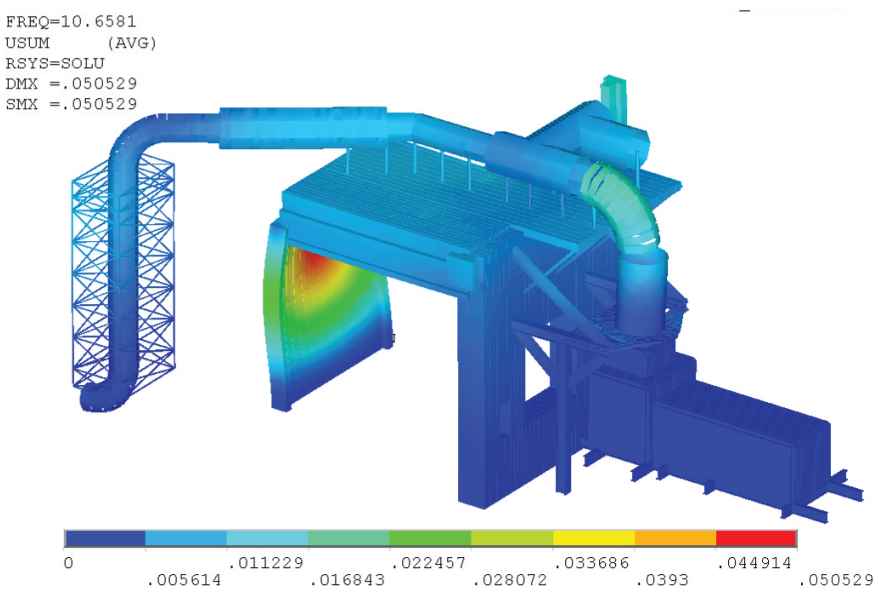

Figure 6.6.9: Vibrational mode corresponding to 10.6581 Hz (Y).

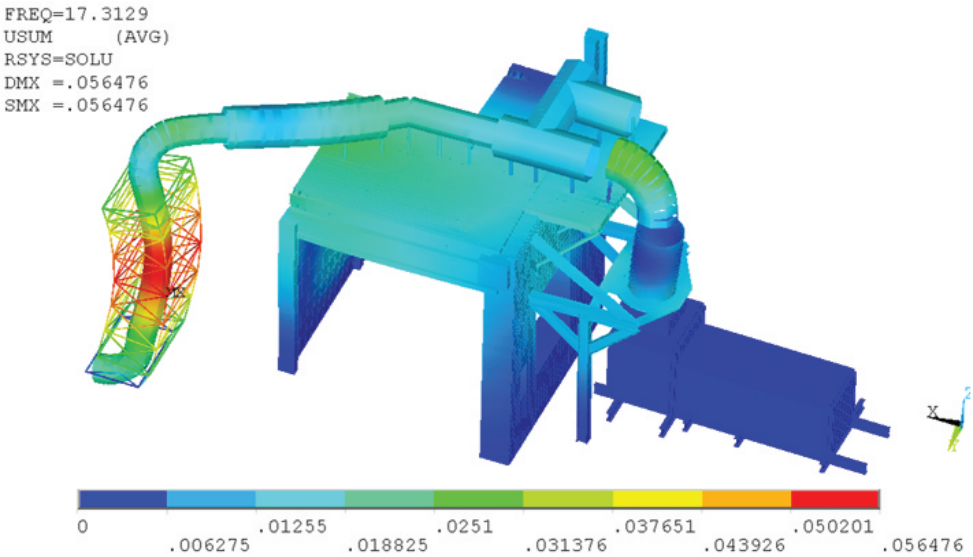

Figure 6.6.10: Vibrational mode corresponding to 17.3129 Hz (X).

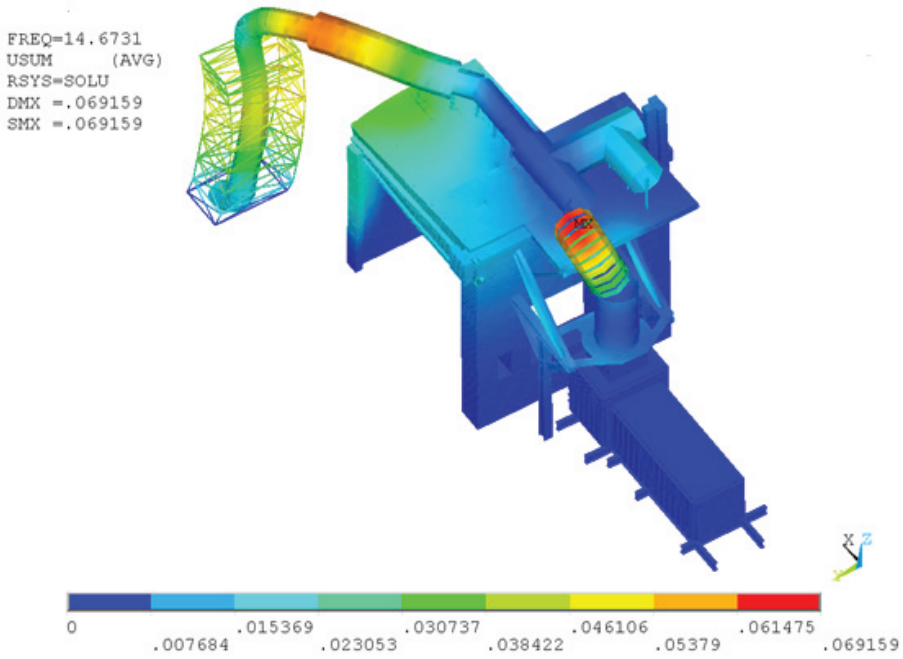

Figure 6.6.11: Vibrational mode corresponding to 14.6731 Hz (X).

Results from response spectrum analyses

Configuration 1

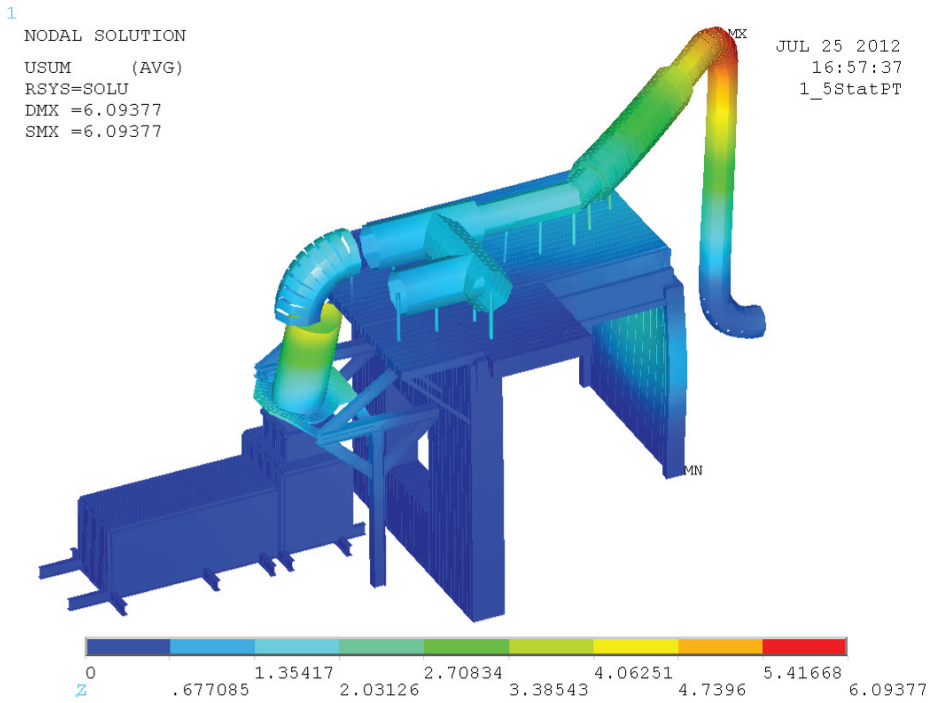

Figure 6.6.12: Displacements (D_{XYZ}) [mm]. Seismic analysis with seismic action along X direction.

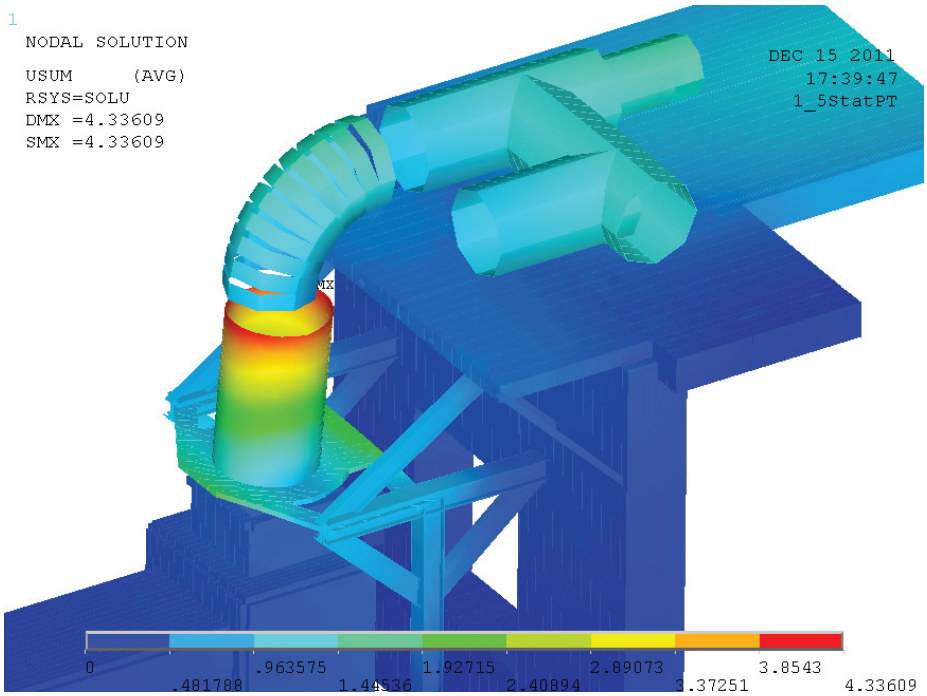

Figure 6.6.13: Displacements (D_{XYZ}) [mm]. Seismic analysis with seismic action along X direction. Detail.

Configuration 2

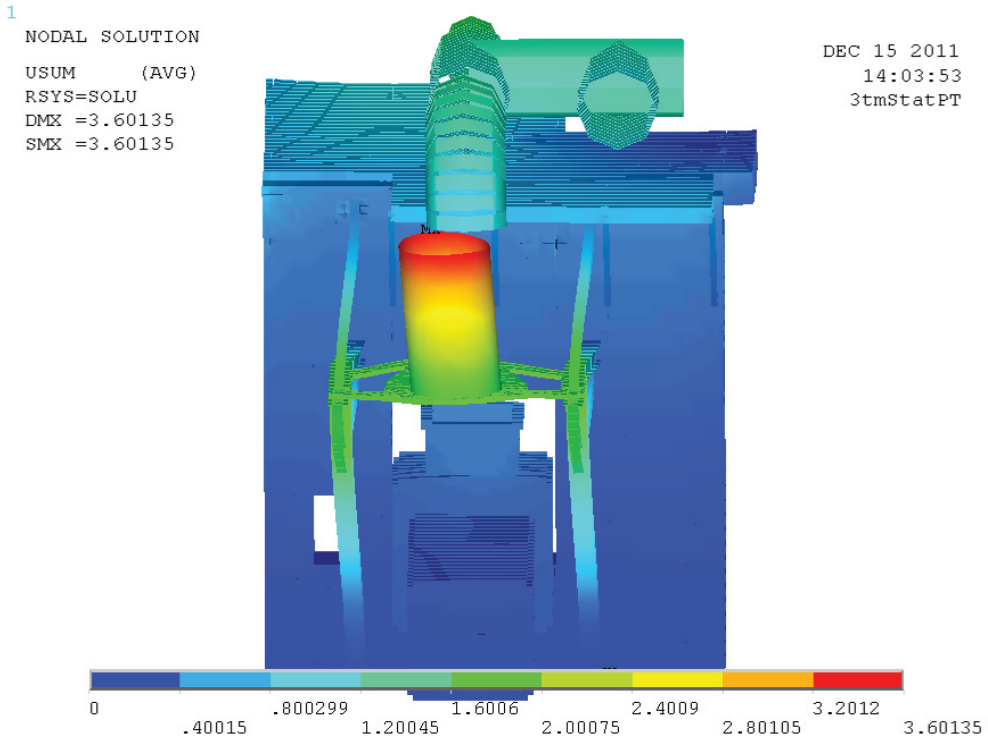

Figure 6.6.14: Displacements (D_{XYZ}) [mm]. Seismic analysis with seismic action along Y direction. Detail.

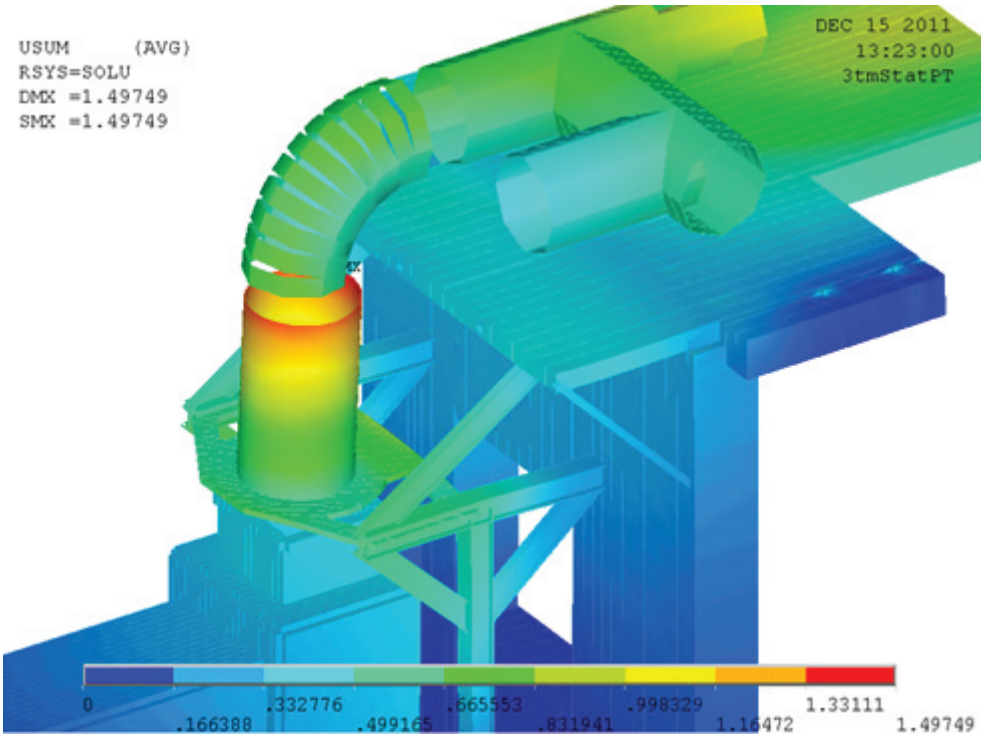

Figure 6.6.15: Displacements (D_{XYZ}) [mm]. Seismic analysis with seismic action along Z direction. Detail.

Configuration 3

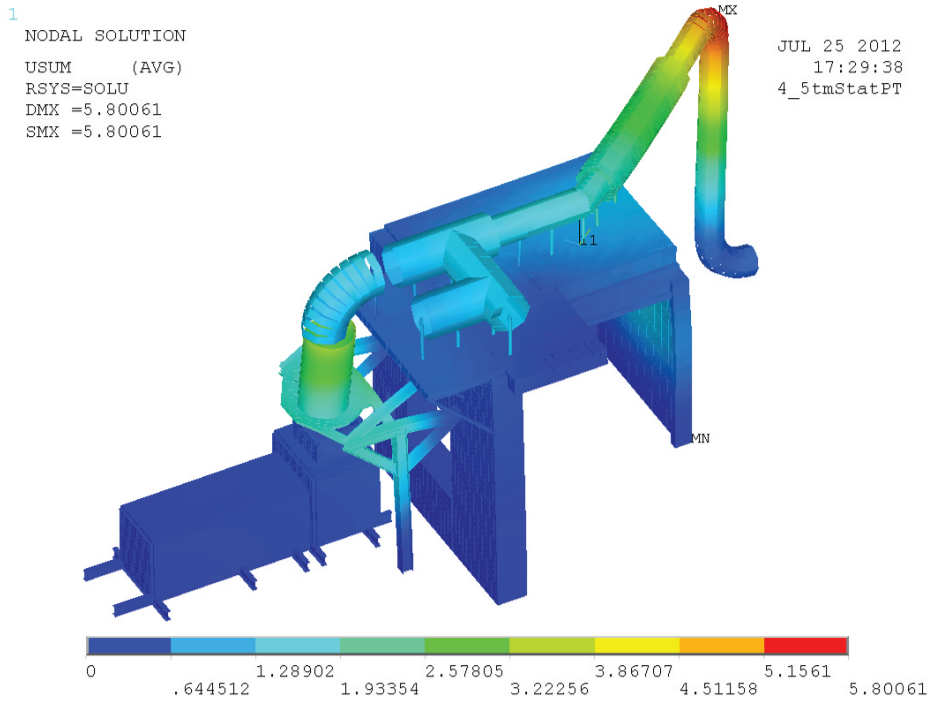

Figure 6.6.16: Displacements (D_{XYZ}) [mm]. Seismic analysis with seismic action along Y direction.

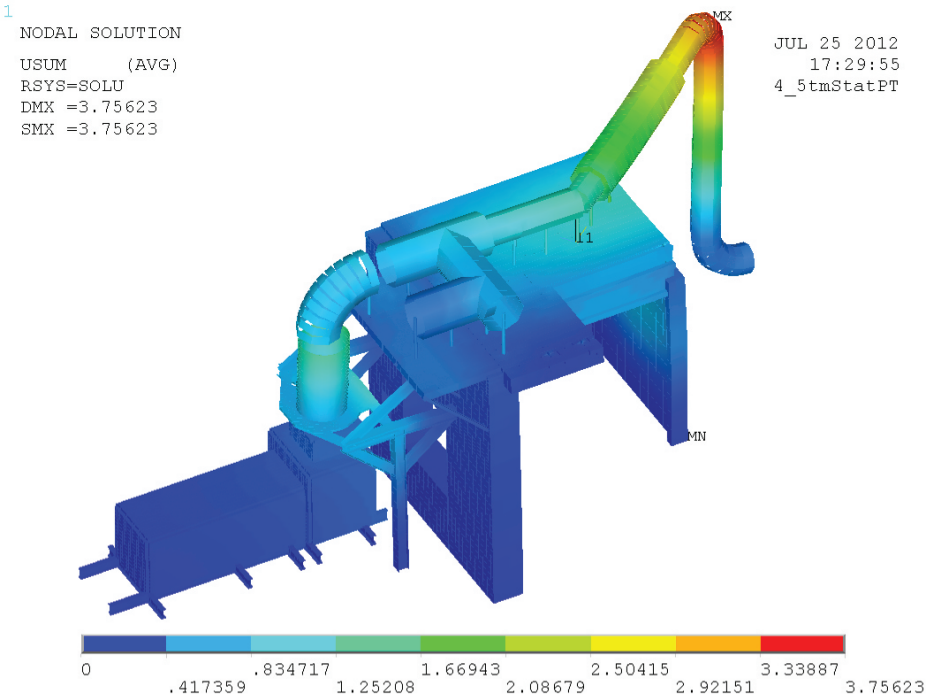

Figure 6.6.17: Displacements (D_{XYZ}) [mm]. Seismic analysis with seismic action along Z direction.

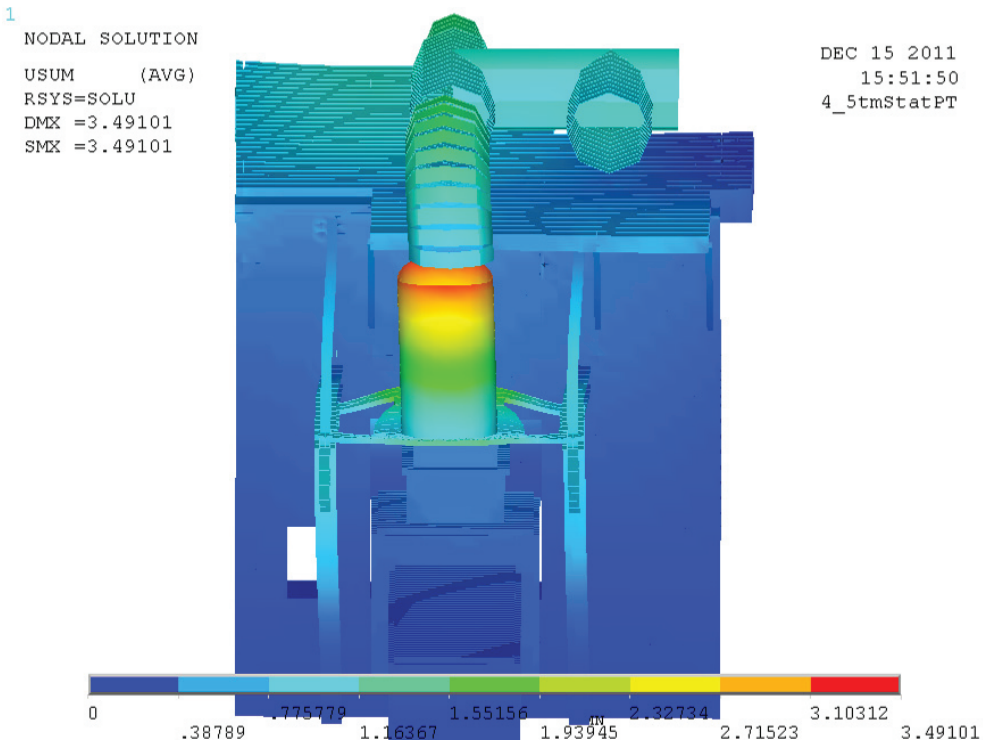

Figure 6.6.18: Displacements (D_{XYZ}) [mm]. Seismic analysis with seismic action along X direction. Detail.

Configuration 4

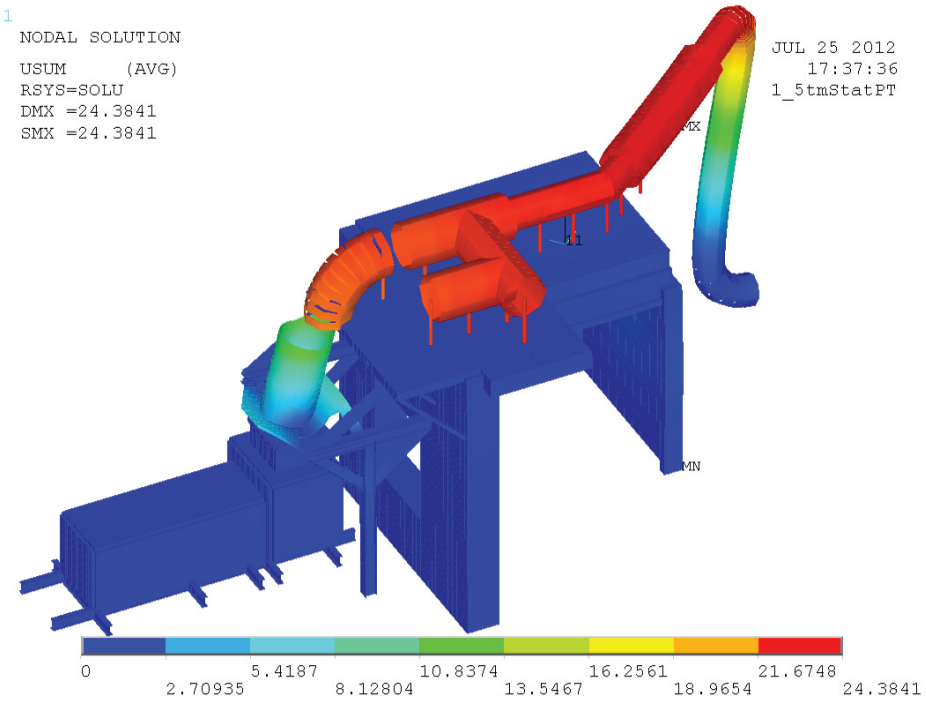

Figure 6.6.19: Displacements (D_{XYZ}) [mm]. Seismic analysis with seismic action along X direction.

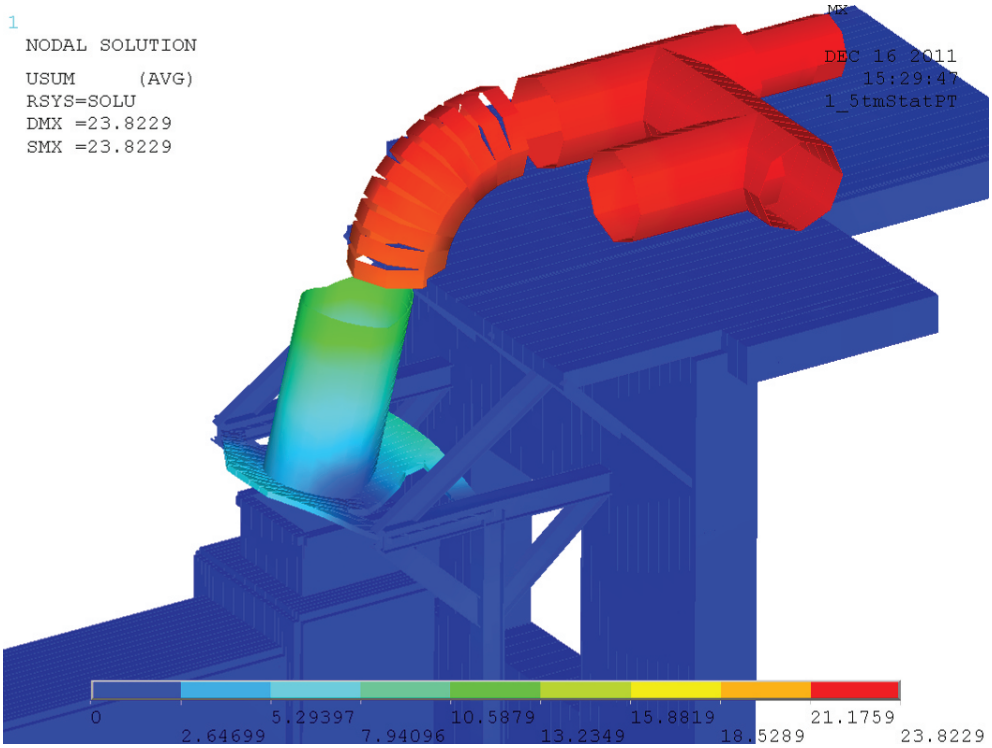

Figure 6.6.20: Displacements (D_{XYZ}) [mm]. Seismic analysis with seismic action along X direction. Detail.

Results Comments

As shown in the table above, static results in terms of displacements (Table 6.6.3) are quite similar for the firsts three configurations. In general configuration 4 returns the maximum displacement, both in static and dynamic analyses, due to a lack of constraining action, along the longitudinal direction of the line. The maximum displacement occurs when the seismic load is in X direction, as main direction.

The difference in terms of maximum displacement in the bellows are negligible for Configurations 2 and 3, in fact they are pretty similar. Configuration 4 returns the maximum displacement result (in X direction), that is higher about four time than the previous configurations results.

Finally, one can observe that, with a lack of constraints along the transmission line (Configuration 4), the behaviour of the transmission line is strongly influenced by the remaining constraint conditions. In particular, the pin-jointed structure out from the MITICA Building, designed to vertically support the line, seems to strongly influence the magnitude of the displacements, under this freedom case, leading to results near to the bellows that are widely beyond the threshold imposed by the design bellows.

6.7. Conclusions

An integrated model of the RFX neutral beam injector with the MITICA building that surrounds and houses all the experimental devices has been done [4]. Furthermore, the MITICA building has the function to prevent the diffusion of the nuclear radiations that represent a danger for health and life, in the proximities of the plant. This critical task is done by the concrete bio-shielding that offer enough protection from the hazardous environment.

Different load configurations applied to the structure and inner devices has been considered in the case of dynamic events, such an earthquake, in order to ensure the reliability of the whole plant, to check the behaviour of the transmission line and beam source and line vessels and design the linkage and support structures for the various parts of equipment that are heavy and delicate.

An accurate integrated modelling of the MITICA system and buildings is mandatory to evaluate correctly the overall structural response and carry out all the necessary verifications. Several static and dynamic FEM analyses have been performed considering both the assembly–disassembly and operational conditions, in order to

allow design optimization. In particular, analyses helped to design the high voltage bushing support structure, finding the best configuration for the truss elements that provides that stress and strain are far below the material limits and a high buckling factor. A suitable combination of sliding supports and bellows with different stiffness values allowed a first design optimization.

The integrated models will be further used for next design verifications, following the on-going activities for design and integration of MITICA components.

Bibliography

1. Rigato, W., et al., *Vessel design and interfaces development for the 1MV ITER Neutral Beam Injector and Test Facility.* Fusion Engineering and Design, 2009. **84**(7): p. 1606-1610.

2. Masiello, A., et al., *The European contribution to the development of the ITER NB injector.* Fusion Engineering and Design, 2011. **86**(6): p. 860-863.

3. Hemsworth, R., et al., *Status of the ITER heating neutral beam system.* Nuclear Fusion, 2009. **49**(4): p. 045006.

4. Mazzucco, G., et al., *Structural analyses and integrated design of the MITICA Injector assembly.* Fusion Engineering and Design, 2013.

5. Code, A.P.V., *Rules for Construction of Pressure Vessels.* Section VIII, Divisions, 1992. **1**.

6. 2010, A., *Boiler and Pressure Vessel Code, section VIII, div. 2.*

7. Infrastrutture, M.d., *Decreto Ministeriale 14 gennaio 2008 - Approvazione delle nuove norme tecniche per le costruzioni* 2008.

7 Complete Bibliography

1. ASME 2010, Boiler and Pressure Vessel Code, section VIII, div. 2.

2. Ahuja, L. and D. Swartzendruber, An improved form of soil-water diffusivity function. Soil Science Society of America Journal, 1972. **36**(1): p. 9-14.

3. America, S.S.S.O., Methods of Soil Analysis. Part 4. Physical Methods. SSSA Book Series, no. 5, 2002.

4. Anderson, E., LAPACK Users' guide. Vol. 9. 1999: Siam.

5. Anderson, E., et al., LAPACK Users' guide. 1995: Society for Industrial and Applied Mathematics Philadelphia.

6. Bachmat, Y. and J. Bear, On the concept and size of a representative elementary volume (REV), in Advances in transport phenomena in porous media. 1987, Springer. p. 3-20.

7. Baggio, P., C. Bonacina, and M. Strada, Trasporto di calore e massa nel calcestruzzo cellulare. Termotecnica, 1993. **47**(12): p. 53-59.

8. Biot, M., General solutions of the equations of elasticity and consolidation for a porous material. J. appl. Mech, 1956. **23**(1): p. 91-96.

9. Biot, M., Theory of stability and consolidation of a porous medium under initial stress. 1963.

10. Biot, M.A., General theory of three-dimensional consolidation. Journal of applied physics, 1941. **12**(2): p. 155-164.

11. Biot, M.A., Consolidation settlement under a rectangular load distribution. Journal of Applied Physics, 1941. **12**(5): p. 426-430.

12. Biot, M.A., Theory of elasticity and consolidation for a porous anisotropic solid. Journal of Applied Physics, 1955. **26**(2): p. 182-185.

13. Biot, M.A., Thermoelasticity and irreversible thermodynamics. Journal of Applied Physics, 1956. **27**(3): p. 240-253.

14. Biot, M.A. and P.G. Willis, The elastic coefficients of the theory of consolidation. J. Appl. Mech., 1957. **24**: p. 594 - 601.

15. Bird, R.B., W.E. Stewart, and E.N. Lightfoot, Transport phenomena. 2007: Wiley. com.

16. Bolzon, G., B. Schrefler, and O. Zienkiewicz, Elastoplastic soil constitutive laws generalized to partially saturated states. Géotechnique, 1996. **46**(2): p. 279-289.

17. Bomberg, M. and C. Shirtliffe, Influence of moisture and moisture gradients on heat transfer through porous building materials. ASTM STP, 1978. **660**: p. 211-233.

18. Brooks, R. and A. Corey, Hydraulic properties of porous media. Hydrology Papers, Colorado State University, Fort Collins, 1964. **3**.

19. Brooks, R. and A. Corey, Hydraulic Properties of Porous Media, of Colorado State University Hydrology Paper, 3. Colorado State University, 1964.

20. Brooks, R.H. and A.T. Corey. Properties of porous media affecting fluid flow. in Journal of the Irrigation and Drainage Division, Proceedings of the American Society of Civil Engineers. 1966.

21. Brutsaert, W., Probability laws for pore-size distributions. Soil Science, 1966. **101**(2): p. 85-92.

22. Burdine, N., Relative permeability calculations from pore size distribution data. Journal of Petroleum Technology, 1953. **5**(3): p. 71-78.

23. Campbell, G.S., A simple method for determining unsaturated conductivity from moisture retention data. Soil Science, 1974. **117**(6): p. 311-314.

24. Carsel, R.F. and R.S. Parrish, Developing joint probability distributions of soil water retention characteristics. Water Resources Research, 1988. **24**(5): p. 755-769.

25. Císlerová, M., J. Šimůnek, and T. Vogel, Changes of steady-state infiltration rates in recurrent ponding infiltration experiments. Journal of Hydrology, 1988. **104**(1): p. 1-16.

26. ASME 2010, Rules for Construction of Pressure Vessels. Section VIII, divisions 2, 1992. **1**.

27. Soilmoisture equipment Corp., The Use of Porous Materials in Devices for Sampling Moisture in the Vadose Zone. Engineering details, 2001. **05/2001**.

28. Intel Corporation, Intel® Math Kernel Library 11.0.3 Reference Manual, 2011

29. de Boer, R., Porous Media: A Survey of Differential Approaches. 1991: Universität-Gesamthochschule-Essen, Fachbereich Bauwesen.

30. E. Anderson, Z.B., C. Bischof, S. Blackford, J. Demmel, J. Dongarra, J. Du Croz, A. Greenbaum, S. Hammarling, A. McKenney, and D. Sorensen, Linear Algebra PACKage (LAPACK). 1991, 1992 and 1998.

31. Fernandez, R. and V. Schrock. Natural convection from cylinders buried in a liquid-saturated porous medium. Proceedings of the 7th International Heat Transfer Conference. 1982.

32. Fernandez, R.T., Natural convection from cylinders buried in porous media, 1972, University of California, Berkeley

33. Fincato, R., 3D nonlinear coupled modelling of geomaterials using the unconventional Subloading Surface approach, 2013.http://paduaresearch.cab.unipd.it/5567/

34. Fleureau, J. and S. Taibi. Water-air permeabilities of unsaturated soils. Proceedings of the first international conference on unsaturated soils (UNSAT'95), Paris (France), 6-8 september 1995. Volume 2. 1995.

35. Gabriele, G., Modellazione numerica di problemi idro- termo- meccanici nei mezzi porosi parzialmente saturi. Department of Civil, Environmental and Architectural Engineering, DICEA, Padua, 2010-2011.

36. Galerkin, B.G., Series solution of some problems of elastic equilibrium of rods and plates. Vestn. Inzh. Tekh, 1915. **19**: p. 897-908.

37. Gawin, D., P. Baggio, and B.A. Schrefler, Coupled heat, water and gas flow in deformable porous media. International Journal for numerical methods in fluids, 1995. **20**(8-9): p. 969-987.

38. Gawin, D. and B.A. Schrefler, Modelling of saturated-unsaturated transition in porous media. Proceedings of the GIMC-AMC Conference, Padua, 1996.

39. Gawin, D., B.A. Schrefler, and M. Galindo, Thermo-hydro-mechanical analysis of partially saturated porous materials. Engineering Computations, 1996. **13**(7): p. 113-143.

40. Gawin, D., B.A. Schrefler, and M. Galindo, Thermo-hydro-mechanical analysis of partially saturated porous materials. Engineering Computations, 1996. **13**(7): p. 113-143.

41. Ghaboussi, J., E.L. Wilson, and J. Isenberg, Finite element for rock joints and interfaces. Journal of the soil mechanics and foundations division, 1973. **99**(10): p. 849-862.

42. Hassanizadeh, M. and W.G. Gray, General conservation equations for multi-phase systems: 1. Averaging procedure. Advances in Water Resources, 1979. **2**: p. 131-144.

43. Hassanizadeh, M. and W.G. Gray, General conservation equations for multi-phase systems: 2. Mass, momenta, energy, and entropy equations. Advances in Water Resources, 1979. **2**: p. 191-203.

44. Hassanizadeh, M. and W.G. Gray, General conservation equations for multi-phase systems: 3. Constitutive theory for porous media flow. Advances in Water Resources, 1980. **3**(1): p. 25-40.

45. Hassanizadeh, S.M., Derivation of basic equations of mass transport in porous media, Part 1. Macroscopic balance laws. Adv. Water Resour, 1986. **9**: p. 196-206.

46. Hassanizadeh, S.M., Derivation of basic equations of mass transport in porous media, Part 2. Generalized Darcy's law and Fick's law. Adv. Water Resources, 1986. **9**: p. 207-222.

47. Haverkamp, R., et al., A comparison of numerical simulation models for one-dimensional infiltration. Soil Science Society of America Journal, 1977. **41**(2): p. 285-294.

48. Hemsworth, R., et al., Status of the ITER heating neutral beam system. Nuclear Fusion, 2009. **49**(4): p. 045006.

49. Ho, C.K. and S.W. Webb, Gas transport in porous media. Vol. 20. 2006: Springer.

50. Hwang, C., N. Morgenstern, and D. Murray, On solutions of plane strain consolidation problems by finite element methods. Canadian Geotechnical Journal, 1971. **8**(1): p. 109-118.

51. Incropera, F.P. and D.P. DeWitt, Fundamentals of heat and mass transfer, 1990, Wiley (New York)

52. Ministero delle Infrastrutture, Decreto Ministeriale 14 gennaio 2008 - Approvazione delle nuove norme tecniche per le costruzioni 2008 (N.T.C. 2008).

53. Jennings, A., A compact storage scheme for the solution of symmetric linear simultaneous equations. The Computer Journal, 1966. **9**(3): p. 281-285.

54. Terzaghi K., Die Berechnung der Durchlässigkeitsziffer des Tones aus dem Verlauf der hydrodynamischen Spannungserscheinungen. Ak. der Wissenschaften in Wien, Sitzungsberichte mathematisch-naturwissenschaftliche Klasse, part IIa, 1923. **132 (3/4)**: p. 125 - 138.

55. Katz, D.L.V. and E.R. Lady, Compressed air storage for electric power generation. 1976: May be ordered from Ulrich's Books.

56. Kosugi, K.J., Three-parameter lognormal distribution model for soil water retention. Water Resources Research, 1994. **30**(4): p. 891-901.

57. Laloui, L., G. Klubertanz, and L. Vulliet, Solid–liquid–air coupling in multiphase porous media. International journal for numerical and analytical methods in geomechanics, 2003. **27**(3): p. 183-206.

58. Leij, F.J., UNSODA unsaturated soil hydraulic database. 1996.

59. Lewis, R.W. and B.A. Schrefler, The finite element method in the deformation and consolidation of porous media. 1987.

60. Lewis, R.W. and B.A. Schrefler, The finite element method in the deformation and consolidation of porous media. 1998.

61. Lewis, R.W., B.A. Schrefler, and N.A. Rahman, A finite element analysis of multiphase immiscible flow in deforming porous media for subsurface systems. Communications in numerical methods in engineering, 1998. **14**(2): p. 135-149.

62. Liakopoulos, A.C., Transient flow through unsaturated porous media, 1964, University of California, Berkeley

63. Liakopoulos, A.C., Transient flow through unsaturated porous media, 1964, University of California, Berkeley

64. Liu, J.W., A compact row storage scheme for Cholesky factors using elimination trees. ACM Transactions on Mathematical Software (TOMS), 1986. **12**(2): p. 127-148.

65. Lloret, A. and E.E. Alonso, State surfaces for partially saturated soils. Proceedings of the 11th International Conference on Soil Mechanics and

Foundation Engineering, San Francisco, 12-16 august 1985. Publication of Balkema, 1985.

66. Lloret, A., et al. Flow and deformation analysis of partially saturated soils. in European conference on soil mechanics and foundation engineering. 9. 1987.

67. Luckner, L., M.T. Van Genuchten, and D. Nielsen, A consistent set of parametric models for the two-phase flow of immiscible fluids in the subsurface. Water Resources Research, 1989. **25**(10): p. 2187-2193.

68. Befi M., Modelli tridimensionali per l'analisi termomeccanica di geomateriali Department of Civil, Environmental and Architectural Engineering, 1993: p. 271.

69. MAJORANA, C., Modelli tridimensionali per l'analisi termomeccanica di geomateriali. Tecnica Italiana, 1994. **59**(4): p. 265-290.

70. Majorana, C., R. Lewis, and B. Schrefler, Two-dimensional non-linear thermo-elastoplastic consolidation program Plascon. The Finite Element Method in the Deformation and Consolidation of Porous Media, Lewis RW, Schrefler BA (eds), 1987.

71. Masiello, A., et al., The European contribution to the development of the ITER NB injector. Fusion Engineering and Design, 2011. **86**(6): p. 860-863.

72. Mazzucco, G., et al., Structural analyses and integrated design of the MITICA Injector assembly. Fusion Engineering and Design, 2013.

73. McWhorter, D.B. and D.K. Sunada, Exact integral solutions for two-phase flow. Water Resources Research, 1990. **26**(3): p. 399-413.

74. Meiri, D., Analysis of compressed air aquifer storage by finite element method, 1979, University of Wisconsin-Milwaukee.

75. Meiri, D., Two-phase flow simulation of air storage in an aquifer. Water Resources Research, 1981. **17**(5): p. 1360-1366.

76. Meiri, D. and G.M. Karadi, Simulation of air storage aquifer by finite element model. International Journal for Numerical and Analytical Methods in Geomechanics, 1982. **6**(3): p. 339-351.

77. Milly, P., Estimation of Brooks-Corey parameters from water retention data. Water Resources Research, 1987. **23**(6): p. 1085-1089.

78. Moran, M.J., et al., Fundamentals of engineering thermodynamics. 2010: Wiley. com.

79. Morris, J.L., Computational methods in elementary numerical analysis. 1983: Wiley New York.

80. Mualem, Y., A new model for predicting the hydraulic conductivity of unsaturated porous media. Water resources research, 1976. **12**(3): p. 513-522.

81. Mualem, Y., catalogue of the hydraulic properties of unsaturated soils. 1976.

82. Narasimhan, T. and P. Witherspoon, Numerical model for saturated-unsaturated flow in deformable porous media: 3. Applications. Water Resources Research, 1978. **14**(6): p. 1017-1034.

83. Nozad, I., R. Carbonell, and S. Whitaker, Heat conduction in multiphase systems—I: theory and experiment for two-phase systems. Chemical Engineering Science, 1985. **40**(5): p. 843-855.

84. Parker, J. and R. Lenhard, A model for hysteretic constitutive relations governing multiphase flow: 1. Saturation-pressure relations. Water Resources Research, 1987. **23**(12): p. 2187-2196.

85. Parker, J., R. Lenhard, and T. Kuppusamy, A parametric model for constitutive properties governing multiphase flow in porous media. Water Resources Research, 1987. **23**(4): p. 618-624.

86. Pastor, M., O. Zienkiewicz, and A. Chan, Generalized plasticity and the modelling of soil behaviour. International Journal for Numerical and Analytical Methods in Geomechanics, 1990. **14**(3): p. 151-190.

87. Richtmyer, R. and K. Morton, Difference methods for initial-value problems. New York: Interscience, 1967.

88. Rigato, W., et al., Vessel design and interfaces development for the 1MV ITER Neutral Beam Injector and Test Facility. Fusion Engineering and Design, 2009. **84**(7): p. 1606-1610.

89. Roscoe, K.H. and J. Burland, On the generalized stress-strain behaviour of wet clay. 1968.

90. Salomoni, V.A. and R. Fincato. 3D modelling of geomaterials accounting for an unconventional plasticity approach. 2011.

91. Salomoni, V.A. and R. Fincato, Subloading surface plasticity model algorithm for 3D subsidence analyses above gas reservoirs. International Journal of Geomechanics, 2012. **12**(4): p. 414-427.

92. Salomoni, V.A. and R. Fincato, 3D subsidence analyses above gas reservoirs accounting for an unconventional plasticity model. International Journal for Numerical and Analytical Methods in Geomechanics, 2012. **36**(8): p. 959-976.

93. Salomoni, V.A. and R.L. Fincato. Subloading surface plasticity model algorithm for 3D subsidence analyses above gas reservoirs. 2011.

94. Sandhu, R.S., Fluid flow in saturated porous elastic media. 1968: University Microfilms.

95. Schenk, O. and K. Gärtner, Solving unsymmetric sparse systems of linear equations with PARDISO. Future Generation Computer Systems, 2004. **20**(3): p. 475-487.

96. Schenk, O., et al., PARDISO: a high-performance serial and parallel sparse linear solver in semiconductor device simulation. Future Generation Computer Systems, 2001. **18**(1): p. 69-78.

97. Schrefler, B., et al., Pollutant transport in deforming porous media. European journal of mechanics. A. Solids, 1994. **13**: p. 175-194.

98. Schrefler, B. and L. Simoni, A unified approach to the analysis of saturated-unsaturated elastoplastic porous media. Numerical Methods in Geomechanics, 1988: p. 205-212.

99. Schrefler, B. and Z. Xiaoyong, A fully coupled model for water flow and airflow in deformable porous media. Water Resources Research, 1993. **29**(1): p. 155-167.

100. Schrefler, B.A., X. Zhan, and L. Simoni, A coupled model for water flow, airflow and heat flow in deformable porous media. International Journal of Numerical Methods for Heat & Fluid Flow, 1995. **5**(6): p. 531-547.

101. Šimůnek, J., et al., Parameter estimation of unsaturated soil hydraulic properties from transient flow processes. Soil and Tillage Research, 1998. **47**(1): p. 27-36.

102. Stephens, D.B., Vadose zone hydrology. 1996: CRC press.

103. Stephens, D.B., K. Lambert, and D. Watson, Regression models for hydraulic conductivity and field test of the borehole permeameter. Water Resources Research, 1987. **23**(12): p. 2207-2214.

104. Strassen, V., Gaussian elimination is not optimal. Numerische Mathematik, 1969. **13**(4): p. 354-356.

105. Tyler, S.W. and S.W. Wheatcraft, Application of fractal mathematics to soil water retention estimation. Soil Science Society of America Journal, 1989. **53**(4): p. 987-996.

106. Tyler, S.W. and S.W. Wheatcraft, Fractal processes in soil water retention. Water Resources Research, 1990. **26**(5): p. 1047-1054.

107. van Genuchten, M.T., A closed-form equation for predicting the hydraulic conductivity of unsaturated soils. Soil Science Society of America Journal, 1980. **44**(5): p. 892-898.

108. van Genuchten, M.T., F. Leij, and S. Yates, The RETC code for quantifying the hydraulic functions of unsaturated soils. 1991.

109. van Genuchten, M.T. and D. Nielsen, On describing and predicting the hydraulic properties of unsaturated soils. Ann. Geophys, 1985. **3**(5): p. 615-628.

110. van Genuchten, R., Calculating the unsaturated hydraulic conductivity with a new closed-form analytical model. 1978: International Ground Water Modeling Center.

111. Webb, S.W., Steady-state saturation profiles for linear immiscible fluid displacement in porous media, 1991, Sandia National Labs., Albuquerque, NM (United States)

112. Withaker, S., Simultaneous heat, mass and momentum transfer in porous media. A theory of drying porous media. Adv. Heat Transfer, 1977. **13**: p. 119-200.

113. Zanetti, S., Analisi tridimensionale di problemi di subsidenza per estrazione di fluidi. Master Thesis, Departement of Civili, Environmental and Architectural Engineering, Padua, 1995-1996: p. 133.

114. Zienkiewicz, O.C., The Finite Element Method. 1989.

115. Zienkiewicz, O.C., et al., Static and dynamic behaviour of soils: a rational approach to quantitative solutions. I. Fully saturated problems. Proceedings of the Royal Society of London. A. Mathematical and Physical Sciences, 1990. **429**(1877): p. 285-309.

116. Zienkiewicz, O.C., C. Humpheson, and R. Lewis, A unified approach to soil mechanics problems (including plasticity and viscoplasticity), 1977, Wiley: New York. p. 151-179

117. Zienkiewicz, O.C. and T. Shiomi, Dynamic behaviour of saturated porous media; the generalized Biot formulation and its numerical solution. International journal for numerical and analytical methods in geomechanics, 1984. **8**(1): p. 71-96.

118. Zienkiewicz, O.C., et al., Static and dynamic behaviour of soils: a rational approach to quantitative solutions. II. Semi-saturated problems. Proceedings of the Royal Society of London. A. Mathematical and Physical Sciences, 1990. **429**(1877): p. 311-321.

119. Zienkiewicz, O.C., et al., Static and dynamic behaviour of soils: a rational approach to quantitative solutions. II. Semi-saturated problems. Proceedings of the Royal Society of London. A. Mathematical and Physical Sciences, 1990. **429**(1877): p. 311-321.